



This book is provided in digital form with the permission of the rightsholder as part of a Google project to make the world's books discoverable online.



This book is licensed under a Creative Commons license. By using a Creative Commons license, the rightsholder chose to give you more freedom to share or re-use the book than would otherwise be possible under copyright law.

This license allows distribution of this book with attribution but prohibits commercial use or derivative works. Terms available here: <http://creativecommons.org/licenses/by-nc-nd/3.0/>

### **About Google Books**

Google's mission is to organize the world's information and to make it universally accessible and useful. Google Books helps readers discover the world's books while helping authors and publishers reach new audiences. You can search through the full text of this book on the web at <http://books.google.com/>

UC-NRLF



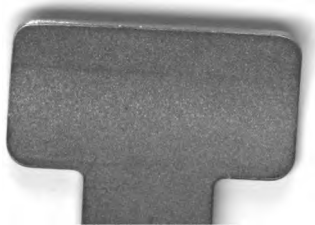
B 4 431 850

UNIVERSITY OF BELGRADE  
FACULTY OF CIVIL ENGINEERING  
and  
INSTITUTE OF TECHNICAL SCIENCES  
OF SERBIAN ACADEMY OF SCIENCES AND ARTS

# MISCELLANY

DEDICATED TO THE 65<sup>th</sup> BIRTHDAY  
OF ACADEMICIAN PROFESSOR  
Dr. NIKOLA HAJDIN

BELGRADE, 1988



**MISCELLANY**  
**Dedicated to the 65<sup>th</sup> Birthday**  
**of Academician Professor Dr. Nikola Hajdin**



**UNIVERSITY OF BELGRADE  
FACULTY OF CIVIL ENGINEERING  
and  
INSTITUTE OF TECHNICAL SCIENCES  
OF SERBIAN ACADEMY OF SCIENCES AND ARTS**

# **MISCELLANY**

**DEDICATED TO THE 65<sup>th</sup> BIRTHDAY  
OF ACADEMICIAN PROFESSOR  
Dr. NIKOLA HAJDIN**

**Edited by  
NATALIJA NAERLOVIĆ - VELJKOVIĆ**

**BELGRADE, 1988**

5482-3341

**Published by**  
**University of Belgrade**  
**Faculty of Civil Engineering**  
**and**  
**Institute of Technical Sciences**  
**of Serbian Academy of Sciences and Arts**

The publication of this book was financially supported by  
Science Association of the Socialist Republic of Serbia  
and  
"Kirilo Savić" Institute, Belgrade

*Original*

Technical Editor  
Rastislav Mandić

Printed and bound by  
GOŠA - RO Institute, Belgrade

This book is printed from direct litographs of authors' manuscripts

TAG  
M5  
195  
EN

## CONTENTS

<b>NIKOLA HAJDIN AS A PERSONALITY, SCIENTIST, TEACHER AND ENGINEER</b>	1
N. Naerlović-Veljković, Prof., Dr. Faculty of Civil Engineering, University of Belgrade	
<b>CONGRATULATIONS FROM SWITZERLAND</b>	5
B. Thürlimann, Prof., Dr. Eidgenössische Technische Hochschule Zürich (ETH)	
<b>NIKOLA HAJDIN - A PERSONAL TRIBUTE TO A FRIEND AND TEACHER</b>	6
D. Krajčinović, Prof., Dr. University of Illinois at Chicago	
<b>VERSUCHE ZUR REIBERMUEDUNG EINBETONIERTER SPANNKABEL</b>	9
B. Thürlimann, Prof., Dr. und J. Oertle, dipl. Bauing. ETH Eidgenössische Technische Hochschule Zürich (ETH)	
<b>ZWEI BEITRÄGE ZUR STABILITÄTSTHEORIE IM STAHLBAU</b>	19
P. Dubas, Prof., Dr. Eidgenössische Technische Hochschule Zürich (ETH)	
<b>LOCAL DAMAGE EFFECTS IN CYLINDERS STIFFENED BY RINGS AND STRINGERS</b>	29
B.F. Ronalds, Lecturer, Dr. and P.J. Dowling, Prof., Dr. Department of Civil Engineering, Imperial College of Science and Technology, University of London	
<b>MAN-INDUCED VIBRATIONS IN STRUCTURES – MEASURES AND PRACTICAL CASES</b>	43
H. Bachmann, Prof., Dr. Eidgenössische Technische Hochschule Zürich (ETH)	
<b>SOME PROBLEMS OF TWO-CHORD SYSTEMS</b>	55
M. Ivković, Prof., Dr. Faculty of Civil Engineering, University of Belgrade	
<b>THE ESSENTIAL STRUCTURE OF DAMAGE THEORIES</b>	65
D. Krajčinović, Prof., Dr. University of Illinois at Chicago	



<b>APPLICATIONS DE CONNAISSANCES RÉCENTES DANS LA CONCEPTION D'OUVRAGES EN BÉTON</b>	<b>75</b>
R. Favre, Prof. École Polytechnique Fédérale de Lausanne	
<b>FEM SOLUTION OF THE COUPLED PLANE PROBLEM OF THE THERMOELASTICITY</b>	<b>87</b>
N. Naerlović-Veljковиć, Prof., Dr. and D. Šumarac, Assist. Prof., Dr. Faculty of Civil Engineering, University of Belgrade	
<b>MODELLING OF THE BEHAVIOUR OF COLUMN WEB PANELS IN SEMI-RIGID JOINTS</b>	<b>97</b>
R. Maquoi, Prof., Dr. and J.P. Jaspard, Assistant Institut de Génie Civil, Université de Liège	
<b>LONG-SPAN BRIDGES</b>	<b>107</b>
F. de Miranda, Prof. Milan Polytechnic	
<b>CONTRIBUTION TO NONLINEAR ANALYSIS OF R.C. THIN-WALLED BEAMS AND FRAMES BY FINITE ELEMENT METHOD</b>	<b>125</b>
M. Sekulović, Prof., Dr. and B. Pujević, Assistant, M.Sc. Faculty of Civil Engineering, University of Belgrade	
<b>SHEAR LAG IN ARCH-SHAPED STEEL BOX GIRDERS</b>	<b>135</b>
V. Kristek, Prof., Dr. Faculty of Civil Engineering, Czech Technical University, Prague and M. Skaloud, Prof., Dr. Institute of Theoretical and Applied Mechanics, Czechoslovak Academy of Sciences, Prague	
<b>A CONTRIBUTION TO THE SOLUTION OF ULTIMATE CARRYING CAPACITY OF POLYGONAL SLABS</b>	<b>143</b>
M. Milićević, Prof., Dr. Faculty of Civil Engineering, University of Niš	
<b>ON TORSIONAL BUCKLING OF THIN-WALLED CONTINUOUS MEMBERS</b>	<b>151</b>
Z. Cywiński, Prof., Dr. habil. Technical University of Gdańsk and University of Tokyo	
<b>ON NONLINER FUNCTIONALS FOR SHALLOW SHELLS AND GEOMETRICALLY IMPERFECT PLATES</b>	<b>161</b>
R. Dabrowski, Prof., Dr. Technical University of Gdańsk	
<b>THE GENERAL NUMERICAL SOLUTION OF THE LAME'S EQUATIONS BY HAJDIN'S METHOD</b>	<b>169</b>
P.S. Petrović, Prof., Dr. Faculty of Civil Engineering, University of Belgrade	

<b>A RAYLEIGH ESTIMATE OF THE FUNDAMENTAL FREQUENCY OF SIMPLY SUPPORTED SLABS WITH INTERMEDIATE COLUMN SUPPORTS</b>	183
M.N. Pavlović, Reader, Dr. Department of Civil Engineering, Imperial College of Science and Technology, University of London	
<b>LINEAR PROGRAMMING APPROACH TO LIMIT ANALYSIS OF THIN-WALLED STRUCTURES</b>	193
Š. Dunica, Prof., Dr. Faculty of Civil Engineering, University of Belgrade	
<b>COLLAPSE OF PLATE GIRDERS SUBJECTED TO PATCH LOADING</b>	203
T.M. Roberts, Lecturer, Dr. University College, Department of Civil and Structural Engineering, Cardiff and B. Corić, Assist. Prof., Dr. Faculty of Civil Engineering, University of Belgrade	
<b>RISIKOANALYSE ÜBER DEN BETRIEBSZUSTAND DER 109-JAEHRIGEN SCHWEISSEISERNEN WETTSTEINBRÜCKE IN BASEL (SCHWEIZ)</b>	211
J. Grob, Dr.-Ing. Universal Ingenieur AG, Zürich	
<b>SCHRÄGKABELBRÜCKEN MIT PARALLELDRAHTKABELN</b>	221
H.R. Müller, Dipl. Ing. ETH Bureau BBR Ltd./Stahlton AG, Zürich	
<b>FATIGUE CRACK GROWTH AT LARGE DEFLECTIONS OF WEB LOADED IN SHEAR</b>	227
J. Djubek, Assoc. Prof., Dr. Institut of Construction and Architecture of SAS, Bratislava	
<b>NEW LIGHTING TECHNOLOGIES IN TV AND FILM STUDIOS AND THEIR REFLEXES TO THE STRUCTURAL STEELWORK</b>	237
S. Cvetković, Civil Eng. Mostprojekt, Belgrade	
<b>CONTRIBUTION TO THE NUMERICAL SOLUTION OF THE CABLE</b>	247
D. Grbić, Assist. Prof., Dr. Faculty of Civil Engineering, University of Belgrade	
<b>A FINITE ELEMENT SIMULATION OF 2D FLUID FLOW AROUND RIGID STRUCTURES - IBM PC/AT IMPLEMENTATION</b>	253
S. Brčić, Assist. Prof., Dr. Faculty of Civil Engineering, University of Belgrade	
<b>SOME ASPECTS OF NONLINEAR FINITE ELEMENT ANALYSIS OF WELDED GUSSET PLATES</b>	261
Dj. Vuksanović, Assistant, M. Sc. and B. Pujević, Assistant, M.Sc. Faculty of Civil Engineering, University of Belgrade	

<b>NON-LINEAR ANALYSIS OF CABLE-STAYED BRIDGES</b>	<b>273</b>
<b>B. Stipanić, Assistant, M.Sc.</b>	
<b>Faculty of Civil Engineering, University of Belgrade</b>	
<b>ON THE DETERMINATION OF FINITE INCREMENTS IN PERFECT PLASTICITY</b>	<b>283</b>
<b>Lj. Savić, Assistant, M.Sc.</b>	
<b>Faculty of Civil Engineering, University of Belgrade</b>	
<b>ANALYSIS OF THIN-WALLED BEAMS WITH DEFORMABLE CROSS SECTION</b>	<b>293</b>
<b>R. Mandić, Assistant, M.Sc.</b>	
<b>Faculty of Civil Engineering, University of Belgrade</b>	
<b>ACADEMICIAN NIKOLA HAJDIN - CURRICULUM VITAE</b>	<b>301</b>
<b>LIST OF PAPERS AND BOOKS BY NIKOLA HAJDIN</b>	<b>305</b>
<b>SOME OF THE MORE IMPORTANT STRUCTURES DESIGNED BY NIKOLA HAJDIN</b>	<b>315</b>



*Nru Hayden*



## **NIKOLA HAJDIN AS A PERSONALITY, SCIENTIST, TEACHER AND ENGINEER**

Academician Nikola Hajdin belongs to the first generation of students who enrolled in the Civil Engineering Faculty of Belgrade University after the Second World War, in 1945. The University had been closed for four years, and the first post-war generation, with an accumulated thirst for science, eagerly assimilated the knowledge so amply delivered to them by their professors, who had likewise long been deprived of their chairs. For my generation, which immediately followed them, the 1945 generation represented an ideal which attracted and inspired many of us to devote ourselves to our studies in the same way. A large number of very good civil engineers and several university professors emerged from that generation. This special emotional relationship, based on admiration, towards the 1945 generation has faded out in time. However, when Nikola Hajdin is concerned, and in view of his professional and scientific opus, this relationship has with time grown into a completely conscious insight that he is a particularly creative and special figure: his values are completely personal ones which far exceed the average of this generation, and which truly inspired us younger students.

There is an old saying that any truth is perfectly simple. It seems to me that this can be applied in many ways to academician Nikola Hajdin. Having discovered his professional interest in the field of civil engineering structures, he pursues his path of truth as scientist, professor and structural engineer, achieving a balanced relationship between the three aspects of his activity, synthesizing them into a harmonic whole. The way in which he thinks is perfectly simple – direct and crystal clear. Hence the way in which he creates looks as easy as a game. Sharp-sighted in everyday life, he is also this in his professional solutions which are original, imaginative and unexpected in their wittiness.

Nikola Hajdin published his first scientific paper, "Torsion of a Triangular Tube" when he was still a student.

The two works that followed (nos. 2 and 3), together with his first paper represented a contribution in the field of Mathematical Theory of Elasticity. However, it soon

became clear that life is much richer in questions than in answers in the domain of exact solutions. Thus, as early as 1956, Nikola Hajdin turned his interest to the field of numerical solutions. In his doctoral thesis, "A Method for the Numerical Solution of Boundary Value Problems and its Application to Some Problems of the Theory of Elasticity", which he successfully defended in 1956 at Civil Engineering Faculty in Belgrade, Hajdin provides a witty numerical solution based on the integral formulation of equilibrium equations, largely applied to the theory of one- and two- dimensional problems. This method has been used and quoted in the works of over 40 authors in various parts in the world. His numerical analysis actually came at the very timely moment, on the eve of the expansion of computer techniques.

When one examines the scientific opus of academician Hajdin, one can notice a sort of loyalty towards fields once taken up; he has occasionally returned to them as if they were old friends to whom he always had something to impart. We first encounter the shell as a subject in his paper no. 2, written in 1952. It appears again in paper no. 6 (in 1958) and then, with intervals, there follows a series of papers devoted to plates and shells as well as to the application of numerical analysis of arch dams (papers nos. 7, 9, 11, 14, 16, 23, 31, 73). Thus, arch dams have been appearing for years as a preoccupation of academician Hajdin as a structural engineer. Dams were also the first major structures in which Hajdin's numerical procedure was widely applied, as it was on the basis of this procedure that the biggest dams in Yugoslavia: Grančarevo, Mratinje and Glažnja were analysed and constructed. However, as we shall see later, first place in academician Hajdin's opus belongs to bridges.

As a designer, Hajdin chose steel as his favourite material. Perhaps this is somehow secretly connected with his previous friendship with the Theory of Elasticity. And obviously – where steel structures are present, there is the problem of buckling, or in general, the problem of behaviour in critical and post-critical domains (papers nos. 10, 12, 43, 49, 54, 57, 76, 94), as well as the problem of thin-walled beams. The problem of torsion, broached in his first, student paper, treated within the framework of St. Venant's theory, emerged ten or more years later as a problem of warping torsion, within the Theory of Thin-Walled Beams.

The Theory of Thin-Walled Beams, side by side with his contribution in the domain of numerical analysis of deformable systems, represents another major scientific field to which academician Hajdin made a great contribution. The majority of his papers belongs to this field (nos. 17, 18, 20, 21, 22, 24, 25, 26, 27, 29, 30, 32, 34, 38, 39, 42, 48, 55, 58, 62, 74, 83, 87, 88, 103, 104, 105, 107, 111). In this part of his opus, two exceptionally valuable monographs (nos. 36 and 47) written together with Dr. C.F. Kollbrunner, should be emphasised: "Dünnwandige Stäbe, Band 1: Stäbe mit undeformierbaren Querschnitten" (1972) and "Dünnwandige Stäbe, Band 2: Stäbe mit deformierbaren Querschnitten. Nichtelastisches Verhalten dünnwandiger Stäbe" (1975). These two monographs, the result of two decades of collaboration of the authors, provide a full picture of the knowledge embodied in the Theory of Thin-Walled Beams at the time.

Through the Theory of Thin-Walled Beams, other current preoccupations of academician Hajdin are refracted: non-elastic behaviour (the second volume of the monograph) and non-linear relations (paper no. 83). Girders with curvilinear axis have appeared as well (nos. 30, 32, 88). Physically more complex states and behaviours and their analytical modelling in an acceptable form in the engineering sense, were subjects of other papers: in paper no. 30 the effects of creep and shrinkage of concrete are considered: plasticity and ultimate limit state appeared in his papers nos. 33, 48, 53, 87, 99, 105; other publications dealing with ultimate limit state (no. 51.), elastoplastic behaviour (nos. 62, 103), interaction of soil and structure (nos. 84, 101), composite structures (nos. 40, 58, 100), vibrations of elastic systems and wind effects on structures (nos. 45, 55, 60, 95) followed.

In the recent years, two exceptional structures have been created as a result of Hajdin's design activity: the railway bridge over the Sava river in Belgrade, with a span of 254 m, completed in 1979 (designed together with Professor Jevtović) represented the first use of the system known as "cable-stayed bridge" for what was solely a railway bridge. Then, the Novi Sad Bridge, with a span of 351 m had at the time of its completion in 1981, the longest span in the system with cables in a single vertical plane.

It would be wrong to think that bridges did not preoccupy academician Hajdin until he reached full maturity in his structural engineering work. On the contrary, even as a young designer, he was awarded first prize in the anonymous competitions for designing bridges over the river Tisa near Žablje and the river Sava near Orašje, which were later constructed according to his designs.

The railway bridge over the Sava and the Novi Sad Bridge combine imagination and experience on the one hand and very rigorous theoretical and experimental research and investigation on the other. In connection with the system of cable-stayed bridges, academician Hajdin solved a series of theoretical problems and published his views in over 20 papers and briefings given at congresses (papers nos. 56, 60, 61, 64, 65, 66, 68, 70, 71, 72, 75, 78, 81, 82, 85, 86, 89, 90, 91, 92, 93, 96, 100, 109). The first of the above mentioned works was given at Tenth Congress of the International Association for Bridge and Structural Engineering held in Tokyo in 1976. The paper no. 75, prepared together with Dr. C.F. Kollbrunner and B. Stipančić: "A Contribution to the Analysis of Cable-Stayed Bridges" was published in Zürich in 1980 and later translated into Japanese and printed in the Japanese magazine "Steel Bridges" at the request of its editors (no. 85).

A particular page in the professional and personal life and work of academician Hajdin is dedicated to his sojourn in Zürich and his long-lasting cooperation and friendships there, especially with Dr. C.F. Kollbrunner. This has resulted in more than 20 publications, a number of which are monographs in character. In 1977, the two scientists together wrote an article under the title: *Zwanzig Jahre der Zusammenarbeit* (no. 59).

Surveying the titles of his publications, it occurs to one, that the numerous original theoretical research works of academician Hajdin have almost always been induced



by questions arising from practical problems in his work as a designer. There is no doubt that these new, daring solutions, so characteristic of his structures, could not have been accomplished without extensive previous theoretical and experimental research. Herein lies the explanation of the fact that all his theoretical considerations, regardless of how complex they are, have always been brought to the utmost possible level of applicability. His papers on thin-walled structures and bridges have been used and quoted in several hundred Yugoslav papers and in more than 80 papers in foreign literature.

One should not fail to point out another of academician Hajdin's attributes – his openness to cooperation and his communicativeness in contacts with collaborators. This, coupled with his attitude towards the future of the profession, confirmed his particular ability as a “teacher”. And truly, wherever he goes, academician Hajdin can always meet his students: among masters of science, doctors of philosophy, assistants and lecturers in civil engineering faculties, in the design bureaus of large consulting organizations, on building sites. Sharing his meditations, his dilemmas and the possible ways out of them with capable young people, introducing them to his own work, he finds contentment in following their development and, accordingly, in the continuation of his ideas through their work.

And when I say that academician Hajdin achieves satisfaction in the harmony of his creation, then I have in mind all the facts I have been considering.

Natalija Naerlović – Veljković

## CONGRATULATIONS FROM SWITZERLAND

After completing his doctoral work in 1956, the young Dr. N. Hajdin was looking for a position in a foreign country to broaden his academic as well as his practical experience. At that time Yugoslavia started to normalize its relations with the Western Countries. Mr. Hajdin found a position as structural engineer with the steel fabricators AG Konrad Zschokke, Döttingen, Switzerland, during 1958-59. Within a short time he impressed the director of Zschokke, Dr. C.F. Kollbrunner, with his profound theoretical knowledge of structural analysis and design.

Dr. Kollbrunner was an impressive and imposing personality in many ways, firstly by his physical frame and his voice and then by his almost legendary fame as an innovative and inspiring officer in the Swiss Army. He had also gained a scientific reputation for his research work on structural stability of steel structures and in the field of soil mechanics and foundation engineering. He had a good eye for young talents. Many young engineers have been discovered, supported and promoted by him.

This first contact between the two led to a very fruitful scientific collaboration. In a review entitled 'Zwanzig Jahre der Zusammenarbeit' (Twenty Years of Collaboration), published in 1977, 20 publications co-authored by Kollbrunner and Hajdin within a periode of 20 years (1958-77) with a total of about 2000 pages are listed.

During 1963 Mr. Hajdin, by now an associate professor at the University of Belgrad, was invited by the Technical Commission of the Swiss Steel Fabricators as a visiting scientist to do research work in the field of thin-walled steel members. Out of professional contacts with colleagues at the Swiss Federal Institute of Technology Zürich, a continuing cooperation was initiated. During the summer semesters of 1971 and 1973 Professor Hajdin was a visiting professor lecturing on the subject of "Thin-walled Members". More recently he presented a lecture on the design and erection of the cable-stayed railway bridge in Belgrad for which he was the chief designer.

These professional contacts, social relations and personal friendships between Professor Hajdin and his Swiss colleagues at the Swiss Federal Institute of Technology have grown.

On the occasion of your 65th Birthday we express to you, dear Nikola, our sincere thanks and appreciation for your valuable academic contributions and your warm friendship. With our best wishes for the years ahead of you, yours

Zürich, April 4, 1988

Bruno Thürlimann

## NIKOLA HAJDIN - A PERSONAL TRIBUTE TO A FRIEND AND TEACHER

A teacher affects eternity; he can never  
tell where his influence stops.  
Henry Adams.

Somebody once stated that every engineer is a closet physicist. I often wonder to what extent is that true in my case. No doubt, however, in the case of Nikola Hajdin. The man is exactly what he wants to be - perfectly at ease with himself. No trace of any doubt in himself, a picture of self confidence. A twinkle in his eye and a smile always ready to stretch his lips.

A consummate professional, a man who wears many hats and yet a straightforward person. Most of all a warm human being, a friend if I ever had one. And that is exactly why I do not intend to write about those magnificent bridges spanning mighty rivers, about those high dams, list his papers and books or name all of us who are proud to call ourselves his students. All of these are a matter of record for all of us to see and admire. There are people better with words and anything I can say will add little to those facts.

Getting long in teeth myself, a hesitant but frequent traveler, I was fortunate to rub elbows with people whose names you would recognize. If the truth is to be served some of them were better mathematicians, some knew more about arcane and esoteric continuum theories. Yet the more of them I get to know in a strange way the better Šef, as we call him, looks. Neither the time nor the physical distance were able to subtract from the impression of him I carried and cherished for three decades.

Being a closet physicist and amateur psychologist myself I sometimes wonder about the roots of my admiration and attachment to Šef, and the basis for the high regard I have for the man who we honor with this volume. Am I impressed by these magnificent bridges, and Springer-Verlag books? Of course I am. But that is not all. This most renaissance man I happen to know is not only an engineer and a scientist. He is also a teacher, an educator, a focal point for the young people aspiring to fulfill their ambitions and live up to their potential. And he did all of that with little or no help. He was not backed by a modern lab, institute, an army of technicians and graduate students. To paraphrase our greatest poet he is a lion who came out of a little bush. More than that he transformed the bush into a forest.

He accomplished all of it with a flair that the nature sparingly bestows to chosen few. Well, this suffices to explain the respect for his accomplishment. But, as you guessed by now, I truly love the man. He is my friend. He taught me more than plates and shells. He was there to help, to share his time, to discuss a myriad of things a young man, as I was then, wants to know. His friendship showed no limits and I always felt wiser, better, calmer and more content after talking to him. Infrequently we had difference in opinions and even disagreements and I found that a friendship means not to have to say that I was sorry.

The picture of Šef, which I in an admittedly personal and perhaps biased way, painted would be incomplete without mentioning his wife Milena and son Rade. They are undoubtedly one of the significant sources of his strength. As strong as he is I doubt that he would have reached as far as he did if it was not for their unreserved support. They understood his devotion to his job and shared his time with the rest of us without complaint. In a way this is then my tribute to them as well.

Thank you my friend. This little tribute does not even begin to show how much you did for so many of us. You are a significant part of our lives and you will live in our students and hopefully in theirs as well. Even though, as I understand, you plan to retire at the end of this year knowing you as well as I do this will have little effect on your activities. You will still be here to teach, advise and design. May you enjoy many more years as much as we enjoyed our association with you.

Dusan Krajinovic  
Chicago, May 1988



## VERSUCHE ZUR REIBERMÜDUNG EINBETONIRTER SPANNKABEL

Prof. Dr. Bruno Thürlimann und J. Oertle, dipl. Bauing. ETH  
Eidgenössische Technische Hochschule Zürich (ETH)

### ZUSAMMENFASSUNG

Die Ermüdungsfestigkeit von Spannkabeln aus Litzen oder parallelen Drähten wird in entscheidendem Masse durch die Art des Hüllrohrmaterials mitbestimmt. Die Verwendung von Kunststoff anstelle von Stahl führte annähernd zu einer Verdoppelung der erträglichen Spannungsschwingbreite. Ebenso führt eine Reduktion der zwischen Spanndraht und Hüllrohr herrschenden Querpressung zu einer erhöhten Ermüdungsfestigkeit. Dies kann durch eine Begrenzung der Kabelkrümmung und/oder durch eine günstige Formgebung der Hüllrohrwandung erreicht werden. Weiterführende Detailuntersuchungen und theoretische Ueberlegungen zum Phänomen Reibermüdung sowie deren Bedeutung für teilweise vorgespannte Betontragwerke werden demnächst veröffentlicht [12].

### 1. Einleitung

Bauteile mit voller Vorspannung weisen in der Regel eine hohe Sicherheit gegen Ermüdungsversagen der Spannstähle auf. Ein Nachweis der Dauerfestigkeit ist ausser in Verankerungsbereichen und bei Koppelstellen von Spanngliedern im allgemeinen nicht erforderlich [1]. Da die Bemessung Zugspannungen im Beton ausschliesst, überschreiten die aus Schwingbelastung entstehenden Spannungsschwingbreiten der Spann- und Bewehrungsstähle den Bereich von  $\Delta\sigma = 50 \text{ N/mm}^2$  im allgemeinen nicht und sind somit, verglichen mit ihren Dauerfestigkeiten, klein. Demgegenüber können bei teilweiser Vorspannung bereits unter Gebrauchslasten Risse auftreten. Dadurch werden die Spannungsschwingbreiten der Spann- und Bewehrungsstähle bedeutend grösser. Sogar voll vorgespannte Bauwerke können infolge unvorhergesehener Umstände (Setzungen, Schwinden, Temperatureinwirkungen, etc.) an kritischen Stellen Risse aufweisen. Die Spannungsverhältnisse in der Umgebung des Betonrisses sind dann mit denjenigen in teilweise vorgespannten Bauteilen vergleichbar.

Früher beschränkte sich die Forschungstätigkeit meist auf experimentelle Untersuchungen schwingend beanspruchter, teilweise vorgespannter Träger, die im Spannbettverfahren hergestellt worden waren und deshalb gerade verlaufende

Spannglieder hatten. Erst zu Beginn der achtziger Jahre kamen systematische Untersuchungen an teilweise vorgespannten Trägern, deren Spannglieder gekrümmt geführt waren und der Verbund nachträglich hergestellt wurde, hinzu [2, 3, 4].

Das Institut für Baustatik und Konstruktion der ETH Zürich forscht seit Jahren auf diesem Gebiet. In verschiedenen Publikationen wurde über Teilprojekte wie Schubbewehrung [5], Ermüdungsfestigkeit nackter Stähle [6], Einfluss der Länge von Spanngliedern [7] sowie Ermüdungsverhalten teilweise vorgespannter Träger [2, 8] berichtet. Im Jahre 1981 wurde eine Versuchsserie von 15 Balken von je 6.7 m Länge begonnen. Bereits die ersten Versuche zeigten völlig überraschend, dass das Ermüdungsverhalten einbetonierter, injizierter Spannglieder wesentlich ungünstiger ist als dasjenige nackter Proben von Spanndrähten und -litzen. Ursache dieses unerwarteten Verhaltens ist hauptsächlich die Reiberermüdung, welcher bisher beim Spannbeton keine Beachtung geschenkt worden war. Ein Riss im Träger hat zur Folge, dass in dessen unmittelbarer Umgebung kleine Relativverschiebungen zwischen dem Spannkabel und dem Hüllrohr auftreten. Ist das Spannkabel in diesem Bereich noch gekrümmt, so entstehen durch die Umlenkkräfte bedeutende Querverpressungen und entsprechende Reibkräfte an den Kontaktstellen zwischen dem Spannkabel und den Rippen des Hüllrohrs. Die dabei erzeugte Reibung führt zu einer frühzeitigen Ermüdung. Dieses Phänomen ist im Maschinenbau schon länger bekannt [9, 10].

## 2. Zielsetzung

Um die Reiberermüdung in Kabeln teilweise vorgespannter Betonträger genauer abklären zu können, wurde eine neue Versuchsanlage entwickelt (Bild 1a). Dabei wurde darauf geachtet, dass im Kleinkörper der Bereich um den Riss der Risszone im teilweise vorgespannten Bauteil, in der Ermüdungsbrüche auftreten, möglichst gut entsprach. Im weiteren wurden übersichtliche statische Verhältnisse angestrebt, damit der Kraftverlauf eindeutig feststand (Bild 1b). Die Kleinkörper sollten nicht zu gross und geometrisch einfach geformt sein, um deren Herstellung und Prüfung zu erleichtern, ganz besonders, weil eine grössere Anzahl Kleinkörperversuche geplant wurde, um eine gewisse statistische Absicherung der Versuchsergebnisse zu erreichen.

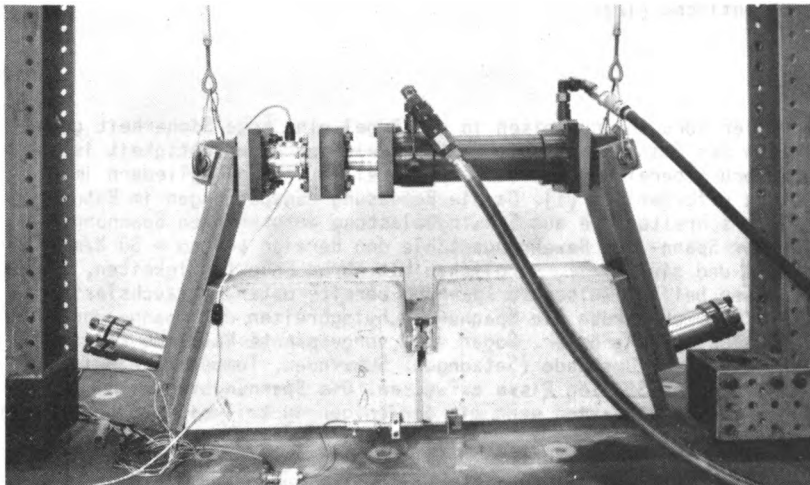


Bild 1a: Versuchsanlage

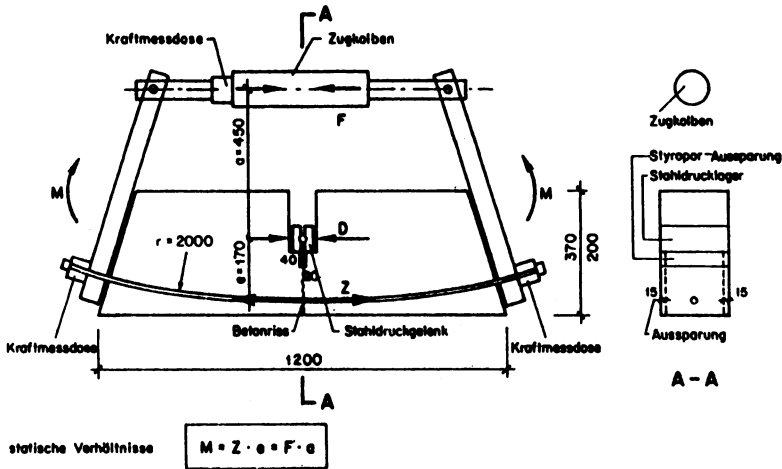


Bild 1b: Schema des Kleinkörpers und seiner Belastung

Nach Abschluss der Versuche an Kleinkörpern wurde aufgrund der gewonnenen Erkenntnisse eine begrenzte Anzahl Balkenversuche durchgeführt, um neu zu entwickelnde Bemessungskriterien überprüfen zu können.

### 3. Versuchsdurchführung an Kleinkörpern

Der im Bild 1b dargestellte Kleinkörper wies eine Länge von 1200 mm und einen Querschnitt von 200 x 350 mm auf. Ein nachträglich eingegossenes Stahldruckgelenk legte den inneren Hebelarm zwischen den Druck- und Zugresultierenden eindeutig fest, so dass die Spannungen im Spannstahl exakt bestimmt werden konnten. Das Hüllrohr wurde während der Betonierphase mit Hilfe eines kreisförmig vorgebogenen Führungsrohres, welches später beim Ausschalen herausgezogen werden konnte, fixiert. Dadurch war der Krümmungsradius - und somit die Querpressung - des Spannkabels definiert. Das Vorspannen der Kleinkörper erfolgte über einen Verankerungskopf mit je drei Schrauben. Die entstehende Vorspannkraft konnte auf beiden Seiten über je eine Kraftmessdose kontrolliert werden. Die freie Aufhängung des Prüfsystems stellte sicher, dass keine Zwängungen auftreten konnten und somit alle auf die Rissregion einwirkenden Kräfte genau bekannt waren.

Die Kleinkörper mit Einzellitze  $\varnothing 0.6''$  oder mit fünf Paralleldrähten  $\varnothing 7$  mm wurden in der Regel solange geprüft, bis drei Brüche im Spannglied erfolgt waren. Nach einem Drahtbruch wurden beide Kraftgrenzen derart reduziert, dass die Prüfung des restlichen Kabelquerschnittes bei konstanter Spannungsschwingbreite und konstantem Spannungsniveau durchgeführt werden konnte. Würde der Schwingversuch ohne Rücksicht auf erfolgte Drahtbrüche mit konstant gehaltenen Kraftgrenzen gefahren, hätte dies nach jedem Bruch eine sprungartige Erhöhung der Spannungen im verbleibenden Kabelquerschnitt zur Folge.



#### 4. Ergebnisse der Kleinkörperversuche

Bei den Darstellungen der Spannungsschwingbreite über der Lastspielzahl (Bilder 2 bis 5, 8, 9) ist speziell zu beachten, dass die Lastspielzahl auf der Abszisse nicht wie üblich im logarithmischen Massstab, sondern im linearen Massstab aufgetragen ist. Bei logarithmischer Auftragung treten die Aenderungen und Vorgänge zu Beginn der Lebensdauer besonders deutlich hervor. In bezug auf das Ermüdungsverhalten von Spannstählen gilt jedoch das Interesse in gleicher Weise der gesamten Lebensdauer.

Bei den Versuchen mit Stahlhüllrohr und einer Litze (Bild 2) ging der Ermüdungsanriss der zuerst gebrochenen Drähte regelmässig von den Kontaktstellen zwischen einem Aussendraht und einer Rippe des Hüllrohrs aus. Die folgenden Drahtbrüche hingegen wurden an Kontaktstellen zwischen Aussen- und Zentraldraht erzeugt. Demgegenüber erfolgte bei Versuchen mit Kunststoffhüllrohr der Ermüdungsanriss der gebrochenen Litzendrähte ohne Ausnahme zwischen Aussen- und Zentraldraht (Bild 3). Der Einfluss der Art des Reibpartners ist beachtlich, wenn man die Ermüdungsfestigkeit der Kleinkörper mit Stahlhüllrohr (Bild 2) mit derjenigen der Kleinkörper mit Kunststoffhüllrohr (Bild 3) vergleicht.

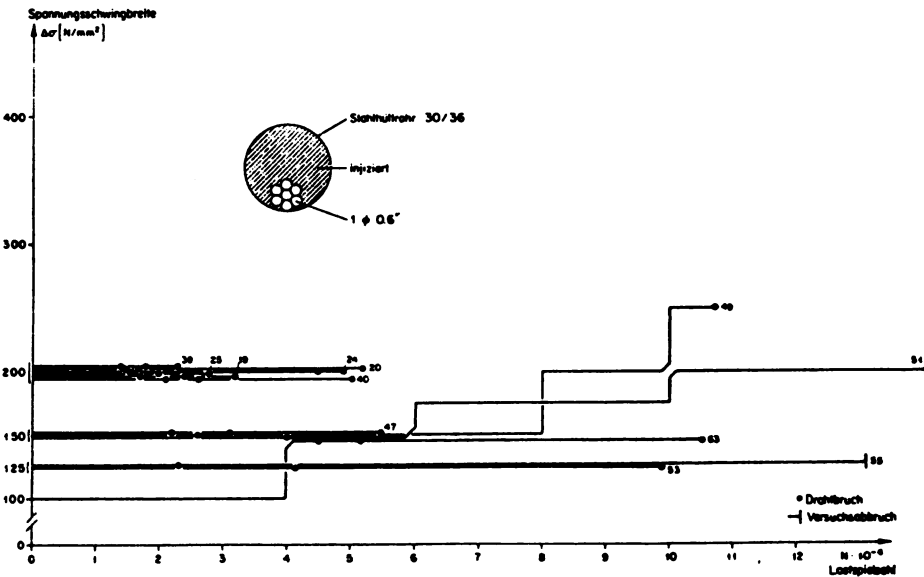


Bild 2: Kleinkörperversuche

Bei den Versuchen mit fünf Paralleldrähten ging es besonders darum, den Einfluss der Gruppenwirkung so gut als möglich zu beurteilen, um Basiswerte in bezug auf die Ermüdungsfestigkeit für die geplanten Balkenversuche erarbeiten zu können. Aus geometrischen und versuchstechnischen Gründen konnten Spannglieder aus mehr als fünf Einzeldrähten nicht geprüft werden.

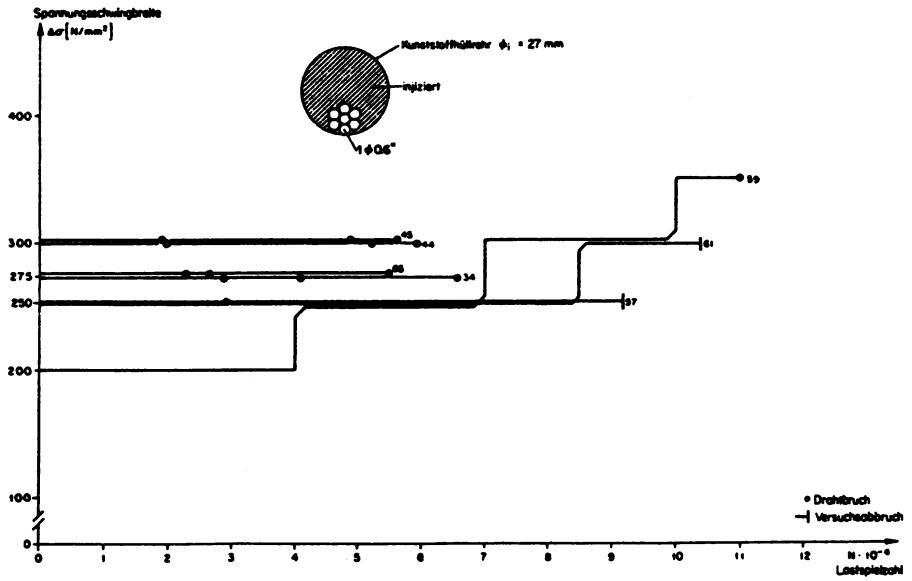


Bild 3: Kleinkörperversuche

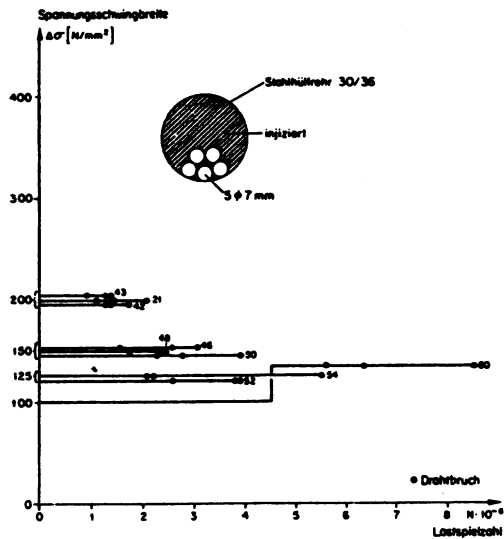


Bild 4: Kleinkörperversuche

Eine grössere Anzahl Versuche mit Stahlhüllrohr (Bild 4) sollte die Abschätzung der unteren Grenze der Ermüdungsfestigkeit erlauben. Die Ergebnisse der Versuche mit Kunststoffhüllrohr sind im Bild 5 dargestellt. Entsprechend den Versuchen mit Einzellitze ist auch hier im Vergleich zu den Versuchen mit Stahlhüllrohr mit der Verwendung eines Kunststoffhüllrohres eine wesentliche Erhöhung der Ermüdungsfestigkeit zu verzeichnen. Bei sämtlichen Versuchen war keine Kontaktstelle zwischen dem Spannglied und dem Kunststoffhüllrohr durchgerieben. Um die Phänomene beim Durchreibevorgang während des Vorspannens kennenzulernen, wurden im Anschluss an die Kleinkörperversuche entsprechende Durchreiberversuche durchgeführt [12].

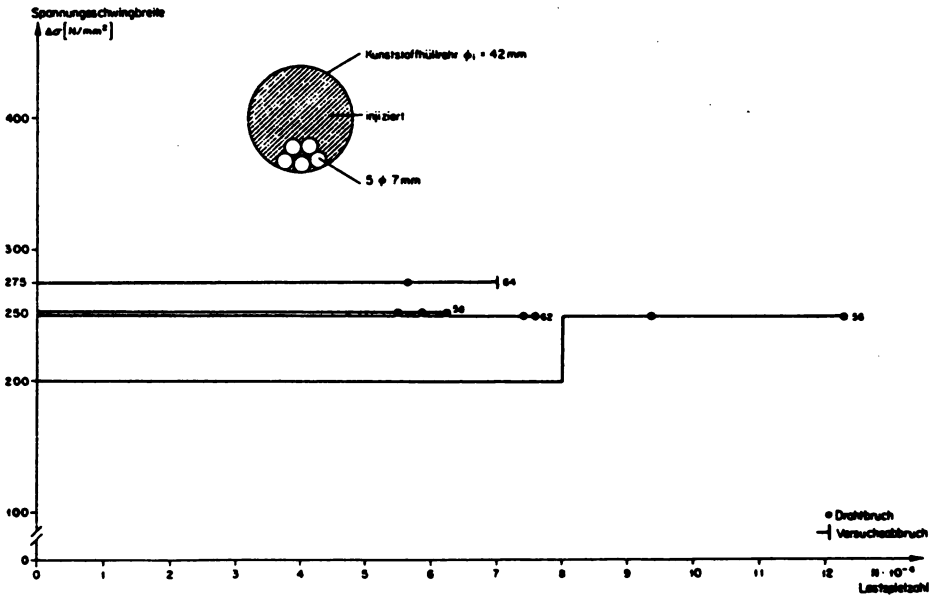


Bild 5: Kleinkörperversuche

### 5. Versuchsdurchführung an Balken

Da die Resultate der neuen Balkenversuche mit denjenigen aus [2] vergleichbar sein sollten, wurden die gleichen geometrischen Abmessungen und die gleiche Bewehrung gewählt. Bild 6 zeigt die Dimensionen und weitere Details der Bewehrung. Um örtliche Knickstellen in der Spanngliedführung zu verhindern, wurde das Hüllrohr in Abständen von 50 mm an ein Stützblech mit exaktem Krümmungsradius von  $r = 3500 \text{ mm}$  befestigt.

Die Belastungsanordnung für alle Balken ist im Bild 7 dargestellt. Der Balken war statisch bestimmt gelagert, und die äussere Belastung wurde über Stahlquerträger in den Balken eingeleitet. Die Kolbenkräfte wurden mit Kraftmessdosen kontrolliert. Um dynamische Einflüsse klein halten zu können, wurde die Belastungsfrequenz auf 5 Hz festgelegt. Zur Verhinderung eines sprungartigen Anstiegs des Spannungsniveaus und der Spannungsschwingbreite nach Drahtbrüchen im restlichen Querschnitt wurden die obere Kraftgrenze wegkontrolliert und die untere Kraftgrenze kraftkontrolliert gesteuert.

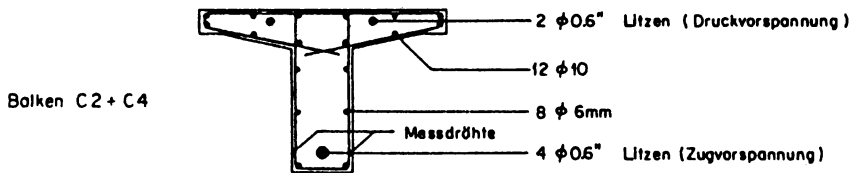
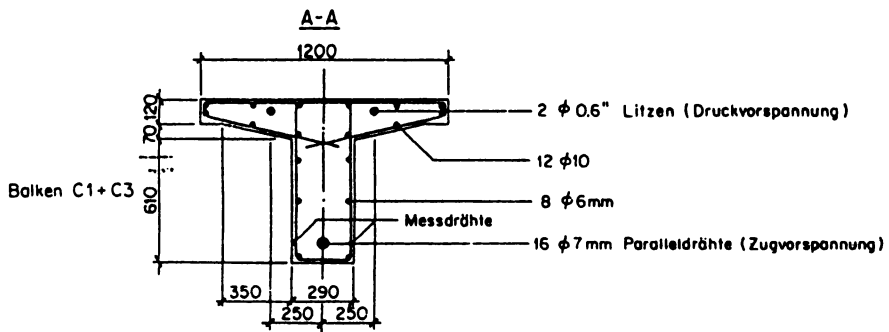
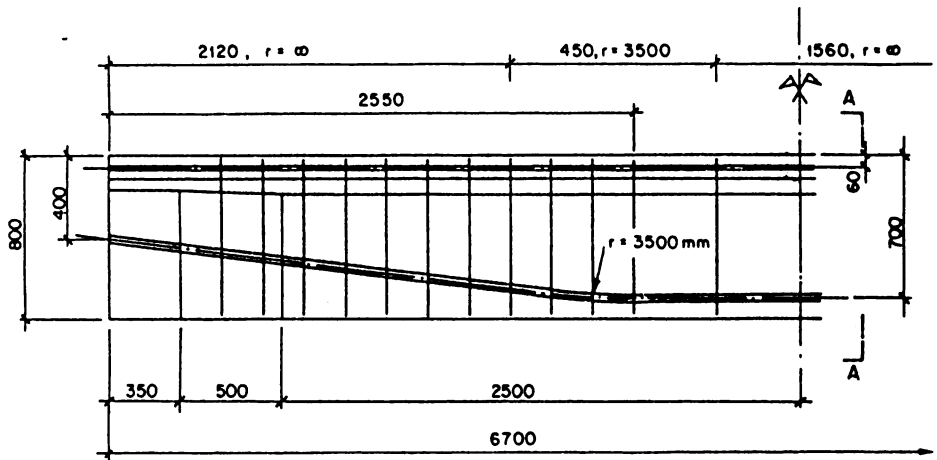


Bild 6: Balkenabmessungen, schlaffe Bewehrung, Vorspanndetails

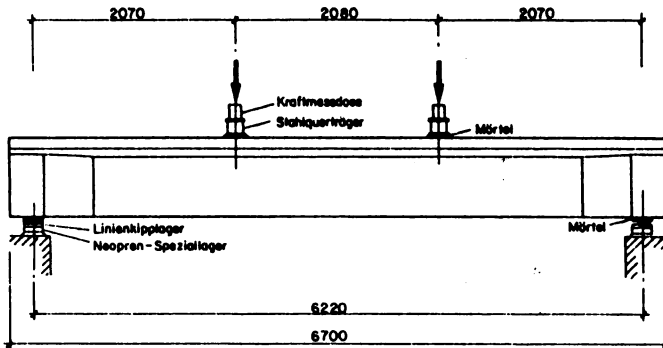


Bild 7: Balkenversuche; Belastungsanordnung

Die mit einem Personal Computer (PC) erfassten Werte der Dehnungsmessungen an der Betonoberfläche liessen es zu, die Lastspielzahl bei einem Drahtbruch nachträglich zu bestimmen. Die automatische Überwachung der Spitzenwerte erlaubte auch bei Litzenversuchen, Drahtbrüche örtlich festzulegen und deren Lastspielzahl bei Bruch anzugeben.

Im Balken C1 wurde in Trägermitte ein Trennblech eingebaut, um Zugspannungen im Beton zu vermeiden. Es zeigte sich, dass die totalen Vorspannverluste infolge von Reibung, Schwinden, Kriechen und Relaxation etwa 15% betragen. Mit der Höhe des gewählten Vorspanniveaus und der Grösse der gewählten Spannungsschwingbreite ergaben sich stets Belastungen, die über dem Dekompressionsniveau lagen. Damit konnte der Einfluss einer Ungenauigkeit in der Bestimmung des Vorspannverlustes auf die Berechnung der Spannungsschwingbreite praktisch vernachlässigbar klein gehalten werden [12]. Wird hingegen beim Schwingen das Dekompressionsniveau durchfahren [2], so wird die Spannungsschwingbreite sehr stark von diesem Niveau und damit von den meistens nur ungenau bekannten Vorspannverlusten abhängig.

## 6. Ergebnisse der Balkenversuche

Aus der Darstellung der Versuchsergebnisse in den Bildern 8 und 9 geht hervor, dass der erste Drahtbruch bei sämtlichen Versuchen erst während der zweiten oder dritten Laststufe erfolgte. Vergleicht man die Bruchlastspielzahlen mit den entsprechenden Werten der Kleinkörperversuche, so stellt man fest, dass die Versuchsergebnisse sowohl bei Verwendung von Stahl- als auch von Kunststoffhüllrohren gut übereinstimmen. Die in [11] in bezug auf Kleinkörper gemachten Aussagen, wonach im Ermüdungsverhalten einbetonierter Spannglieder aus Litzen oder parallelen Drähten keine ausgeprägten Unterschiede auftreten, bestätigten sich auch in den Balkenversuchen.

Wie bei den Kleinkörperversuchen mit injiziertem Kunststoffhüllrohr traten auch hier keine durchgeriebenen Stellen in der Hüllrohrwandung auf. Im weiteren fiel auf, dass beide Spannglieder mit Kunststoffhüllrohr am Spannstahl einen geringeren Abrieb an den Kontaktstellen aufwiesen als diejenigen mit Stahlhüllrohr. Beim Spannglied des Balkens C4 mit neuentwickeltem Kunststoffhüllrohr [12] waren auf der gesamten Länge des Kabels an der Oberfläche nur kleine Spuren von Reibrost sichtbar.

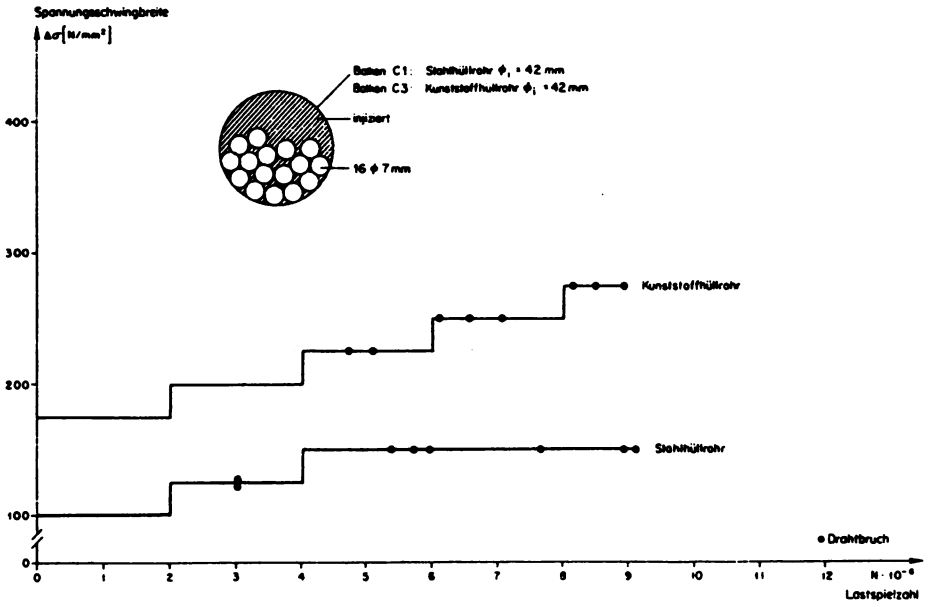


Bild 8: Balkenversuche

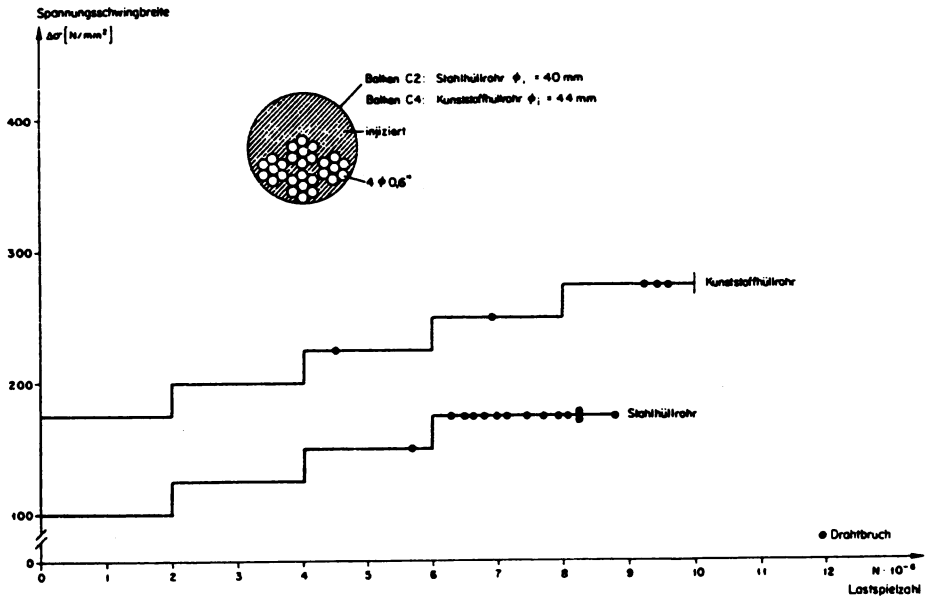


Bild 9: Balkenversuche

## Literatur

- [1] Warner R.F., Hulsbos C.L., "Probable Fatigue Life of Prestressed Concrete Beams", Journal of the Prestressed Concrete Institute, Vol. 11, No.2, 1966.
- [2] Rigon C., Thürlimann B., "Fatigue Tests on Post-Tensioned Concrete Beams", Institut für Baustatik und Konstruktion, ETH Zürich, Versuchsbericht Nr. 8101-1, August 1985, Birkhäuser Verlag Basel.
- [3] Müller H.H., "Abschlussbericht zum Forschungsvorhaben: Prüfverfahren für die Dauerschwingfestigkeit von Spannstählen", Technische Universität München, Institut für Bauingenieurwesen III, Nr. 1111, Mai 1985.
- [4] Cordes H., "Dauerhaftigkeit von Spanngliedern unter zyklischen Beanspruchungen", Rheinisch-Westfälische Technische Hochschule Aachen, Institut für Massivbau, Deutscher Ausschuss für Stahlbeton, Heft 370, Berlin 1986.
- [5] Frey R., Thürlimann B., "Ermüdungsversuche an Stahlbetonbalken mit und ohne Schubbewehrung", Institut für Baustatik und Konstruktion, ETH Zürich, Versuchsbericht Nr. 7801-1, September 1983, Birkhäuser Verlag Basel.
- [6] Fernandez-Canteli A., Esslinger V., Thürlimann B., "Ermüdungsfestigkeit von Bewehrungs- und Spannstählen", Institut für Baustatik und Konstruktion, ETH Zürich, Versuchsbericht Nr. 8002-1, 1984, Birkhäuser Verlag Basel.
- [7] Castillo E., Fernandez-Canteli A., Esslinger V., Thürlimann B., "Statistical Model for Fatigue Analysis of Wires, Strands and Cables", International Association for Bridge and Structural Engineering (IABSE), Zürich, IABSE Periodica 1, 1985.
- [8] Oertle J., Thürlimann B., Esslinger V., "Versuche zur Reibermüdung einbetonierter Spannkabel", Institut für Baustatik und Konstruktion, ETH Zürich, Versuchsbericht Nr. 8101-2, Oktober 1987, Birkhäuser Verlag Basel.
- [9] Waterhouse R.B., "Fretting Fatigue", Applied Publishers Ltd., London, 1981.
- [10] Kreitner L., "Die Auswirkung von Reibkorrosion und von Reibdauerbeanspruchung auf die Dauerhaltbarkeit zusammengesetzter Maschinenteile", Technische Hochschule Darmstadt, Dissertation, 1976.
- [11] Oertle J., Thürlimann B., "Reibermüdung einbetonierter Spannkabel", Schweizer Ingenieur und Architekt 12, März 1987.
- [12] Oertle J., "Reibermüdung einbetonierter Spannkabel", Institut für Baustatik und Konstruktion, ETH Zürich, Dissertation (wird im Sommer 1988 veröffentlicht).

# ZWEI BEITRÄGE ZUR STABILITÄTSTHEORIE IM STAHLBAU

PIERRE DUBAS

BAUSTATIK UND STAHLBAU  
EIDG. TECHNISCHE HOCHSCHULE ZÜRICH  
CH-8093 ZÜRICH, SCHWEIZ

## ZUSAMMENFASSUNG

Für die Bemessung von Stäben unter Druck und einachsiger Biegung werden oft Interaktionsformeln verwendet. Die Ergebnisse einiger dieser Formeln werden mit Resultaten verglichen, die mit der Fließzonenmethode 2. Ordnung gewonnen worden sind.

Im zweiten Teil des Aufsatzes werden Versuche an Blechträger vorgestellt, mit denen die Interaktion zwischen steifenloser Krafeinleitung und Gesamtbiegung untersucht worden ist.

## 1. BEMESSUNG VON STÄBEN UNTER DRUCK UND EINACHSIGER BIEGUNG

### 1.1 Einleitung

Bei Stäben unter Druck und einachsiger Biegung sind die Einflüsse 2. Ordnung zu berücksichtigen: die seitlichen Auslenkungen bedingen eine Vergrößerung der Exzentrizität der Druckkraft und somit eine Zunahme der Biegemomente.

Bei einer rein elastischen Betrachtung ist das Problem einfach zu lösen, hängt doch die Biegesteifigkeit  $EI$  nicht von der Höhe der Schnittkräfte ab. Wenn man die geometrischen Imperfektionen in der Form passend gewählter Anfangsauslenkungen einführt, liefert dieses Verfahren meistens auf der sicheren Seite liegende Ergebnisse. In Wirklichkeit kompensieren sich, mindestens teilweise, zwei gegenteilige Einflüsse: die Einführung eines idealelastischen-idealplastischen Materialverhaltens ist an sich zu optimistisch, weil dabei die Wirkung der Eigenspannungen auf die Biegesteifigkeit vernachlässigt wird; auf der anderen Seite wird die Grenzlast dem Erreichen der Fließgrenze am meistbeanspruchten Rand gleichgesetzt, d.h. die Querschnittsplastifizierungen werden vernachlässigt.



Will man diese plastischen Reserven mobilisieren, so ist der Einfluss der Höhe der Schnittkräfte und der Eigenspannungen auf die Biegesteifigkeit einzuschließen. In diesem Rahmen führt die Fließzonenmethode 2. Ordnung, wie sie im nächsten Abschnitt kurz erläutert wird, zur bestmöglichen Simulation der physikalischen Wirklichkeit. Für die Konstruktionspraxis ist dieses Verfahren allerdings zu aufwendig, so dass in der Regel mehr oder weniger genaue Interaktionsformeln zwischen der Normalkraft und dem Biegemoment verwendet werden. Die Ergebnisse der Fließzonenmethode 2. Ordnung sollen mit einigen solchen Interaktionsformeln verglichen werden.

### 1.2 Durchgeführte Untersuchungen mit der Fließzonenmethode 2. Ordnung

Gegenstand der in [1] veröffentlichten Untersuchungen ist ein beidseitig gelenkig gelagerter Stab unter Druck und einachsiger Biegung. Die Aussermittigkeit  $e$  ist an beiden Stabenden gleich gross, so dass die primären Momente  $N \cdot e$  über die Länge konstant verlaufen. **Biegedrillknicken ist ausgeschlossen.** Als Ergänzung wurde auch der Fall einer gleichmässig verteilten Querlast untersucht.

Für die bei der Anwendung der Fließzonenmethode 2. Ordnung benützten Grundlagen kann auf [2] hingewiesen werden. Zur Illustration zeigt Bild 1 Interaktionsdiagramme zwischen den Biegemomenten, bezogen auf das plastische Moment  $M_{pl}$  für die Biegung eines HEA 200 um die schwache Achse, und den relativen Biegesteifigkeiten  $T_B I / EI$ . Die Normalkraft, ebenfalls auf  $N_{pl}$  bezogen, erscheint als Parameter.

Die angenommenen Anfangsauslenkungen verlaufen sinusförmig, mit einer Ordinate von  $l/1000$  in Stabmitte. Die Computerberechnungen wurden inkrementell und mit Gleichgewichtsiterationen an Stäben verschiedener Schlankheit, alle mit dem Querschnitt HEA 200 durchgeführt. Als Materialkennwerte gelten eine Fließgrenze  $f_y = 235 \text{ N/mm}^2$  sowie ein E-Modul von  $210 \text{ kN/mm}^2$ .

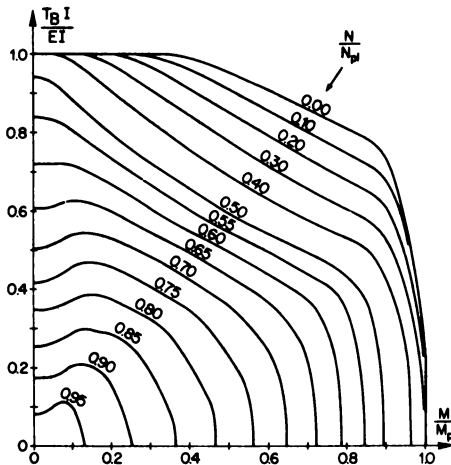


Bild 1 : Interaktionsdiagramme M-T<sub>B</sub> mit N als Parameter (HEA 200).

Da die Ergebnisse aller durchgeführten Berechnungen tabellarisch in [1] wiedergegeben sind, werden in Bild 2 die Resultate in graphischer Form als Interaktionsdiagramme zwischen der Traglast  $N$  und dem dazugehörigen Moment  $M$  bei der Erschöpfung der Tragfähigkeit dargestellt. Dabei ist das Moment  $M$  als  $N \cdot e$  definiert. Es handelt sich somit nicht um das tatsächlich vor-

kommende maximale Moment in Stabmitte, sondern um einen Bezugswert 1. Ordnung, wie er in den Interaktionsformeln benützt wird. Die Traglast  $N$  ist auf die Knicklast  $N_K$  des planmässig zentrisch gedrückten Stabes bezogen, die mit dem gleichen Programm ermittelt worden ist.

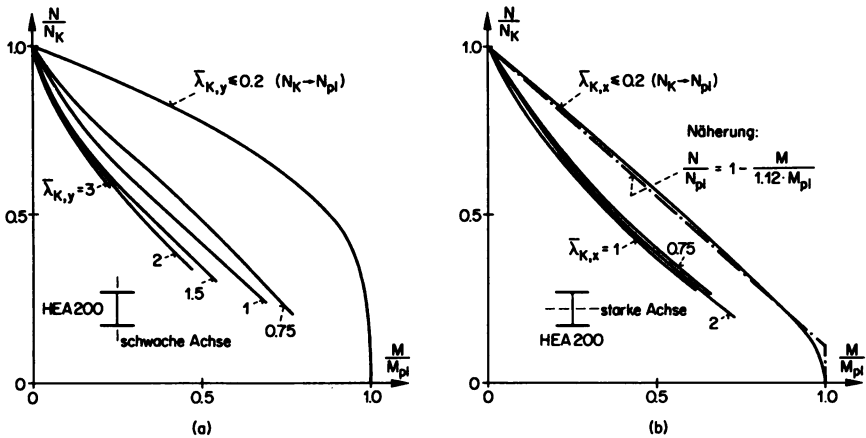


Bild 2a und b: Interaktionsdiagramme N-M für zweiseitig gelagerte, exzentrisch beanspruchte Stäbe aus HEA 200; Exzentrizität  $e = M/N = \text{konstant}$ .

Bild 2a bezieht sich auf die Biegung eines Profils HEA 200 um die schwache Achse, Bild 2b auf die Biegung des gleichen Querschnittes um die starke Achse. Als Parameter erscheint in beiden Fällen die bezogene Schlankheit  $\bar{\lambda}_{K,y}$  oder  $\bar{\lambda}_{K,x}$ . Gegenüber der ebenfalls dargestellten plastischen Interaktion für Stäbe mit verschwindender Schlankheit sind die N-M Kurven durch ihren konkaven Verlauf gekennzeichnet, der auf die Wirkung des Verformungseinflusses zurückzuführen ist.

Zudem ist ein deutlicher Unterschied zwischen der Biegung um die schwache Achse nach Bild 2a und derjenigen um die starke Achse nach Bild 2b festzustellen. Im ersten Fall übersteigt das Verhältnis des plastischen Momentes  $M_{pl}$  zum Fließmoment  $W \cdot f_y$  einen Wert von 1,5. Zudem verringert sich das plastische Moment kaum, solange die Normalkraft von der Steg- und Hohlkehlenfläche aufgenommen werden kann. Dieses günstige Verhalten im plastischen Bereich ist nur mittels einer beträchtlichen Spannungumlagerung möglich, die erst bei grösseren Dehnungen eintreten kann und somit eine erhebliche Verminderung der Biegesteifigkeit bewirkt. Besonders bei schlanken Stäben führt dies zu einer deutlichen Zunahme der Auslenkungen und somit der Einflüsse 2. Ordnung. Bei der Biegung um die starke Achse sind dagegen die plastischen Reserven kleiner, und die Spannungumlagerung spielt eine kleinere Rolle: für alle betrachteten Schlankheiten liegen hier die Interaktionskurven nahe beieinander.

### 1.3 Mögliche Interaktionsformeln

Im Entwurf 1983 zum EUROCODE 3 (Stahlbauten) wurde eine Interaktionsformel folgender Form aufgenommen (vgl. dazu [3])

$$\frac{N}{N_K} + \frac{1}{1 - (N/N_{cr})} \frac{M}{M_R} \leq 1 \quad \text{mit } N_K = \kappa_K \cdot N_{pl} \quad \text{und} \quad N_{cr} = \frac{N_{pl}}{\lambda_K^2} \quad (1)$$

Bild 3 zeigt die Ergebnisse entsprechender Vergleichsuntersuchungen, dargestellt in der Form

$N(\text{Interaktionsformel})/N(\text{FE-Berechnung})$

wobei  $N$  als "ertragbare" Last (Interaktionsformel genau erfüllt) bzw. als Traglast zu verstehen ist. Ein Verhältnis grösser als "1" bedeutet, dass die Interaktionsformel (1) zu hohe, auf der unsicheren Seite liegende Ergebnisse liefert. Im Bild sind für die Biegung um die schwache Achse folgende Varianten berücksichtigt:

- elastischer Nachweis nach Formel (1), mit  $M_R = W \cdot f_y$  (Fliessmoment)
- plastischer Nachweis nach Formel (1), mit  $M_R = M_{pl}$  (plastisches Moment)
- elastischer Nachweis mit  $M = 1,1 \cdot N \cdot e$
- plastischer Nachweis mit  $M = 1,1 \cdot N \cdot e$

Die Momentenverteilungszahl  $\omega = 1,1$  deckt näherungsweise den Unterschied zwischen dem Vergrösserungsfaktor 2. Ordnung  $1/(1-N/N_{Cr})$ , der für eine sinusförmige Verteilung der primären Momente gilt, und dem für konstante Momente einzusetzenden genaueren Faktor der Form  $(1+0,25 \cdot N/N_{Cr})/(1-N/N_{Cr})$ .

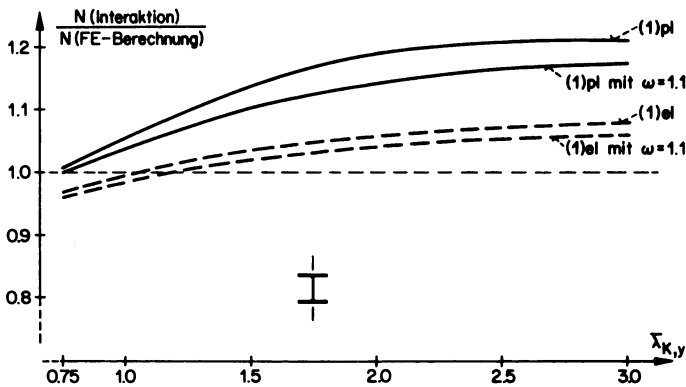


Bild 3 : Vergleich der Ergebnisse der Formel (1) mit den FE-Berechnungen, bei Biegung um die schwache Achse: maximale Abweichungen für die betrachteten Exzentrizitäten  $e$ .

Mit zunehmender Schlankheit liefern alle Varianten der Interaktionsformel (1) grössere, auf der unsicheren Seite liegende Abweichungen gegenüber den Ergebnissen der Fliesszonenmethode 2. Ordnung. Bei hohen Schlankheiten führt nur die letzte Variante, d.h. der elastische Nachweis mit  $\omega = 1,1$ , zu noch vertretbaren Fehlern in der Grössenordnung von 5%. Dieses Verfahren ist allerdings für gedrungene Stäbe konservativ.

Für die Biegung um die starke Achse liegen aus den vorher erwähnten Gründen günstigere Verhältnisse vor, so dass auf eine Wiedergabe des entsprechenden Bildes verzichtet werden kann.

Um die Ergebnisse der Interaktionsformel (1) zu verbessern, ist der Biege­widerstand  $M_R$  in Funktion der Schlankheit auszudrücken. Aufgrund umfangreicher Untersuchungen haben wir in [1] vorgeschlagen, folgenden Verlauf anzunehmen:

$$M_R = 1,12 \cdot M_{pl} \quad \text{für } \bar{\lambda}_K \leq 0,75$$

$$M_R = 1,12 \cdot M_{pl} - (1,12 \cdot M_{pl} - M_y)(\bar{\lambda}_K - 0,75)/1,25 \quad \text{für } 0,75 < \bar{\lambda}_K < 2,0 \quad (2)$$

$$M_R = M_y = W \cdot f_y \quad \text{für } \bar{\lambda}_K \geq 2,0$$

Gleichung (2) entspricht einer linearen Interpolation, im Schlankheitsbereich 0,75 bis 2,0, zwischen dem Wert  $1,12 \cdot M_{pl}$  und dem Flie遨moment  $M_y$ . Der Ausdruck  $1,12 \cdot M_{pl}$  wird in zahlreichen Vorschriften als Bezugsgrö遨e für die Interaktion zwischen Zug/Druck und Biegung 1. Ordnung von I-Querschnitten um die starke Achse verwendet. Es handelt sich dabei um eine linearisierte Näherung für die in Bild 2b gezeigte Interaktionskurve beim Grenzfall  $N_K \rightarrow N_{pl}$ . Für die Biegung um die schwache Achse liegt diese Annahme auf der sicheren Seite.

Bild 4 zeigt die extremen Abweichungen - für die betrachteten Exzentrizitäten  $e$  - zwischen den Resultaten der Interaktionsformel (1), ausgewertet mit den Werten  $M_R$  nach Gl. (2), und der Ergebnissen der FE-Berechnungen. Dabei wurde der Knickwiderstand  $N_K$  bzw. der Knickbeiwert  $\kappa_K$  mit dem gleichen Computerprogramm ermittelt; diese  $\kappa_K$ -Werte stimmen für die schwache Achse sehr gut mit denjenigen aus der europäischen Knickspannungskurve "c" überein, währenddem für die starke Achse die Kurve "b" zu kleine Werte liefert (sie entspricht dem Knicken eines Querschnittes PE 160 um die schwache Achse). Zudem wurde als Moment  $M$  der Ausdruck  $1,1 \cdot N \cdot e$ , d.h.  $\omega = 1,1$  eingeführt.

Das vorgeschlagene Verfahren führt zu einer befriedigenden Übereinstimmung der Interaktionsformel mit der genauen Lösung. Die Einführung eines von der Schlankheit abhängigen Biege widerstandes stellt allerdings eine gewisse Komplikation dar. Zudem verliert die Methode an Übersichtlichkeit.

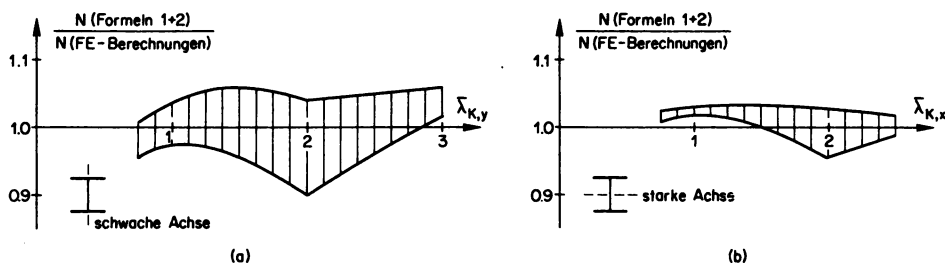


Bild 4: Vergleich der Ergebnisse der Formel (1), ausgewertet mit den Biege widerständen nach Gl. (2), mit den FE-Berechnungen: maximale und minimale Abweichungen für die betrachteten Exzentrizitäten  $e$ .

In neueren Entwürfen zum EUROCODE 3 (vgl. z.B. [4]) sowie in der Normvorlage zur DIN 18800, Teil 2, wurde versucht, durch Einschränkungen bei der Anwendung des plastischen Nachweises nach Formel (1) mit  $M_R = M_{pl}$ , zu hohe Abweichungen bei schlanken Stäben zu vermeiden. Wir wollen auf dieses Vorgehen nicht näher eingehen und auf die entsprechenden Bemerkungen in [1] hinweisen.

Im Rahmen der in Angriff genommenen Revision der Schweizer Norm SIA 161/1979 wurde folgende verblüffend genaue und zugleich einfache Näherung vorgeschlagen. Gegenüber Formel (1) wird im Nenner des Vergrößerungsfaktors die Korrektur  $N_K/N_{pl}$  weggelassen, zudem auch bei konstanten Momenten  $\omega$  zu 1,0 gesetzt, und die Interaktion somit in folgender Form geschrieben, die im ganzen Schlankheitsbereich gültig ist:

schwache Achse 
$$\frac{N}{N_K} + \frac{1}{1 - N/N_{cr}} \frac{N \cdot e}{M_{pl}} \leq 1 \quad (3a)$$

mit 
$$N_{cr} = \frac{N_{pl}}{\bar{\lambda}_K^2}$$

starke Achse 
$$\frac{N}{N_K} + \frac{1}{1 - N/N_{cr}} \frac{N \cdot e}{1,12 \cdot M_{pl}} \leq 1 \quad (3b)$$

Bild 5 zeigt den Vergleich der Ergebnisse dieser Formel mit den Resultaten der FE-Berechnungen. Grenzverhältnisse höher als 1,0 bedeuten auch hier, dass das Näherungsverfahren Ergebnisse auf der unsicheren Seite liefert. Es handelt sich aber um wenige Procente, wobei für die schwache Achse die Abweichungen kleiner sind als nach Bild 4a. Zudem ist zu berücksichtigen, dass bei einer Beanspruchung auf Druck mit Biegung alle Variablen, d.h. N und e auf der Lastseite, sowie die Grenzmomente  $M_{pl}$  auf der Widerstandsseite gleichzeitig ihren Extremwert annehmen müssen. Weiterhin ist stillschweigend vorausgesetzt, dass die anfängliche Auslenkung und die Aussermittigkeit e sich immer addieren. Durch diese Annahmen ergibt sich eine kleinere Auftretenswahrscheinlichkeit für die Erschöpfung des Tragwiderstandes als beim gelenkig gelagerten Knickstab.

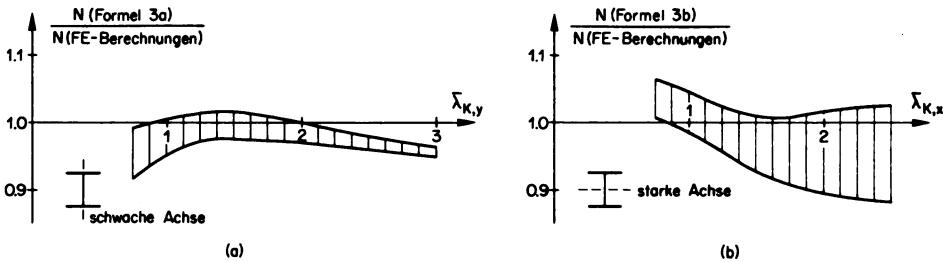


Bild 5: Vergleich der Ergebnisse der Formeln (3a) und (3b) mit den FE-Berechnungen: maximale und minimale Abweichungen für die betrachteten Exzentrizitäten e .

Für die Bemessung führen die unten aufgeführten Formeln zu einer direkten Lösung.

- Exzentrizität e bekannt, gesucht die "ertragbare" Normalkraft N :

$$\frac{N}{N_K} = \beta - \sqrt{\beta^2 - \frac{1}{\kappa_K \cdot \bar{\lambda}_K^2}} \quad \text{mit} \quad \beta = \frac{1}{2 \cdot \bar{\lambda}_K^2} \left( \frac{N_K \cdot e}{\kappa_K \cdot M_R} + \frac{\bar{\lambda}_K^2}{\kappa_K} + \frac{1}{\kappa_K} \right) \quad \text{und} \quad \kappa_K = \frac{N_K}{N_{pl}} = \frac{\sigma_K}{f_y} \quad (4)$$

- N bekannt, zugehöriges Moment M bzw. Exzentrizität e = M/N gesucht:

$$\frac{M}{M_R} = \left( 1 - \frac{N}{N_K} \right) \left( 1 - \frac{N}{N_K} \kappa_K \bar{\lambda}_K^2 \right) \quad (5)$$

Dabei ist für die schwache Achse  $M_R = M_{pl}$ , für die starke Achse  $M_R = 1,12 \cdot M_{pl}$  einzusetzen.

Schliesslich soll erwähnt werden, dass der Formelaufbau der Gleichung (3) dem bekannten PERRY-ROBERTSON-Typ entspricht. Ähnliche Interaktionsformeln werden seit längerer Zeit hauptsächlich in Nordamerika verwendet (vgl. z.B. [5]).

## 2. INTERAKTION ZWISCHEN EINZELLASTEN UND GESAMTBIEGUNG BEI DÜNNWANDIGEN BLECHTRÄGERN

### 2.1 Problemstellung

In zahlreichen Fällen sind grössere Druckkräfte steifenlos in den Steg eines dünnwandigen Blechträgers einzuführen. Falls in der gleichen Zone hohe Biegebeanspruchungen auftreten, ist deren Einfluss auf den Grenzwiderstand für die rippenlose Krafteinleitung zu berücksichtigen. Als Beispiel für eine solche Interaktion können die Verhältnisse über dem massgebenden Pfeiler beim Längseinschieben einer Vollwandbrücke erwähnt werden: hier treten gleichzeitig hohe Auflagerdrücke und Biegemomente auf, die in der Nähe des Biegeverbandes liegen. Ähnliche Bedingungen sind bei Kranbahnträgern anzutreffen, allerdings mit dem wesentlichen Unterschied, dass hier wegen der zahlreichen Lastwechsel der Ermüdungsnachweis massgebend ist. Die Ergebnisse der anschliessend beschriebenen Versuche, bei denen schon vor dem Erreichen des Tragwiderstandes grössere Plastifizierungen und bleibende Verformungen zu beobachten waren, dürfen daher bei Kranbahnträgern oder anderen einer wiederholten Krafteinleitung ausgesetzten Elementen nicht verwendet werden.

### 2.2 Durchgeführte Versuche

Am Institut für Baustatik und Stahlbau der Eidg. Techn. Hochschule Zürich sind Interaktionsversuche durchgeführt worden. Zudem wird das Problem mit Hilfe der FE-Methode untersucht. Anschliessend sollen die Ergebnisse der experimentellen Forschung kurz vorgestellt werden.

Bild 6 zeigt die Hauptabmessungen der ersten drei Träger sowie die Belastungsanordnung. Die zwei etwa im Drittel der Spannweite wirkenden Lasten werden mit Quersteifen eingeleitet und bestimmen, zugleich mit der zentralen Kraft  $F$ , die Höhe der Biegemomente. Für jeden Träger wurden folgende sechs Tragversuche durchgeführt:

- Interaktion einer Einzellast  $F$  in Trägermitte mit hohen Biegemomenten, wobei für jeden der drei Träger eine andere Kombination gewählt wurde.
- Bestimmung des Biegeverbandes, ohne Kraft  $F$ . Zu diesem Zwecke wurde der Träger umgedreht, so dass der im ersten Versuch als Druckgurt wirkende Flansch dann auf Zug beansprucht war. Die eingetretenen plastischen Verformungen wirkten sich daher nicht nachteilig aus. Auf alle Fälle wurde bei allen Versuchen der Biegeverband durch das Fließen des Druckgutes, gefolgt von örtlichen Kipp- oder Beulverformungen, eingeleitet.
- Vier Versuche für die Endfelder des Trägers. Die hier vorkommenden Biegemomente (Spannweite 1800 mm) sind so klein, dass die Traglast den Grenzwiderstand  $F_U$  für die rippenlose Krafteinleitung ohne Gesamtbiegung darstellt.

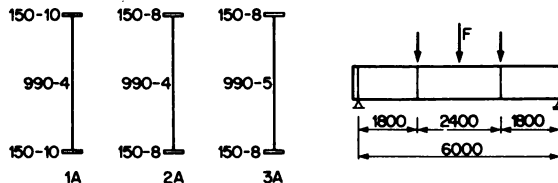


Bild 6: Trägerquerschnitte und Versuchsanordnung für die Untersuchung der Interaktion zwischen Querlast und Hauptbiegung.

Für die Hauptversuche sind ähnliche Querschnitte gewählt worden. Die Abmessungen sind in der Tabelle 1 zusammengefasst.

Träger	VT1	VT2	VT3	VT4	VT5	VT6
Steg	1000·4	1000·4	1000·5	1000·5	800·5	800·5
Flansche	150·8	100·12	150·12	150·12	150·8	150·12

Tabelle 1: Querschnitte der Versuchsträger VT1 - VT6.

Die Stegslankheit variiert somit zwischen 160 und 250 und ist für die heute in der Schweiz gebauten Vollwandträger ohne Längssteifen repräsentativ. Zudem wurden vier längsversteifte Träger untersucht, auf die hier nicht eingegangen wird.

Gegenüber Bild 6 sind die Längsabmessungen leicht geändert und betragen jetzt 1760+2480+1760 mm. Zudem wurde der Biege widerstand  $M_U$  nicht für jeden Versuchsträger bestimmt, so dass mehr Interaktionspunkte gewonnen werden konnten. Der Wert  $M_U$  wurde dann rechnerisch ermittelt, wobei die zahlreichen durchgeführten Biegeversuche eine Kalibrierung des Berechnungsverfahrens erlaubten. Für diese Versuche kann zudem auf [6] hingewiesen werden. In dieser Veröffentlichung sind einige experimentelle Ergebnisse mit verschiedenen Bemessungsverfahren verglichen.

Die gemessenen Versuchswerte  $F_U$  für die rippenlose Krafteinleitung bei vernachlässigbarer Gesamtbiegung zeigen zudem, dass die untenstehende in der Schweizer Norm SIA 161/1979 angegebene Formel (43) auf der sicheren Seite liegende Ergebnisse liefert

$$F_u = 0,5 \cdot t_w^2 \cdot f_y \sqrt{\frac{E \cdot t_f}{f_y \cdot t_w}} \cdot \text{Korrekturbeiwerte} \quad (6)$$

mit  $t_w$  = Stegstärke und  $t_f$  = Flanschdicke.

Im Durchschnitt beträgt der experimentell bestimmte Faktor rund 0,65 statt 0,5. Je nach Träger erreicht die Fließgrenze des Steges Werte  $f_{y,w}$  zwischen 290 und 360 N/mm<sup>2</sup>, während für die Flansche die Streckgrenzwerte  $f_{y,f}$  zwischen 275 und 325 N/mm<sup>2</sup> variieren.

Bei den reinen Krüppelversuchen, praktisch ohne Hauptbiegung, ist die Höhe der sich unmittelbar unterhalb des Druckflansches bildenden Beule klein und übersteigt für die vorliegenden Versuchsträger kaum 50 mm. Gleichzeitig wirkende Biegemomente, genauer gesagt die dazugehörigen Längsdruckspannungen im oberen Stegbereich führen zu einer deutlichen Vergrößerung der Beulabmessungen und zu einer entsprechenden Reduktion des Tragwiderstandes  $F$  gegenüber  $F_U$ . Es wurde bereits in [7] darauf hingewiesen, dass bei einer rippenlosen Krafteinleitung der obere Stegbereich - zusammen mit dem Flansch - als eine Art Verteilungsträger wirkt, so dass weiter unten nur mässige vertikale Druckspannungen auftreten. Man kann sich vorstellen, dass diese Wirkung durch die gleichzeitig wirkenden Biegedruckspannungen beeinträchtigt ist.

### 2.3 Interaktionsdiagramm

Die Hauptergebnisse der durchgeführten Versuche sind in Bild 7 graphisch zusammengefasst. Es handelt sich um die Beziehung zwischen dem Tragwiderstand  $F$  im Interaktionsfall, bezogen auf den jeweiligen Mittelwert  $F_U$  der Versuche mit vernachlässigbarer Biegung, und dem gleichzeitig wirkenden Biegemoment  $M$  in Trägermitte, bezogen auf den Biegewiderstand  $M_U$  bei einer Lasteinleitung über Quersteifen nach Bild 6.

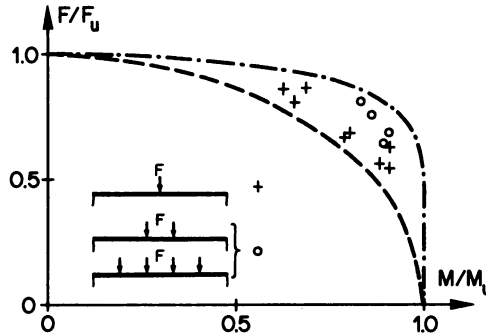


Bild 7: Interaktionsdiagramm zwischen der rippenlos eingeleiteten Querlast  $F$  und dem Biegemoment  $M$  im gleichen Querschnitt.

Die mit einem Kreuz bezeichneten Werte gelten für eine Kräfteinleitung durch eine Einzellast, mit einer Lastangriffslänge von 40 mm. Bei den mit einem Punkt dargestellten Versuchen wurden zwei Lasten (Lastangriffslänge jeweils 40 mm, Zwischenlänge 200 mm) oder vier Lasten (Lastangriffslänge jeweils 40 mm, Zwischenlängen jeweils 200 mm) eingeführt. Diese Versuchsordnung entspricht der beim Einschleiben von Brücken anzutreffenden Belastung durch Rollenbatterien. Durch diese mehrfache Belastung erniedrigt sich die Grösse des Tragwiderstandes  $F$  oder  $F_U$  pro Lastpunkt, während die Gesamtlast selbstverständlich höher ist. Die vorher erwähnte Wirkung des oberen Trägerteils als Verteilbalken erklärt qualitativ diesen Tatbestand.

Bild 7 zeigt, dass die Interaktion nicht sehr ausgeprägt ist, besonders wenn mehrere Lasten  $F$  gleichzeitig wirken. Alle Ergebnisse liegen zudem zwischen den in Bild wiedergegebenen Interaktionskurven. Die obere wurde in [8] aufgrund einer beschränkten Anzahl von Versuchswerten vorgeschlagen und entspricht der Gleichung

$$\frac{F}{F_U} = \left[ 1 - \left( \frac{M}{M_U} \right)^2 \right]^{1/8} \quad (7)$$

Die untere wurde unter anderem von ROBERTS [9] eingeführt

$$\frac{F}{F_U} = \left[ 1 - \left( \frac{M}{M_U} \right)^2 \right]^{1/2} \quad (8)$$



Diese Formel (8) kann aus einer verallgemeinerten von KÄRMÄNSchen Beziehung der Form (vgl. [10])

$$F_u = \sqrt{F_{cr} \cdot F_y} \quad (9)$$

abgeleitet werden. Dabei nimmt man an, dass die Quetschlast  $F_y$  linear vom Flanschbiegewiderstand  $M_{pl,f}$  abhängt. Dieses plastische Flanschmodent, das für die örtliche Verteilung der Einzellast  $F$  mobilisiert wird, ist durch die Flanschnormalkraft aus dem Biegemoment des Trägers im Rahmen der plastischen Interaktion zwischen einem Biegemoment und einer Normalkraft für den rechteckigen Flanschquerschnitt im Verhältnis  $1 - (N/N_{pl})^2$  abzumindern.

Schliesslich soll ausdrücklich festgehalten werden, dass bei den Versuchen eine Verdrehung des Druckflansches im Kräfteeinleitungsbereich durch die Biegesteifigkeit der Pressekolben praktisch behindert war. In dieser Zone war der Steg somit eingespannt. In den meisten Anwendungen ist eine solche Drehbehinderung durch die Art der Kräfteeinleitung - z.B. durch breite Rollen bei Batterien für das Längseinschieben von Brücken - ebenfalls gewährleistet. Für eine gelenkige Kräfteeinleitung, d.h. wenn sich der Flansch und der daran geschweisste Steg im Bereich der Kräfteeinleitung frei verdrehen können, ergeben sich deutlich geringere Tragwiderstände  $F_u$ , die durch die üblichen Bemessungsformeln nicht mehr abgedeckt werden.

#### LITERATURANGABEN

1. DUBAS, P. - 'Bemerkungen zur Bemessung von Stäben unter Druck mit Biegung'. Publ. Nr. 86-1, Baustatik und Stahlbau, ETH Höngerberg, 1986.
2. DUBAS, P. - 'Tragwiderstand von Stäben und Stabsystemen unter Druck und Biegung'. Schweiz. Ing. und Arch., 1979, 9Z, 609-615.
3. ECCS (Europ. Convention for Constr. Steelwork) - Second Intern. Coll. on Stability, Introductory Report, ECCS, Brussels, 1977, 209-227.
4. EUROCODE 3, Entwurf Sept. 1985. RWTH Aachen, Stahlbau (Prof. Sedlacek).
5. Canadian Standards Association - Steel Structures for Buildings (Limit States Design). CAN3-S16.1-M84, Toronto, 1984, 57-59.
6. DUBAS, P. - 'Limit State Design of Plate Girders', Steel Structures - Advances, Design and Construction, Ed. Narayanan, R., Elsevier Applied Science, 1987, 98-107.
7. DUBAS, P. - 'Some Remarks on the Post-Critical Behaviour of Plated Structures', Steel Structures, Recent Research Advances and their Applications to Design, Ed. Pavlović, M.N., Elsevier Applied Science Publ., 1986, 247-263.
8. BERGFELT, A. - 'Studies and Tests on Slender Plate Girders without Stiffeners - Shear Strength and Local Web Crippling', IABSE Reports of the Working Commissions, Vol. 11, Zurich 1971, 67-83.
9. ROBERTS, T.M. - 'Slender Plate Girders Subjected to Edge Loading', Proc. Inst. Civ. Engrs (Part 2), 1981, 71, 805-819.
10. ECCS - Technical Working Group 8.3 - Behaviour and Design of Steel Plated Structures, Ed. Dubas, P. and Gehri, E., ECCS n<sup>o</sup> 44, Brussels 1986, 121-126.

## LOCAL DAMAGE EFFECTS IN CYLINDERS STIFFENED BY RINGS AND STRINGERS

B.F. Ronalds and P.J. Dowling

Department of Civil Engineering, Imperial College of Science and Technology  
London, SW7 2BU, U.K.

### SYNOPSIS

Analytical techniques are outlined which have been developed to complement damage tests on orthogonally stiffened cylindrical shells. The extent of damage caused by characteristic quantities of kinetic energy in an accidental impact, and its effect on the strength of orthogonally stiffened shells under compressive loading, are both addressed.

Experimentally, lateral loading was applied across the stringers through a wedge-shaped indenter. A mechanism approach is used to model the damage development, including the deepening of the dent centre and its spread along the member length. The equations demonstrate the influence of heavier stringers and rings at closer spacing in reducing the damage. The residual compressive strength may be simply estimated by neglecting the damaged material. The results are related to the likely intact capacity of shells with imperfections satisfying recommended tolerances.

### NOTATION

$A_t$	cross sectional area of cylinder
$b$	stringer spacing = $\alpha R$
$ecc$	eccentricity of axial load application from cylinder centre
$j$	stringer number
$n$	nondimensionalized membrane force in stringer beam = $N/N_p$
$N_{P_t}$	cylinder squash force = $\sigma_Y A_t$
$P_{Am}$	compressive load capacity of damaged cylinder
$s$	number of stringers around circumference
$s_D$	number of stringers in dent
$t$	shell thickness
$\alpha$	angle between adjacent stringers = $2\pi/s$
$\sigma_m$	compressive strength of intact shell
$\sigma_Y$	yield stress (tensile or compressive)
$\varphi$	angle to stringer $j$ from dent centre = $j\alpha$
$\varphi_c$	angle to edge of dent at cross section under load
$\varphi_r$	angle to edge of dent at ring frame cross section

## INTRODUCTION

The Department of Energy and the Science and Engineering Research Council have jointly sponsored several projects investigating the consequences of local damage in stiffened cylindrical shells. This paper describes results from part of that programme of research, involving tests on orthogonally stiffened cylinders. The models were in the slenderness range  $190 < R/t < 267$ , the upper value being limited economically by the size of fabrication apparatus and existing testing rigs. The shells had twenty or forty longitudinal stiffeners (stringers) and were either one or three bays in length. The model numbers and other dimensions are given in Table 2.

As in other experimental programmes [1,2] the shells were damaged through a wedge-shaped indenter aligned parallel to the rings. The lateral load was applied slowly, avoiding any dynamic effects. Inertia forces may be neglected in modelling collisions when the duration of impact is much greater than the period of vibration of the structure [3]. De Oliveira [4] and Jones [5] have demonstrated this to be true for components of typical offshore structures. However strain rate effects might be of some importance in impacts, by elevating the yield stress and reducing the fracture strain [3].

The residual strength in the presence of the dent was determined by compression tests. Analyses have been developed for both denting and compression aspects of the testwork and these are outlined in the following sections.

## DENTING ANALYSIS

The dent formation during lateral loading has been modelled by simplifying the stiffened shell to a series of longitudinal beams carried by ring frames. Each longitudinal beam is treated as a plastic mechanism with several modes of response. These modes are illustrated in Fig. 1, with a line of symmetry assumed at the load application point. The load is supported by reactions at the ring frames and is transferred there by bending moment and membrane force in the beam. The tension is generated by the beam stretching to accommodate lateral deflection.

In the first mechanism mode the deflections are contained by the two nearest rings; the dent thus deepens and widens but does not spread longitudinally in this phase. When the load is large enough these two rings begin to deflect and the dent grows in length to extend over three bays. The hogging plastic hinge  $M_h$  moves to the new boundary and the moment  $M_r$  at the intermediate ring unloads elastically as the ring deflects. Because the mechanism rotates only at the centre and ends the ring deflects at two-thirds of the rate of the central deflection. For the three bay dents tested in this programme the next phase of behaviour (mode 3) occurs when  $M_r$  becomes a sagging plastic hinge  $-M_s$ . The entire central bay is then a sagging hinge and its inclination to the horizontal remains constant throughout further loading.

If the beam had more than three bays mode 2 might be terminated by either of two occurrences. One possibility is a sagging hinge at the inner ring, mentioned above, and the other is the collapse of the next ring frame (mode 2a). Both modes 3 and 2a are likely to be followed by mode 3a where  $M_r = -M_s$  and two ring frames are deflecting. The configurations of further modes depend on the failure of additional rings and the formation of sagging hinges at their locations.

Equations describing the shapes of the mechanisms and the values of forces and moments as the dent develops are given in Ref. [6]. Because of the importance of membrane effects in these tests an estimate of the lateral load relationship with deflection may be made very simply by putting the tension force  $N$  at yield. The resulting equations are linear and are listed in Table 1.

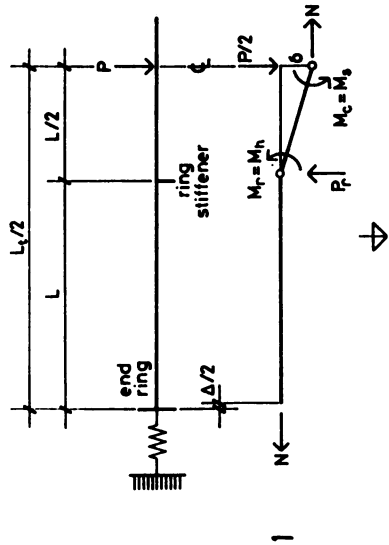
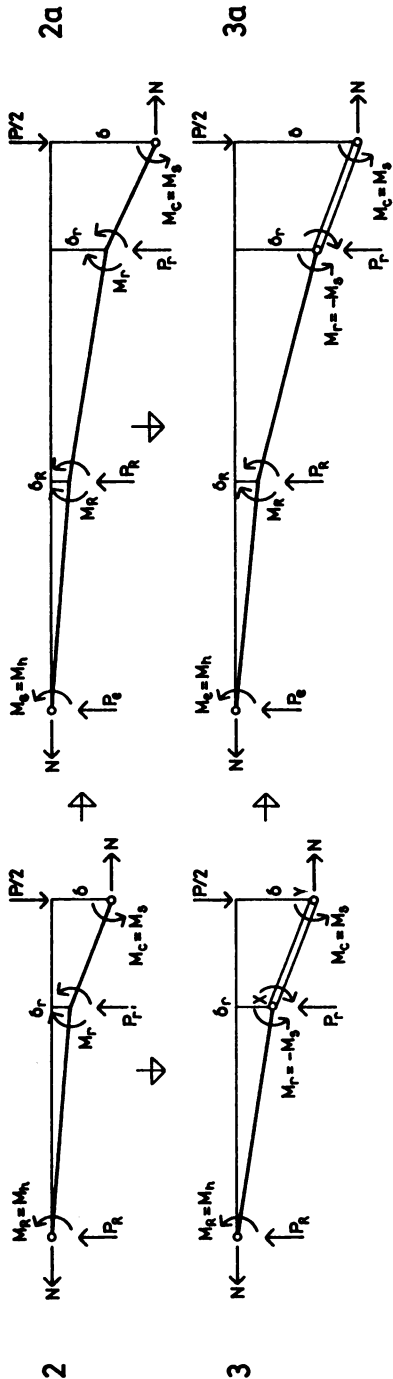


Fig. 1 Beam mechanism modes during denting

31



MODE	DEFLECTION RANGE	RING DEFLECTIONS	MEMBRANE SOLUTION
1	$\delta < \delta'$	$\delta_r = 0$	$\frac{P}{N_P} = 4\frac{\delta}{L}$
2	$\delta' < \delta < \delta''$	$\delta_r = \frac{2}{3}(\delta - \delta')$	$\frac{P}{N_P} = 4\left[\frac{\delta}{L} + 2\frac{\delta''}{L}\right]$
3	$\delta > \delta''$	$\delta_r = \delta - \delta'' + \delta_r'$	$\frac{P}{N_P} = 4\left[\frac{\delta''}{L} - \frac{\delta_r'}{L}\right]$

Table 1 Denting mechanism modes for three bay dent

The behaviour of the entire shell is the sum of the individual beam responses. Results for one of the three bay models tested are given in Figs. 2 to 4. The shell was sparsely stiffened, having only twenty stringers and a resulting panel slenderness of  $b/t = 84$ . Thus two types of longitudinal beam element were chosen. The stringers were assumed to act with an effective width of shell giving  $b_e/t = 30$ . Between the stringer beams the shell was considered to be made up of thin rectangular strips. The response is insensitive to the exact width of stringer beam and so the  $b_e$  value chosen is not important.

Relationships between the ring deflection and the central deflection are given in Fig. 3 showing the various modes of behaviour. Positions in line with stringer beam 0 at  $\varphi = 0$  and stringer 1 ( $\varphi = \alpha$ ) are plotted, where  $\varphi$  is the angle from the longitudinal dent centre-line. Fig. 2 shows the membrane force in the stringer beams, nondimensionalized with respect to the yield force. The theoretical curves are plotted for particular values of  $\gamma$ . This is a measure of the restraint against longitudinal pull-in provided at the ends of the mechanism [6] and is represented by a spring in Fig. 1. A value  $\gamma = 0.5$  means that the total stiffness at the supports is equal to the axial stiffness of the beam.

The experimental damage load response of the shell is compared with two theoretical curves in Fig. 4. The thicker line takes account of the gradual build up of membrane tension in the dented beams and its effect on the moment capacity of the plastic hinges. The membrane solution, combining the simple equations in Table 1, is marked in a thinner broken line.

If the test models had been more than three bays in length the damage would have extended axially as successive ring frames deflected. The predicted shape of the dent zone in a longer forty stringer shell with the geometry of Cylinder 3B2 is illustrated in Fig. 5. This is compared with the idealized deflections of the actual three bay model. Although the central cross section under the indenter is flat, the light ring frames assume a curved shape as dictated by the deforming stringer beams.

Fig. 5 indicates that the curve of the ring frames extends beyond the longitudinal edge of the dent zone. At the end of the denting tests, when the lateral load was removed, residual outward deflections of up to  $\delta/t = 3.7$  were measured in this "undamaged" material. The bulge was localized and typically the deflections became very slightly inward within an angle of about  $3\pi/20$  from the dent edge [7].

## COMPRESSIVE STRESSES ADJACENT TO DENT

The damage spreads circumferentially as it deepens and Fig. 2 shows that membrane tension forces begin to develop in each stringer when the dent edge reaches it. The tension in the dent pulls in the adjacent ring frames and so longitudinal compressive stresses are induced in the undamaged material further around the dent. The axial

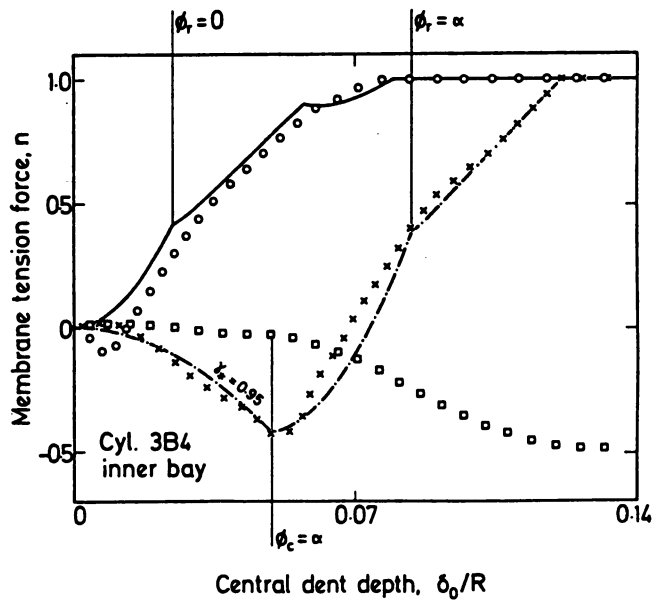
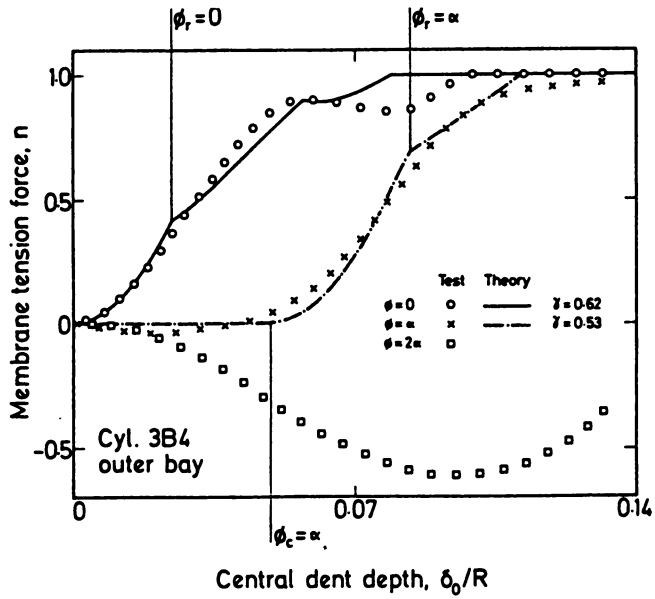


Fig. 2 Longitudinal membrane forces in dent zone

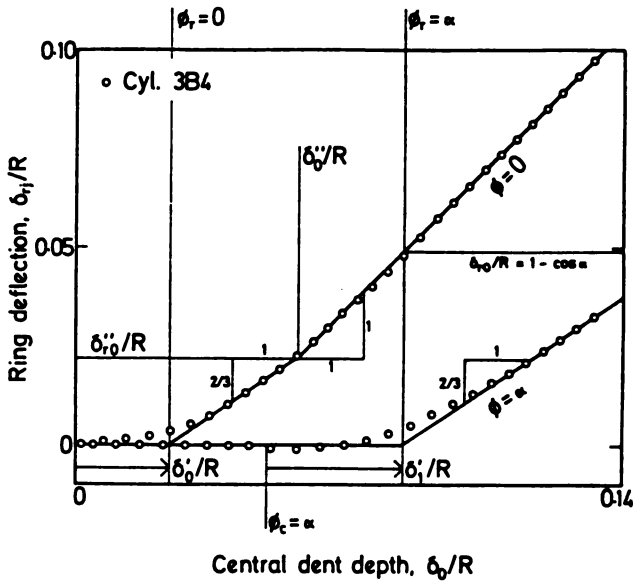


Fig. 3 Lateral deflections of ring frame

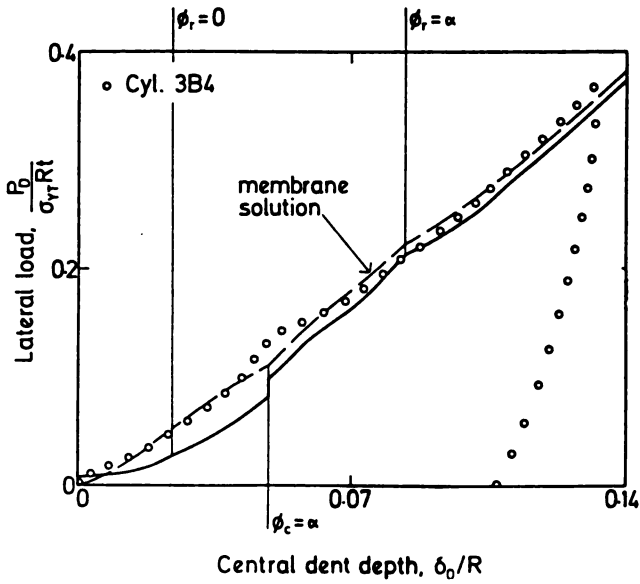


Fig. 4 Lateral loading response of shell

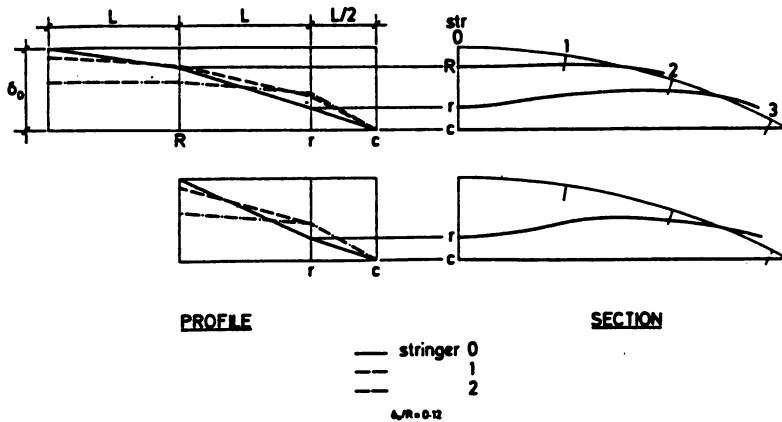


Fig. 5 Computed geometry of dent

rigidity of the undamaged material restrains the inward movement of the rings and thus allows the membrane tension to develop. When the stringers are attached to sturdy rings compressive stresses develop from the beginning of the denting process [8] because the rings pull in relatively uniformly. However the light intermediate rings in the series 3B models could distort locally and so the development of compressive stresses beyond the dent was delayed in the inner bay until material immediately adjacent began to deflect laterally and pull in (Fig. 2(b)).

The compressive stresses grow parabolically with dent depth [8], in the form

$$n_j = -2 \frac{E}{\sigma_Y} (1 - \gamma_x) \left[ \frac{\delta_j}{L} - 1 \right]^2 \quad (1)$$

This relationship is drawn in Fig. 2(b) using a best fit value of  $\gamma_x = 0.95$ . The  $\gamma_x$  values used in Eqn.(1) are always close to unity. For axially stiff supports the amount of pull-in is small and thus the compressive stresses develop gradually. Axially flexible supports cause the tension to develop very slowly and thus little equilibrating compression is generated. This is achieved by the ends pulling in nonuniformly, with larger movement near the centre of the dent and little beyond. The insertion of a small  $\gamma_x$  value in Eqn.(1) would predict the rapid attainment of compressive yield which would not occur in practice.

In Fig. 2 the growth of compressive stresses is seen to diminish at higher dent depths, invalidating the parabolic representation. This behaviour was only observed in the longer dents and is attributed to the development of outward bulging (Fig. 5) which relieves the longitudinal compressive strain. Bulging was restricted in the short dents by the proximity of strong rings [8]. The compressive stresses introduce the possibility of buckling at the edges of the dent which will affect the lateral stiffness under damage loading. While a reduced rate of compression development could delay buckling, the benefits may be counteracted by the radial deflections and additional surface strains produced by the bulge [7].

The stresses in the undamaged material around the dent may also be presented in a different form. The tension forces in the dent pull the ends of the shell inward and caused a reacting stress distribution in the undamaged arc. These stresses may be computed very simply if the ends are assumed to remain planar, as shown in Fig. 6.



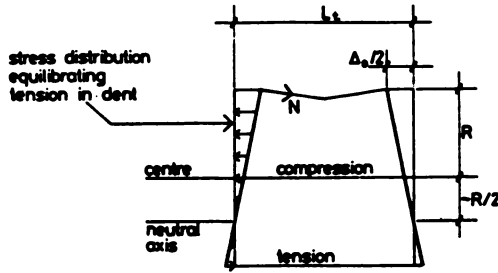


Fig. 6 End rotation and pull-in

Hence

$$\frac{\sigma}{\sigma_Y} = \sum_j \frac{n_j}{s} \left[ 1 + \frac{(\bar{y}/R + 1)(\bar{y}/R + \cos\varphi)}{I_{te}/A_{te}R^2} \right] \cdot \frac{A_t}{A_{te}} \quad (2)$$

Here  $\bar{y}$ ,  $A_{te}$  and  $I_{te}$  define the centroid, cross sectional area and second moment of area, respectively, of the arc of undamaged material [9].

Eqn.(2) is plotted in Fig. 7 for various positions around the circumference of Cylinder 3B2. The readings of longitudinal strain gauges at  $\varphi = \frac{1}{2}\pi$  and  $\pi$  in the centre bay compare very well with the predictions. At  $\varphi = 4\pi/20$ , just outside the dent, strain gauges were placed in both inner and outer bays, with the results plotted in Fig. 7(b). This is the same position as the  $\varphi = 2\alpha$  results in Fig. 2. The inner and outer bays behave differently [6] because the compression strains are modified by the movement of the intermediate ring frame, as discussed above. However the average strain over the three bays is very close to the simple prediction.

An effective strain was also computed at the dent centre ( $\varphi = 0$ ) from the longitudinal movement of the ends, which was measured with displacement transducers. The measured pull-in here is larger than predicted (Fig. 7(a)). This indicates some inward flexural and shear deformation of the end rings in the dent zone, superimposed on the planar displacement. Extremely rigid supports would be needed to prevent nonlinear pull-in.

Fig. 7 shows, finally, that the rate of pull-in increases at larger dent depths, because both the total tension force in the dent increases and the arc of resisting material diminishes. This is the reason why the effective stiffness  $\gamma$  at the ends of the dented beam elements is smaller at higher  $\varphi$  values in Fig. 2.

### COMPRESSIVE STRENGTH ANALYSIS

The application of simple analytical techniques continued in assessing the loss of axial strength caused by the local damage. The large radial deflections of the beam strips in the dent ensured that they had very little longitudinal stiffness under compressive loading. The damaged zone was therefore neglected and the undamaged arc of material was assumed to provide all the stiffness and strength. The asymmetry of the arc meant that the effective material was stressed nonuniformly, with the maximum stresses found adjacent to the dent. Collapse was computed to occur when these critical stresses reached the compressive capacity of the geometry [9].

The intact strengths of the models were determined from tests undertaken by other researchers [10,11] and by finite element analysis. Results are given in column 4 of Table

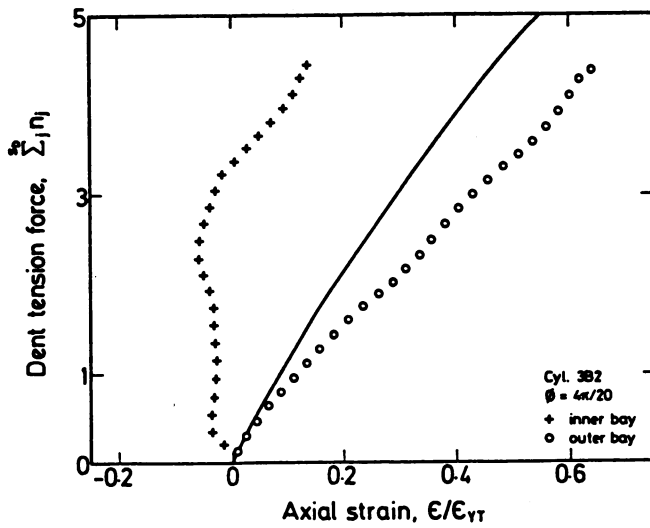
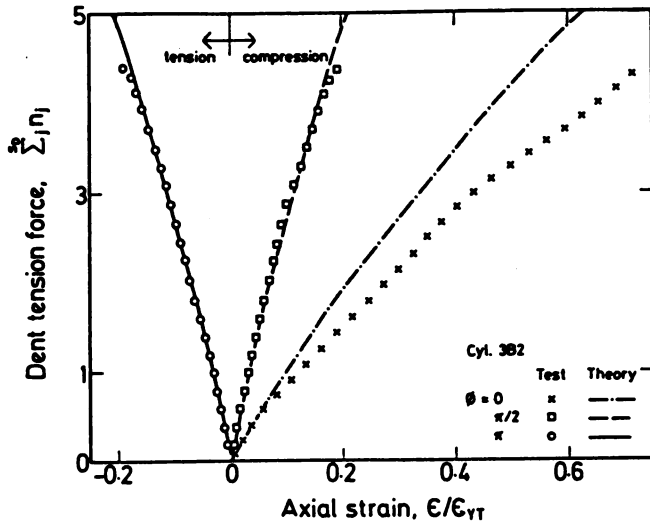


Fig. 7 Axial strains around cross section

CYL.	SLENDERNESS		INTACT STRENGTH		DAMAGED STRENGTH		DENT DEPTH
	L/R	b/t	$\sigma_m/\sigma_{YC}$		$P_{Am}/N_{Pt}$		$\delta_{De}/t$
			Model Imperfections	DnV	Theory	Test	
3A3	0.33	30	1.0	0.96	0.79	0.86	9.8
1A2	0.42	60	0.96	0.69	0.77	0.76	8.9
3B1	0.60	42	1.0		0.81	0.90	12.4
3B2	0.60	42	1.0		0.75	0.79	20.7
3B3	0.60	84	0.79	0.49	0.59	0.57	21.6
3B4	0.60	84	0.79	0.49	0.54	0.55	28.5
1B1	1.08	40	1.0		0.67	0.59	26.5
1B2	1.08	80	0.79	0.78	0.55	0.46	26.4

Table 2 Compression test results

2. The Table also compares the damaged strengths predicted using these intact capacities with the experimentally observed values. With the exception of Cylinders 1B the correlation supports the simple analysis.

The numerical analysis of the undamaged shells modelled one stringer beam and was therefore suitable for geometries failing in a local panel mode. The approach was developed and validated by Agelidis [10] and the mesh used is shown in Fig. 8. Initial imperfections sympathetic to the buckling mode were incorporated into the mesh, using the largest magnitude measured on the undamaged cylinder.

For models failing in a local mode the predicted strength for a panel containing the maximum imperfection complying with the tolerances of the DnV Buckling Analysis Notes [12] is also listed in Table 2 (column 5). These imperfection amplitudes were computed using the approach of Agelidis [10]. Being in the range  $0.26 < b/t < 0.84$  they were larger than the imperfections contained in the models.

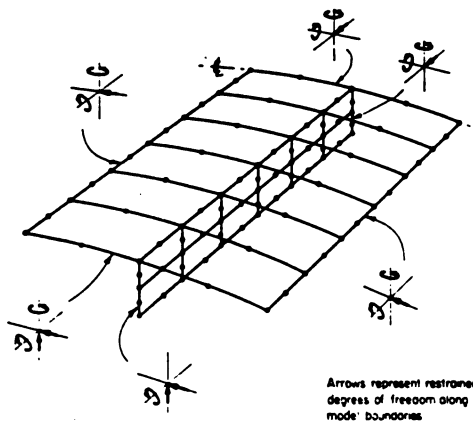


Fig. 8 Finite element mesh of stringer beam (from [10])

For Cylinders 1A2, 3B3 and 3B4, comparison of columns 4 and 5 in Table 2 indicates a strong imperfection sensitivity in the assumed mode. The DnV imperfection tolerance produces a significantly lower strength than the maximum magnitude of imperfection actually measured in the model. Cylinder 1B2 is also affected by imperfection amplitude: the predicted strength of a perfect model is  $\sigma_m/\sigma_{YC} = 0.96$ . However the maximum measured imperfection was only slightly smaller than the tolerance for this geometry and so the additional strength reduction is slight. The similarity of the two strength values for Cylinder 3A3 occurs, in contrast, because imperfections are not important for this stocky model.

A curious observation for Cylinders 1A2, 3B3 and 3B4 is that their strengths when *damaged* are larger than the predicted *intact* capacities when the shells contain the largest imperfections specified by DnV [12]. This is despite the dents being of the order of thirty times deeper than the recommended tolerances. The edge of the dent has tight circumferential curvature which stiffens its response under compressive loading. Additionally the significant outward bulge beyond the dent in the longer models is not sympathetic with the preferred modes of buckling of the shell. Thus this part of the cylinder can support high stresses, and considering it to be fully intact in the effective section analysis gives realistic strength estimates.

Very much smaller imperfections in critical buckling modes may, however, reduce the strength markedly, as noted above. It appears, in fact, that the small inward deflection adjacent to the outward bulge next to the dent was very important in the compression tests of series 1B and 3B. This inward imperfection was compatible with a general buckling mode in the stringer stiffened bay and grew to form such a buckle during loading [7]. The presence of this secondary imperfection may explain the larger strength reductions found in the damaged Cylinders 1B, although further studies are necessary to confirm this.

In Fig. 9 the effective section analysis is compared with two shell tests having similar dent sizes. The stronger response curve is for Cylinder 3B2, a forty stringer model. This model was 5% stronger than predicted due its ability to redistribute stress after first yield occurs adjacent to the dent. The other model is geometrically similar to Cylinder 3B2 but has only twenty stringers. Being more slender the intact shell material collapsed at lower load and with little possibility of stress redistribution. The residual compressive strengths of all the damaged shells tested in this Department of Energy/SERC Programme are plotted in Fig. 10 and compare quite well with the effective section analysis.

## CONCLUSIONS

Damage tests on orthogonally stiffened cylindrical shells have furnished useful information on the consequences of accidental impact. Using the experimental data simple, approximate analyses have been developed and calibrated. Plastic mechanism techniques were used to model the lateral loading process, taking account of both bending and membrane action in the dented material. This enabled a relationship between impact energy and extent of damage to be quantified. The manner in which different stiffening geometries affect the energy absorbing capability has been studied [14]. Where high axial restraint is provided at the ends of the dent, membrane effects dominate and the response equations are greatly simplified.

The damage weakens the compressive response of the shells because the dent carries very little axial stress. An analysis has been developed which considers material outside the dent to be fully effective and thus the residual dent depth is the only parameter required to estimate the strength loss. This approach gives good agreement with experimental data for most of the geometries tested. It appears, however, that small radial imperfections circumferentially remote from the dent, but produced during lateral loading, may have an additional affect on the compressive response of the most slender shells.

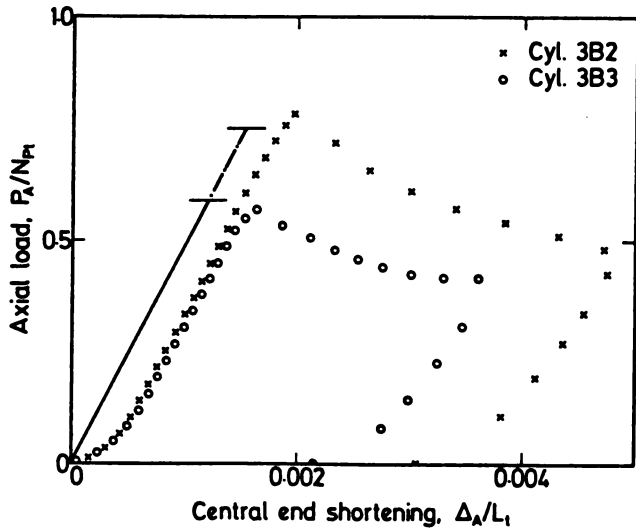


Fig. 9 Compression loading response

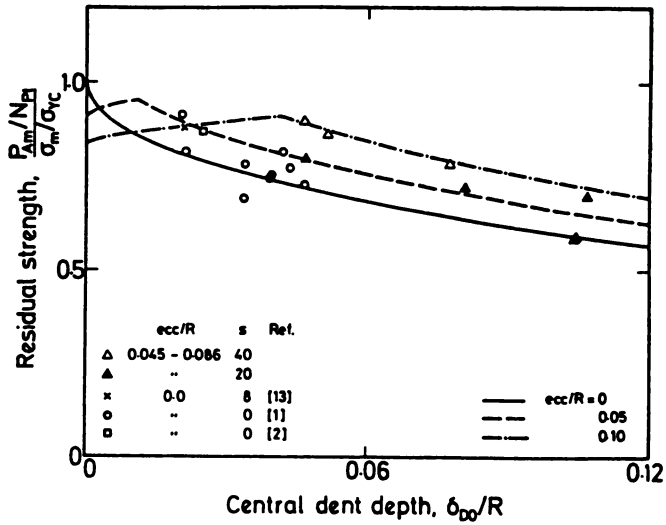


Fig. 10 Residual compressive strength of damaged shells

## ACKNOWLEDGEMENTS

The authors wish to thank the Department of Energy and the Science and Engineering Research Council for their financial support. The finite element analyses discussed in this paper were undertaken using the program FINAS which was developed by Dr. U. Trueb and Dr. D.N. Bates.

## REFERENCES

1. ONOUFRIOU A., HARDING J.E. and DOWLING P.J., 'Impact damage on ring stiffened cylinders'. Stability of Plate and Shell Structures, Proc. Int. Colloq., Ghent, ed Dubas P. and Vandepitte D., 493 (1987)
2. WALKER A.C. and McCALL S. 'Combined loading of damaged cylinders'. Univ. of Surrey (1986)
3. JONES N., 'Structural aspects of ship collisions'. Structural Crashworthiness, 1st. Int. Symp., Liverpool, ed. Jones N. and Wierzbicki T., 308 (1983)
4. DE OLIVEIRA J.G., 'Simple methods of estimating the energy absorption capability of steel tubular members used in offshore structures'. Report SK/R50, Division of Marine Structures, Norwegian Institute of Technology, Trondheim (1979)
5. JONES N., Written discussion on 'Tanker structural analysis for minor collisions'. McDermott J.F. *et al*, Trans. SNAME, New York, 82, 408 (1974)
6. RONALDS B.F. and DOWLING P.J., 'A denting mechanism for orthogonally stiffened cylinders'. Int. J. Mech. Sci., 29, 743 (1987)
7. RONALDS B.F. and DOWLING P.J., 'Collision resistance of orthogonally stiffened shell structures'. Proc. Int. Conf. Steel Structures, Yugoslavia, ed. Hajdin N. *et al*, II, 555 (1986) also J. Construct. Steel Research, 9, 179 (1988)
8. RONALDS B.F. and DOWLING P.J., 'Finite deformations of stringer stiffened plates and shells under knife edge loading'. Proc. 5th. Int. OMAE Symp., Tokyo, ed. Chung J.S. *et al*, III, 323 (1986)
9. RONALDS B.F. and DOWLING P.J., 'Residual compressive strength of damaged orthogonally stiffened cylinders'. Stability of Plate and Shell Structures, Proc. Int. Colloq., Ghent, ed. Dubas P. and Vandepitte D., 503 (1987)
10. AGELIDIS N., 'Collapse of stringer-stiffened cylinders'. Ph.D thesis, Imperial College, Univ. of London (1984)
11. FAHY W.G., 'Collapse of longitudinally stiffened cylinders subject to axial and pressure loading'. Ph.D thesis, Imperial College, Univ. of London (1985)
12. DET NORSKE VERITAS, 'Classification notes - buckling strength analysis of mobile offshore units'. Hovik, Norway (1984)
13. WALKER A.C. and DAVIES P., 'The collapse of stiffened cylinders'. Steel Plated Structures, ed. Dowling P.J. *et al*, 791 (1976)
14. RONALDS B.F. and DOWLING P.J., 'Stiffening of steel cylindrical shells for accidental lateral impact'. Proc. Instn. Civ. Engrs., Part 2, 83, 799 (1987)



## MAN-INDUCED VIBRATIONS IN STRUCTURES - MEASURES AND PRACTICAL CASES

Hugo Bachmann  
Professor of Structural Engineering  
Swiss Federal Institute of Technology (ETH) Zürich, Switzerland

### SUMMARY

Man-induced vibrations in structures can lead to serious problems to the extent to render a structure unserviceable. At the beginning of this paper, the following points, important for the objective of avoiding excessive vibrations, are considered: major parameters, possible countermeasures, classification of structures with man-induced vibrations, representative types of motion and dynamic loads, and frequency tuning. Then, case reports of footbridges, gymnasia and sports halls, dance halls and concert halls without fixed seating, and concert halls with fixed seating are presented. In some cases, existing buildings had to be upgraded. In other cases, where structures were still in the planning stage, significant modifications to the design were necessary.

### 1. PRELIMINARIES

Lately, man-induced vibrations in structures have caused serious problems. Only recently has it become possible to establish guidelines on how to avoid problems of man-induced vibrations [1,2]. While some theoretical considerations did play a role, experience and understanding of the phenomena were gained, however, through practical case studies. Most important were tests, carried out in situ before and after rehabilitation of a structure.

Before describing such practical cases, attention is drawn to some general characteristics.

#### 1.1 Major parameters

In the case of vibrating structures the following parameters dominate the dynamic behaviour

- dynamic loads
- dynamic system
- dynamic bending stiffness
- damping

These four parameters govern the structural response. In existing structures, response can mostly be measured. For structures in the planning stage, the structural response can only be estimated and this represents a much more difficult



task. Sufficient knowledge of these four major parameters is vital for conceiving anti-vibration measures.

### 1.2 Possible measures

Three classes of measures can be distinguished with reference to the forementioned major parameters:

- Frequency tuning of the structure, based on the loading frequency, i.e. the spectrum of Fourier amplitudes of the dynamic load. For frequency tuning beside of the load-time function the dynamic system and the dynamic bending stiffness are also important, whereas damping is less important.
- Calculating the forced vibration of the structure and comparing the amplitudes to certain acceptance criteria. For the calculation of a forced vibration, the load-time function, the dynamic system, the dynamic bending stiffness and especially the damping are important.
- Taking special measures such as, for instance, general stiffening of the structure, increasing the damping, installing tuned vibration absorbers, or, instead, restricting the use of the building or facilities.

Depending on circumstances, these measures can differ greatly in potential, their feasibility and expenditure.

### 1.3 Classification of structures with man-induced vibrations

Based on the various dynamic loads and the countermeasures applicable, structures affected by man-induced vibrations can be grouped as follows:

- pedestrian structures
- office buildings
- gymnasias and sports halls
- dance halls and concert halls without fixed seating
- concert halls with fixed seating
- high-diving platforms in swimming pools

Man-induced vibrations are primarily a problem of serviceability, in terms of annoying or disturbing the respective users. On pedestrian structures and high-diving platforms the causative person himself may feel disturbed, whereas in other buildings only users not directly involved in creating vibrations are affected. In rare cases, a safety problem may arise, i.e. the stability of the structure is at risk. A detailed description of serviceability and safety problems of man-induced vibrations in structures is given in the book [1].

### 1.4 Representative types of motion and dynamic loads

Knowing the dynamic loads is the basis to the understanding of the vibration phenomena. This understanding allows measures to be taken to reduce vibrations. The innumerate variances of rhythmical human body motions constitute a large variety of possible dynamic loads. Of those, rhythmical motions often performed to music by several people at the same time synchronising their movements have to be especially considered. When lasting up to 20 seconds or more, they lead to almost periodic loads resulting in more or less steady-state structural vibrations. Although the loads differ in their dominant frequencies and their load-time function, they can be grouped into the following representative types of motion and the corresponding dynamic loads:

- walking
- running
- jumping

- dancing
- clapping

One can say that until recently the understanding of the dynamic loads induced by man was very limited. Calculations were based on a single harmonic function of the basic loading frequency (e.g. the pacing rate). Over the last few years, however, incidences of structural inadequacies shed light on the contribution of upper harmonics (as part of the Fourier decomposition of the loading function), which may become critical for the dynamic design of a structure [1,2,3].

### 1.5 Frequency tuning

The simplest countermeasure, which proved efficient in numerous practical cases, is frequency tuning of the structure. The structural frequency, mostly the fundamental natural frequency, has to be established with regard to the most critical frequencies of the load-time function. This is quite often not the nominal loading frequency itself, but the frequency of an upper or lower harmonic in the spectrum of the load-time function.

The following criteria can be used for frequency tuning in the forementioned structural classes:

- Pedestrian structures:  
Avoidance of the 1st and 2nd harmonic of the dynamic load due to "walking".
- Office buildings:  
High-frequency tuning with respect to the 3rd harmonic of the dynamic load due to "walking".
- Gymnasias and sports halls:  
High-frequency tuning with respect to the 2nd harmonic of the dynamic load due to "jumping" (see [1]).
- Dance halls and concert halls without fixed seating:  
High-frequency tuning with respect to the 2nd harmonic of the dynamic load due to "dancing" (see [1]).
- Concert halls with fixed seating:  
High-frequency tuning with respect to the 1st harmonic due to "clapping" [4]. In structures with low damping, the frequency of the 2nd harmonic of the same load should be considered (avoidance or high tuning).
- High-diving platforms in swimming pools:  
Consideration of special frequency and stiffness criteria (see [1]).

On determining the frequency bounds for different structural types, the accurate stiffness, mass and damping have to be taken into account.

The above mentioned criteria together with a general consideration of the properties of the different structural types lead to the recommendations for eigenfrequencies given in Table 1 (fundamental and higher frequencies). Observing these frequency bounds should in most cases result in adequate dynamic performance. In the following, several practical cases are described. Some cases deal with existing structures most of which had to be upgraded. The other cases are projects, the design of which had to be substantially modified. In most cases, the above frequency criteria became relevant.

Structural class	Structural type	Reinforced concrete	Prestressed concrete	Composite steel-concrete	Steel
Pedestrian structures		Avoidance of 1.6 to 2.4 Hz and 3.5 to 4.5 Hz			
Office buildings		> 7.5	> 8.0	> 8.5	> 9.0
Gymnasies and sports halls		> 7.5	> 8.0	> 8.5	> 9.0
Dance halls and concert halls without fixed seating		> 6.5	> 7.0	> 7.5	> 8.0
Concert halls with fixed seating		> 3.4			

Table 1: Recommendations for the eigenfrequencies [Hz] of structures with man-induced vibrations

## 2. FOOTBRIDGES

### 2.1 Footbridge of ~ 2 Hz

A 4 m wide footbridge was planned to cross a canal over a total length of ca. 91 m, divided into three spans of 25.7 m – 40 m – 25.7 m, Figure 1a. The U-shaped cross-section is made up from a ~ 20 cm thick slab and two 40 cm thick parapet walls of 1 m inner height, topped by a 30 cm high metal non-loadbearing metal railing. Above the intermediate supports, the slab is haunched to 40 cm. The girder will be prefabricated in 3.5 m segments and assembled on the site with resin joints and post-tensioned by means of longitudinal prestressing cables.

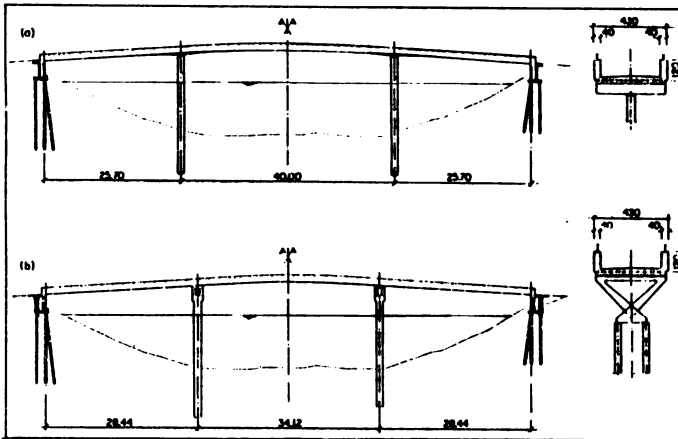


Fig.1: Project of a footbridge before and after dynamic calculations

During the design, the dynamic behaviour was calculated, and the fundamental frequency was found to be ~ 2.0 Hz. A forced vibration was calculated, estimating the damping ratio to 0.5% of critical, a value which was found in similar structures. For a mean flow rate of 20 pedestrians per minute an acceleration of ~ 8% g was obtained (after [1]). As the acceleration in footbridges should not much exceed 5% g and peak flow rate could well be higher, design modifications were envisaged to reduce the proneness to vibration.

The following measures were examined:

- increasing the height of the parapet walls
- making a much heavier railing part of the load-bearing structure

- further haunching of the slab over the intermediate supports
- changing the ratio of spans.

Heightening the parapets or thickening the slab seemed aesthetically undesirable. Stiffening of the bridge by the railing was kept as a last resort for post-structural upgrading. Hence the lengths of the spans were altered from 25.7 m - 40 m - 25.7 m to 28.44 m - 34.12 m - 28.44 m, Figure 1b. This raised the calculated fundamental frequency to  $\sim 2.4$  Hz and reduced the acceleration at 20 persons/minute to  $\sim 4\%$  g. In addition, the structural detailing provided for a certain encastrement of the girder in the piers.

The bridge is going to be built in the spring of 1988. After completion, dynamic tests will be carried out and the results compared with the design calculations.

## 2.2 Footbridge of $\sim 4$ Hz

When a steel footbridge showed noticeable vertical vibration, its frequency and amplitude were measured during normal evening peak traffic [1]. The number of people crossing varied between 30 and 55 per minute. It became obvious that the bridge vibrated predominantly in its fundamental frequency of about 4 Hz. This was excited by the second harmonic of the load-time function with a pacing rate frequency of about 2 Hz.

## 3. GYMNASIA AND SPORTS HALLS

### 3.1 Gymnasium of $\sim 5.2$ Hz

A two-storey gymnasium showed severe vibrations of the intermediate floor caused through normal gymnastics, especially rhythmical exercises. These vibrations were disturbing and raised doubts about the safety of the floor. The floor is a ribbed slab of reinforced in-situ concrete, spanning an area of ca. 15 m x 27 m. The load is carried across the short span by 0.15 m thick and 0.46 m high ribs spaced about 0.65 m apart. On one side, along the glazed front of the building, the ribs are indirectly supported via an edge beam by slender columns, which provides virtually no rotational restraint; on the opposite side, the ribs are fixed rigid in the concrete walls and adjacent floor slabs.

In order to determine the dynamic behaviour of the floor, drop tests were performed as well as resonance excitation by jumping and running of schoolchildren from two classes. A total of 34 pupils, aged about 14 years, carried out a standard test of jumping on the spot synchronized by a metronome with frequencies between 1.4 and 3.5 Hz. This way, the frequency response curve of Figure 2a was obtained. The strongest vibration resulted from jumping at 2.58 Hz. The fundamental frequency of the floor was 5.15 Hz. Thus resonance was excited by the 2nd harmonic of the load-time function or - figuratively speaking - pupils exerted a thrust in (shifted) phase with every second downward swing of the floor. However, Figure 2a shows another resonance with the 3rd harmonic, which time did not permit to explore further. The peak amplitudes obtained were  $\pm 50$  mm/s velocity and  $\pm 1.65$  m/s<sup>2</sup> acceleration.

The damping ratio was determined to 3% of critical, which is fairly high for gymnasium floors. It was derived from a sudden stand-still of the jumping pupils, so that the decaying vibration could be monitored. Because the pupils standing on the vibrating floor provided extra energy dissipation, the damping ratio of the unloaded floor must be expected to be smaller than the 3% measured.

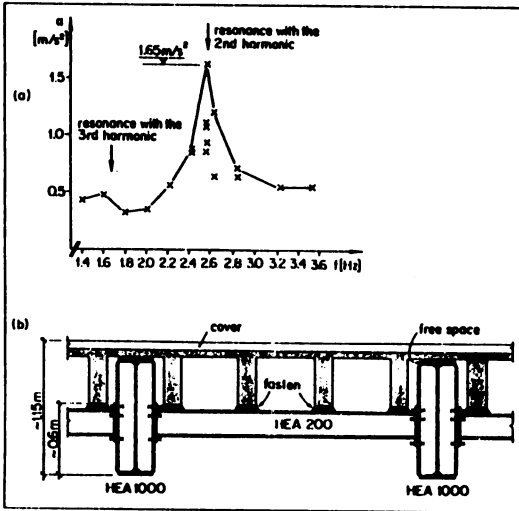


Fig. 2: Gymnasium floor; a) resonance curve from jumping exercises; b) section of the upgraded structure

Serviceability of floors in gymnasiums limits acceleration to 5% g, at most 10% g. Since the respective gymnasium is used by adults as well, and may host a larger number of participants than in the tests, the owner of the facility decided to upgrade the structure. The fundamental frequency of the floor was to be raised to about 7.5 Hz [1]. Out of six alternatives, two seemed equally cost-effective: (a) to demolish the existing floor and to replace it with a prestressed concrete joist floor, and (b) to install a steel girder grid as supporting structure underneath the existing floor. It was decided to use option (b) for its shorter construction time, although it reduces significantly the clear height of the lower hall. Figure 2b gives a cross-section of the upgraded floor. Post-rehabilitation tests were carried out again with jumping on the spot, this time by a group of 51 pupils, aged about 15 years, who were lined up in the relevant central area of the floor at a high density of one person per  $2 m^2$  [1]. The fundamental frequency of the upgraded floor was measured to  $\sim 7.47$  Hz, the damping ratio from decay measurements was 3.2%. The fundamental frequency could be excited to resonance by both the 3rd and 4th harmonic of the load-time function, i.e. with jumping frequencies of  $\sim 2.5$  Hz and  $\sim 1.9$  Hz. Associated peak accelerations were  $0.74 m/s^2$  and  $0.60 m/s^2$ , respectively. Thus they do not exceed the upper bound of 5 to 10% g. The calculated displacement and acceleration (according to [1]) overestimate the experimental results by about 10%.

### 3.3 Sports hall adjacent to grandstand of $\sim 2.4$ Hz

The design project of a large two-storey sports hall involved 3 m high and 42 m spanning prestressed concrete beams [1]. On one side, the columns had also to support a grandstand (Figure 3a). For a first assessment of the vibrational performance under rhythmic excitation as during fitness classes, dynamic calculations were applied to a simplified but conservative model structure (Figure 3b) and yielded a fundamental frequency of  $\sim 2.4$  Hz. The low value was mainly due to a very adverse contribution of the horizontally swinging grandstand mass. For the resonance case of the excitation frequency being equal to the structural frequency, a forced vibration computation (according to [1]) with 1% damping and a user

density of one person jumping per 4 m<sup>2</sup> indicated amplitudes of  $\pm 34$  mm displacement,  $\pm 560$  mm/s velocity, and 8.6 m/s<sup>2</sup> (!) acceleration. The high stress level was expected to lead to damage or even structural collapse. Therefore, one had to consider substantial design modifications and strengthening with the goal of reaching a fundamental frequency of the floor of about 8 Hz.

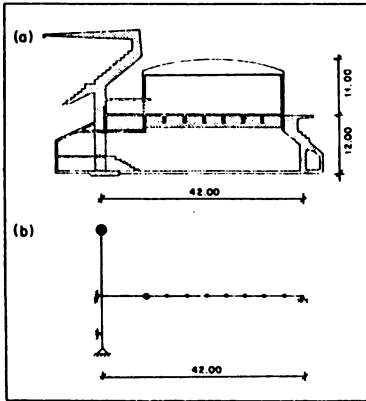


Fig. 3: Sports hall connected to grandstand;  
a) cross-section, b) simple dynamic model

#### 4. DANCE HALLS AND CONCERT HALLS WITHOUT FIXED SEATING

##### 4.1 Concert hall without fixed seating of $\sim 6.2$ Hz

A medium-size hall of 32.8 m x 55 m area exhibited strong floor vibration during pop concerts [1]. These events were attended by up to 4000 people, a part of the audience was always enthused to activities such as clapping of hands, body rocking or light bouncing up and down to the music. Several hall areas without fixed seats brought about differences in density of the audience with a particular grouping (estimated up to a maximum of 6 persons per m<sup>2</sup>) towards the stage whenever the musicians were on show. The plan and the sections of the floor structure in Figure 4 reveal a hollow-block slab of 0.45 m thickness and about 450 kg/m<sup>2</sup> mass. The floor is supported by two rows of columns spaced 6.62 m apart, across which runs in longitudinal direction an internal joist (a cast-in strengthened steel section DIE 38). The structural action can thus be described as a predominantly crosswise-spanning continuous plate over three openings of 8.6 m/14 m/-8.6 m. The floor is bisected by a dilatational joint. Designated originally as an exhibition hall, the building had merely been designed for static loads, so that the new problems are to be attributed to the unanticipated utilization for concerts.

Measurements were made at several concerts, showing that the vibration intensity depended more or less on the kind of music influencing the activities of the audience, and on its beat frequency. For example, soft pop music (Band "Simple Minds") with a beat frequency of  $\approx 2.0$  Hz  $\pm 2.5$  Hz and 3500 relatively quiet spectators yielded at a beat frequency of  $\approx 2$  Hz  $\pm 3$  Hz a peak vibration amplitude of  $\pm 4.6$  mm vertical displacement and  $\pm 1.66$  m/s<sup>2</sup> acceleration. During hard rock music (Band "Status Quo"), however, with a beat frequency of  $\approx 2.1$  Hz  $\pm 3$  Hz and an audience of about 2000 (of which about one third was quite electrified), the displacement at a beat frequency of  $\approx 2.1$  Hz reached  $\pm 9.5$  mm, the peak velocity  $\pm 177$  mm/s and the maximum acceleration 2.7 m/s<sup>2</sup>.

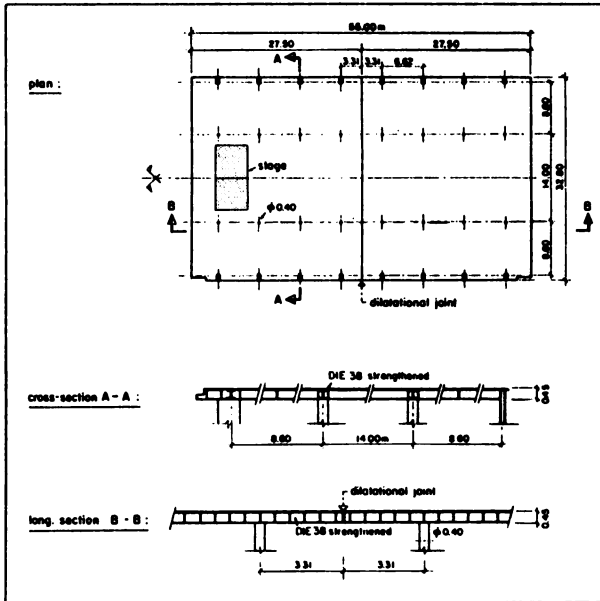


Fig. 4: Concert hall with hollow-cast floor structure (from [1])

When excited by a local impulse, the unloaded floor showed a fundamental frequency of  $\sim 6.2$  Hz. Dynamic loadings on a larger area would probably bring out the inherent structural action in the crosswise direction of the building and - with the additional mass of the audience - a fundamental frequency in the range of double the beat frequency of the music ( $\sim 4.0$  Hz +  $4.5$  Hz). This indicates a resonance-like excitation of the fundamental frequency of the structure, as found for the gymnasium floor described under 3.1, by the 2nd harmonic of the audience's bouncing-time function.

The measured vibration magnitudes and concluded stressing of the floor exceeded the admissible values by far so that the hall had to be closed for pop concerts. For upgrading, the floor would have to be supported by additional beams in the cross-direction, or temporary props would have to be fitted and removed before and after every concert if the use of the lower storey was not to be greatly restricted. Finally, the discussion became inconsequential as another location for such concerts was found with a much higher floor frequency of about 12 Hz (unloaded).

## 5. CONCERT HALLS WITH FIXED SEATING

### 5.1 Concert hall with fixed seating of $\sim 2.5$ Hz

The floor of a concert hall with approximately 2000 seats span on an area of about 40 m x 40 m. The floor vibrated considerably whenever the audience clapped their hands rhythmically (seated or standing up). This phenomenon is quite common in pop-concerts while clapping in rhythm to the music or demanding encors. It may also occur in classical concerts when clapping to a piece like the Radetzky March by Strauss. The floor in question had a measured fundamental frequency of  $\sim 2.5$  Hz (unloaded), which dropped to  $\sim 2.4$  Hz due to the audience present; this

corresponds to a usual rhythm or clapping frequency. Dynamic loads due to clapping are usually of minor importance [4]. In this case, however, the audience was able to excite the floor to near-resonance by clapping with the natural frequency of the structure (1st harmonic of the load = 1st structural frequency).

As no plausible magnitudes for the dynamic load were available, special experiments had to be carried out. Figure 5 shows the load-time function and the Fourier amplitude spectrum of the dynamic load exerted by a seated person clapping hands. Figure 6 shows the Fourier amplitudes of the different harmonics created through various ways of rhythmical clapping (after [4]).

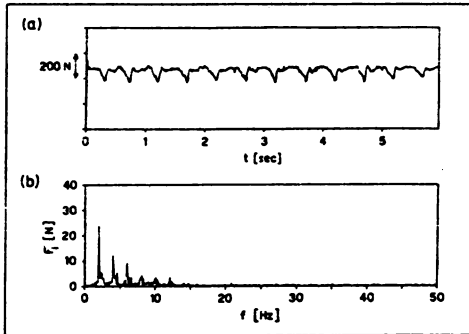


Fig. 5: Rhythmical hand clapping (2 Hz) of a person being seated (from [4]):  
 a) Load-time function of dynamic load;  
 b) Fourier-amplitude spectrum created

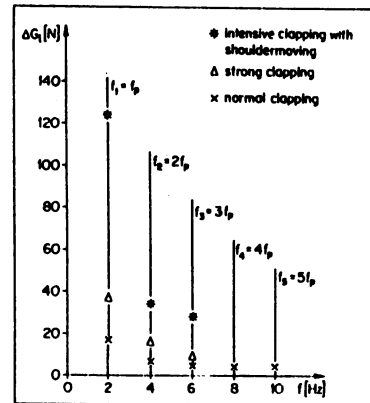


Fig. 6: Amplitudes and harmonics created through various types of hand clapping (2 Hz) (from [4])

## 6. HIGH-DIVING PLATFORMS

### 6.1 Diving platform with torsional vibrations

The shaft of a 3 m and a 5 m platform showed intolerably large twisting vibration soon after completion [1]. The two reinforced-concrete platforms are each supported by two steel columns with cantilever beams, resulting in an excentric layout of the facility with the four columns forming the corners of an open rectangular shaft. The columns were braced horizontally only near the foundation. The design engineer, although he had calculated the fundamental bending frequency and had found it uncritical, must have overlooked the low torsional rigidity of his design. Subsequently, two concrete wall members were erected between the foundation and each platform parallel to the flights of stairs, combining an architecturally satisfying solution with a much improved dynamic behaviour.

### 6.2 Diving platform of ~ 2.8 Hz

A reinforced concrete diving platform has two slabs at 3 m and 5 m elevation, supported by a Y-shaped shaft (Figure 7). The shaft arms are connected by a tie-beam at the height of the lower slab. Below the ground the shaft is joined to the wall of the pool from the foundation base upwards to 1.20 m below surface.



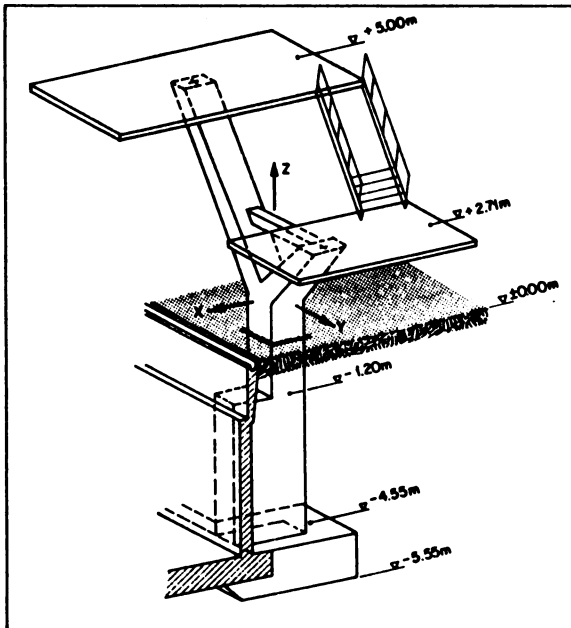


Figure 7: Diving platform

The lower slab is equipped with a soft spring-board. During normal use, irritating vibrations were felt when diving off the spring-board. Moreover, the entire platform could deliberately be excited by jumping on the upper slab or rhythmical pushing and pulling on its railing ("vandal loading" by youngsters). Because of the frightening amplitudes thereby obtained, the owner of the facility became concerned about long-term deterioration of the structure. The Swiss Federal Laboratory for Testing Materials and Research (EMPA) was called in to investigate. For an experimental modal analysis, the platform was excited with a hammer (including a contact-force sensor) and the resulting accelerations were measured at 50 points in all three orthogonal axes, in groups of 6 points.

By a phase-separation technique, the following basic modes were identified:

- Mode 1 (lateral sway about the x-axis):  $f_1 \approx 2.8 \text{ Hz}$ ,  $\xi = 1.64\%$ .
- Mode 2 (shaft nodding about the y-axis):  $f_2 \approx 4.2 \text{ Hz}$ ,  $\xi = 1.18\%$ .
- Mode 3 (Torsion of the upper slab about the z-axis):  $f_3 \approx 4.8 \text{ Hz}$ ,  $\xi = 0.88\%$ .

Higher modes at  $f_4 \approx 10.8 \text{ Hz}$ ,  $f_5 \approx 11.8 \text{ Hz}$ ,  $f_6 \approx 14.6 \text{ Hz}$ , etc. show a combination of these spatial components.

Additional resonance excitations were performed through test persons. Rhythmical jumping of a person on the upper slab caused vertical displacements at the slab center of max. 5.7 mm and accelerations of max.  $2.8 \text{ m/s}^2$  at the rear edge of the slab. The fundamental frequency decreased by about 5% because larger sway amplitudes decreased the flexural rigidity about the x-axis (opening of cracks). From single-jump tests with amplitudes of a few mm (especially in mode 1), the damping ratio was derived to  $\sim 2\%$  of critical. A high-diver jumping off the spring board

on the lower slab caused accelerations at the rear end of this slab of max.  $4.6 \text{ m/s}^2$  lateral (y-direction) and max.  $2.6 \text{ m/s}^2$  vertical.

The acceptance criteria in [1] require the following lower bounds on shaft vibrations:

- slab without springboard:  $f \geq 3.5 \text{ Hz}$
- slab with springboard:  $f \geq 5.0 \text{ Hz}$

The platform in case does not meet the frequency criteria, although in this particular case the most critical vibration is not in take-off direction. Stiffening the structure without gross changes in its appearance will be difficult. No decision on upgrading has been made to date.

## 7. CONCLUSIONS

In practical cases frequency tuning of the structure is a useful countermeasure to curb excessive vibrations. The structural frequency, mostly the fundamental frequency, has to be established in view of the most critical frequency of the spectrum of the load-time function. This is quite often not the nominal loading frequency itself, but the frequency of an upper or lower harmonic of the dynamic load.

## REFERENCES

- [1] Bachmann H., Ammann W., Vibrations in Structures Induced by Man and Machines, Structural Engineering Document No. 3e, International Association for Bridge and Structural Engineering (IABSE), Zürich, 1987.
- [2] Allen D.E., Rainer J.H. and Pernica G., Building Vibrations due to Human Activities, Proceedings of the Structures Congress of the American Society of Civil Engineers (ASCE), Orlando, FL, USA, 1987.
- [3] Baumann K., Bachmann H., Durch Menschen verursachte dynamische Lasten und deren Auswirkungen auf Balkentragwerke (Man-induced dynamic loads and their influence on beam structures), Institute of Structural Engineering (IBK), Swiss Federal Institute of Technology (ETH) Zürich, Report No. 7501-3, December 1987, Editor Birkhäuser, Basel.
- [4] Vogt R., Bachmann H., Dynamische Lasten durch rhythmisches Klatschen, Fussstampfen und Wippen (Dynamic loads from rhythmic hand clapping, footstamping and moving up and down), Institute of Structural Engineering (IBK), Swiss Federal Institute of Technology (ETH) Zürich, Report No. 7501-4, September 1987, Editor Birkhäuser, Basel.
- [5] Peterson C., Theorie der Zufallsschwingungen und Anwendungen (Theory of random vibrations and applications), work report No. 2/72, Structural Engineering Laboratory, Technical University Munich, FRG, 1972.
- [6] Bachmann H., Vibrations of building structures caused by human activities, case study of a gymnasium, National Research Council of Canada, Ottawa, Ontario, Technical Translation 2077, 1984.



## SOME PROBLEMS OF TWO-CHORD SYSTEMS

Milorad IVKOVIĆ

Professor at the Faculty of Civil Engineering  
University of Belgrade  
Belgrade, Yugoslavia

The problems of two-chord linear systems which have high elastoplastic properties are considered in this attachment. The analysis is made for the systems which possess the different sign curve so that the gaus curve of the system in negative. Fig. 1. shows a structural possibility of such systems which is frequently used in engineering practice for beam prestressed girders with tendons outside the cross section.

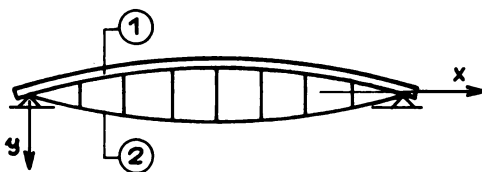


Fig. 1.

As it is evident from Fig. 1, the system consists of two chords connected by the web which is supposed to be rigid in vertical direction. The elementar par with external and internal (forces in the section) that act upon it is presented in the Fig. 2.

$$\epsilon(t, \tau) = \frac{\sigma(t)}{E(t)} + \int_{\tau}^t \kappa(t, \tau) \cdot \frac{\sigma(\tau)}{E(\tau)} d\tau + \epsilon_s(t, \tau) + d\theta(t) \quad (1)$$

The relation between stress and strain in the form of Volttera - Integral equation

of the second order is assumed for the material which has high elastoplastic properties.

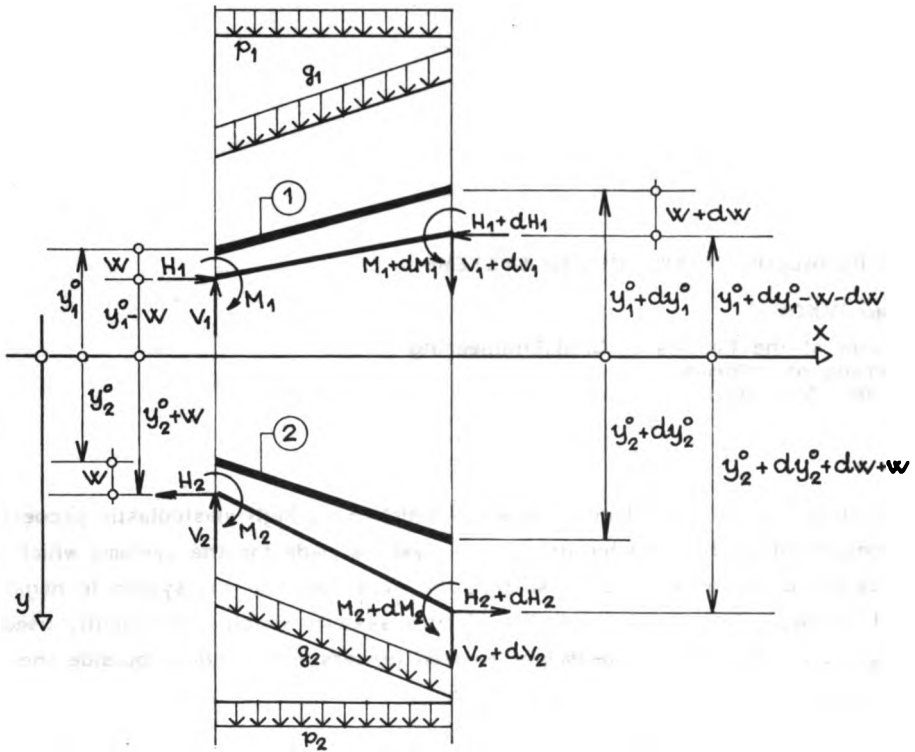


Fig. 2.

or its resolvent form

$$\sigma(t) = E(t) [E(t) - \epsilon_s(t) - \alpha \theta(t)] - E(t) \int_{\tau}^t R(t, \tau) [E(\tau) - \epsilon_s(\tau) - \alpha \theta(\tau)] d\tau \quad (2)$$

where  $K(t, \tau)$  - the core and  $R(t, \tau)$  its resolvent with the known relation in the form,

$$K(t, \tau) = R(t, \tau) - \int_{\tau}^t K(t, \eta) R(\eta, \tau) d\eta \quad (3)$$

- $\epsilon_s(t, \tau)$  - shrinkage deformation
- $\alpha$  - thermal coefficient
- $\theta(t)$  - change of temperature with time.

From the equilibrium condition of the differential element of the girder the following is obtained:

$$\frac{d^2 M_1}{dx^2} + \frac{d^2 M_2}{dx^2} - (H_1 - H_2) \frac{d^2 w}{dx^2} + H_1 \frac{d^2 y_1^0}{dx^2} + H_2 \frac{d^2 y_2^0}{dx^2} + g_1 \frac{ds_1}{dx} + g_2 \frac{ds_2}{dx} + p_1(x) + p_2(x) = 0 \quad (4)$$

where,

$$y_1 = y_1^0 + w \quad y_2 = y_2^0 + w.$$

It is valid for technical theory taking into consideration the relations (1) or (2),

$$\frac{1}{f_i} = \mathcal{E}_i(t) = \frac{M_i(x,t)}{E(t)J(x,t)} + \int_0^t K(t,\tau) \frac{M_i(x,\tau)}{E(\tau)J(x,\tau)} d\tau, \quad (5)$$

or

$$M_i(x,t) = E(t)J_i(x,t) \left[ \mathcal{E}_i(x,t) \right] - \int_0^t \mathcal{E}_i(x,\tau) E(\tau)J(x,\tau) R(t,\tau) d\tau, \quad (6)$$

as well as

$$\mathcal{E}_i(x,t) = \frac{M_i(x,t)}{E_i(t)J_i(x,t)} = \frac{d^2 w(x,t)}{dx^2}, \quad \text{namely}$$

$$\mathcal{E}_i(x,\tau) = \frac{M_i(x,\tau)}{E_i(\tau)J_i(x,\tau)} = \frac{d^2 w(x,\tau)}{dx^2}$$

so with the assumption that not much preciseness is lost if the change of the modulus of deformation  $E(t)$  with time and the moment of laziness are neglected  $J(x,t) \approx J(x,\tau)$ , the equation (4) finally acquires the following form,

$$\frac{d^4 w(x,t)}{dx^4} + \int_0^t \frac{d^4 w(x,\tau)}{dx^4} R(t,\tau) d\tau + (K_1^2 - K_2^2) \frac{d^2 w(x,t)}{dx^2} - \varphi(x) = 0 \quad (7)$$

where,

$$K_1^2 = \frac{H_1}{R_1 + R_2}, \quad K_2^2 = \frac{H_2}{R_1 + R_2} \quad R_1 = E_1(\tau)J_1 \quad \text{and} \quad R_2 = E_2J_2$$

$$\varphi(x) = H_1 \frac{d^2 y_1^0}{dx^2} + H_2 \frac{d^2 y_2^0}{dx^2} + g_1 \frac{ds_1}{dx} + g_2 \frac{ds_2}{dx} + p_1(x) + p_2(x)$$

For the case  $t = \tau$  (momentary elastic solution) integral differential equation (7) is transmitted into a non-homogenous bi-square total differential equation the solution of which is relatively easily attained. The function  $\varphi(x)$  as it is easily

noticed, is the function of the initial geometry as well as of the quantity and distribution of the external forces acting upon the girder.

Integral differential equation (7) with the corresponding boundary conditions provides the possibility to determine the displacement condition of both of the systems  $w(x,t)$ , in the function of parameters  $H_1(t)$  and  $H_2(t)$ . In order to finally determine the state of stress and strain it is necessary to use (meet) the deformations conditions. In this case, the conditions for calculation of the "lengths" of the members after the action of the external forces most frequently called the conditions of "length" are the required conditions.

So, if

$$L_{i0} + \Delta L_{i0} = L_i$$

(8)

$$L_{i0} = l + \frac{1}{2} \int_0^l \left( \frac{dy_i^0}{dx} \right)^2 dx$$

$$L_i = l + \frac{1}{2} \int_0^l \left[ \frac{dy_i^0}{dx^2} + 2 \frac{dy_i^0}{dx} \frac{dw(x,t)}{dx} + \frac{d^2w(x,t)}{dx^2} \right] dx,$$

$$\Delta L_{i0} = \left[ H_i(t) + \int_{\tau}^t H_i(\tau) K(t,\tau) d\tau \right] \frac{3L_{i0} - 2l}{E_i(\tau) F_i},$$

for,  $\int_0^l \frac{1}{\cos^3 \varphi} dx = 3L_{i0} - 2l$ , if the angles between the system lines and positive direction of the x-axis are the conditions of length (8) acquire the final form,

$$\left[ H_i(t) + \int_{\tau}^t H_i(\tau) K(t,\tau) d\tau \right] \frac{3L_{i0} - 2l}{E_i(\tau) F_i} - \int_0^l \left( \frac{dy_i^0}{dx} \right) \left( \frac{dw(t,\tau)}{dx} \right) dx - \frac{1}{2} \int_0^l \left( \frac{dw(x,t)}{dx} \right)^2 dx = 0. \quad (9)$$

Integral differential equation (7) and the conditions of length (9) make it possible to achieve the general solution for the values of stress and strain state with two-chord systems under any kind of loading.

For engineering practice, however, the solution of equation (7) and the condition (9) is a task very difficult to solve. Sufficiently precise solution of the problem for engineering practice can be attained by the introduction of algebraic relations between stress and strain instead of the relation in the form of Volterra's integral equation of the second order.

Algebraic form of the equations (5) and (6) for this case when the percentage of reinforcement is small, can acquire the following form:

$$\mathcal{Z}_i(x,t) = \frac{1}{J_i(\tau)E_i(\tau)} \left[ b_t M_i(x,t) + (a_t - b_t) M_i(x,\tau) \right] \quad (10)$$

namely

$$M_i(x,t) = J_i(\tau)E_i(\tau) \left[ C_t \mathcal{Z}_i(x,t) + (c_t - d_t) \mathcal{Z}_i(x,\tau) \right] \quad (11)$$

where  $a_t, b_t, c_t, d_t$  are determined known functions of time and age (when concrete or some other material changing its mechanical properties with time is in question).

With the equation (11) using the relations (6) the equation (7) becomes

$$\left[ C_t \frac{d^4 w(x,t)}{dx^4} + (c_t - d_t) \frac{d^4 w(x,\tau)}{dx^4} \right] + (K_{1t}^e - K_{2t}^e) \frac{d^2 w(x,t)}{dx^2} - \varphi(x) = 0 \quad (12)$$

where,

$$K_{1t}^e = \frac{H_1(t)}{R_1 + R_2}, \quad K_{2t}^e = \frac{H_2(t)}{R_1 + R_2}; \quad K^e = \frac{H_1(t) + H_2(t)}{R_1 + R_2},$$

while

$$R_1 = E_1 J_1, \quad R_2 = E_2 J_2$$

In this case, equation (12) is, for algebraic relations (11), a total non-homogeneous differential equation of the fourth order with quasi-constant coefficients.

The task is solved in two steps. First of all, in the first step, the so called momentary elastic task should be solved. That will be acquired if, in the equation (12)  $C_t = d_t = 1$  is inserted  $t = \tau$  and differential equation of the form is firstly solved

$$\frac{d^4 \bar{w}(x,\tau)}{dx^4} + (K_{1\tau}^e - K_{2\tau}^e) \frac{d^2 \bar{w}(x,\tau)}{dx^2} - \varphi(x) = 0 \quad (13)$$

where

$$K_{1\tau}^e = \frac{H_1(\tau)}{R_1 + R_2}, \quad K_{2\tau}^e = \frac{H_2(\tau)}{R_1 + R_2}$$

The general solution for this case must be searched depending on the values of parameters  $K_1^e$  and  $K_2^e$ . Namely, when

a)  $K_1^e > K_2^e$  the general solution is obtained in the form

$$\bar{w}(x,\tau) = C_{20} \sin K_{\tau} x + C_{20} \cos K_{\tau} x + C_{30} x + C_{40} + \int \left[ \int \bar{\varphi}(x) dx \right] dx \quad (14)$$



where

$$K_{\tau}^e = \frac{H_1(\tau) - H_2(\tau)}{R_1 + R_2}$$

while  $\bar{\varphi}(x)$  - particular integral of the differential equation (13)

b) When  $K_1^2 < K_2^2$  then

$$\bar{w}(x, \tau) = C_{1b} \int h k_{\tau} x + C_{2b} C h k_{\tau} x + C_{3b} x + C_{4b} + \int \left[ \int \bar{\varphi}(x) dx \right] dx \quad (15)$$

When however,

c)  $K_1^2 = K_2^2$  therefore, when  $H_1(\tau) = H_2(\tau)$  (the case of vertical loading only) then

$$\frac{d^4 \bar{w}(x, \tau)}{dx^4} - \varphi(x) = 0 \quad (16)$$

so the unknown function is acquired by direct successive integration of the known function given in advance  $\varphi(x)$ .

In all those cases, integration constants are obtained from the conditions along the deformations and forces in the section at the ends of the member.

When  $\bar{w}(x, \tau)$  is known, horizontal forces are determined directly from the conditions of the "length" which, in this case, with algebraic relations is

$$\left[ b_t H_i(t) + (a_t - b_t) H_i(\tau) \right] \frac{3L_i - 2L}{K_{Ni}} - \int_0^l \left( \frac{dy_i}{dx} \right) \left( \frac{dw(x, t)}{dx} \right) dx - \frac{1}{2} \int_0^l \left( \frac{dw(x, t)}{dx} \right)^2 dx = 0 \quad (17)$$

where  $a_t = (1 + \varphi_t)$ ,  $b_t = (1 + \varphi_t) \gamma_t$

$$K_{Ni} = E_i A_i$$

$\varphi_t$  - coefficient of creep

$\gamma_t$  - ageing coefficient

$A_i$  - cross section surface

In case of momentary elastic solution for  $t=\tau$  when  $\alpha_t = b_t = 1$  the conditions (17) is acquired in the form

$$H_i(\tau) \frac{3L_i - 2l}{K_{Ni}} - \int_0^l \left( \frac{dy_i}{dx} \right) \left( \frac{d\bar{w}(x,\tau)}{dx} \right) dx - \frac{1}{2} \int_0^l \left( \frac{d\bar{w}(x,\tau)}{dx} \right) dx = 0 \quad (18)$$

With the solution (14), (15) or (16) and the conditions (18) the task to establish the state of stress and strain for momentary elastic condition of the two-chord system is determined with a single sign.

When  $H_1(\tau)$ ,  $H_2(\tau)$  and  $\bar{w}(x,\tau)$  is determined, then, as the second step, it is possible to determine  $H_i(t)$  and  $w(x,t)$  for any moment of time  $t$  and any age of the material  $\tau$ .

Equation (12) in this case, is

$$C_t \frac{d^4 w(x,t)}{dx^4} + K_t^e \frac{d^2 w(x,t)}{dx^2} - \varphi(x) + (C_t - d_t) \cdot \psi(x,\tau) = 0 \quad (19)$$

where,

$$\psi(x,\tau) = \frac{d^4 \bar{w}(x,\tau)}{dx^4}$$

$C_t$  and  $d_t$  is the determined function of age and of time, and

$$K_t^e = \frac{H_1(t) - H_2(t)}{R_1 + R_2}.$$

It is now possible to write the general solution in the form for

a)  $K_t^e > 0$

$$w(t,x) = C_{1t}^a \sin K_t x + C_{2t}^a \cos K_t x + C_{3t}^a x + C_{4t}^a + \int \left[ \int \bar{\varphi}_t(x) dx \right] dx - (C_t - d_t) \int \left[ \int \psi(x,\tau) dx \right] d\tau \quad (20)$$

b)  $K_t^e < 0$

$$w(t,x) = C_{1t}^b \sinh K_t x + C_{2t}^b \cosh K_t x + C_{3t}^b x + C_{4t}^b + \int \left[ \int \bar{\varphi}_t(x) dx \right] dx - (C_t - d_t) \int \left[ \int \bar{\psi}(x,\tau) dx \right] d\tau \quad (21)$$

for the case  $K_t^e = 0$ , the function  $w(t,x)$  is obtained by the direct integration of the equation

$$\frac{d^4 w(t,x)}{dx^4} - \varphi_t(x) + (C_t - d_t) \psi(x,\tau) = 0 \quad (22)$$

Now, when  $W(t,x)$  is known from the equations (20), (21) and (22), horizontal forces are determined directly from the condition (17).

- THE CASE OF PRESTRESSED CONCRETE SYSTEMS WITH PRESTRESSING TENDONS OUTSIDE THE CROSS SECTION

The sketch 1 presents a beam system of the type with which the chord (1) is of classical reinforced concrete and the chord (2) of prestressed tendons as a case of prestressed system of reinforced concrete with prestressing tendons with one, usually upper chord, convex "upwards" made of classical reinforced concrete with significant bending rigidity while the lower chord (concave "upwards" is of classical steel or of prestressing steel and is, as a rule, without bending rigidity.

In this case, determination of stress and strain state, taking into consideration the general solution given in the preceding chapter, is significantly simplified and is reduced to solving the differential equation (12) where, it should be taken into consideration that

$$K_{tt}^2 = \frac{H_1(t)}{R_1} \quad , \quad K_{zz}^2 = \frac{H_2(t)}{R_1} \quad , \quad R_1 = E_1 J_1$$

$$R_2 = 0 \quad K_t^2 = \frac{H_1(t) - H_2(t)}{R_1}$$

and the conditions (17) with which it should be taken into account that the system (2) does not possess the property of creep.

In this case, the task is also solved in two steps. First of all, the state of stress and strain for  $t = \tau$  is determined (momentary elastic task). With the determined  $w(\tau, x)$  and  $H_1(\tau)$  and  $H_2(\tau)$  and  $w(t, x)$ ,  $H_1(t, x)$  and  $H_2(t, x)$  by modified (adaptable) equations (14), (15) or (16) namely (20), (21) or (22) with the conditions of "length" (17) and (18).

For the case of vertical loading only, when  $K_\tau^2 = K_t^2 = 0$ , the task to determine the state of stress and strain is reduced to determination of  $\bar{w}(x, \tau)$  and  $w(x, t)$  and significantly simplified conditions of the "length" (17) and (18) which, in this case, are simple algebraic equations.

## REFERENCES

- /1/ NEVILLE A.M., DILGER W.H., BROOKS J.J., Creep of plain and structural concrete. Construction Press, 1983.
- /2/ CEB-FIP Model Code for concrete structures. Bulletin d'Information CEB No. 124-125/1978.
- /3/ MØLLMAN H., Analysis of hanging roofs by means of the displacement method. Polyteknisk Forlag, Lyngby 1974.
- /4/ IVKOVIĆ M., PRAŠČEVIĆ Ž., KLEM N., Contribution of the computer analysis of hanging roofs, (in Serbo-Croatian). 14 Congress of the Yugoslav Association for Theoretical and Applied Mechanics, 1976.



## **THE ESSENTIAL STRUCTURE OF DAMAGE THEORIES**

Dusan Krajcinovic

University of Illinois at Chicago  
Chicago, Illinois 60680, U.S.A.

### **SUMMARY**

Brittle deformation processes are characterized by nucleation and growth of the grain size micro-cracks (evolution of damage) gradually weakening the meso-structure of the solid and leading ultimately to the failure of the specimen. This short state-of-art review discusses some of the seminal aspects of the newly emerging damage mechanics dealing with this class of problems. The paper discusses both mesomechanical and phenomenological theories emphasizing their accomplishments and shortcomings.

### **1. INTRODUCTION**

Until rather recently the constitutive modeling was based on the premise that a solid is a continuum with scale independent properties. The state and internal variables were selected primarily on the basis of macroscopic observations and had little in common with the underlying physics of the phenomenon. The ensuing plethora of clever stratagems and cute artifices created just as many problems as they purportedly solved. Naturally, with an almost limitless supply of 'material' parameters it was not difficult to fit a particular set of curves with a desired accuracy.

Yet as most physicist knew for some time the mechanical properties of the solid entirely depend on its microstructure. The resistance to the reversible stretching of its crystalline lattice (elastic parameters) are related to the primary bonds keeping the particles of the solid together. The inelastic behavior is, in contrast, traceable to the defects in the crystalline lattice and their kinetics during the deformation process. Naturally, keeping track of every bond and each defect requires a horrendously large database relegating such procedures to the realm of statistical physics [1-2].

On the intermediate or meso-scale the bookkeeping becomes much simpler but still prohibitive in the case of nonuniform macro-fields. Each crystal is considered a continuum (with a defined structure), while the atomic defects such

as dislocations and ruptured bonds are lumped into slip systems and microcracks. Despite some spectacular accomplishments [3-6] the engineering community remained if not ignorant than at least unimpressed by these efforts.

With a strongly developed predilection of engineers for the continua and an equally strong suspicion of arcane theories dealing with objects not visible to the naked eye, it appears that the phenomenological single scale theories are here to stay. And, indeed, therein is the crux of the dilemma. A typical phenomenological model combines the computational expedience (inherent to manipulations with gradually changing continuous fields) and the often bewildering uncertainties related to arbitrary choices of the internal variables and flow rules.

A rational approach adhering to the physics of the phenomenon and retaining tractability must by necessity span at least two scales. The distinction between the two scales and the micro- and macro-defect is by no means fortuitous. On the micro-scale an otherwise macro-homogeneous solid is all but homogeneous with randomly distributed material properties. Consequently, a grain size microcrack can propagate only along the cleavage plane even though the stresses in some other planes might be higher. A macro-defect, however, 'sees' the surrounding material as homogeneous and grows according to the dictates of the stress field.

The primary objective of this paper is to discuss some of the basic issues of the mechanical response of brittle solids on both phenomenological and micromechanical grounds. The confines of time and space dictate the reduction of the scope to the isothermal and time-independent brittle processes and infinitesimal strains.

## 2. THERMODYNAMIC PRELIMINARIES

The infinitesimal macro-strain fields admit additive decomposition

$$\underline{\epsilon} = \underline{S} : \underline{\sigma} + \underline{\epsilon}^P \quad (1)$$

where  $\underline{\epsilon} = \underline{\epsilon}^P$  when  $\underline{\sigma} = 0$  is the plastic strain. In (1)  $\underline{S}(x)$  is the compliance tensor reflecting the crystalline lattice of the solid and the already accumulated defects in the neighborhood of the material point  $x$ . Since a point does not have a structure the preceding sentence invokes the notion of the representative volume element (RVE) (or unit cell in sense of Hill) which in a statistical sense defines the smallest volume of the solid which in respect to a given variable behaves as the continuum itself. In other words, the disparity between the statistical moments of a given variable taken over the RVE and any larger volume centered in  $x$  are within a prescribed margin of error.

From the present point of view it is then possible to define a configurational space containing all relevant informations (database) about the defects in the RVE which define the state in  $x$ . This configurational space will be referred to as the recorded history  $H(x)$ . The flux  $dH(\underline{\sigma}, H)$  in a physically acceptable manner will define the irreversible (energy consuming) rearrangements of the crystalline lattice. Disregarding the diffusional growth of spherical vacancies, phase transformations, and some other less frequent mechanisms of structural changes the present paper will briefly emphasize the major differences between the slips and microcracks (i.e. ductile and brittle response). After that the discussion will be limited exclusively to the brittle response.

The process of slip is often depicted by stating that during such a process material slips through the crystalline lattice [4] which remains unperturbed and undistorted. In other words, as a mobile dislocation glides along an operative slip system for every primary bond ruptured ahead of the dislocation another is reinstated in its wake. Hence the number of primary bonds remains virtually unchanged during a plastic deformation. Since the elastic properties depend on the primary bonds they are not affected by ductile processes (excluding geometric instabilities associated with large strains). Since the lattice is not distorted the plastic (residual) strains will not be removed during the removal of stresses (unloading).

In contrast, the microcracking is in essence a process of creation of new internal surfaces, i.e. rupture of primary bonds. Not surprisingly, the microcracking strongly affects the elastic parameters (i.e. the compliance of the solid). The elastic energy stored in the distorted lattice (to accommodate a crack) tends to eliminate the inelastic stresses (associated with the crack opening) in unloading. The residual strains in brittle processes are not the result of ductility (slips) but friction, grain interlock and bridging over the uneven crack surfaces.

Consistent with the physics of the deformation processes reasonable choices for the internal variables defining the ductile and brittle deformation processes are:

- path traversed by an individual dislocation and the number of ruptured bonds on the micro-scale,
- shears on the operative slip bands and active microcracks on the meso-scale, and
- appropriate scalar (work-hardening) or tensorial (strain-hardening) functions of the plastic strain and the compliance on the macro-scale.

In all cases the selected internal variables can be readily measured and identified in experiments satisfying one of the most important requirements for their selection [7]. They can also be related to each other by an averaging or homogenization process starting from the micro- to the macro-scale.

For a path-dependent process the expression (1) should be rewritten in its incremental form

$$d\underline{\underline{\varepsilon}} = \underline{\underline{S}} : d\underline{\underline{\sigma}} + d\underline{\underline{S}}^d : \underline{\underline{\sigma}} + d\underline{\underline{\varepsilon}}^p \quad (2)$$

where as in [8]

$$d\underline{\underline{S}}^d(\underline{\underline{\sigma}}, H) = \underline{\underline{S}}(\underline{\underline{\sigma}}, H + dH) - \underline{\underline{S}}(\underline{\underline{\sigma}}, H) \quad (3)$$

represents the change in compliance attributable to the evolution of damage. In keeping with the objective the plastic strain will be neglected in the sequel.

Introduce the Gibbs energy of the RVE with volume  $V$  as

$$\Psi(\underline{\underline{\sigma}}, H) = V \underline{\underline{\sigma}} : \underline{\underline{\varepsilon}} - \Phi(\underline{\underline{\varepsilon}}, H) \quad (4)$$



where  $\phi$  is the Helmholtz free energy of the RVE. Consequently,

$$\tilde{\epsilon} = \frac{1}{V} \frac{\partial \Psi}{\partial \sigma} \quad (5)$$

Also, from (2) and (5)

$$\tilde{S} = \frac{1}{V} \frac{\partial^2 \Psi}{\partial \sigma \partial \sigma} \quad (6)$$

while

$$d^1 \tilde{S} = \frac{1}{V} \frac{\partial^2 (d^1 \Psi)}{\partial \sigma \partial \sigma} \quad (7)$$

where as in (3) the superscript '1' denotes inelastic changes in a process during which  $H$  changes into  $H + dH$ .

As a consequence of the second law of thermodynamics [8]

$$d^1 \Psi = \frac{\partial \Psi}{\partial H} dH \geq 0 \quad (8)$$

The utility of the stress-strain relation (2) is contingent on the availability of the expression for the inelastic change in the Gibbs energy of the RVE containing a crack. To explore the possibility of accomplishing this task consider a single crack, circumscribed by a closed contour  $L$ , embedded into volume  $V$  of elastic material. Consider a process during which the surface area is increased through rupture of the bonds at the crack tip. The change in the Gibbs energy [8,9] consists of two parts

$$d^1 \Psi = \int_L \left[ \left( \frac{\partial W}{\partial a} - 2\gamma \right) \delta a \right] dL \geq 0 \quad (9)$$

where  $W(\sigma, H)$  is the elastic energy associated with the distortion of the elastic lattice accommodating the crack and  $\gamma$  the surface energy. Also  $\delta a$  is the advance of the crack tip in the direction normal to  $L$ .

The first term under the integral in (9) can be computed as in [8,9]

$$\frac{\partial W}{\partial a} = \lim_{\Delta a \rightarrow 0} \frac{1}{\Delta a} \frac{1}{2} \int_0^{\Delta a} T_1 [u_1] dr \quad (10)$$

The tractions  $T$  at the distance  $r$  ahead of the original crack tip are

$$T_1 = K_1 r^{-1/2} + \dots \quad (11)$$

where  $K$  are the stress intensity factors (SIF). Similarly the crack opening displacements (COD) behind the crack tip are

$$[u_i] = C_{ij}K_j(\Delta a - r)^{-1/2} + \dots \quad (12)$$

Thus, from expressions (10) to (12) it follows that

$$d^1\psi = \int_L [(G - 2\gamma)\delta a] dL \geq 0 \quad (13)$$

where

$$G = \frac{\pi}{4} C_{ij}K_iK_j \quad (14)$$

is the energy release rate. Thermodynamically,  $G$  and  $2\gamma$  are the driving and resisting thermodynamic forces conjugate to the flux  $\delta a$  (increase in the crack size).

From (7), (12) and (14) the inelastic change in the compliance (which can be selected as the internal variable [10]) is

$$d^1S_{ijmn} = \frac{\pi}{2V} \int_L \left[ C_{pq} \frac{\partial K_p}{\partial \sigma_{ij}} \frac{\partial K_q}{\partial \sigma_{mn}} \delta a \right] dL \quad (15)$$

An entirely equivalent formulation is possible via the Eshelby inclusion method [11,12] identifying the CODs with the eigenstrains [5]. The identity can be verified using the expressions for the SIFs and CODs from [13].

The inequality (9) assuming it to be valid pointwise can be written for the case when the healing is excluded ( $\delta a > 0$ ) in the form of Griffith's inequality

$$F(\sigma, H) = G - 2\gamma \geq 0 \quad (16)$$

such that

$$\delta a = 0 \quad \text{when} \quad F < 0 \quad (17)$$

In the case of many cracks in RVE the conditions (15) written for individual cracks form a polyhedral hypersurface enveloping the loci of all points in the stress space reachable without energy

### 3. ANALYTICAL MODEL

#### 3.1 Mesomechanical Models

As demonstrated above the stress-strain relationship (2) for a volume  $V$  of brittle solid containing a single crack (and mapping on a point  $x$  of the continuum) can be written providing that it is possible to derive the expressions for  $C$  and  $K$  in (14), and that a kinetic equation  $\delta a = \delta a(\sigma, H)$  is available. In reality the problem is further complicated by the presence of many cracks of different sizes and orientations in  $V$ . The determination of the

external fields of  $N$  cracks embedded in  $V$  entails solution of  $N$  coupled integral equations [6]. Since  $N$  is by definition large and crack fields random the problem does not admit an analytical solution.

The prohibitive computational effort associated with the more rigorous models motivated formulation of the effective field theories. Assuming [6] that: (a) the external fields of a particular defect weakly depend on the exact position of the adjacent defects in  $V$ , and that (b) the external stress field of each defect is equal to the macro-stress, the problem becomes solvable via a formalism known as the self-consistent model. The assumption (b) eliminates the need for the integral equations. The assumption (a) reduces the number of random variables by  $3N$  and eliminates from considerations the direct interaction of the neighboring defects. Consequently, the method becomes suspect for higher defect concentrations characteristic of incipient localization. Within the framework of these models the compliance of the RVE is obtained summing the contributions of all cracks over all sizes and orientations. For a large number of cracks  $N$  the sums are recast into integrals over the probability density functions for the radii and orientations of active cracks [11,12].

The principal advantage of the micromechanical methods based on the effective continua [11,12,15], etc. is a direct consequence of their adherence to the physics of the phenomena. The kinetic laws are derived (rather than a priori postulated) from the distribution of toughnesses in the meso-structure allowing unambiguous identification of the material parameters. Nevertheless, despite considerable success in replicating the experimentally determined trends the referenced literature also identifies the limitations of these methods. Most of those limitations stem from the paucity of the analytical solutions for the SIFs embedded in anisotropic solids, branched or kinked cracks, etc. In fact, with possible but rare exceptions the mesomechanical solutions are limited to the uniform macro-fields and loading cases resulting in isotropic and transversely isotropic crack distributions.

### 3.2 Phenomenological Models.

The above mentioned limitations of the mesomechanical models present a strong stimulus to the development of phenomenological theories. An entire class of models have been formulated (see Lemaitre or Murakami in [11], or [16]) following this simple recipe: select a priori a suitable damage variable, define an objective form of the Helmholtz free energy, select (somewhat arbitrarily) a damage law (either in form of a damage potential or a set of evolution equations) and use a sufficient number of parameters to fit a given set of experimental curves. While computationally efficient these methods are by their very nature restricted in application to the cases for which they are fitted.

Rather recently Ortiz [10] proposed an interesting model. Integrating twice the expression (6)

$$\psi(\underline{\sigma}, H) = \frac{1}{2} \underline{\sigma} : \underline{S}(H) : \underline{\sigma} - \psi^0(H) \quad (18)$$

where  $\psi^0(H)$  is the energy dissipated in creation of new (crack) surfaces in  $V$ . From the second law of thermodynamics (8)

$$D = \frac{1}{2} \underline{\sigma} : d^1 \underline{S} : \underline{\sigma} - d^1 \psi^0 \geq 0 \quad (19)$$

Provided that a flow rule such as [10,17]

$$d^1 \underline{S} = \dot{\mu} R(\underline{\sigma}) \quad (20)$$

can be specified the flow potential can be derived directly from (19). Denoting

$$B(\underline{\sigma}) = \frac{1}{2} \underline{\sigma} : \underline{R}(\underline{\sigma}) : \underline{\sigma} \quad d^1 \psi^0 = \dot{\mu} f(\mu) \quad (21)$$

the flow potential is from (19)

$$F(\underline{\sigma}, \mu) = B(\underline{\sigma}) - f(\mu) \geq 0 \quad (22)$$

since excluding healing  $\mu > 0$ . The identity of (16) and (22) for a single crack, when  $B = G$ ,  $\mu = a$  and  $f(\mu) = 2\gamma$ , is evident. As in plasticity it is now possible to write from (19)

$$\begin{aligned} \dot{\mu} > 0 & \quad \text{iff} \quad F = 0 \quad \text{and} \quad (\partial F / \partial \underline{\sigma}) : \underline{\sigma} \geq 0 \\ \dot{\mu} = 0 & \quad \text{otherwise} \end{aligned} \quad (23)$$

which provides the distinction between loading and unloading.

The unilateral constraints imposed by cracks on the displacement fields are, perhaps, the primary impediment in the formulation of a reasonably simple but rational phenomenological damage theory. The single most distinguishing aspect of the damage process is the dependence of the COD and crack growth mode on the sign of the normal stresses to which it is exposed. Since the flux, the change in compliance (15), depends on the mode of the crack growth it appears reasonable to modify the algorithm in [10] in a manner conforming to the physics of the phenomenon. This task would require the establishment of the deformation maps (not unlike those in [18]) defining regions in the stress space in which a particular crack growth mode governs.

As an illustration consider a case when one of the three principal stresses is negative and held constant. If the other two principal stresses are tensile and approximately equal the existing cracks will grow in a self-similar manner remaining planar. If one of the stresses is much smaller a crack will exhibit directional instability [19] and kink into the direction minimizing the shear stresses on the kinked part. The kinking becomes much more pronounced when the larger of two stresses is compressive. Finally, when all three principal stresses are compressive the deformation becomes ductile. The brittle-ductile transition depends on the size of the pupative crack and the yield stress and critical SIF of the material (i.e. the ductility ratio [20]).

Consequently, the two types of the damage evolution are never coincidental in a given point as suggested in [10]. Instead it is an either-or proposition since a crack either kinks or grows in its own plane depending on the state of stress.

In the case when the kinking is either absent or can be neglected the inelastic compliance rates can be written as [11,21]

$$d^1 S_{ijmn}^I = \dot{\mu} C n_i n_j n_m n_n \quad (24)$$

$$d^i S_{ijmn}^{II} = \mu \frac{2C}{2-\nu} (\delta_{in} n_j n_m + \delta_{jm} n_i n_n - 2n_i n_j n_m n_n) \quad (25)$$

where the two components of the  $d^i S$  are associated with the normal (tensile) and shear stresses in the plane of the crack. For the  $N$  non-interacting penny-shaped crack of the same radius  $a$

$$C = 8 \frac{1 - \nu^2}{E} \quad (26)$$

while

$$\mu = \frac{Na^3}{\nu} \quad (27)$$

is the crack density parameter suggested first in [22].

The derivation is somewhat more complicated in the case of the kinking cracks. However, using the modified first order solution of Cotterell and Rice [23] the SIFs  $K$  of the kinked crack can be determined with a surprising degree of accuracy from the stresses external to the pupative (straight) crack. Thus, it is always, at least in principle, possible to write

$$K_i = M_{ijk} k_j \quad (28)$$

where  $k$  are the SIFs of the pupative crack. The coefficients  $M$  are readily available when the length of the kink is much smaller than the radius of the pupative crack  $l \ll a$ . If  $l \gg a$  the derivation of the coefficients  $M$  involves the determination of the stresses external to the pupative crack along the path of the prospective kink and a numerical quadrature of a definite integral. A simpler deduction of the SIFs  $K$ , using approximate expressions (such as one in [20]) may ultimately be a much more appealing alternative.

The proposed strategy is sketched here using a broad brush. A number of outstanding problems remains open. Among them is the formulation of the flow potential in the case when the crack kinking dominates (compression). The presence of friction will preclude from consideration the normality structure of the kinetic processes [23] and introduce a number of problems in modeling the unloading phase of the process.

Finally, it must be pointed out that the kinetic equations must be consistent with the mode of the ultimate failure. In the presence of substantial tensile stresses the macrofailure is typically a result of the runaway instability of a single, critical crack. In contrast, when confined and exposed to compressive stresses an otherwise brittle material fails in the localization mode [20] during which the microcrack density in a narrow band becomes so large that the direct interaction between cracks cannot be neglected.

#### 4. CONCLUSIONS

This short and unpretentious state-of-art review obviously presents the personal opinion of the author. The somewhat unsettled state of affairs of this relatively new branch of mechanics makes this enterprise a risky one. A variety of different and often contradictory concepts and models have yet to be reconciled with each other and sorted into a theory with a well defined structure. Succinctly stated, the damage mechanics is, as expected, still in the state of flux. However, a lot has been done in the last decade and pieces of the mosaic

are emerging in the literature at an increasing rate. In particular, the development of the mesomechanical models is presently at a stage allowing a careful look at the phenomenological models. And that is, in the opinion of the author, the most important part of the development of the damage mechanics.

### 5. ACKNOWLEDGEMENT

The author gratefully acknowledges the financial support rendered by the U.S. Department of Energy (Office of Basic Energy Sciences) and Air Force Office of Scientific Research (Directorate of Aerospace Science, Civil Engineering Program) research grants which made this work possible.

### REFERENCES

1. WEINER, J. H. - Statistical Mechanics of Elasticity, A Wiley- Interscience Publ. J. Wiley and Sons, New York, 1983.
2. LATANISION, R. M. and PICKENS, R. J. Eds. - Atomistics of Fracture, Plenum Press, New York, 1983.
3. GITTS, J. and ZARCA, J. Eds.- Modelling Small Deformations of Polycrystals, Elsevier Applied Science Publ., London, 1986.
4. ASARO, R.J. - 'Micromechanics of Crystals and Polycrystals', Advances in Applied Mechanics, Vol. 23, Eds. J. W. Hutchinson, T. Y. Wu, Academic Press, Inc., New York, 1983.
5. MURA, T. - Micromechanics of Defects in Solids, Martinus Nijhoff Publ., The Hague, 1982.
6. KUNIN, I. A. - Elastic media with Microstructure II, Springer- Verlag, Berlin, 1983.
7. HART, E. W., LI, C.-Y. and WIRE, G. L. - 'Phenomenological Theory A Guide to Constitutive Relations and Fundamental Deformation Properties', Constitutive Relations in Plasticity, Ed. A. S. Argon, the MIT Press, Cambridge, MA., 1975.
8. RICE, J. R. - 'Continuum Mechanics and Thermodynamics of Plasticity in Relation to Microscale Deformation Mechanisms', Constitutive Relations in Plasticity, Ed. A. S. Argon, The MIT Press, Cambridge, MA., 1975.
9. IRWIN, G. R. - 'Analysis of Stresses and Strains Near the End of a Crack Traversing a Plate', J. Appl. Mech. 1957, 24, 361.
10. ORTIZ, M. - 'A Constitutive Theory for the Inelastic Behavior of Concrete', Mech. of Materials, 1985, 4, 67.
11. KRAJCINOVIC, D. and LEMAITRE J., Eds. - Continuum Damage Mechanics: Theory and Applications, Springer Verlag, Wien, 1987.
12. SUMARAC, D. and KRAJCINOVIC, D. - 'A Self-Consistent Model for Microcrack Weakened Solids', Mech. of Materials, 1987, 6, 39.
13. HOENIG, A. - 'The Behavior of a Flat Elliptical Crack in an Anisotropic Body', Int. J. Solids Structures, 1978, 14, 925.
14. RUDNICKI, J. W. and RICE, J. R. - 'Conditions for the Localization of Deformation in Pressure-Sensitive Dilatant Materials J. Mech. Phys. Solids, 1975, 23, 371.

15. KRAJCIKOVIC, D. and FANELLA, D. - 'A Micromechanical Damage Model for Concrete', Eng. Fracture Mech., 1986, 25, 585.
16. KRAJCIKOVIC, D. - 'Continuous Damage Mechanics - 1986 Update' Applied Mechanics Update 1986, Eds. Steele, C. R. and Springer G. S., ASME Publ., New York, 1986.
17. LUBLINER, J. - 'On Thermodynamic Yield Criteria', Acta Mech., 1980, 37, 259.
18. ASHBY, M. F. - 'Micromechanics of Fracture in Static and Cyclic Failure', Fracture Mechanics, Ed. R. A. Smith, Pergamon Press, Oxford, U.K., 1979.
19. LAWN, B. R. and WILSHAW, T. R. - Fracture of Brittle Solids, Cambridge Univ. Press., Cambridge, U.K., 1975.
20. HORII, H. and NEMAT-NASSER, S. - 'Brittle Failure in Compression: Splitting, Faulting and Brittle-Ductile Transition', Phil. Trans. Royal Soc., London, 1986, A319, 337.
21. SUMARAC, D. - Self-Consistent Model for the Brittle Response of Solids, Ph.D. thesis, CEMM Dept., Univ. of Illinois at Chicago, 1987.
22. BUDIANSKY, B. and O'CONNELL, R. J. - 'Elastic Moduli of a Cracked Solid', Int. J. Solids Structures, 1976, 12, 81.
23. COTTERELL, B. and RICE, J. R. - 'Slightly Curved or Kinked Cracks', Int. J. of Fracture, 1980, 155.

APPLICATIONS DE CONNAISSANCES RÉCENTES DANS LA CONCEPTION D'OUVRAGES  
EN BÉTON

Renaud FAVRE

Professeur à l'Ecole Polytechnique Fédérale de Lausanne  
EPFL/IBAP, 1015 Lausanne (Suisse)

RÉSUMÉ

Cette contribution tente de montrer quelques répercussions concrètes que peuvent avoir des résultats de recherches théoriques et expérimentales sur la conception d'ouvrages en béton armé ou précontraint. Dans le cas d'élargissement ou de renforcement de ponts avec du nouveau béton, on montre la part importante d'une force de précontrainte qui se diffuse du nouveau dans l'ancien béton, malgré la disposition d'une brèche. Cette diffusion peut en particulier créer des problèmes de couture.

D'autre part, un exemple de piles encastrées malgré la complexité de l'ouvrage est présenté, permettant une conception simplifiée en évitant entre autres des palées obliques inesthétiques ou des mesures contre le soulèvement des appuis.



## 1. INTRODUCTION

Afin d'être compétitif, l'ingénieur doit continuellement s'adapter aux progrès des connaissances dans son domaine. En ce qui concerne les ouvrages en béton armé ou précontraint, la recherche a fait d'énormes progrès depuis une dizaine d'années pour mieux saisir le comportement réel des structures et mieux discerner les éléments et critères essentiels qui interviennent dans la conception d'un ouvrage de bonne qualité, durable, sûr et néanmoins économique.

C'est ainsi qu'une meilleure connaissance sur la réalisation de bétons à haute performance permet de réduire la fissuration et la déformation des structures. Elle permet grâce à des bétons plus fluides et contenant moins d'eau, de réaliser un enrobage de l'armature plus compact, plus dense, plus imperméable ce qui favorise grandement la protection anticorrosive du béton. Les connaissances accrues concernant le rôle primordial de l'état permanent sur l'aptitude au service et la durabilité ont permis de concevoir des ouvrages qui travaillent dans les meilleures conditions possibles sous l'effet des charges permanentes en tenant compte des effets différés. Les charges mobiles, rarement à l'origine d'ennuis, peuvent être traitées de façon beaucoup plus permissives en ce qui concerne l'aptitude au service.

En Suisse, on tâche de tirer profit des enseignements de la recherche en portant un soin particulier à la conception des ouvrages, aux détails constructifs, à la qualité du béton, à son enrobage et à sa ductilité. C'est ainsi que la nouvelle norme SIA 162 prévoit une armature minimale, graduée en fonction des différents cas, mais devant toujours assurer une ductilité suffisante et limiter l'ouverture des fissures [1]. Elle prévoit également, pour des structures exposées aux intempéries ou agents agressifs (béton apparents, ponts, tunnels) de limiter les contraintes dans l'acier sous l'effet des charges quasi-permanentes.

Une conséquence de la ductilité élevée du béton armé est la possibilité d'espacer ou même de supprimer les joints de dilatation. Elle permet également d'accepter des déformations imposées importantes dans les structures (variations de température, retrait,

tassements) sans compromettre leur qualité à l'état de service ni leur résistance à l'état de ruine.

2. ELARGISSEMENT OU RENFORCEMENT DE PONTS

Toute une série de ponts d'autoroute construits en Suisse entre 1960 et 1970 ne comportent pas de voies d'arrêt et doivent être élargis afin de créer le même profil que sur le tracé en terre plein et afin de faciliter l'entretien. C'est ainsi p.ex. que la plupart des ponts d'autoroute entre Genève et Lausanne sont en train d'être élargis (Fig. 1).

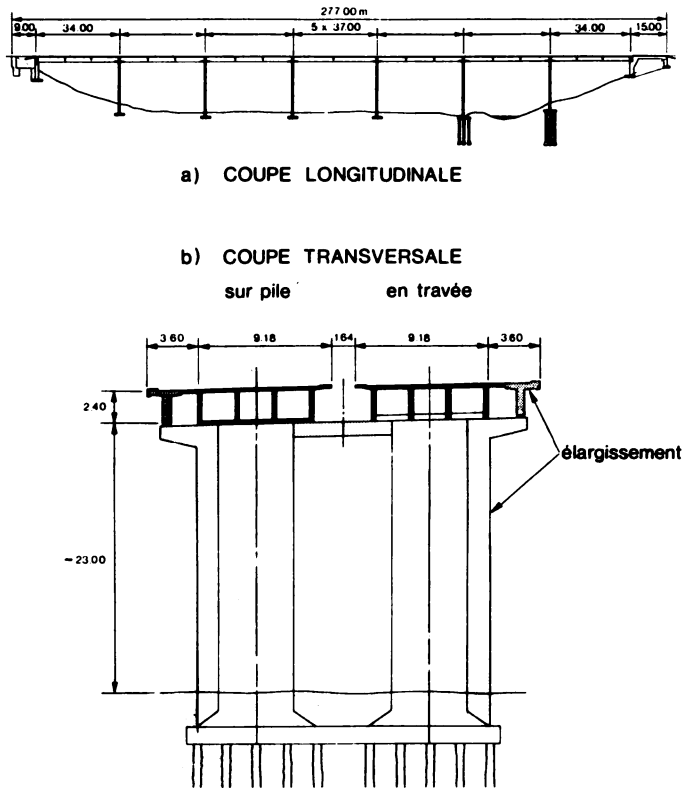


Fig. 1 Pont sur l'Aubonne de 1962  
 a) coupe longitudinale  
 b) coupe en travers avec l'élargissement projeté

D'autres ouvrages, en particulier des ponts biais en béton armé sans précontrainte, doivent être renforcés pour endiguer l'évolution continuelle des flèches. A titre d'exemple, nous montrons à la Fig. 2 le pont très biais de Bibersee près de Cham, canton de Zoug [2]. Ce pont, construit en 1969, accusait des flèches de près de 300 mm qui continuaient à augmenter année après année. C'est pourquoi il a dû être renforcé par des poutres précontraintes.

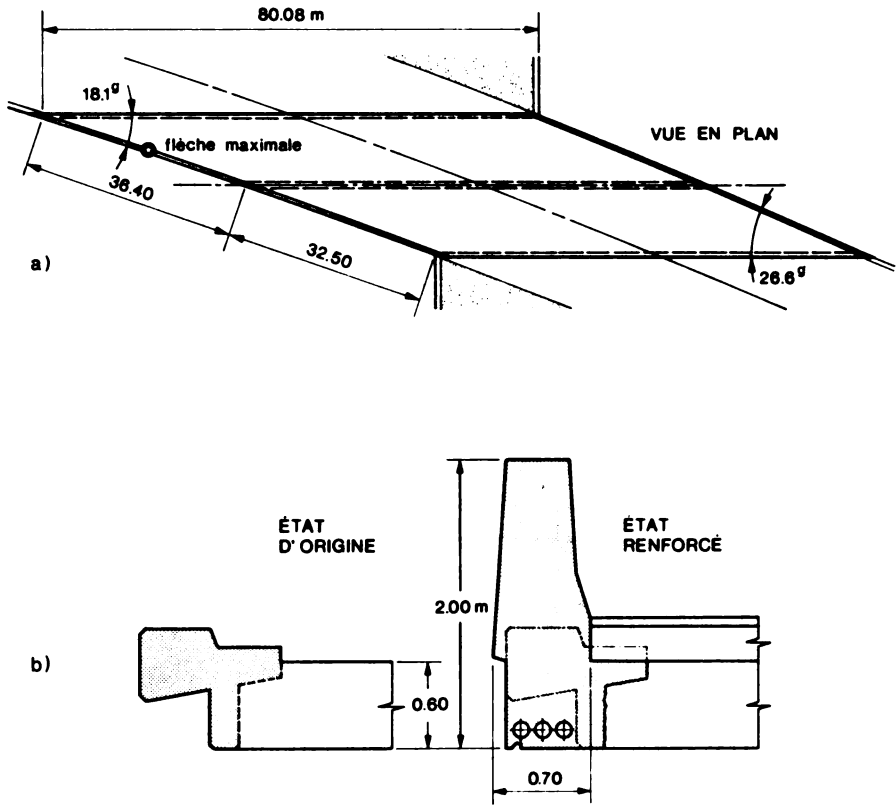


Fig. 2 Pont biais de Cham  
a) vue en plan  
b) coupe en travers

Le problème qui se pose lorsque du béton jeune est ajouté à un béton ancien provient des effets différés de ce jeune béton. Pour limiter ces effets, on tâche de laisser une brèche provisoire, si possible pendant quelques semaines, entre l'ancien et le nouveau béton. Ainsi, lors de la mise en précontrainte de ce dernier, il pourra se raccourcir librement et commencer à subir les effets du fluage et du retrait sans être entravé par l'ancien béton. Néanmoins, dès la suppression de cette brèche, le raccourcissement résiduel du béton jeune va être entravé par le béton ancien. Cette entrave, en vertu du principe de St-Venant, va avoir lieu sur une petite longueur du joint entre ancien et nouveau béton. Cette petite longueur est de l'ordre de 1 à 1,5 fois la largeur de l'élargissement  $b$  (Fig. 3).

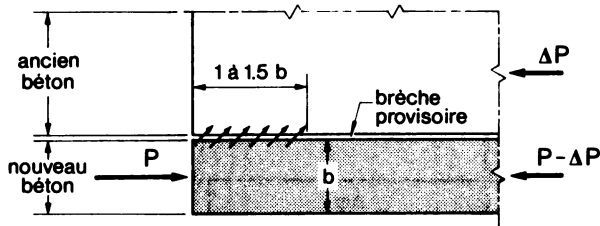


Fig. 3 Vue en plan de la diffusion de la précontrainte  $P$

Etudions quelle est l'importance de  $\Delta P$ , donc de la partie de l'effort normal dû à la précontrainte  $P$  qui va quitter le béton jeune et pénétrer dans l'ancien béton [3, 4, 5]. Admettons que le problème soit symétrique (Fig. 4).

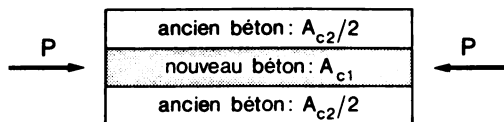


Fig. 4 Modèle de calcul (vue en plan)

L'équation de compatibilité de déformation au temps  $t_{..}$  s'écrit :

$$\Delta\phi \frac{P}{A_{c1} \cdot E_{c1}} - (1 + \chi \cdot \Delta\phi) \frac{\Delta P}{A_{c1} \cdot E_{c1}} = \frac{\Delta P}{A_{c2} \cdot E_{c2}} (1 + 0.4) \quad (1)$$

S'il n'y a pas de brèche, l'équation (1) devient

$$(1 + \phi) \frac{P}{A_{c1} \cdot E_{c1}} - (1 + \chi \cdot \phi) \frac{\Delta P}{A_{c1} \cdot E_{c1}} = \frac{\Delta P}{A_{c2} \cdot E_{c2}} (1 + 0.4) \quad (2)$$

Mais revenons au cas plus favorable (1) où nous voulons montrer que  $\Delta P$  est néanmoins très important.  $\Delta\phi$  représente le coefficient de fluage qui reste après la liaison,  $\chi$  le coefficient de vieillissement. 0.4 représente la partie différée de la déformation élastique du vieux béton.

Admettons  $A_{c2} = 2.7 A_{c1}$  et  $E_{c2} = 1.1 E_{c1}$  :

$$\Delta\phi \cdot P - (1 + \chi \cdot \Delta\phi) \Delta P = 0.47 \cdot \Delta P$$

d'où

$$\Delta P = \frac{\Delta\phi}{1.47 + \chi \cdot \Delta\phi} \cdot P \quad (3)$$

Exemples numériques :

$$\begin{aligned} \Delta\phi = 1.0 & , \quad \chi = 0.8 & \rightarrow & \Delta P = 0.44 P \\ \Delta\phi = 1.5 & , \quad \chi = 0.8 & \rightarrow & \Delta P = 0.56 P \\ \Delta\phi = 2.0 & , \quad \chi = 0.8 & \rightarrow & \Delta P = 0.65 P \end{aligned}$$

On constate donc, que même si on attend longtemps avant de lier le nouveau béton à l'ancien et que  $\phi \rightarrow 1$ , il y aura avec le temps néanmoins une part très importante de  $P$  qui va quitter le nouveau béton ( $\Delta P \geq 0.44 P$ ) et créer des problèmes de couture sur la longueur  $l$  à  $1,5 b$  de la liaison (voir Fig. 3). Il faudra donc créer une liaison appropriée transversalement au joint de bétonnage, qui soit capable de reprendre l'effort rasant  $\Delta P$ , ce qui n'est pas aisé, du moins dans l'ancien béton.

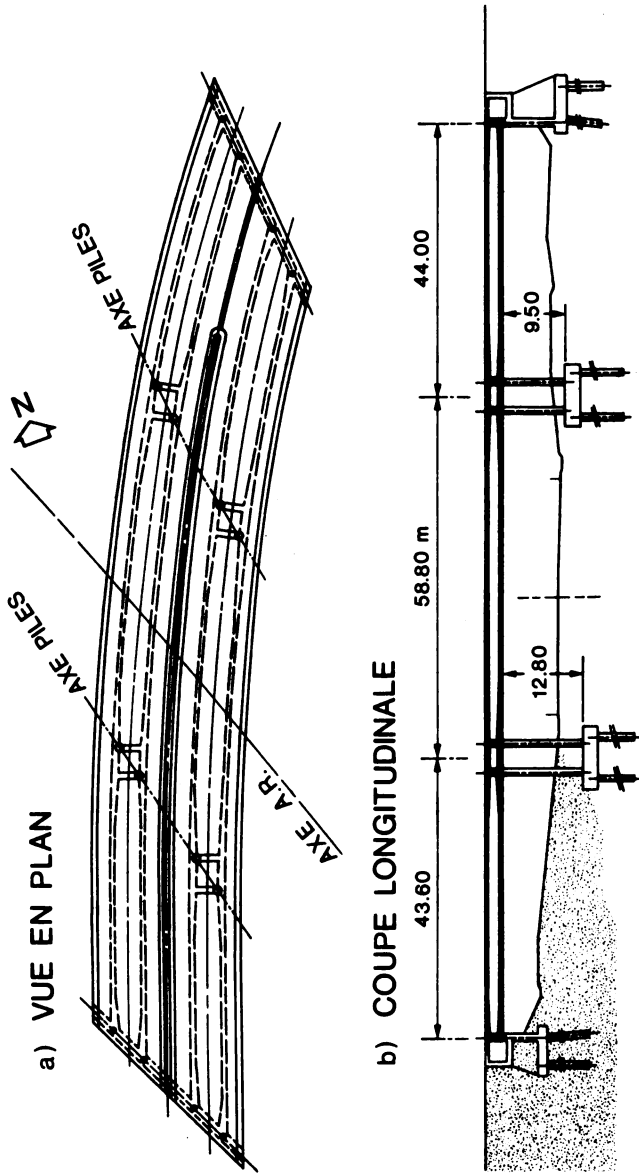
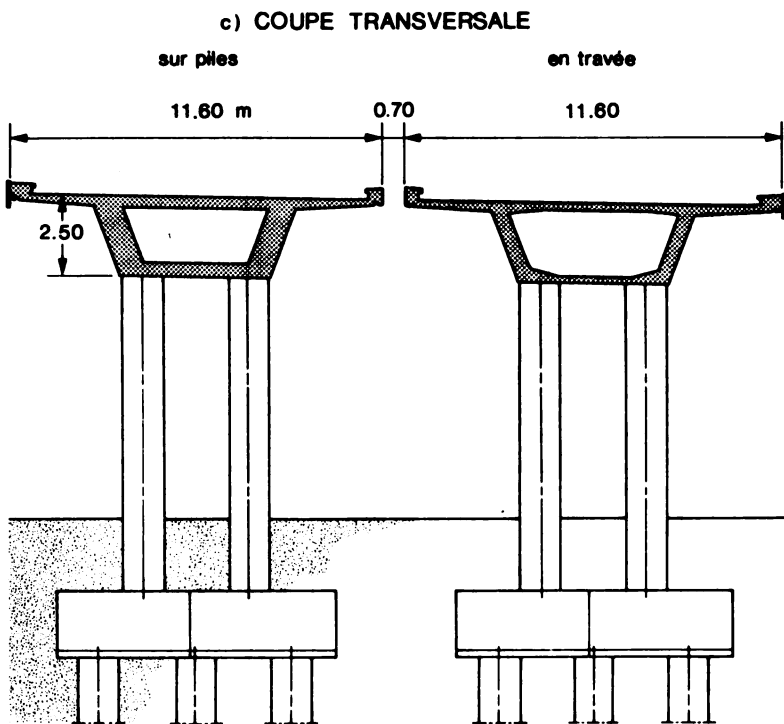


Fig. 5 L'ouvrage d'art OA 418 à St-Julien, Genève  
 a) vue en plan  
 b) coupe longitudinale



**Fig. 5** L'ouvrage d'art OA 418 à St-Julien, Genève  
 c) coupe en travers

### 3. EXEMPLE D'UN PONT BIAIS ET COURBE À PILES ENCASTRÉES

L'autoroute de contournement de Genève actuellement en construction nécessite la création d'un grand échangeur à St-Julien. Une route cantonale importante y franchira l'autoroute sur deux grands ponts contigus biais et courbes. Le début des travaux est programmé pour l'automne 1988 (Fig. 5).

Notons que les points hauts des câbles de précontrainte sont situés au droit des piles pour chacune des âmes. De plus, la précontrainte balance entièrement les charges permanentes.

Grâce aux travaux de thèse [6, 7, 8] dont celui de D. Najdanovic de l'Université de Belgrade, il a été possible de concevoir ce pont en simplifiant grandement les problèmes d'appui. En effet, des piles encastrées dans les fondations et la superstructure assurent la stabilité de l'ensemble, encastrant le caisson à la torsion; ces piles reprennent les efforts longitudinaux et transversaux tout en étant capable de supporter le raccourcissement du tablier par suite du retrait, du fluage et d'une baisse de température. La grande ductilité de ces piliers, grâce en particulier à un frettage adéquat, à la relaxation du béton et la prise en compte du comportement réel permettent d'assurer une aptitude au service et une sécurité à la ruine satisfaisantes. Il s'agit là d'un exemple d'application concret de colonnes sollicitées, outre l'effort normal  $N$ , par des déformations imposées dues surtout au raccourcissement du tablier et par certains moments  $M$  dus à des actions directes (forces de freinage, de frottement des appuis sur culées et du vent), pour lesquels la capacité portante doit être vérifiée. Les applications aux bâtiments, où il y a un noyau stabilisateur, sont déjà fréquentes en Suisse. Dans ce cas, aucun moment dû aux actions directes n'est à reprendre et le problème en est simplifié. Jusqu'à des angles imposés aux extrémités des colonnes de 1 à 2 %, la capacité portante vis-à-vis de l'effort normal  $N$  n'est pratiquement pas affectée. Il y a en effet un recentrage de  $N$  dans la colonne, grâce à la formation de rotules plastiques, pour autant que la ductilité soit assurée par un frettage adéquat.



Quant à l'aptitude au service, il s'agit d'éviter une fissuration des colonnes et un éclatement du béton d'enrobage. Dans le bâtiment, on adoptera en Suisse comme critères, des limitations pour les déformations relatives de l'acier à  $\epsilon_s = 1.5 \%$ . (acier tendu) et  $- 2.3 \%$ . (acier comprimé). Pour le pont de la Fig. 5, on a adopté des critères plus sévères afin de tenir compte de l'exposition aux intempéries, à savoir  $1.0 \%$  resp.  $- 1.5 \%$ .

#### 4. CONCLUSIONS

Il nous paraît indispensable de faire bénéficier la conception d'un ouvrage des enseignements récents de la recherche. Il ne s'agit pas du tout de vouloir rendre les ouvrages meilleurs marché au détriment de la qualité, mais bien au contraire d'introduire dans la pratique des notions et des outils qui permettent une amélioration du comportement (p.ex. suppression de joints, d'appareils d'appuis, amélioration de la sécurité au renversement, renforcement efficace par précontrainte additionnelle etc.). Ce qui est également essentiel, c'est que les normes et règlements en vigueur autorisent l'application de ces connaissances récentes et que les ingénieurs apprennent à les maîtriser.

#### RÉFÉRENCES

1. JACCOUD, J.-P. - Armature minimale pour le contrôle de la fissuration des structures en béton - thèse de doctorat, Ecole Polytechnique Fédérale de Lausanne, 1987.
2. ANDREY, D., SUTER, R. - Maintenance des ouvrages d'art - Ecole Polytechnique Fédérale de Lausanne, 1986.
3. KOPRNA, M - Effets différés : fluage, retrait, relaxation - Ecole Polytechnique Fédérale de Lausanne, 1986.
4. GHALI, A., FAVRE, R. - Concrete Structures : Stresses and Deformations - Chapman and Hall, 11 New Fetter Lane, London EC4P 4EE, 1986.

5. TREVINO, J. - Méthode directe de calcul de l'état de déformation et de contrainte à long terme d'une structure composée - thèse de doctorat, Ecole Polytechnique Fédérale de Lausanne, 1988.
6. THÜRLIMANN, Chr. - Bemessung von Stahlbetonstützen unter Zwangsverformungen - thèse de doctorat, Ecole Polytechnique Fédérale de Lausanne, 1984.
7. NAJDANOVIC, D. - Contribution à la vérification de l'état d'utilisation des colonnes sous déformations imposées - thèse de doctorat, Ecole Polytechnique Fédérale de Lausanne, 1987.
8. DAL BUSCO, S. - Déformabilité et capacité portante des colonnes en béton armé - thèse de doctorat, Ecole Polytechnique Fédérale de Lausanne, 1988.



## FEM SOLUTION OF THE COUPLED PLANE PROBLEM OF THERMOELASTICITY

Natalija Naerlović-Veljković and Dragoslav Šumarac

Department of Applied Mechanics and Structural Analysis,  
Faculty of Civil Engineering, University of Belgrade

### SUMMARY

A computer program (TRE) was written for the linear coupled thermoelastic theory of plane or axisymmetric problems, using Finite Element Method (FEM) formulation. The programme is checked comparing obtained results with the existing solutions of thermoelastic problem for the half-space subjected to the temperature increment at its boundary.

### 1. INTRODUCTION

New development in the field of technology and application of new classes of materials, requires also a development of more rigorous theories of materials behaviour. Regarding the behaviour of materials under elevated temperature, up to 1952 [1] and further 1960 [2], coupled thermoelasticity theory was subject of research of a sequence of authors [3]. Explicit form of the second order thermoelasticity field equations may be found in [4] (1971). General thermoelastic theory is also incorporated in [5] (1976). In spite of the development of the nonlinear theory, classical form of thermoelastic field equations [1], [2] remained the basis of solving particular problems [6], [7]. The present paper yields a numerical solution of the linear coupled thermoelasticity field equations [2], using the Finite Element Method (FEM). The computer programme TRE (ThermoElasticity) is written to solve plane and axisymmetric problems of coupled theory formulated by equations (1) and (2) for arbitrary boundary and initial conditions. As it is evident, equation (2) exhibits nonlinearity in the second term on the left-hand side of the equation. The programme is tested on the three well known examples [8], [10] and [11].

### 2. FIELD EQUATIONS

Coupled thermoelastic theory as formulated by Chadwick [2], is expressed by the following set of field equations:

$$C_{iprs} U_{r,ps} - \beta_{ip} \theta_{,p} + \rho f_i = \rho \ddot{u}_i \quad (1)$$

$$\rho c \dot{\theta} + T \beta_{pq} \dot{u}_{p,q} = k_{pq} \theta_{,pq} + \rho h \quad (2)$$

Performing strict linearization, the actual temperature  $T$  in eq. (2) may be substituted by the value  $T_0$ , corresponding to the reference state [2]. In the equations (1) and (2) usual notation are used:  $u_i$  - component of the displacement vector,  $T$  - absolute temperature at the current time,  $T_0$  - uniform temperature at the reference state,  $\theta = T - T_0$  temperature increment related to the reference state. The description of the problem in particular cases is completed by the boundary and initial conditions.

### 2.1. Half-space subjected to external temperature increment on its boundary

One among classical problems of thermoelasticity is that of half-space being suddenly subjected to uniform temperature increment at its boundary. The solution of the problem includes the determination of temperature, displacement and stress fields at an arbitrary time  $t$ . The problem was first solved by Danilovskaya in 1952 [8], [9], but without coupling term in the equation (2) (first Danilovskaya problem). Later on, Sternberg and Chakravorty [10] considered a similar problem examining the influence of the duration of the temperature excitation at the boundary of the half-space; on the ground of uncoupled theory. Further on, authors such as Hetnarsky [11], Boley and Tolins [12], Nickell and Sackman [13] were analysing the Danilovskaya problem within the framework of the linear coupled thermoelastic theory (second Danilovskaya problem).

The governing thermoelastic field equations for the halfspace  $y \leq 0$  (Fig. 1) reduce to two equations in terms of displacement  $u_y = u_y(y, t)$  and  $T = T(y, t)$ . Using dimensionless variables these field equations may be expressed in the form:

$$\frac{\partial^2 v}{\partial \eta^2} = \frac{\partial^2 v}{\partial \tau^2} + \frac{\partial q}{\partial \eta} \quad (3)$$

$$\frac{\partial^2 q}{\partial \eta^2} = \frac{\partial q}{\partial \tau} + \delta \frac{\partial^2 v}{\partial \eta \partial \tau} \quad (4)$$

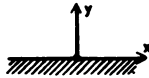


Fig. 1 Half-space

Following notation were used:

$$\eta = \frac{ay}{K}; \quad \tau = \frac{a^2 t}{K}; \quad \sigma = \frac{\sigma_y}{\beta T_0}; \quad q = \frac{T - T_0}{T_0} = \frac{\theta}{T_0}$$

$$v = \frac{a(\lambda + 2\mu)u_y}{K\beta T_0}; \quad K = \frac{k}{\rho c v}; \quad a^2 = \frac{\lambda + 2\mu}{\rho}$$

$$\beta = \alpha(3\lambda + 2\mu); \quad h = \frac{k \cdot h_T}{a \cdot k}; \quad \delta = \delta(T) = \frac{\beta^2 T}{\rho c(\lambda + 2\mu)}; \quad \delta_0 = \delta(T_0) = \frac{\beta^2 T_0}{\rho c(\lambda + 2\mu)}$$

with  $\sigma_y$  being the normal stress,  $\lambda, \mu$  - Lamé's coefficients,  $k$  - thermal conductivity,  $h_T$  - boundary-layer conductance, and  $c$  - specific heat.

The initial conditions for the equations (3), (4) are:

$$v(\eta, 0) = \frac{\partial v}{\partial \tau}(\eta, 0) = 0 \quad (5)$$

$$q(\eta, 0) = 0 \quad (6)$$

On the free surface the following boundary conditions for mechanical and thermal variables take place:

$$\sigma(0, \tau) = 0 \quad (7)$$

$$q(0, \tau) = 1 \quad (8a)$$

$$q(0, \tau) = \begin{cases} \frac{\tau}{\tau_0} & 0 < \tau < \tau_0 \\ 1 & \tau > \tau_0 \end{cases} \quad (8b)$$

The exact solutions of the uncoupled dynamical theory, [8] and [10] for boundary conditions (8a) and (8b) respectively, will be compared with the numerical solution obtained here using FEM. Numerical solution for the coupled theory, obtained for the boundary conditions (8a) by programme TRE, will be compared with the solution [11].

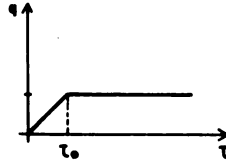


Fig. 2 Boundary condition for the Sternberg-Chakravorty problem

### 3. FINITE ELEMENT SOLUTION OF THE PROBLEM

The differential equations of the coupled problem of Thermoelasticity are cast in the form of the FEM equations. The basic FEM equations are:

$$\underline{\underline{M}} \ddot{\underline{\underline{v}}} + \underline{\underline{K}} \underline{\underline{v}} = \underline{\underline{R}} \quad (9)$$

$$\underline{\underline{P}} \underline{\underline{T}} + \underline{\underline{C}} \dot{\underline{\underline{T}}} = \underline{\underline{Q}} \quad (10)$$

where the introduced matrices and vectors are:

$$\underline{\underline{M}} = \sum_e \left( \int_{V_e} \underline{\underline{N}}^T \rho \underline{\underline{N}} dV \right) \quad \text{- global mass matrix}$$

$$\underline{\underline{K}} = \sum_e \left( \int_{V_e} \underline{\underline{B}}^T \underline{\underline{D}} \underline{\underline{B}} dV \right) \quad \text{- global stiffness matrix}$$

$$\underline{\underline{P}} = \sum_e \left( \int_{V_e} \underline{\underline{\beta}}^T \underline{\underline{K}} \underline{\underline{\beta}} dV + \int_{S_e} \underline{\underline{N}}^T h_T \underline{\underline{N}} dS \right) \quad \text{- global conductivity matrix (11)}$$

$$\underline{\underline{C}} = \sum_e \left( \int_{V_e} \underline{\underline{N}}^T \underline{\underline{c}} \underline{\underline{N}} \rho dV \right) \quad \text{- global heat capacity matrix}$$

$$\underline{\underline{R}} = \sum_e \left( \int_{V_e} \underline{\underline{N}}^T \underline{\underline{p}} ds + \int_{V_e} \underline{\underline{N}}^T \rho \underline{\underline{f}} dV + \int_{V_e} \underline{\underline{\beta}}^T \underline{\underline{\sigma}}_0 dV \right) \quad \text{- global node force vector}$$

$$\underline{\underline{Q}} = \sum_e \left( \int_{S_q} \underline{\underline{N}}^T q ds + \int_{V_e} \underline{\underline{N}}^T \rho h dV + \int_{V_e} \underline{\underline{N}}^T \alpha \underline{\underline{I}}_\sigma \underline{\underline{N}} \underline{\underline{T}} dV + \int_{S_h} \underline{\underline{N}}^T h_T ds \right) \quad \text{- effective heat flow vector (12)}$$

Additional notation includes:  $N_i$  - shape function vector,  $f$  - body force vector,  $h$  - internal heat generation,  $\dot{I}_\sigma$  - rate of the first invariant of the stress tensor.

The programme TRE has been based on the equations (9) and (10) (including the possibility of strict linearization of the heat conductivity equation). In the programme plane and axisymmetric elements with four to eight nodes were incorporated. The number of Gauss points for the numerical integration with respect to space variable can be also varied between four and sixteen.

Integration of the differential equations (9) and (10) with respect to time is performed by Wilson -  $\theta$  method, in the case of equation of motion, and "step by step" method for the temperature field equation. Both methods are numerically stable. Equations (9) and (10) are coupled and simultaneous. Therefore, the solution procedure for any time interval has to be iterative. The coupling term is included as a part of the effective heat flow vector, containing stress invariant. The rate of the stress invariant in any time can be calculated as:

$$\dot{I}_\sigma = \frac{1}{\Delta t} [\sigma_{jj}^{t+\Delta t} - \sigma_{jj}^t] \quad (13)$$

where  $\Delta t$  stands for the time interval.

At the first time interval, beginning with  $t=0$ , temperature field is determined neglecting the  $\dot{I}_\sigma$  term. Then, vector  $R$  is calculated and equation (9) is solved. After that, term (13) can be found. Substituting (13) in (12), second iteration for the temperature field is obtained from (10). Using this result the second iteration for the deformation and the stress field is determined from (9). This procedure, corresponding to the same time interval, is repeated until the difference in the norm of the heat flow vector from the two successive iterations becomes less than required one. In each subsequent time interval ( $t+\Delta t$ ) the part of the heat flow vector, depending of the stress invariant for the  $i+1$  iteration can be written as:

$$\dot{Q}^{(i+1)t+\Delta t} = \int_{V_e} N^T \frac{1}{\Delta t} [\sigma_{jj}^{(i)t+\Delta t} - \sigma_{jj}^t] N^T^{(i)t+\Delta t} \quad (14)$$

In the expression (14) the coupling coefficient  $\delta = \delta(T)$  is introduced. The further iteration procedure for an arbitrary time increment is identical to one already described above.

#### 4. NUMERICAL EXAMPLES

To check the TRE program three examples are considered: the first Danilovskaya problem, next Strenberg-Chakravorty problem and finally the second Danilovskaya problem. The same finite element mesh, given in Fig. 3, is used for all examples. Such mesh pattern is imposed by the nature of the problem itself. The density of the mesh is increased from the bottom to the top, where the boundary conditions are prescribed. For  $\eta = 0$  up to  $\eta = -2.0$  there are 20 elements with a width 0.1 each, and from  $\eta = -2.0$  up to  $\eta = -3.0$  there are 4 elements 0.25 with. Finally between  $\eta = -3.0$  up to  $\eta = -10.0$  the elements are of 0.5 width. The total number of elements is 38 and the total number of nodes is 78. The density of the mesh is satisfactory. Namely, increasing the number of points, and introducing elements with 8 nodes, the results didn't change significantly. Bottom of the mesh is far enough from the free edge, and the reflective waves do not exist.

The problem is set in the dimensionless form. According to this, the characteristics of the material are:  $E = 1.0$ ;  $\mu = 1/3$ ;  $k = 1.0$ ;  $c_v = 1.0$ ;  $\rho = 1.5$ . It follows here from:  $a = K = 1.0$ ;  $\eta = y$ ;  $\tau = t$ ;  $v = 1/2(u_y) \times 10^5$ .

The convective element is introduced with the value  $h_T = \infty$  on the element 1, between nodes 1 and 40. This is equivalent to the boundary conditions (8).

#### 4.1. Sternberg-Chakravorty problem

Sternberg-Chakravorty problem is defined for the boundary condition (8b) (Fig.2). The closed form solution is obtained by means of Laplace's transformations [10]. The numerical solution is obtained for the same boundary conditions. To check the convergence two time intervals  $t=0.1$  and  $t=0.05$  are used. The dimensionless displacement, stress and temperature distributions are presented in Fig. 4, 5 and 6, including the closed form and two FEM solutions, for  $\tau_0 = 0.5$ . All diagrams are given on  $\eta = -1$ . The convergence of the numerical solution is apparent. The decrease of the time interval improves the accuracy of the analysis.

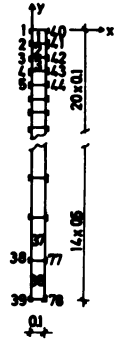
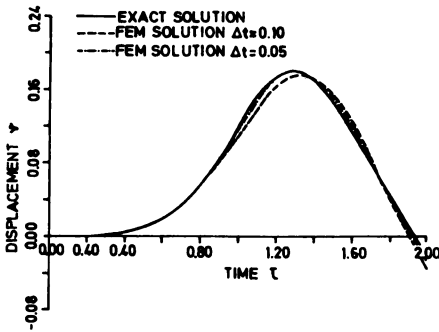


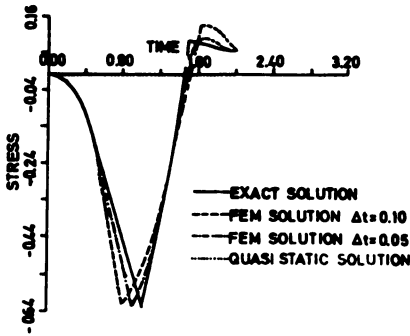
Fig.3 FEM mesh



TIME $\tau$	EXACT SOLUTION	FEM TIME INCREMENT $\Delta t = 0.1$	FEM TIME INCREMENT $\Delta t = 0.05$
0.100000	0.000005	0.000047	0.000022
0.200000	0.000133	0.000431	0.000289
0.300000	0.000941	0.001743	0.001375
0.400000	0.003363	0.004824	0.004151
0.500000	0.008488	0.010700	0.009696
0.600000	0.017672	0.020472	0.019220
0.700000	0.032211	0.035024	0.033839
0.800000	0.053092	0.054779	0.054302
0.900000	0.081155	0.079409	0.080668
1.000000	0.117192	0.107411	0.111594
1.100000	0.151535	0.135898	0.143310
1.200000	0.173251	0.159585	0.169228
1.300000	0.180883	0.173546	0.181597
1.400000	0.172828	0.172860	0.175281
1.500000	0.147461	0.155590	0.151168
1.600000	0.112975	0.123813	0.115788
1.700000	0.079121	0.083166	0.077066
1.800000	0.046351	0.040617	0.040154
1.900000	0.013492	0.001569	0.006624
2.000000	-0.018934	-0.032029	-0.02417

Fig. 4. Displacement for the Sternberg-Chakravorty problem,  $\tau_0 = 0.5$

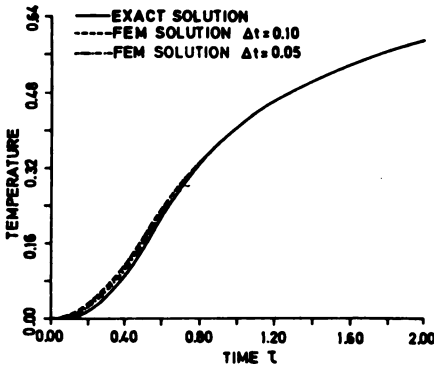




TIME $\tau$	EXACT SOLUTION	FEM $\Delta t=0.1$	FEM $\Delta t=0.05$
0.100000	-0.001153	-0.001574	-0.001403
0.200000	-0.015496	-0.017429	-0.016856
0.300000	-0.049923	-0.051909	-0.050365
0.400000	-0.103714	-0.108438	-0.104086
0.500000	-0.175829	-0.183682	-0.179342
0.600000	-0.264607	-0.314563	-0.281210
0.700000	-0.358114	-0.479679	-0.389421
0.800000	-0.450022	-0.621578	-0.525323
0.900000	-0.541934	-0.591522	-0.632122
1.000000	-0.636122	-0.536350	-0.580347
1.100000	-0.524281	-0.449689	-0.489329
1.200000	-0.396323	-0.348768	-0.383438
1.300000	-0.251458	-0.258563	-0.253630
1.400000	-0.088592	-0.134856	-0.103489
1.500000	0.093732	-0.029651	0.039763
1.600000	0.086744	0.133243	0.093974
1.700000	0.080618	0.131521	0.099563
1.800000	0.075378	0.124785	0.081234
1.900000	0.070520	0.098568	0.072324
2.000000	0.066290	0.073240	0.067259

Fig. 5 Stress for the Sternberg-Chakravorty problem,  $\tau_0 = 0.5$

The curve on the Fig.7 shows the influence of the parameter  $\tau_0$  on the change of stress in time. The stress for  $\eta = -1.0$  has an extremum  $s = -0.89$ , for  $\tau_0 = 0$ . For  $\tau_0 \rightarrow \infty$  stress reduces to quasi - static solution ( $s=0$ ). This example clearly shows the inertia effects.



TIME $\tau$	EXACT SOLUTION	FEM $\Delta t=0.1$	FEM $\Delta t=0.05$
0.100000	0.001125	0.008580	0.004950
0.200000	0.014807	0.030550	0.023350
0.300000	0.046839	0.066400	0.057010
0.400000	0.092401	0.114760	0.104230
0.500000	0.150678	0.173820	0.162790
0.600000	0.217556	0.233370	0.225810
0.700000	0.279914	0.287230	0.283260
0.800000	0.331391	0.333780	0.332150
0.900000	0.373709	0.373530	0.373210
1.000000	0.411797	0.407540	0.407930
1.100000	0.439045	0.436880	0.437650
1.200000	0.464920	0.462430	0.463380
1.300000	0.487521	0.484890	0.485930
1.400000	0.507482	0.504820	0.505880
1.500000	0.525278	0.522630	0.523690
1.600000	0.541269	0.538680	0.539710
1.700000	0.555747	0.553220	0.554220
1.800000	0.568933	0.566490	0.567440
1.900000	0.581014	0.578640	0.579560
2.000000	0.592120	0.589840	0.590710

Fig.6 Temperature for the Sternberg-Chakravorty problem,  $\tau_0 = 0.5$

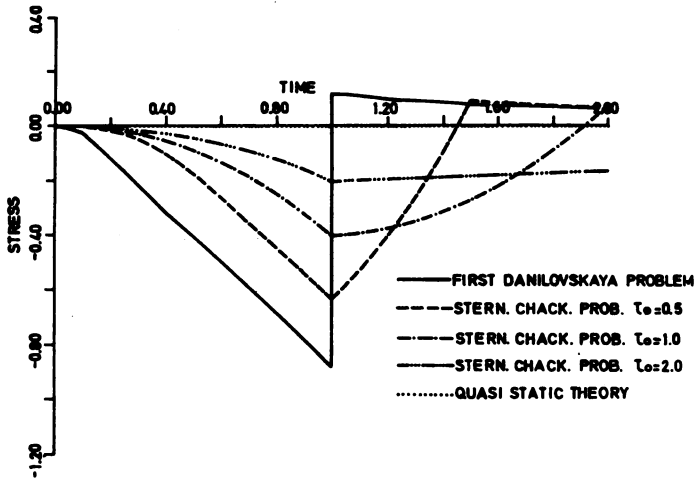
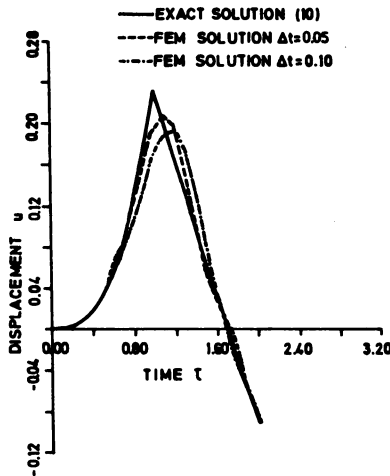


Fig. 7 The change of stress in time for different values of  $\tau_0$

#### 4.2. First and Second Danilovskaya Problems

The Danilovskaya problem differs from the Sternberg-Chakravorty in the thermal condition on the boundary. Here the temperature excitation is represented by a jump on the free surface as given by the expression (8a). First Danilovskaya problem requires a solution of the uncoupled dynamic theory of Thermoelasticity. In Fig. 8 analytic and numerical solution for two time intervals are presented. Convergence of the FEM solution is again apparent.



TIME $\tau$	EXACT SOLUTION	FEM TIME INCREMENT $\Delta t=0.1$	FEM TIME INCREMENT $\Delta t=0.05$
0.500	0.032	0.029	0.031
0.600	0.063	0.049	0.053
0.700	0.086	0.075	0.082
0.800	0.129	0.105	0.117
0.900	0.176	0.138	0.155
1.000	0.234	0.169	0.190
1.100	0.198	0.190	0.209
1.200	0.160	0.194	0.199
1.300	0.128	0.175	0.157
1.400	0.099	0.135	0.099
1.500	0.060	0.083	0.051
1.600	0.034	0.032	0.024
1.700	0.001	-0.009	0.006
1.800	-0.034	-0.038	-0.023
1.900	-0.067	-0.060	-0.065
2.000	-0.093	-0.085	-0.092

Fig. 8 Displacement for the first Danilovskaya problem

For the second Danilovskaya problem, a small number of analytical solutions exists. There is the Hetnarski solution [11]. On Fig.9 numerical solution obtained with the TRE program and Hetnarski's solution are compared. The curve shows the distribution of the temperature with respect to  $\eta$  coordinate, for two different times  $\tau=1.0$  and  $\tau=2.0$ .

TIME $\tau$	COORDI-NATE $\eta$	HETNARSKI UNCOUPLED	HETNARSKI COUPLED	FEM UNCOUPLED $\Delta t = 0.1$	FEM COUPLED $\Delta t = 0.1$
1.0	0.100	0.944	0.943	0.414	0.941
	2.000	0.157	0.158	0.152	0.152
	3.000	0.034	0.034	0.036	0.036
	4.000	0.005	0.000	0.007	0.007
2.0	0.100	0.960	0.959	0.959	0.959
	3.000	0.134	0.135	0.131	0.131
	3.500	0.080	0.081	0.079	0.079

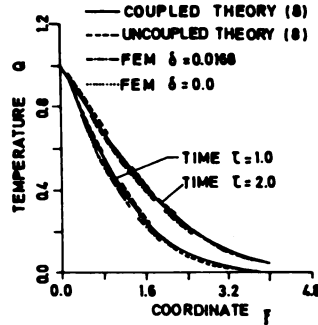


Fig.9 Temperature vs. space for the second Danilovskaya problem

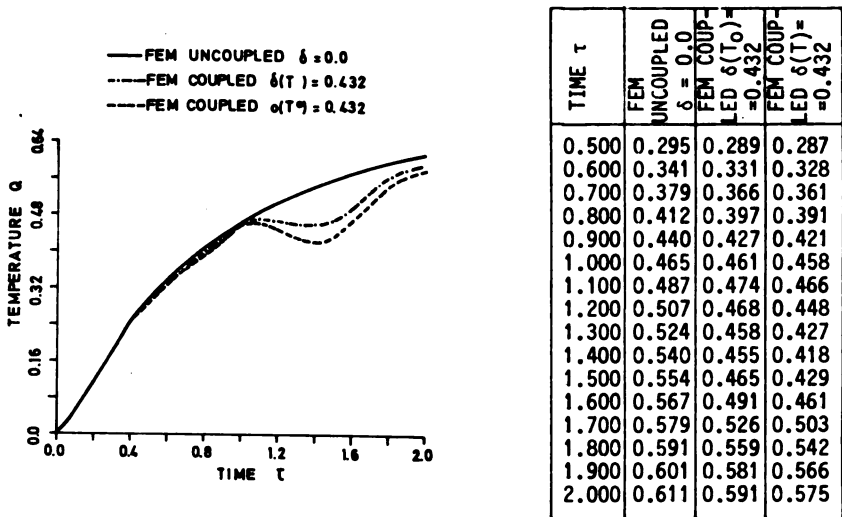


Fig.10 Temperature vs. time for the second Danilovskaya problem

Finally in Fig.10 (curve and table) temperature vs time, at the level  $\eta=-1.0$ , is presented as obtained numerically from the TRE program. Diagram clearly shows the influence of substituting  $\delta(t)$  instead of  $\delta(T_0)$  for the value of the coupling coefficient. From Fig.10 it can also be seen that no jump in the temperature distribution exists for  $\tau = -\eta = 1.0$ . This fact contributes to the known discussion concerning the form of the temperature curves [14], [11].

## REFERENCES

1. Biot, M.A. - Thermoelasticity and irreversible thermodynamics , J.Appl.Phys., 1952, 27, 240-253.
2. Chadwick, P. - Thermoelasticity , Progress in Solid Mechanics, Ed. Sneddon, I.N. and Hill, R., North-Holland, 1960, Vol I, p. 265.
3. Truesdell, C. and Noll, W. - The non-linear field theories of mechanics , Handbuch der Physik, Ed. Flugge, S., Springer-Verlag, 196E, Vol. III/3.
4. Chadwick, P. and Seet, L.T.C. - Second-order thermoelasticity theory for isotropic and transversely isotropic materials , Trends in Elasticity and Thermoelasticity, W. Nowacki Anniversary Volume, 1971, p. 30.
5. Parkus, H. - Thermoelasticity, Springer-Verlag, Wien, New York, 1976.
6. Nowacki, W. - Thermoelasticity, (Second edition) PWN - Polish Scientific Publishers, Warszawa, 1986.
7. Progres in Thermoelasticity , VIII th European Mechanics Colloquim, Ed. W.K. Nowacki, Inst. Fund. Techn. Research, Pol. Acad. Sci., 1969, Warszawa.
8. Danilovskaya, V.I. - Thermal Stresses in an Elastic Half Space Arising After a Sudden Heating at Its Boundary , Prikladnaya Matematika i Mehanika, 1950, 14, 3, 316-318.
9. Danilovskaya, V.I. - On a Dynamical Problem of Thermoelasticity , Prikladnaya Matematika i Mehanika, 1952, 16, 3, 341-344.
10. Sternberg, E. and Chakravorty, J.G. - On Inertia Effects in a Transient Thermoelastic Problem , J. of Appl. Mech., 1959, 26, 4, 503-509.
11. Hetnarski, R. - Coupled Thermoelastic problem for the Half Space , Bulletin de L Academie Polonaise des Sciences, Series des Sciences Techniques, 1964, 12, 49-57.
12. Boley, B.A. and Tolins, I.S. - Transient Coupled Thermoelastic Boundary Value Problems in the Half Space , J. of Appl. Mech., 1963, 29, 4, 637-646.
13. Nickell, R.E. and Sackman, J.L. - Approximate solutions in Linear, Coupled Thermoelasticity , J. of Appl. Mech., 1968, 35, 2, 255-266.
14. Paria, F. - Coupling of Elastic and Thermal Deformations, Appl. Scientific Research, 1959, 7, 463-475.
15. Naerlović-Veljković, N. - Introduction to Thermoelasticity (In Serbo-Croatian), Scientific Press, Belgrade, 1977.
16. Naerlović-Veljković, N. and Stojanović, R. - Large thermal deformations of the hollow cylinder (In Serbo-Croatian), Tehnika, 1966, 6, 134.
17. Naerlović-Veljković, N. - On Maxwell - Cattaneo's Equation for Anisotropic Media - Extrait du Bulletin T. LXXVI de L Academie serbe des Sciences et des Arts, Classe des Sciences mathematiques et naturelles, Sciences mathematiques, 1981, 11.
18. Sumarac D. - A contribution to the Numerical solution of the coupled problem of Thermoelasticity, Master degree work (In serbo-croatian), 1983, Faculty of Civil. Eng., Belgrade.
19. Sumarac, D. - A Solution of the Two-dimensional Thermoelasticity Problem by the Finite Element Method, Numerical Methods in Thermal Problems (IV International Conference), Ed. Lewis, R.W. and Morgan, K., Pineridge Press, 1985, Vol II, p. 1248.



## MODELLING OF THE BEHAVIOUR OF COLUMN WEB PANELS IN SEMI-RIGID JOINTS.

René MAQUOI, Professor

Jean-Pierre JASPART, Assistant

Institut du Génie Civil, Université de Liège, Belgique.

### SUMMARY

Present paper is aimed at assessing the non linear shear deformability of unstiffened column web panels in the vicinity of bolted and/or welded beam-to-column semi-rigid joints. A general expression providing the associated  $M-\theta$  curve is suggested and formulae for the evaluation of the different terms are presented. The agreement between experiments and modelling is found quite satisfactory.

### 1. INTRODUCTION

For some years much experimental and/or theoretical research work has been devoted to the actual behaviour of beam-to-column joints in steel buildings and more especially to semi-rigid joints. There are the result of a search for simple and cheap connections with a view to a reduction of the labour cost, which grew much faster than the material cost. Thus for the sake of economy bolted joints and joints without any stiffener became a common practice. Unfortunately such joints have a non linear behaviour : when subject to an applied bending moment  $M$ , the axis of the connected members do not rotate a same angle, so that there is a relative rotation  $\theta$ , which is not proportional to the applied bending moment  $M$ .

Both strength and stability of steel frames are affected by the semi-rigid behaviour of the joints [1]. Though several computer programmes, which allow for material and geometrical non linearities - including semi-rigid connections - are available, there is an urgent need of knowledge for the  $M-\theta$  characteristics of the joints.

In the authors' laboratory a lot of experimental investigations were recently carried out [2, 3]; in addition, the junior author is developing a mathematical modelling of the two components of the joint flexibility : i) the deformability of the connection properly, and ii) the shear flexibility of the column

web panel adjacent to the beam.

Present paper is aimed at presenting a mathematical model that is likely to provide the  $M-\theta$  curve associated to the shear rotation of the column web panel. This model is demonstrated to give results in close agreement with experiments.

## 2. EXPERIMENTAL INVESTIGATION.

Tests were carried out in Liège on strong axis -, weak axis - and 3 D beam-to-column joints. As far as column web panel is concerned within present paper, it will be referred to strong axis connections only ; the beam is connected to one flange of the column, so that any transverse loading on the beam induces bending about the strong axis of the column cross section. Beam and column are made with hot-rolled H or I sections ; they are assembled by either an end plate, or web cleats, or flange cleats. The load is applied at the end of the cantilever beam while the column is subject to an additional axial load (fig.1).

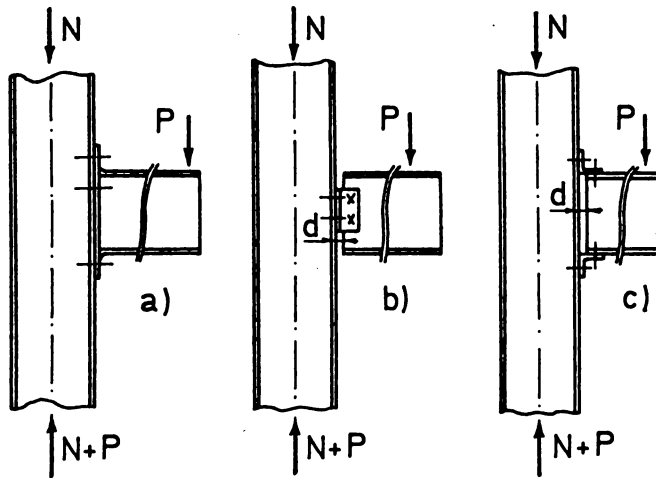


Figure 1 - Strong axis joints tested in Liège.

The relative rotation of the joint, as well as the one of the connection properly and the shear flexibility of the column web panel are directly measured or deduced from measurements with transducers (fig. 2).

It results from experimental evidence that the effect of the axial force in the column on the shear flexibility of the column web panel can be disregarded as far as it does not exceed half the squash load. However that is not actually a severe restriction in practice.

Comments can be made on the physical meaning of the contributions of the joint rotation depicted in figure 2 by referring for instance to figure 3. From a static point of view the bending moment that is applied to the beam can be substituted by two equivalent forces C and T - equal but opposite - acting in both compressive and tensile flange respectively. Because of the tensile force T, the end plate and the adjacent flange of the column bend locally and the shank of the bolts in the tensile zone elongates. For the same reason, a part of the column web is subject to transverse tensile stresses and will consequent-

ly deform in the plane of the web. The sole effect of the compressive force  $C$  is to generate transverse compressive stresses in another part of the column web that is adjacent to the lower flange of the beam.

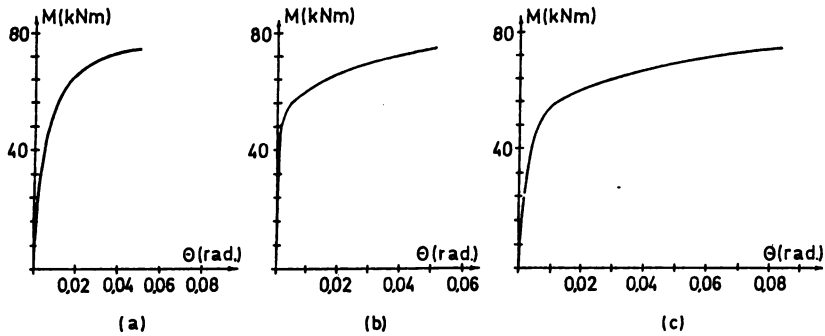


Figure 2 - M- $\theta$  curves for an end plate connection : a) of the connection ; b) of the joint ; c) due to the shear deformability of the column web panel.

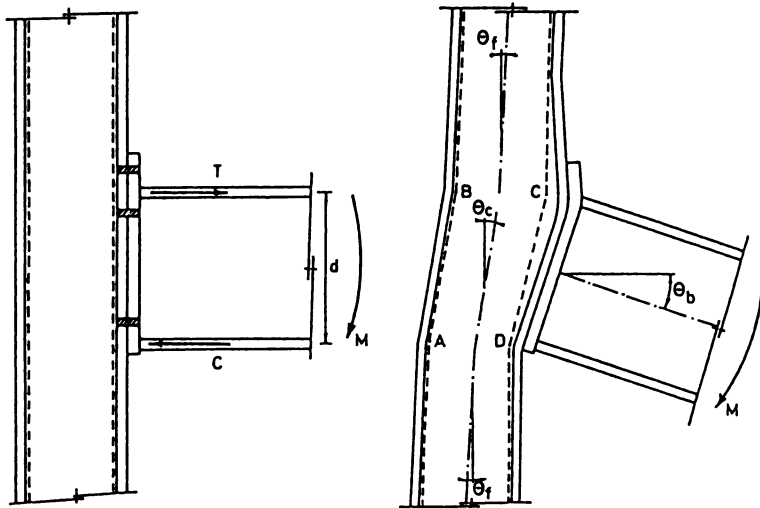


Figure 3 - Deformation during test of a joint using an end plate connection.

The rotation associated to the aforementioned deformations due to  $C$  and  $T$  forces constitutes the relative rotation of the connection ; the latter is obtained as the difference between the rotations  $\theta_b$  and  $\theta_c$  (fig. 3). This connection rotation is increased by a rotation resulting from the shear flexibility of the column web panel ABCD - in short, the shear rotation -, because of the combined



effects of tensile  $T$  and compressive  $C$  forces. This shear rotation is quantified by the difference between rotations  $\theta_c$  and  $\theta_b$  (fig. 3), where  $\theta_c$  would be the flexural rotation of the column when subject to a concentrated bending moment  $M$ . The relative rotation of the joints is simply obtained by adding the relative rotation of the connection and the shear rotation of the column web panel.

Within the frame of present paper, only the non-linear  $M-\theta$  curve dealing with the shear rotation of the column web panel (fig. 2.c.) is concerned with. First the column web panel behaves elastically, as if it was quasi rigid in shear. In a second step, yielding occurs in the column web ; the connecting flange of the column begins to bend appreciably, with consequently a sudden and fast increase of the shear deformation of the web. Finally the ultimate strength of the joint is reached.

### 3. MATHEMATICAL MODELLING OF THE BEHAVIOUR OF A COLUMN WEB PANEL.

To be general let us consider an internal joint of a structure that is subject to shear forces and bending moments (fig. 4).

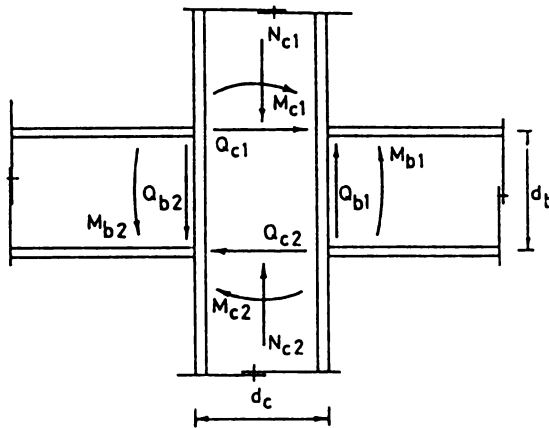


Figure 4 - Loading of an internal joint.

The loading of such a joint is composed of two parts [4] which are associated to gravity loads and horizontal forces respectively. The loading components are simply computed as follows :

#### Horizontal forces

$$M_b = 0.5 (M_{b1} + M_{b2}) \quad (1.a.)$$

$$M_c = 0.5 (M_{c1} + M_{c2}) \quad (1.b.)$$

$$Q_b = 0.5 (Q_{b1} + Q_{b2}) \quad (1.c.)$$

$$Q_c = 0.5 (Q_{c1} + Q_{c2}) \quad (1.d.)$$

#### Gravity loads

$$M_b^x = 0.5 (M_{b1} - M_{b2}) \quad (2.a.)$$

$$M_c^x = 0.5 (M_{c1} - M_{c2}) \quad (2.b.)$$

$$Q_b^x = 0.5 (Q_{b1} - Q_{b2}) \quad (2.c.)$$

$$Q_c^x = 0.5 (Q_{c1} - Q_{c2}) \quad (2.d.)$$

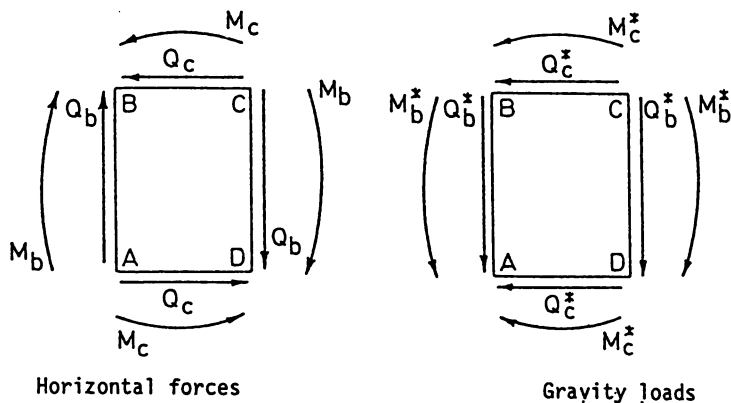


Figure 5 - Loading components in a column web panel.

The shear in the column web panel is thus clearly shown (fig. 5) to result from the effect of horizontal forces. By assuming that the bending moments are mainly transmitted by the flanges, the computation of the shear forces in the column web panel can be conducted as follows (fig. 5) :

$$\bar{Q}_b = (2M'_c/d_c) - Q_b = (M_{c1} + M_{c2})/d_c - 0.5 (Q_{b1} + Q_{b2}) \quad (3.a.)$$

$$\bar{Q}_c = (2M'_b/d_b) - Q_c = (M_{b1} + M_{b2})/d_b - 0.5 (Q_{c1} + Q_{c2}). \quad (3.b.)$$

A bending moment ( $pM$ ) can be associated to this loading ; it writes :

$$(pM) = \bar{Q}_b d_c = \bar{Q}_c d_b \quad (4)$$

Let us now investigate the successive steps of the behaviour of the column web panel.

### 3.1. Range of elastic strength and behaviour.

At the first beginning of the loading, the column web has a purely elastic behaviour. It is reasonably assumed that the shear stresses  $\bar{\tau}$  are distributed uniformly across the column web depth of thickness  $t_p$  ; then it writes simply :

$$\bar{\tau} = \bar{Q}_b/d_b t_p = \bar{Q}_c/d_c t_p \quad (5)$$

The elastic behaviour is subject to the condition :

$$\bar{\tau} \leq \tau_y \quad (6)$$

where the shear yield stress is derived from the von MISES's yield criterion, according to :

$$\tau_y = f_y/\sqrt{3} \quad (7)$$

$f_y$  being the tensile yield stress of the material. (Let us remind that the effect of axial force in the column can be disregarded).

The shear strain is given as :

$$\bar{\gamma} = \bar{\tau}/G \quad (8)$$

where  $G$  is the shear modulus.

Thus the bending moment that is associated to the end of the elastic range behaviour writes :

$$(pM)_y = V_p \tau_y \quad (9)$$

with :

$$V_p = d_b d_c t_p \quad (10)$$

On the other hand, one has immediately :

$$\theta_y = \gamma_y = \tau_y/G \quad (11)$$

### 3.2. Inelastic range.

As soon as the web yields, a deformation range associated to a constant bending moment - and thus to the yield plateau of the material stress-strain diagram-could be expected. The truth is else.

The shear strength is increased as a result of the bending resistance of the column web panel fitted with its boundary elements : column flanges and restraints provided by the adjacent beam(s). Obviously this bending resistance is already present in the elastic range, where it is there not significant because of the large shear rigidity of the elastic web.

The inelastic range ends when the column web material reaches the strain hardening range. The associated bending moment  $(pM)_{st}$  can be found as follows [5] :

$$(pM)_{st} = 0.75 (pM)_y + 0.50 (mM)_y \quad (12)$$

where  $(mM)_y$  is the elastic bending moment of the column or of the beam cross section, according to which is the lesser. The validity of (12) is subject to following condition :

$$(pM)_y \leq 2 (mM)_y \quad (13)$$

which is not actually restrictive for most of the joints used in practice.

The shear rotation of the column web panel writes :

$$\theta_{st} = \theta_y + \sqrt{3} (\epsilon_{st} - \epsilon_y) \quad (14)$$

where  $\epsilon_y$  and  $\epsilon_{st}$  are the strains associated respectively to the start and the end of  $\gamma_y$  the yield plateau ( $\sigma = f_y$ ) in the relevant  $\sigma - \epsilon$  diagram.

### 3.3. Ultimate carrying capacity.

Strain hardening contributes to an increase of the shear strength too. According to [5], the ultimate strength can be assessed as :

$$(pM)_u = V_p \tau_u + 0.5 (mM)_y - 0.25 (pM)_y \quad (15)$$

where the ultimate shear stress  $\tau_u$  writes :

$$\tau_u = f_u / \sqrt{3} \quad (16)$$

$f_u$  being the ultimate tensile strength of the column web material.

Any mathematical function that is likely to represent the shear behaviour of a column web panel must :

- i) be such that  $(pM) = 0$  when  $\theta = 0$  ;
- ii) be asymptotic to  $(pM) = (pM)_u$  when  $\theta$  is increasing infinitely ;
- iii) comply with the coordinates  $((pM)_y, \theta_y)$  ;
- iv) comply with the coordinates  $((pM)_{st}, \theta_{st})$  .

From the several mathematical expressions which were investigated and compared with tests results, the following one is suggested :

$$(pM) = (pM)_u \{1 - \exp [-f(\theta)]\} \quad (17)$$

with :

$$f(\theta) = a\theta^b + c\theta > 0 \quad (18)$$

Parameters  $a$  and  $b$  can be determined by above conditions (iii) and(iv), wherefrom :

$$a = - (\beta + c\theta_y) \theta_y^b = - (\alpha + c\theta_{st}) / \theta_{st}^b \quad (19.a)$$

$$b = \ln [(\alpha + c\theta_{st}) / (\beta + c\theta_y)] / \ln (\theta_{st} / \theta_y) \quad (19.b)$$

with :

$$\alpha = \ln [1 - (pM)_{st} / (pM)_u] \quad (20.a)$$

$$\beta = \ln [1 - (pM)_y / (pM)_u] \quad (20.b)$$

According to requirement (i), parameter  $b$  must be strictly positive ; therefore parameter  $c$  cannot exceed a limiting value  $c_{max}$  :

$$c \leq c_{max} \quad (21)$$

with :

$$c_{max} = (\beta - \alpha) / (\theta_{st} - \theta_y) \quad (22)$$

At last it is easily demonstrated that only positive (or zero) values of  $c$  can warrant the  $pM-\theta$  curve with existence of the horizontal asymptot.

#### 4. COMPARISON BETWEEN THE MATHEMATICAL MODELLING AND EXPERIMENTAL RESULTS

The shape of the  $pM-\theta$  curves is largely dependent on the value of parameter  $c$ , as it is clearly shown in figure 6.

By comparing the results of the mathematical model suggested here with those got from experiments, a very simple value  $c = 0.75 c_{max}$  can be recommended when the column is a HEB section. Indeed a very good agreement is obtained by using this value, as shown in figure 7, which is dealing with end plate connections.

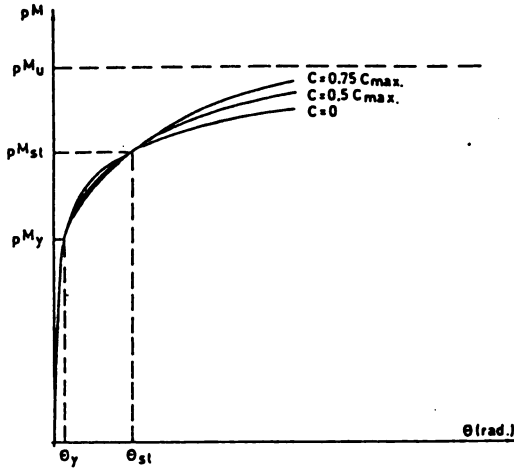
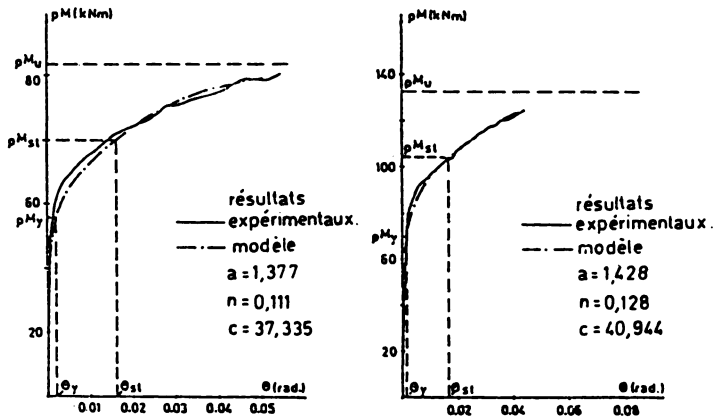


Figure 6 - Influence of  $c$  value on the shape of  $pM-\theta$  curve.



(a) Colonne-HEB 160-poutre-IPE 200      (b) Colonne-HEB 160-poutre-IPE 300

Figure 7 - Comparison between mathematical modelling and experimental results.

The authors' mathematical model complies with the coordinates  $(pM_y, \theta_y)$  and does not develop, as it should be, a linear elastic behaviour in the region of small bending moment. The reason for doing so is the desire of simplicity when expressing mathematically the  $pM-\theta$  curve. As demonstrated by the diagrams, this simplification appears quite justified; indeed the difference between the theoretical approach and the actual behaviour is not significant at all.

Figure 8 is concerned with an end plate connection between a HEB 200 column and an IPE 300 beam; two curves are plotted, which are both dealing with the shear behaviour of the web:

- a) The first one has been obtained by KLEIN [6], on base of a modelling of a joint by means of a set of springs, each of which is associated to a specific source of deformability (shear deformation of the column web panel, compression and tension in the column web,...). It must be noticed that the strain hardening is not accounted for.
- b) The second one is deduced from the authors' model, which has been arranged in order to neglect strain hardening, in accordance with KLEIN's approach.

The agreement between both approaches is here too quite satisfactory.

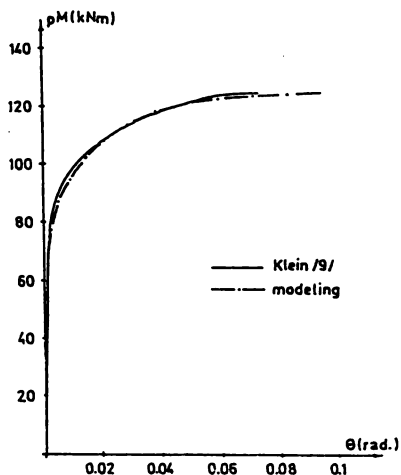


Figure 8 - Comparison between two models.

## 5. CONCLUSIONS

The results of the modelling have been found in a very satisfactory agreement with experiments. Work is still in progress with a view to suggest  $c$  values for several types of sections. The authors are of the opinion that such a modelling is likely to avoid extensive laboratory tests when aimed at quantifying the shear deformability of column web panels.

## 6. REFERENCES.

1. ANDERSON, D., BIJLAARD, F.S.K., NETHERCOT, D.A. and ZANDONINI, R. - 'Analysis and design of steel frames with semi-rigid connections'. IABSE Survey S-39/87, IABSE Periodica 4/87.
2. JANSSE, J., JASPART, J-P. and MAQUOI, R. - 'Experimental study of the non-linear behaviour of beam-to-column bolted joints'. Proceedings Workshop on Connections and the Behaviour, Strength and Design of Steel Structures, Cachan, May 25-28, 1987, pp. 26 - 32.
3. JASPART, J-P. - 'Essais sur assemblages poutre-colonne d'axe fort'. CRIF, Bruxelles (in preparation).
4. KATO, B. - 'Beam-to-column research in Japan'. Journal of Structural Engineering, A.S.C.E., Vol. 108, ST2, February, 1982, pp. 343 - 360.
5. NAKAO, M. - 'Research on the behaviour of steel beam-to-column rigid connections'. Dissertation presented to the University of Tokio, Japan, in 1975, in partial fulfillment of the requirements for the degree of Doctor of Engineering.
6. KLEIN, H. - 'Das elastisch-plastische Last-Verformungsverhalten M- $\theta$  steinlose geschweisster Knoten für die Berechnung von Stahlrahmen mit HEB-Stützen'. Diss. Univ. Innsbruck, 1985.

## LONG SPAN BRIDGES

*Prof. F. DE MIRANDA*

*Associate Professor of Structural Engineering - Milan Polytechnic*

### SUMMARY

First of all the situation in the last century is recalled which thanks to the use of steel, served as a point of departure for an extraordinary development in the field of bridge building. In order to satisfy new traffic requirements, a typical feature of this development was a progressive increase in the length of free spans. After referring to the various and heterogeneous aspects involved in the design of long span bridges, a brief description is offered of the fundamental technical problems which, in the course of a century, have been faced and solved through great works of engineering, thus adding further to the possibilities of reaching the maximum potentialities offered by the use of steel in constructions. As a conclusion, some brief reference will be made to some present research programmes investigating new structural systems for long span bridges.

### 1. INTRODUCTION

Over the centuries the need for rapid road connections has always been felt as a factor of considerable importance, and often led to brilliant solutions in the planning of routes, shown, for example, by the roads of the Roman Empire. However, the limited speed of even horse-drawn vehicles meant that these routes did not really need large spans for crossing natural obstacles. But the arrival of the railways in the last century, and then more recently the development of civil motor traffic and motorways, and the growing operational speed have imposed certain characteristics on these routes, such that more and more often they have to cross natural obstacles with long span bridges.

*This article represents a shortened version of the paper submitted to the ECCS (BSCA International Symposium on Steel Bridges, London 1988)*



Progress up to the 19th century in the fields of mechanics and locomotion also, of course, involved civil engineering, above all for parallel developments in the technology of materials and the science of constructions. In this wide range of development, also in civil engineering steel played a leading part, widely used above all in bridge building, where it gave rise to a profound change in structural engineering. Construction in steel, and bridge building in particular, has always kept a close eye on progress in the steel industry and technologies for its use. The growing homogeneity of steel products had made it possible to increase working stresses, and greater knowledge of states of stress in load bearing structures has led to a more and more rational distribution of the material. However the introduction of steel in bridge construction did not immediately produce those structural systems which are the most efficient for its optimal use. This was mainly due to the centuries long tradition of masonry and woodwork, which still influenced designers and builders, who thus tended to approach new constructions in steel with the structural systems of the past. So to begin with there was a vast range of different typologies of long structures with arches and latticed girders, in general rather heavy both overall and in detail. This was partly because of the great density of the secondary members but also because the only system for connecting them was by hot riveting. For decades this type of construction dominated steel bridges.

It seems reasonable to suggest that steel bridges, like other things, tend to reflect the spirit of the age in which they were built, also because construction in steel is already in itself a particular form of architecture.

There were, however, a few exceptions to this general rule, such as the Britannia Bridge over the Menai Strait (1851), designed by Stephenson and his collaborators. With its well-known self-supporting plate girder it really broke with the past and anticipated by about a century the bridges of self-supporting girders in stiffened steel plate.

In many significant instances, as in suspension bridges, where there was a desire to exploit the new material to the full, new structures were built growing constantly in lightness and elegance. This development, with the help of new techniques and means of construction, has continued without a halt up to our own days, and is ready to launch itself into the future, as will be shown later. So bridges gradually became more slender and efficient, but to begin with still far from the lightness of those structures that could only be achieved with the use of high strength steels and electric welding methods that have made it possible to simplify and lighten the joint very considerably.

If one pauses for a moment to consider certain modern typologies of bridges created from steel over the past 40 years, such as cable stayed bridges, the attentive critic will be struck by an evolution that is so rich and variegated that it might almost be considered a revolution. This evolutionary process, with the help of new construction and assembly techniques, and new technologies for the use of materials, has brought results that are objectively of very great interest in the field of large buildings, even from a formal point of view.

## 2. LONG SPAN BRIDGES - STRUCTURAL TYPOLOGIES

### 2.1 Long span bridges - structural systems

More than sixty years ago aeronautical engineers introduced the "strength/weight factor". It is defined by the ratio  $\sigma_a/\gamma$  between the permissible stress  $\sigma_a$  of the material and its specific weight  $\gamma$ . About thirty years later (1951) Prof. Fritz Stüssi (1) arrived at a formula that was both concise and at the same time highly expressive related the theoretically maximum span that a bridge could be given to the physical parameters involved:

$$g_H = (\psi_F g_F + \psi_P p) \frac{l}{l_c - l} ; \quad l_c = \alpha \frac{\sigma_a}{\gamma}$$

In this formula the values  $g_H$ ,  $g_F$ ,  $p$  are, per unit of length, respectively the dead weight of the principal structures of the bridge, the dead weight of its secondary structures and the live load, while  $\psi_F$  and  $\psi_P$  are, respectively, coefficients depending on the distributions of  $g_F$  and, differentiated of  $p$ . Stüssi's formula still contains the so-called strength/weight factor  $\sigma_a/\gamma$  of the aeronautical engineers, as a fundamental parameter in the problem of long spans. But it also contains a factor  $\alpha$  that depends on the chosen structural system and the relative geometry, that is to say, on a parameter that depends essentially on the ability of the designer, or "the human factor".

Among the various materials available for the construction of bridges - masonry, reinforced concrete, wood, steel-the highest value of  $\sigma_a/\gamma$  is obtained precisely, and only, for high strength steels. So, clearly, construction in steel dominates and will continue to dominate in the field of long span bridges.

Stüssi's study (Fig. 1), although referring to long spans (and by long he meant starting from 300 m), only took into consideration certain well-trying structural systems, such as:

- Simply supported lattice girders
- Lattice gerber girders
- Arches
- Suspension bridges.

He demonstrated their relative technical-economic validity as the span increase or, more exactly, for their average spans

$$l_m = \frac{\sum l_i^2}{\sum l_i}$$

Stüssi's curves show that the first of these systems is the most suitable for smaller spans (100÷200)m, the second for medium spans (200÷300)m, the third for larger spans (300÷600)m, and lastly suspension bridges for the long spans (500÷2000 m and more). But during the evolution of the technique of steel bridges for the larger spans, besides the suspension bridge a new structural typology has been developed over last thirty years - the cable stayed bridge. As will be shown later, it too is valid and efficient for a wide range of spans (300÷2000 m and over), particularly of its great, rapid continuous and growing development during last decades.

So as things are today, in the field of long span steel bridges two basic structural typologies (2) might be considered valid: the suspension bridge and the cable stayed bridge. They will be the next subject of discussion, examining their basic systems and relative

Structural systems

① Simply supported lattice girder

② Lattice girder truss

③ Lattice arch

④ Suspension bridge with stiffening girder

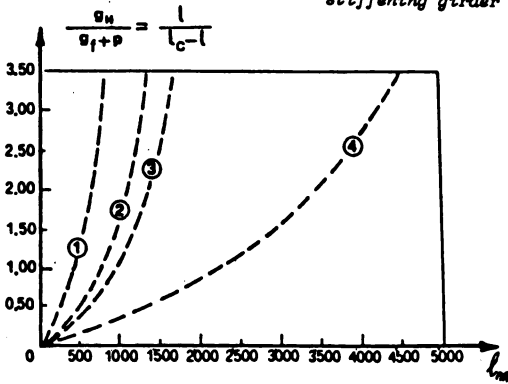
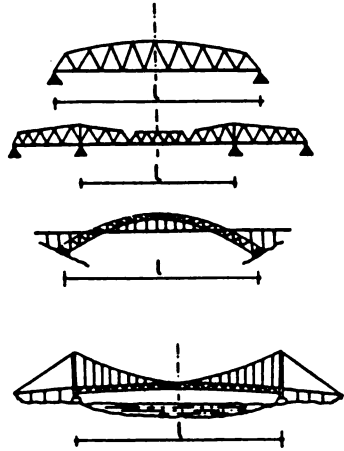


Fig.1: Theoretical limit spans

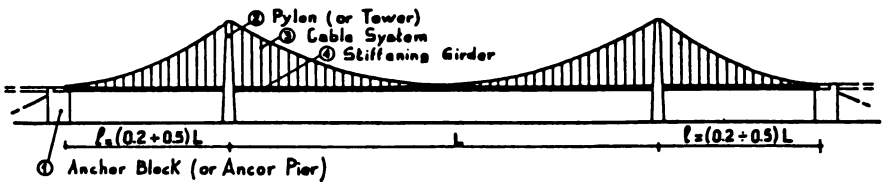


Fig. 2a: Three-span cable supported bridge: main components of a cable supported bridge



Fig 2b: Suspension bridge system: (left) vertical hangers, (right) inclined hangers

erection techniques.

## 2.2 Suspension bridges

The most common type of cable supported bridge has three spans, a large main one flanked by two smaller side spans; the main components of the structural system are indicated in Fig. 2, where the suspension system comprises a parabolic main cable and vertical or slightly inclined hanger cables connecting the stiffening girder to the main cable.

For the concept and design of cable supported bridges, aspects related to erection have a very strong influence, as is the case for any structure of considerable size. Thus, the structural systems and materials, as well as the design of details, must be chosen with due regard to the erection procedure.

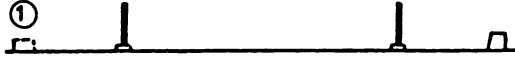
The erection procedure to be used for Bridges with Earth Anchored Cable Systems depends on the anchoring of the cable system, as this will determine the sequence of erecting the cable system and the stiffening girder. With a fully earth anchored cable system as found in all major suspension bridges, the cable system can be completed first and subsequently used to erect the stiffening girder. This feature is illustrated by the erection procedure outlined in Fig. 3, where six stages of a typical suspension bridge erection are indicated. The erection procedure outlined has the advantage that the girder sections adjacent to the pylons are placed when the main cable is reaching its final configuration. This makes it possible to reduce the secondary stresses in the main cable, as the final tightening of the cable bands near the pylons can be postponed to a stage when only insignificant permanent angular changes of the main cable at the pylon top remain. With this procedure the erection crew has to use the catwalk to get to the partially erected stiffening girder in the main span (during stages 3 and 4). The erection procedure of Fig. 3 has been used in several cases, among these for the Severn Bridge.

Another erection procedure to be found within suspension bridges, is illustrated in Fig. 4, where five stages of a typical suspension bridge erection are indicated. The erection procedure of Fig. 4 is advantageous in relation to the planning of the work as the erection crew can easily be transported to the bridge deck from the main piers, and also easily be moved from the main to the side span. The procedure of Fig. 4 was adopted in the erection of the Mackinac Bridge.

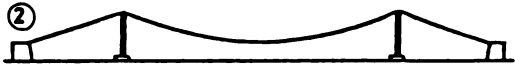
## 2.3 Cable stayed bridges

The cable stayed system (Fig. 5) contains straight cables connecting the stiffening girder to the pylons. In the fan system all stay cables radiate from the pylon top, whereas parallel stay cables are used in the harp system. Besides the two basic cable stayed systems (the fan and the harp system), intermediate systems can also be found; thus, in the modified fan system the cable anchor points at the pylon top are spread sufficiently to separate each cable anchorage. Combined systems containing both the suspension system and the cable stayed system had been applied in cable supported bridges built in the 19th century, such as the Brooklyn Bridge, with its main cable and vertical hangers supplemented by stay cables in the fan configuration.

Stage 1: Construction of the main piers, pylons and anchor blocks.



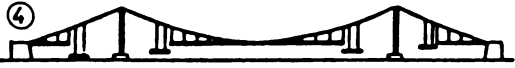
Stage 2: Erection of the main cables



Stage 3: Erection of the stiffening girder starting from the centre of the main span



Stage 4: Erection of the stiffening girder in the side spans to reduce the horizontal displacements of the pylon tops.



Stage 5: Erection of the closing pieces in the stiffening girder systems.



Stage 6: Closing of all joints in the stiffening girder.



*Fig. 3: Earth anchored suspension bridge with stiffening girder erected from midspan towards the pylons*

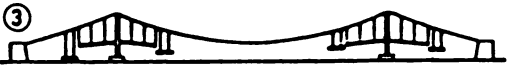
Stage 1: Construction of the main piers, pylons and anchor blocks.



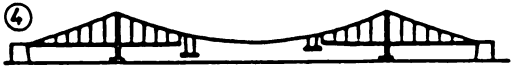
Stage 2: Erection of the main cables.



Stage 3: Erection of the stiffening girder starting symmetrically from both the pylons.



Stage 4: Erection of the central part of the stiffening girder.



Stage 5: Closing of all joints in the stiffening girder.



*Fig. 4: Earth anchored suspension bridge with the stiffening girder erected from the pylons towards midspan.*

The idea of combining the suspension system with stays to achieve more efficient structural systems was proposed already in 1938 by F. Dischinger. In this system the central part of the span would be carried by a suspension system, whereas the outer parts were to be carried by stays radiating from the pylon top. It was intended for a railway cable supported bridge with a 750 m main span across the River Elbe in Hamburg.

In connection with the reconstruction of German bridges after the war, the Dischinger system was proposed on several occasions (Fig. 6), but it was never used, probably because of the pronounced discontinuity of the system with respect to the structural behaviour.

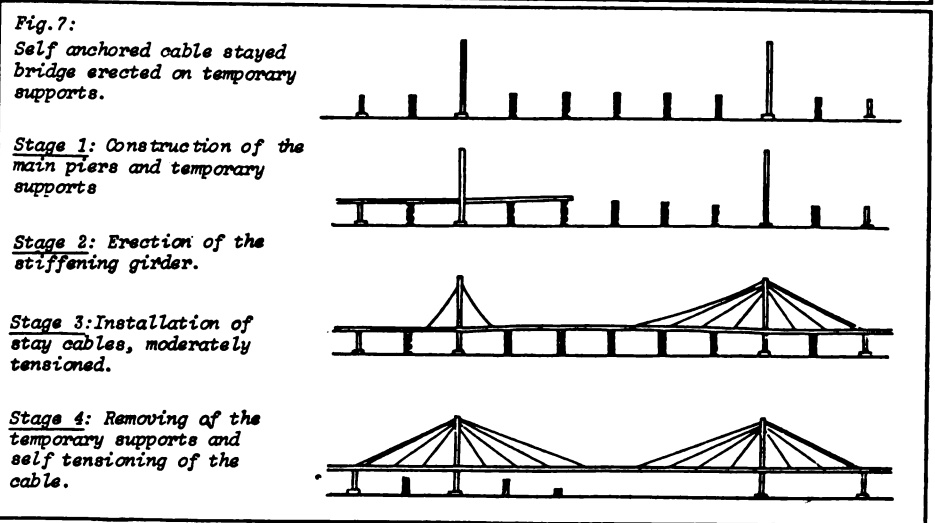
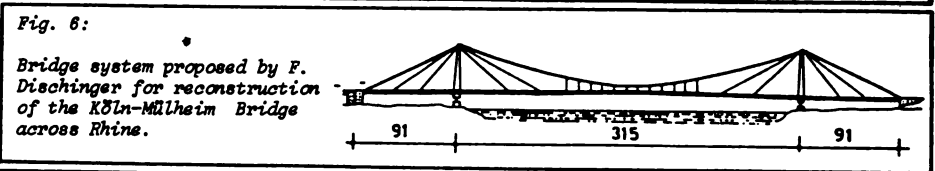
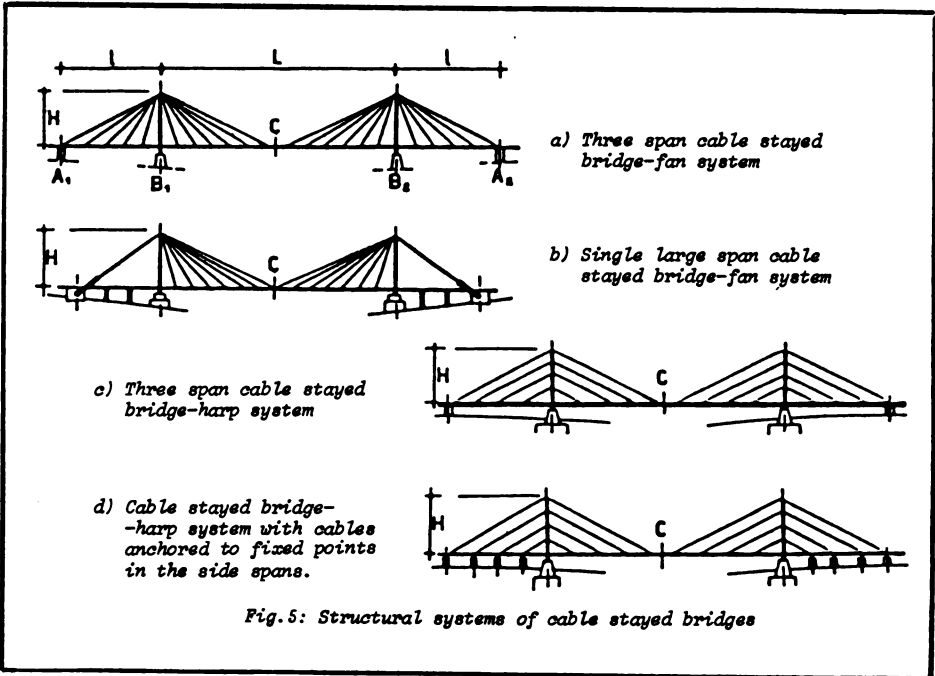
Although the system proposed by Dischinger was never adopted for actual construction, undoubtedly it had a considerable influence on the introduction of the pure cable stayed bridge. For cable stayed bridges the trend has been to move from systems with relatively few heavy stay cables to multi-cable systems with a large number of stay cables supporting the stiffening girder more continuously. For the concept and design of cable stayed bridges too, aspects related to erection have a very strong influence, as is the case for any structure of considerable size. Thus, the structural systems and materials, as well as the design of details, must be chosen with due regard to the erection procedure, as previously mentioned for suspension bridges. A straightforward solution is to erect the entire stiffening girder on temporary supports before adding the cables, as illustrated in Fig. 7 for a fan cable stayed bridge with a Earth Anchored Cable System, where four main stages are indicated.

This erection procedure offers the advantage that the girder can be erected continuously by cantilevering from one end to the other, allowing the transportation of men, equipment, and material on the completed part of the deck (Fig. 8). Also, the procedure leads to an efficient control of the geometry and cable tension. The disadvantage is related to the temporary supports that must be used. In many cases clearance requirements during the construction period, or deep water under the main span, will exclude the installation of the necessary number of temporary supports, and the procedure will not be feasible. Temporary supports can be completely avoided if the bridge is being erected by the free cantilever method, as illustrated in Fig. 9 where four main stages are involved.

With this procedure it is essential to have a very efficient fixity of the super-structure to the main piers throughout the construction period, as the entire stability depends on this fixity until the end pier is reached. Also, the lateral bending stiffness of the girder must be sufficient to ensure the stability of the cantilever arm with a length corresponding to half the main span.

Thus, the procedure is especially advantageous in bridges with a large width-to-span ratio of the girder

The cantilevering of a cable stayed bridge requires that all girder joints are closed as soon as the girder units are in place, to allow the transmission of the normal forces and the bending moments induced during the subsequent tensioning of the stay cables.



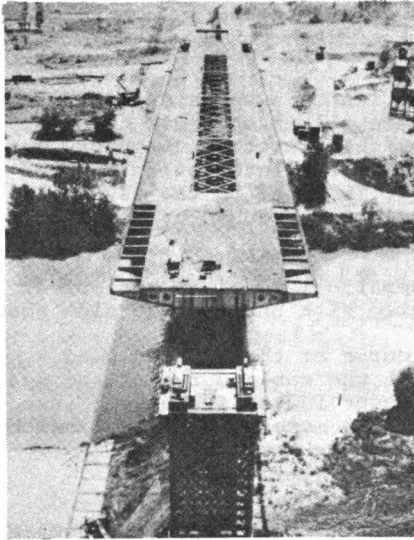


*Fig. 8a: Indiano Bridge (Florence) during deck erection by longitudinal launching.*

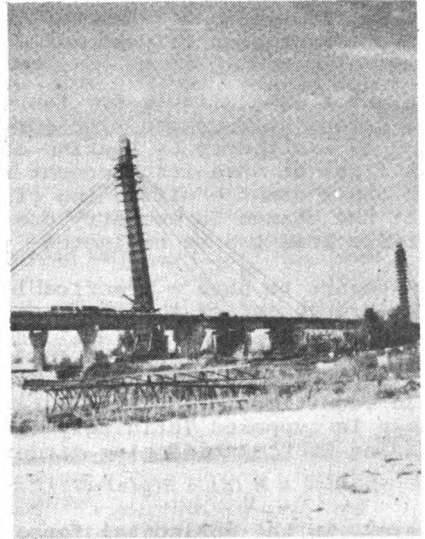
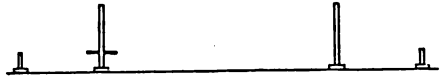


*Fig. 8b: Indiano Bridge in the stage of tensioning of cables.*

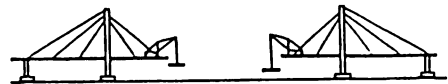
Stage 1: Construction of piers and pylons. The girder units above main piers are erected (temporarily) fixed to the piers.



Stage 2: Erection of deck and cables by balanced free cantilevering.



Stage 3: Erection of central part of the bridge.



Stage 4: Closing main span central, additional dead loads from wearing surface, etc...

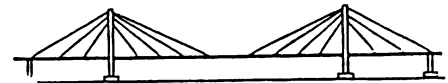


*Fig. 9: Self-anchored cable stayed bridge erected by double sided free cantilevering from the pylons*



### 3. STRUCTURAL ANALYSIS OF LARGE SPAN BRIDGES

#### 3.1 The Evolution of Theories for the Static Analysis of Suspension Bridges

The theories available for the calculation of suspension bridges in the second half of the 19th century were all first order theories, such as the theory by Rankine of 1858. This first order theory was the first to take into account rationally the interaction between the cable and the stiffening girder; it is based on the assumption that the change in geometry due to deflection caused by the applied traffic load can be neglected.

The desire to have a practicable mathematical model is reflected in the arrangement of the structural system with unsuspended side spans.

In Fig. 10 can be seen the funicular curve of the applied dead + traffic load; it does not coincide with the cable curve of the dead load condition, so that moments will occur in the system. Because the cable is supposed infinitely flexible, the moments will be taken by bending in the stiffening girder, and can be expressed by:

$$M(x) = M_0(x) - H(y(x) - \bar{y}(x)) = H \cdot e,$$

where  $H$  is the horizontal force (related to the funicular curve) and  $e$  is the vertical distance from the cable to the funicular curve.

In the evolution of cable supported bridges, the so-called "deflection theory" developed by Melan in 1888, had the effect of progressively increasing shenderness in the design of suspension bridges. The deflection theory is a second order theory taking into account the displacements of the main cable under traffic load when calculating the bending moments in the stiffening girder. In this theory the equilibrium is established more correctly for the deflected system rather than for the system with the dead load geometry.

With reference to a suspension bridge with main span subjected to traffic load in the left half of the span (Fig. 11), it can be seen that, due to the hangers linking the stiffening girder to the main cable, the deflection of the girder will cause a change in the geometry of the cable. The full line is the shape of the cable when deflection of the stiffening girder is taken into account: the cable moves towards the funicular curve, and as equilibrium must exist in the deflected system, the bending moments in the stiffening girder will be:

$$M(x) = H(e(x) - \delta(x)),$$

where  $H$  is the horizontal component of the reaction and  $e - \delta$  is the vertical distance from the funicular curve to the distorted cable. When taking into account the second order effects related to the displacement of the cable, the bending moments in the stiffening girder will be reduced, often to less than half of that found by a first order theory. Actually there are no limits to the reduction that can be achieved, as a suspension bridge with a girder having insignificant bending stiffness will deflect under asymmetrical loading until the displaced cable and the funicular curve coincide. Consequently  $M(x) = 0$  because:  $(e - \delta) = 0$ . As equilibrium can be attained without any stiffening girder at all, the deflection theory will not

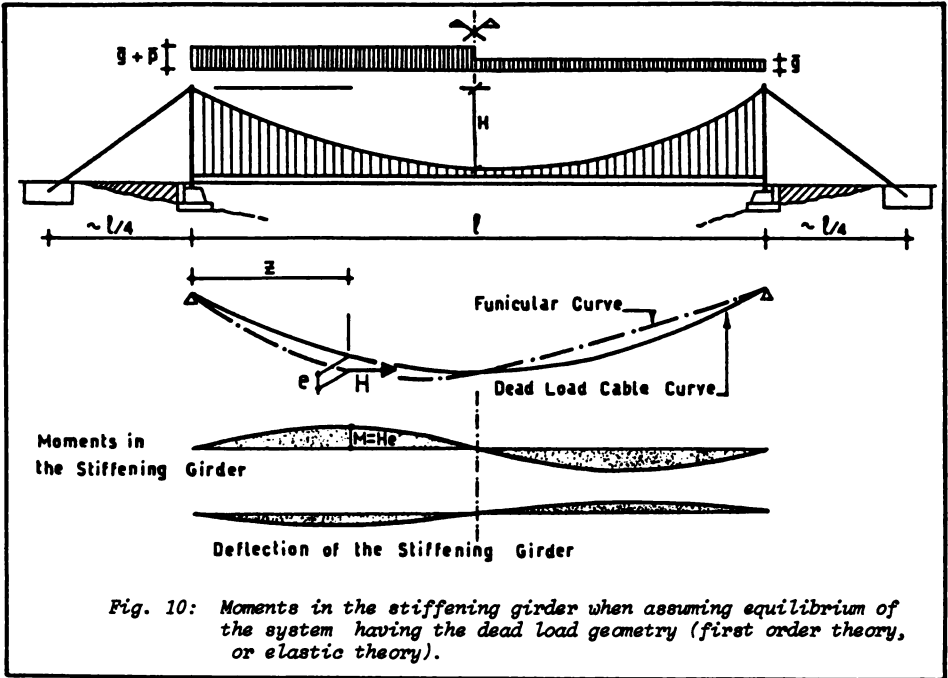


Fig. 10: Moments in the stiffening girder when assuming equilibrium of the system having the dead load geometry (first order theory, or elastic theory).

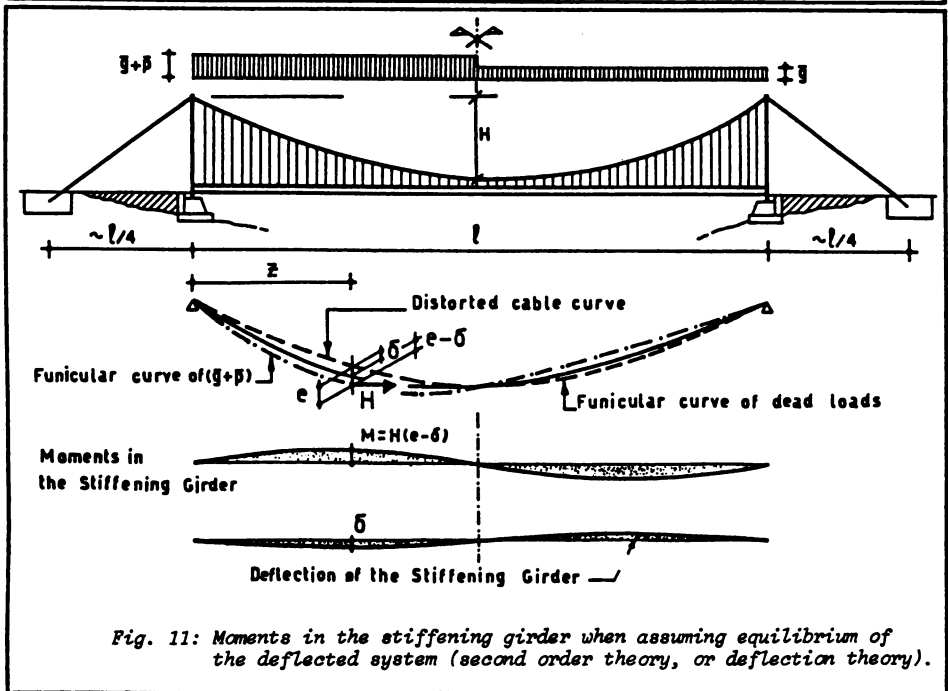


Fig. 11: Moments in the stiffening girder when assuming equilibrium of the deflected system (second order theory, or deflection theory).

ensure a minimum bending stiffness. However to make structural deformations compatible with traffic requirements, in the applications of the deflection theory the authorities recommended a minimum depth of the stiffening truss in the interval from one sixtieth to one ninetieth of the span length. When the deflection theory was introduced, the calculation capacity of the design engineers was still limited, and thus the solution procedure for the non-linear differential equation was difficult and complicated. Consequently, simplifications had to be introduced in the form of charts, tables, and correction curves by which the results of the simpler elastic theory could be corrected to approximate those of the deflection theory (3).

### 3.2 Structural Analysis of Cable Stayed Bridges

Reference is to a continuous stayed bridge with the fan system and with a continuous distribution of cables along the girder, which is the most suitable system for long spans. It is assumed that construction, by regulating the tension in the cable, will ensure a practically straight final configuration with no bending moments. The structural analysis due to permanent loads can be carried out starting from the equilibrium equations of a beam element in the left half of the bridge (Fig. 12):

$$\begin{aligned} \frac{dN}{ds} + n \cos \alpha &= 0 \\ g - n \sin \alpha &= 0 \end{aligned} \quad \left( n = \frac{N_s}{\Delta} \right) \quad (1)$$

in which  $s$  is the abscissa of the cross-section considered,  $N$  is the axial force in the deck,  $N_s$  the axial force in the cable. With reference to the adimensional abscissa  $\xi = s/H$ , and considering that:

$$\operatorname{tg} \alpha = \frac{1}{\xi}; \quad \cos \alpha = \frac{\xi}{\sqrt{1+\xi^2}}; \quad \sin \alpha = \frac{1}{\sqrt{1+\xi^2}},$$

then the second equation of system (1) gives:

$$n = \frac{g}{\sqrt{1+\xi^2}}; \quad N_s = \frac{g\Delta}{\sqrt{1+\xi^2}}, \quad (2)$$

which, when substituted in the first of the equations in (1), gives:

$$\frac{dN}{d\xi} = -gH\xi$$

From this, taking into account that at the centre ( $\xi = L/2H$ ), because of the erection procedure, it can be assumed that  $N=0$ , one finally obtains:

$$N(\xi) = g \frac{H}{2} \left\{ \left( \frac{L}{2H} \right)^2 - \xi^2 \right\} \quad (3)$$

The action of the live loads modifies the initial equilibrium corresponding to the permanent loads, and sets up an additional stress-strain state. The stress state already existing before the action of the mobile loads is made up of tensile stresses in the stays and of compression stresses in the pylons and the girder. Furthermore, the action of the dead loads fixes the equilibrium configuration of the cables, and thus controls their reactions through the value of Dischinger's modulus of virtual elasticity (Fig. 13):

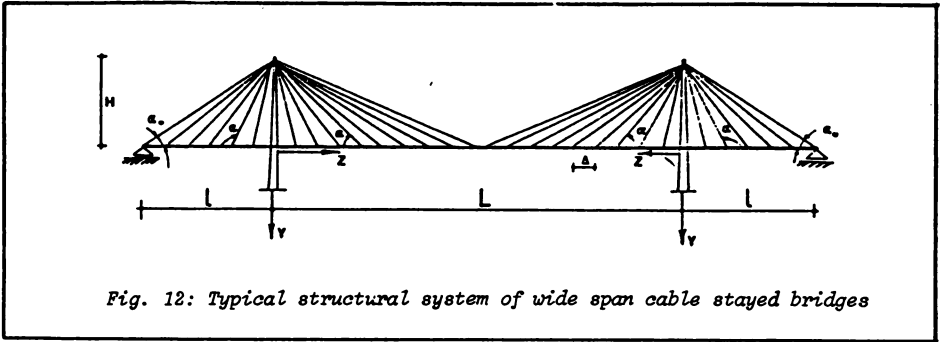


Fig. 12: Typical structural system of wide span cable stayed bridges

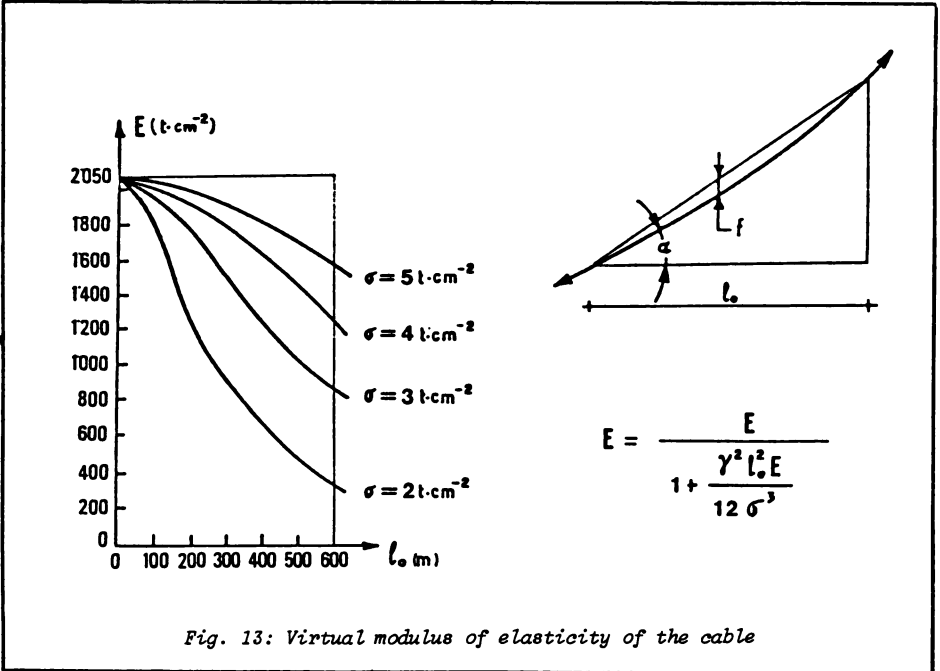


Fig. 13: Virtual modulus of elasticity of the cable

$$E = \frac{E}{1 + \frac{\gamma^2 l_0^2 E}{12 \sigma^3}}$$

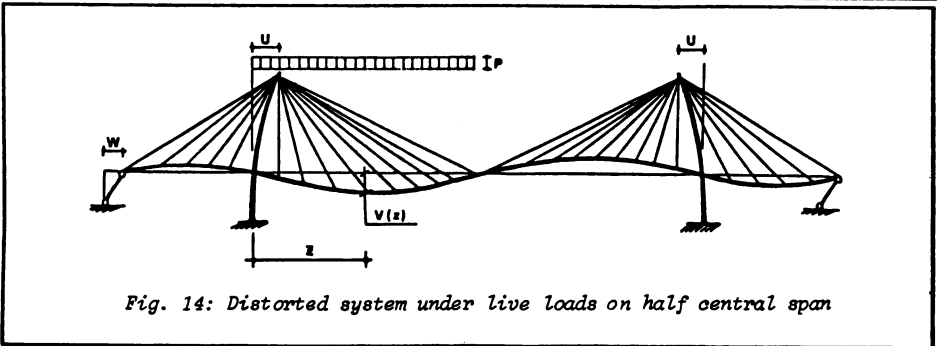


Fig. 14: Distorted system under live loads on half central span

$$E^* = \frac{E}{1 + \frac{\gamma^2 l_o^2}{12\sigma^3}}$$

$$\left\{ \begin{array}{l} \gamma = \text{specific weight of steel in the cable} \\ l_o = \text{horizontal projection of the length of the cable} \\ E = \text{modulus of longitudinal elasticity of the cable} \\ \sigma = \text{tension of the cable.} \end{array} \right.$$

The additional strain in the bridge is further indentified (Fig. 14) by the vertical displacements  $v(z)$  of the girder, by the rigid horizontal displacement  $w$  of the girder itself, and by the elastic horizontal displacement  $u$  of the tops of the pylons.

Structural analysis for evaluating static effects due to live loads, after the first simple applications in the 1950+s, has been studied theoretically by various authors (5) with approximation methods that are very interesting, but tend to be rather laborious and complex.

At the same time, however, the complete and exact structural analysis of the stress-strain state has been carried out systematically by means of a discrete model which also takes into account the effects of non linearity due to strains in the cables and variations in the geometry of the structure. The discrete model can be obtained either by the analysis with a computer of a system with a given number of cables, or by solving with a numerical method (e.g. the finite element method) the equations of the continuous model. The results obtained in this way are very precise and make it possible to state that the earlier analytical obstacles, considerable through they were, have now been overcome, obstacles that were responsible for the initial distrust in the cable stayed bridge and its late development.

In fact, computers have made it possible to conduct investigations and reasearch on stiffening systems of cable stayed bridges for application to long and very long spans.

### 3.3 The Aerodynamic Stability of Long Span Bridges

Among the numerous problems that arise in studying the dynamic behaviour of long span bridges, aerodynamic instability is undoubtedly the most important, since it may lead to destruction. The main forms of aerodynamic instability are:

- Those deriving from self-excited vibrations of the bridge due to vortex shedding by the deck when exposed to wind, vibrations that, as a first approximation, are substantially independent by deck deformation;
- Those deriving from flutter due to periodic variations in aerodynamic lift and the (external) twisting moment, vibrations that depend on the flexural-torsional oscillations of the girder.

### 3.4 Self-excited Oscillations Due to Vortex Shedding

For the sake of a brief discussion on the essentials of the problem of self-excited oscillations of a bridge due to vortex shedding, it should be remembered that if a bridge is exposed to a steady current of air, vortices shed from the deck generating the so-called "Von Karman wake". Each time that a vortex is shed, a noticeable vertical

force develops on the deck. So periodic shedding produces a pulsing lift effect on the deck. For a given value of the velocity of the wind, which corresponds to the so-called critical resonance velocity between the frequency of the formation of vortices and the natural frequency of the bridge, vertical (and sometimes, but more rarely, torsional) oscillations are induced of increasing amplitude. Depending on the particular case, the amplitude of these oscillations may be limited, or may reach catastrophic proportions.

From numerous experiments in wind tunnels, within the range of variability of the Reynolds number:

$$R = \frac{CV_0}{\mu/\rho}$$

(in which  $C$  is a characteristic dimension of the cross-section, normally the half-width of the cross-section of the deck,  $V_0$  the wind speed and  $\mu/\rho$  the so-called kinematic viscosity, i.e. the ratio between the viscosity  $\mu$  and the density  $\rho$  of the air), the frequency  $f_s$  of the vortex shedding is directly proportional to the wind speed  $V_0$ , and inversely proportional to the transversal dimension  $C$  of the deck. For a given cross-section of the deck, the frequency  $f_s$  of vortex shedding can be expressed through the simple relation:

$$f_s = K_s \frac{V_0}{C} \quad (4)$$

in which  $K_s$  is a constant, to be defined for each cross-section, in the technical literature known as a Strouhal number. Then, for a given cross-section of the deck, the evaluation of the ratio:

$$K_s = f_s \frac{C}{V_0}$$

i.e. of the corresponding Strouhal number  $K_s$ , makes it possible to evaluate the frequency of the vertical forcing actions.

The values of  $K_s$  are worked out for each case by testing models of cross-section of the deck in a wind tunnel. Experiments already carried out show that for a circular cylindrical cross-section  $K_s \approx 0,25$  while for thin cross-section, aerodynamically shaped,  $K_s \approx 0,15$  to  $0,10$ .

So it seems reasonable to conclude that for a long span bridge with a fundamental vertical oscillation period of 2.5 sec. and a cross-section with a Strouhal number  $K_s$  for vortex shedding equal to 0.20, the resonance condition would be attained when the wind speed, blowing across the deck, reaches 20 m/sec. But for a more aerodynamic cross-section, e.g. with a  $K_s$  value of 0.10, the critical velocity would be 40 m/sec.

Long span bridges generally have rather low free flexural vibration frequencies, and anyway they decrease as the span increases, as shown by the curves of Fig. 15. Given these frequencies, and  $K_s$  values on average around 0.20, with the usual values of  $C$ , and in the range of variability of the wind speed  $V_0$  (between 5 m/sec. and 50 m/sec., i.e. between 18 Km/h and 180 Km/h), it seems impossible to avoid the onset of resonance conditions between the aerodynamic actions induced by vortex shedding from the deck and the natural oscillation due to vertical displacements of the girder. In the absence of special devices, that do not always work (flaps arranged along the lateral edges of the deck able to destroy the Von Karman wake before it develops), it is impossible to prevent the formation of self-excited vibrations of

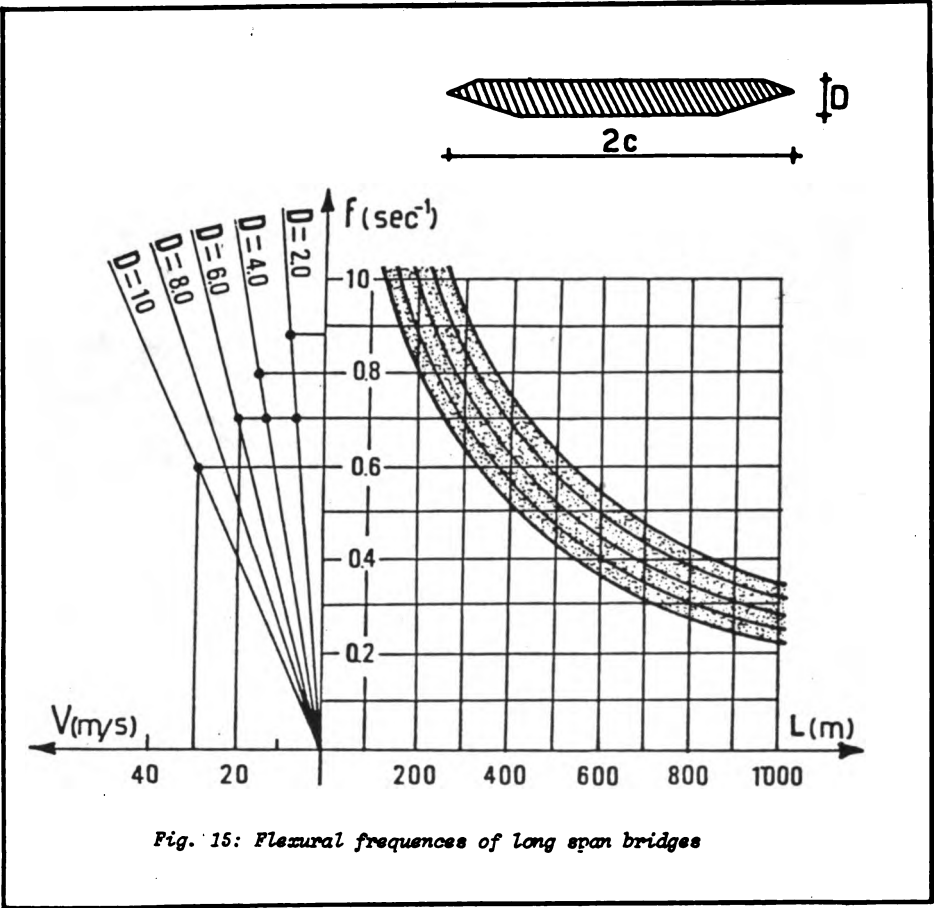


Fig. 15: Flexural frequencies of long span bridges

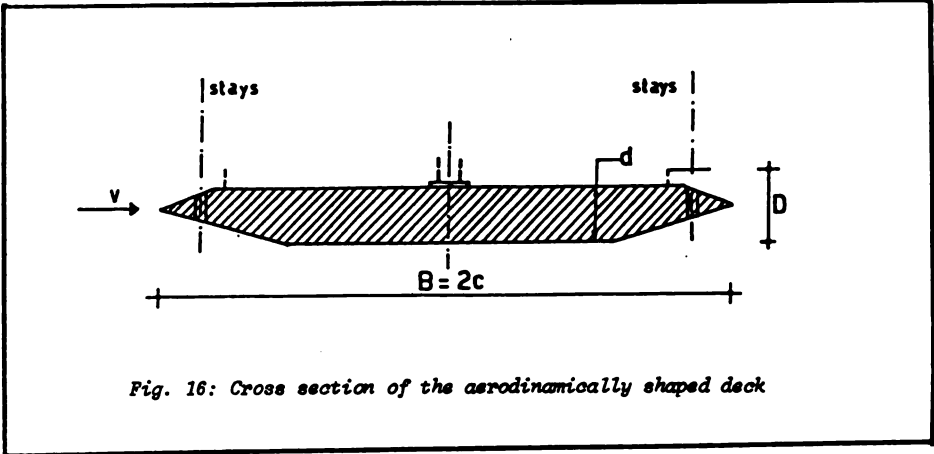


Fig. 16: Cross section of the aerodynamically shaped deck

the deck due to these effects. What is possible, as a counter measure, is to reduce the intensity of the pulsing forces due to the vortices. Studies in wind tunnels in fact make it possible to quantify not only the frequency of the periodic actions transmitted by the wake, as expressed by equation (4), but also the intensity of the pulsing lift forces as a function of such characteristic parameters as the wind speed  $V_0$ , the half-width  $C$  of the deck cross-section, and its shape. In fact, if  $p_s$  is the pulsing lift per unit of length of the deck, then:

$$p_s = \frac{1}{2} \rho V_0^2 (2C) C_p \sin \pi f_s t \quad (5)$$

where  $\rho$  is the density of the air,  $f_s$  the frequency expressed by (4), and  $C_p$  a coefficient depending on the shape of the cross-section to be determined experimentally. Experiments in wind tunnels show that the coefficient  $C_p$  is greatly reduced if the cross-section of the deck is "aerodynamically" shaped (Fig. 16). In this way the intensity of the periodic lift forces can be reduced and so also the energy that the wake transmits to the deck in conditions of resonance for each oscillation cycle of the bridge. In this case the energy which, because of various damping effects, is dissipated during the oscillation of the bridge, can partly absorb the energy transmitted by the vortices, and so reduce the maximum amplitudes of the vertical oscillations of the bridge to acceptable values. So a long span bridge, whether suspended or cable stayed, must have an aerodynamically shaped deck, so as to avoid dangerous amplitudes of self-excited vertical oscillations due to vortex shedding. An aerodynamic shape of the cross-section will have the following characteristics (Fig. 16):

- 1) Tapered leading and trailing edges (with a low drag coefficient)
- 2) High slenderness ratio ( $\approx C/D \approx 10$ )

So for the designer of long span bridges today this is the first problem - to decide on the geometry of the cross-section of the deck and its aerodynamic stability, taking into account resonance with the Von Karman wake. It might be said that for long span bridges the study of this problem can never be undervalued in the design phase, when the geometrical characteristics of the cross-section of the bridge deck are being defined. A further check in a wind tunnel on a suitably reduced scale model is also necessary.

#### 3.4.1 Self-Excited Oscillations Due to Flutter

Problems of flutter, that is, vibrations self-excited by the periodic variations in the lift and by aerodynamic moments due to variations in the angle of attack of the wind on the deck because of its flexural-torsional vibrations, must be neutralized. So the cross-section of a modern long span bridge should typically have one or more longitudinal openings. This was first suggested by Stüssi and Ackeret. But it should only be necessary if those particularly dangerous conditions arise in which the value of the ratio between the natural torsional and flexural vibrations is close to unity. In other words, if there are very small values for the natural torsional frequency. In the case of stall flutter, or aerodynamic instability due to high values of the angle of attack of the wind on the horizontal plane of the deck, such values would lead to very dangerous conditions, as in the case of the first Tacoma Narrows bridge.



During the past 40 years a large amount of theoretical and experimental (windtunnel) work has been done to solve the complex problem of the aerodynamic stability of long span bridges. Various solutions have been proposed, and the most effective have been mentioned here.

The fundamental design criteria in this field for long span bridges, whether suspended or cable stayed, show a definite trend towards reducing the height of the deck to a minimum, forsaking the stiffening contribution of the flexural moment of inertia. This is because it has a very limited effect in countering the deformations compared to the advantages to be drawn from reducing the static and aerodynamic actions of the wind. So at the same time another problem assumes greater importance. How to strengthen the entire structure with other systems so that, from the point of view of deformations, it can cope with service conditions. And since these various aspects so far considered are intimately connected, also the stiffening systems have a considerable and favourable influence on each other (6).

#### BIBLIOGRAPHY

- (1) Stüssi F. : Das Problem der Grössen Spannweite - VSB Verlag, Zürich, 1954.
- (2) Gimsing N.J. : Cable supported Bridges - John Wiley & Sons
- (3) Steinmann D.B. : Suspension Bridges, Their Design, Construction and Erection, John Wiley & Sons, New York, 1922.
- (4) De Miranda F. : Ponti strallati di grande luce Ed.Sc.A.Cremonese - Roma, 1980.
- (5) De Miranda F., Como M., Maceri F. : Basic Problems in Long Span Cable Stayed Bridges - Dept. of Structures, University of Calabria, Report N<sup>o</sup>. 25, 1979.
- (6) De Miranda F. : Paper No. 8. Design - Long Span Bridges. ECCS/BCSA International Symposium on Steel Bridges, London, 1988.

## CONTRIBUTION TO NONLINEAR ANALYSIS OF R.C. THIN-WALLED BEAMS AND FRAMES BY FINITE ELEMENT METHOD

*M. Sekulović and B. Pujević*

*Faculty of Civil Engineering, Belgrade, Yugoslavia*

### ABSTRACT

A method of analysis for three dimensional slender reinforced concrete frames based upon the finite element displacement formulation is presented. A stiffness matrix for the analysis of thin-walled beams with an arbitrary open cross-section made up of longitudinal filaments to represent the concrete and reinforcing steel is derived. The description of the element is based on the assumptions introduced by Vlasov. The warping degree of freedom is added to the conventional degrees of freedom at each end of the element. An updated Lagrangian formulation is used to take into account the material nonlinearities and the effects of changing structural geometry.

### 1. INTRODUCTION

It is well known that the behaviour of reinforced thin-walled concrete structures deviate, even for relative low loading levels from the linear elastic behaviour that classically has been assumed as valid. For ultimate loading levels the behaviour of these structures is highly non-linear not only because of the material properties but also because the change of structural geometry is significant.

The purpose of this paper is to describe a unified numerical procedure for the material and geometric nonlinear analysis of reinforced concrete thin-walled beams and frames.

The stiffness matrix for the general nonlinear analysis of thin-walled members with open cross-section is derived. The description of the element is based on the assumptions introduced by Vlasov.

The approach followed is of a general nature, enabling its implementation in a general-purpose finite element computer program.

### 2. THIN-WALLED BEAM WITH OPEN CROSS-SECTION

The following three basic assumptions, which are usually adopted in the analysis of thin-walled beams, are used in this study:

- a) The cross-section is assumed to be perfectly rigid in its plane while free to warp out of its plane.

- b) The shear strains in the middle surface are very small and can be neglected.  
 c) Normals to the reference surface of the member remain normal to it and undergo no change in length during deformation (the Kirchhoff-Love assumption).  
 According to the first assumption only three displacement components, i.e., two translations and a angle of twist, are required to describe the cross-sectional behaviour. From Fig. 1, the in-plane displacements of on arbitrary point are

$$\begin{aligned} u^* &= \xi - (y - y_p)\theta \\ v^* &= \eta + (x - x_p)\theta \end{aligned} \quad (1)$$

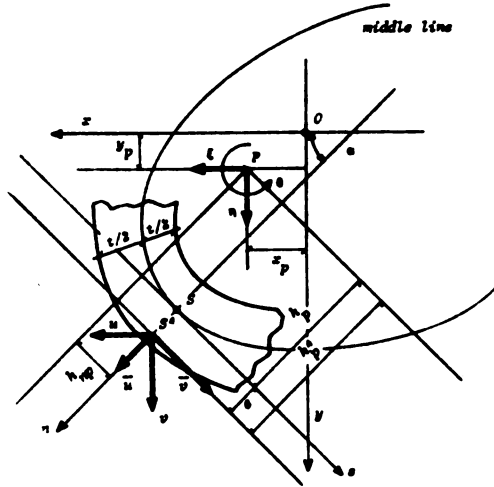


Fig. 1

The longitudinal displacement  $w$  of the arbitrary point, due to the warping of the cross section may be found, concerning the absence of the shearing strain,

$$w^* = w_0 - \xi x - \eta y - \theta z \quad (2)$$

where  $w_0$  is an arbitrary function and

$$w_p = \int_0^s h_p ds + h_{np} e = w_p + h_{np} e \quad (3)$$

is the generalized warping function.

The first three terms on the right hand side of eq. (2) describe longitudinal displacements of the cross-section as contained in a plane surface (Bernoulli's assumption). The last term describes the warping of the cross-section.

From eq. (1), (2) and (3) it is obvious that the displacements  $(u, v, w)$  of a thin-walled beam are dependent only on one coordinate variable, namely the axis of the beam. This is a direct result of the starting assumptions, and thus the thin-walled beam is effectively reduced to a one-dimensional problem.

### 3. FINITE ELEMENT FORMULATION

Figure 2. shows a typical finite element of thin-walled beam as a straight line element with two nodes at the ends of the member. At each node there are seven

displacements as the basic unknown parameters, so that the element has fourteen degrees of freedom. The convention for the positive directions of the incremental displacements and forces at the element nodes is indicated in Fig. 2.

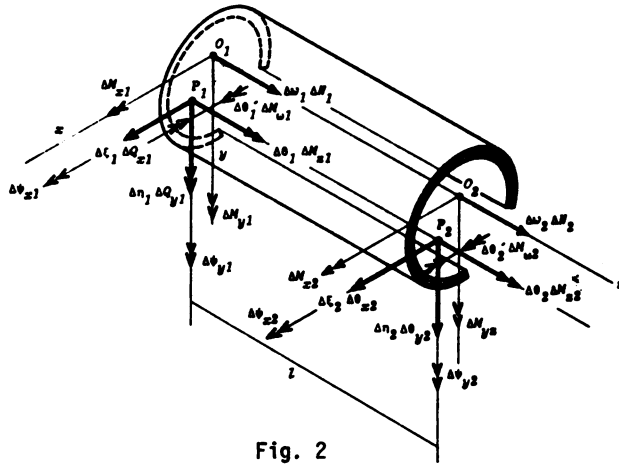


Fig. 2

It should be noted that the normal force  $N$  and the bending moments  $M_x$  and  $M_y$  refer to the centroidal point  $O$  while the other forces refer to the point  $P$ . The distributed loads  $q_x$ ,  $q_y$  and  $q_z$ , and support reactions refer to the axis which pass through the point  $P$ . It should also be noted that the transverse shear forces and the twisting moment can not be defined in terms of deformations as a result of imposed thin-walled beam assumptions. The vector  $\Delta q$  of incremental displacements at the nodes of the member can be written as

$$\Delta q^T = (\Delta q_u \quad \Delta q_v \quad \Delta q_\theta \quad \Delta q_w) \quad (4)$$

where

$$\begin{aligned} \Delta q_u^T &= (\Delta \epsilon_1 \quad \Delta \psi_{y1} \quad \Delta \epsilon_2 \quad \Delta \psi_{y2}) \\ \Delta q_v^T &= (\Delta \eta_1 \quad \Delta \psi_{x1} \quad \Delta \eta_2 \quad \Delta \psi_{x2}) \\ \Delta q_\theta^T &= (\theta_1 \quad \Delta \theta_1' \quad \Delta \theta_2 \quad \Delta \theta_2') \\ \Delta q_w^T &= (\Delta w_1 \quad \Delta w_2) \end{aligned} \quad (5)$$

A linear displacement field is adopted for the axial displacement field, and the cubic displacement field for other displacements

$$\begin{aligned} \Delta \epsilon &= N_u \quad q_u \\ \Delta \eta &= N_v \quad \Delta q_v \\ \Delta \theta &= N_\theta \quad \Delta q_\theta \\ \Delta w &= N_w \quad \Delta q_w \end{aligned} \quad (6)$$

where the shape functions describing the displacement field are

$$\begin{aligned}
 N_u &= N_\theta = N \\
 &= (1-3\xi^2+2\xi^3) \mathcal{L}(\xi-2\xi^2+\xi^3) \quad 3\xi^2-2\xi^3 \quad \mathcal{L}(-\xi^2+\xi^3) \\
 N_v &= (1-3\xi^2+2\xi^3) \mathcal{L}(-\xi+2\xi^2-\xi^3) \quad 3\xi^2-2\xi^3 \quad \mathcal{L}(\xi^2-\xi^3) \\
 N_w &= (1-\xi) \xi
 \end{aligned}
 \tag{7}$$

where

$$\xi = \xi/L$$

The derivation of the equilibrium equation using the principle of virtual displacements and its transformation and linearization in the incremental form following the updated Lagrangian formulation is explained in Ref. 1. Substituting the expressions for incremental displacements eq. 6 it is possible to obtain the following equation of equilibrium in terms of nodal displacements and nodal forces

$$({}^1K_L^T + {}^1K_{NL}) q = {}^2R - {}^1Q \tag{8}$$

$${}^1K_L^T = \int_{V} {}^1B_L^T D^T B_L dV \quad - \text{tangent incremental stiffness matrix} \tag{9}$$

$${}^1K_{NL} = \int_{V} {}^1B_{NL}^T {}^1\sigma {}^1B_{NL} dV \quad - \text{geometric incremental stiffness matrix}$$

${}^2R$  - vector of externally applied nodal-point loads in current configuration

${}^1Q$  - the vector of nodal-point forces equivalent to the element stresses in previous configuration

${}^1\sigma$  and  ${}^1\bar{\sigma}$  - the matrix and vector of Cauchy stresses

$B_L, B_{NL}$  - the linear and nonlinear strain-displacement transformation matrix

$D^T$  - the tangential stress-strain material property matrix.

The more detailed approach of derivation of element matrices of eq. 8 are given in Ref. 1. The final form of the linear stiffness matrix  ${}^1K_L$  is given in Table 1.

Nonlinear (geometric) stiffness  ${}^1K_{NL}$  is derived assuming the following incremental strain components

$$\begin{aligned}
 \Delta\eta_{33} &= \frac{1}{2}((\Delta w_{,z})^2 + (\Delta u_{,z})^2 + (\Delta v_{,z})^2) \\
 2\Delta\eta_{13} &= \Delta v_{,x} \Delta v_{,z} + \Delta w_{,x} \Delta w_{,z} \\
 2\Delta\eta_{23} &= \Delta u_{,y} \Delta u_{,z} + \Delta w_{,y} \Delta w_{,z}
 \end{aligned}
 \tag{10}$$

The final form given in Table 2. is derived assuming constant axial force and linearly varying bending moments and bimoments. It must also be noted that the final form is simplified by neglecting the nonlinear term  $w_{,z} w_{,z}$  in the above expressions for the strain components. The element forces appearing in  ${}^1K_{NL}$  are those existing in previous equilibrium configuration.

The element stiffness matrices of eq. 8 are evaluated with respect to nodal displacements referred to local coordinate system. The element displacements with respect to the local coordinate system are related to those in the global system by the transformation

Table 1.

1	2	3	4	5	6	7	8	9	10	11	12	13	14
6a				3la			-6a				3la		
	6b		-3lb					-6b		-3lb			
		g							-g				
			2l <sup>2</sup> b					3lb		l <sup>2</sup> b			
				2l <sup>2</sup> a			-3la				l <sup>2</sup> a		
					c	d						-c	d
						e						-d	f
							6a				-3la		
								6b		3lb			
									g				
										2l <sup>2</sup> b			
											2l <sup>2</sup> a		
												c	-d
													e

$$a = \frac{2EI_{xx}}{l^3} \quad b = \frac{2EI_{yz}}{l^3} \quad c = \frac{12EI_{xx}}{l^3} + \frac{GI_t}{10} \quad e = \frac{4EI_{xx}}{l} + \frac{2GI_t l}{15} \quad f = \frac{2EI_{xx}}{l^2} - \frac{GI_t l}{30} \quad g = \frac{EA}{l}$$

Table 2.

1	2	3	4	5	6	7	8	9	10	11	12	13	14
36a				36a	36b + 3c	36b	-36a				36a	-36b - 33c	36b + 34c
	36a		-36a		36d + 3e	36d		-36a		-36a		-36d - 33e	36d + 34e
				4l <sup>2</sup> a	-36b - 64c	-4l <sup>2</sup> d - l <sup>2</sup> e	36a	36a		-l <sup>2</sup> a		36d + 64e	l <sup>2</sup> d
				4l <sup>2</sup> a	36b + 64c	4l <sup>2</sup> b + l <sup>2</sup> c	-36a				-l <sup>2</sup> a	-36b - 64c	-l <sup>2</sup> b
					36f + 18g	36f + 34g	-36b - 3c	-36d - 3e		-36d + 34e	36b + 34c	-36f - 18g	36f
						4l <sup>2</sup> f + l <sup>2</sup> g	-36b	-36d		l <sup>2</sup> d + l <sup>2</sup> e	-l <sup>2</sup> b - l <sup>2</sup> c	-36f - 34g	-l <sup>2</sup> f - 6l <sup>2</sup> g
							36a				-36a	36b + 33c	-36b - 34c
								36a		36a		36d + 33e	-36d - 34e
										4l <sup>2</sup> a		36d - 34e	-4l <sup>2</sup> d - 3l <sup>2</sup> e
										4l <sup>2</sup> a		-36b + 34c	4l <sup>2</sup> b + 3l <sup>2</sup> c
												36f + 18g	-36f
													4l <sup>2</sup> f + 3l <sup>2</sup> g

$$a = -\frac{N}{30} \quad b = \frac{1}{30}(-\gamma_x N_x + M_{xx}) \quad c = \frac{Q_x}{30} \quad d = \frac{1}{30}(N_x N_x + M_{xx}) \quad e = -\frac{Q_x}{30}$$
  

$$f = \frac{1}{30} \left( -\frac{l}{4} N_x - \frac{l}{12} M_{xx} + \frac{l}{12} M_{xx} + \frac{l}{12} M_{xx} \right) \quad g = -\frac{1}{30} \left( \frac{l}{12} Q_x + \frac{l}{12} Q_x + \frac{l}{12} \frac{M_{xx} + M_{xx}}{l} \right)$$

$$\Delta q^* = T \Delta q$$

(11)

where  $\Delta q$  are displacements in local coordinate system,  $\Delta q^*$  are displacements in global coordinate system,  $T$  is transformation matrix.

For the case of an arbitrary cross section the transformation matrix is given in Ref. 2. In preparation for computer assembly of thin-walled elements, the conditions of compatibility and equilibrium of nodes are formulated using connectivity matrix (2). The overall stiffness matrix taking into account the boundary conditions is generated following the rules that govern the assembly process used in the finite element analysis.

#### 4. MODELING OF MATERIAL PROPERTIES

Concrete and reinforcing steel are considered homogeneous materials. It is assumed that perfect bond exists between concrete and steel reinforcement, thus the displacement field within a reinforced element can be considered continuous. The material properties of concrete and steel depend on the stress state of the material due to the effect of the nonlinear stress-strain relationships, cracking of concrete and yielding of steel.

As it is shown in Fig. 3 the cross-section of the thin-walled beam element is divided into discrete number of concrete and reinforcing steel filaments. The concrete filament area is  $A_{bi}$ , and its position in the cross-section is defined by the coordinates  $x_{bi}$ ,  $y_{bi}$  with the respect to the reference axes. The value of the tangent modulus of the concrete filament is  $E_{bi}^t$ . Each steel filament has steel area  $A_{aj}$ , and coordinates  $x_{aj}$ ,  $y_{aj}$ . The value of the tangent modulus of the  $j$ -th steel filament is  $E_{aj}^t$ .

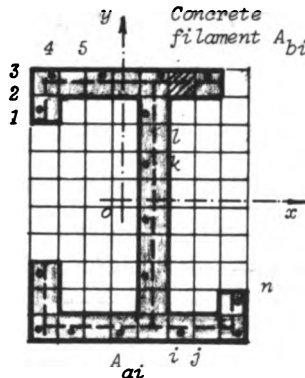


Fig. 3

The stress-strain relation-ship for concrete for short-time loading is the one suggested by Yugoslav preliminary codes shown in Fig. 4.

Tensile failure or cracking of concrete occurs when tensile stress exceeds its maximum tensile strength  $f_g$ .

In this study a bilinear model which is symmetrical about origin, as shown in (Fig. 5) is used for steel reinforcement.

The assumption about the vanishing shearing strain in the middle surface, introduced by Vlasov, allows the separate consideration of bending and warping torsion effects in straight members with open cross-section. In order to simplify the numerical approach the bending and torsional interaction are coupled only thru normal stresses. A trilinear model is used to represent the torsional response of a reinforced thin-walled concrete beam. The experimental curve Fig. 6 can be usually approximated by three straight lines representing the uncracked, cracked and yielded phase, respectively.

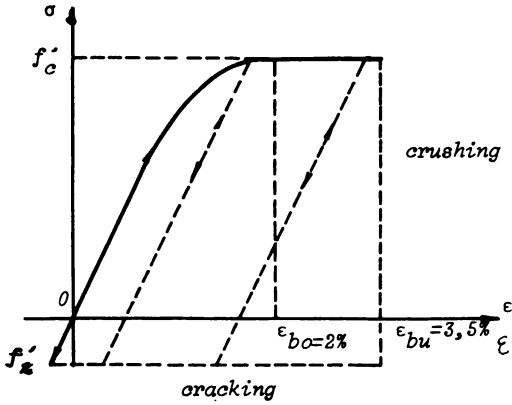


Fig. 4

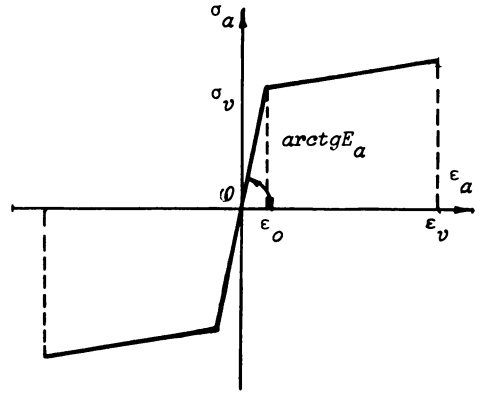


Fig. 5

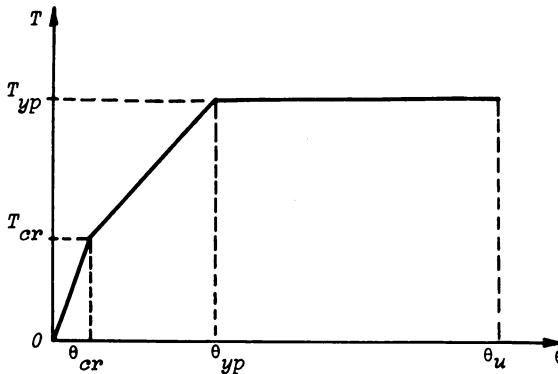


Fig. 6

Taking into account the assumptions about the deformation for straight thin-walled beams with open cross-section, only normal stress contributes to the yielding of the material and the tangent modulus  $E_t$  for both materials at a filament is uniquely determined by the total strain  $\epsilon$  and the incremental strain  $\Delta\epsilon$ . The incremental strain  $\Delta\epsilon$  is given as

$$\Delta\epsilon = \Delta\omega'_0 - x\Delta\xi'' - y\Delta\eta'' - \omega\Delta\theta'' \quad (12)$$

and the stress increment as

$$\Delta\sigma = E^t \Delta\epsilon \quad (13)$$

Substituting the above eq. in the equilibrium equations establishing the stress-force relationships for the cross-section of a thin-walled beam, it is possible to express the generalized stresses  $N$ ,  $M_x$ ,  $M_y$ ,  $M_B$  in terms of generalized strains  $\Delta\omega'_0$ ,  $\Delta\xi''$ ,  $\Delta\eta''$ ,  $\Delta\theta''$  about the reference axes as



$$\begin{pmatrix} \Delta N \\ \Delta M_y \\ \Delta M_x \\ \Delta M_B \end{pmatrix} = \begin{pmatrix} A & S_x & -S_y & -S_\omega \\ & I_y & -I_{yx} & -I_{\omega x} \\ & & I_x & I_{\omega y} \\ & & & I_{\omega\omega} \end{pmatrix} \begin{pmatrix} \Delta \omega' \\ \Delta \xi'' \\ \Delta \eta'' \\ \Delta \theta'' \end{pmatrix} \quad (14)$$

and the St.Venant's torsional moment which has the value

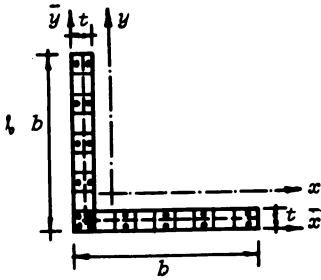
$$\Delta T^{SV} = G K^t \Delta \theta \quad (15)$$

Expressions for the evaluation of the section properties and stress resultants are given in terms of the transformed section assuming the accepted stress-strain curve for concrete and steel reinforcement.

$$\begin{aligned} E^T A &= \int_A E^T dA = \sum_{i=1}^{nB} E_{Bi} A_{Bi} + \sum_{j=1}^{nA} E_{aj} A_{aj} \\ E^T S_x &= \int_A E^T x dA = \sum_{i=1}^{nB} E_{Bi} A_{Bi} x_{Bi} + \sum_{j=1}^{nA} E_{aj} A_{aj} x_{aj} \\ E^T I_{xy} &= \int_A E^T x y dA = \sum_{i=1}^{nB} E_{Bi} A_{Bi} x_{Bi} y_{Bi} + \sum_{j=1}^{nA} E_{aj} A_{aj} x_{aj} y_{aj} \\ E^T I_{yy} &= \int_A E^T x^2 dA = \sum_{i=1}^{nB} E_{Bi} A_{Bi} x_{Bi}^2 + \sum_{j=1}^{nA} E_{aj} A_{aj} x_{aj}^2 + \sum_{i=1}^{nB} E_{Bi} \frac{1}{12} \Delta y_i \Delta x_i^3 \\ E^T I_{xx} &= \int_A E^T y^2 dA = \sum_{i=1}^{nB} E_{Bi} A_{Bi} y_{Bi}^2 + \sum_{j=1}^{nA} E_{aj} A_{aj} y_{aj}^2 + \sum_{i=1}^{nB} E_{Bi} \frac{1}{12} \Delta x_i \Delta y_i^3 \quad (16) \\ E^T S_\omega &= \int_A E^T \omega dA = \sum_{i=1}^{nB} \frac{1}{2} E_{bi} \Delta y_i \Delta x_i (\omega_{li} + \omega_{ki}) \\ E^T I_{x\omega} &= \int_A E^T \omega x dA = \sum_{i=1}^{nB} E_{bi} \frac{\Delta x_i \Delta y_i}{6} (\omega_{li} (x_{ki} + 2x_{li}) + \omega_{ki} (x_{li} + 2x_{ki})) \\ E^T I_{y\omega} &= \int_A E^T \omega y dA = \sum_{i=1}^{nB} E_{bi} \frac{\Delta x_i \Delta y_i}{6} (\omega_{li} (y_{ki} + 2y_{li}) + \omega_{ki} (y_{li} + 2y_{ki})) \\ E^T I_{\omega\omega} &= \int_A E^T \omega^2 dA = \sum_{i=1}^{nB} E_{bi} \frac{\Delta x_i \Delta y_i}{6} (\omega_{li}^2 + \omega_{li} \omega_{ki} + \omega_{ki}^2) \end{aligned}$$

To investigate the performance of the above defined element taking into account the effects of material and geometric nonlinearities the following column in Fig. 7 is analyzed. The geometry and the reinforcement of the cross-section and the material properties are given in Fig. 7.

The column is modeled using 10 equal sized thin-walled beam elements. The cross-section is divided into a grid of 10x10 layers Fig. 7.



$$b/t = 0.2$$

$$I_{bx} = I_{by} = 314222 \text{ cm}^4$$

$$A_a/A_B = 0.0325$$

$$f'_c = 30 \text{ MPa}$$

$$f'_s = 4 \text{ MPa}$$

Fig. 7

An eccentric axial load is applied at the top of the column up to failure. Maximum load was reached in fifteen load increments. The control of the lateral displacement of the top of the column was used to obtain the response of the structure. The resulting load-displacement curve is shown in Fig. 8.

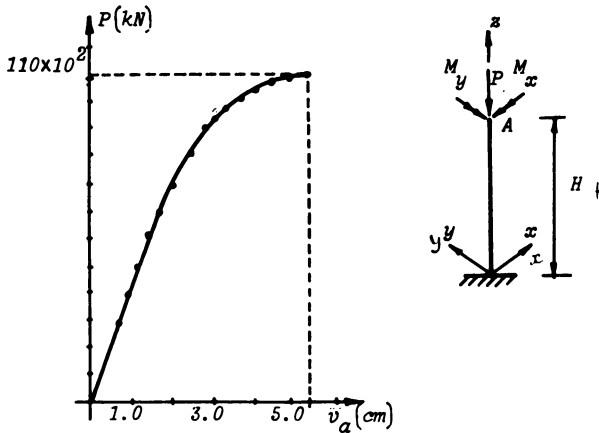


Fig. 8

#### REFERENCES

1. Sekulović, M., "Geometrically Nonlinear Analysis of Thin-Walled Members", Proceedings of the invited papers for the International Conference on Steel Structures - Recent Research Advances and Their Application to Design, Budva, Yugoslavia, September 1986.
2. Sekulović, M., Pujević, B. and Prokić, A., "Contribution to the Nonlinear Analysis of Thin-Walled Frames", Proceedings of the International Conference on Steel Structures - Recent Research Advances and Their Applications to Design, Budva, September 1986.
3. Vlasov, V.Z., "Thin-Walled Elastic Bars" (in Russian), Moscow, Fizmatgiz, 1959.
4. Kollbrunner C.F. and Hajdin, N., "Dünnwandige Stäbe", Band 1, Berlin, Springer 1972.
5. ASCE Task Committee on Finite Element Analysis of Reinforced Concrete Structures, State-of-the-Art Report on "Finite Element Analysis of Reinforced Concrete", ASCE Special Publication, 1982.



## SHEAR LAG IN ARCH-SHAPED STEEL BOX GIRDERS

V. Kristek\* and M. Skaloud\*\*

\* Faculty of Civil Engineering , Czech Technical University ,  
Prague , Czechoslovakia

\*\* Institute of Theoretical and Applied Mechanics , Czechoslovak  
Academy of Sciences , Prague , Czechoslovakia

Research on the shear lag phenomenon in the wide flanges of constructional steelwork, conducted by the authors and their associates, has been under way in Prague for some ten years now. The present paper describes part of the results obtained during the last stage of this research, focused on the problem of shear lag in the flanges of arch-shaped box girders, both longitudinally unstiffened and stiffened flange plates being considered in the analysis. The solution was based on the finite strip method. An analysis of the data obtained reveals that in the flanges of vertically curved box girders is frequently the effect of shear lag more pronounced than in straight girders, the difference increasing with girder curvature.

### 1. PROBLEM STUDIED BY THE AUTHORS

The writers studied the shear lag behaviour of an arch bridge portrayed in Fig. 1a, which is a typical example of vertically curved girders.

As the weight of an arch itself produces a stress distribution that has the character of simple compression only, the present study is focused on an analysis of the effects of point loads which are transmitted into the arch by way of stanchions. Then the thrust line is given by the funicular line to the system of loads applied, which determines, by its distance from the median line of the arch, the eccentricities of the forces acting on the individual sections and thereby the distribution of the bending moments in the arch.

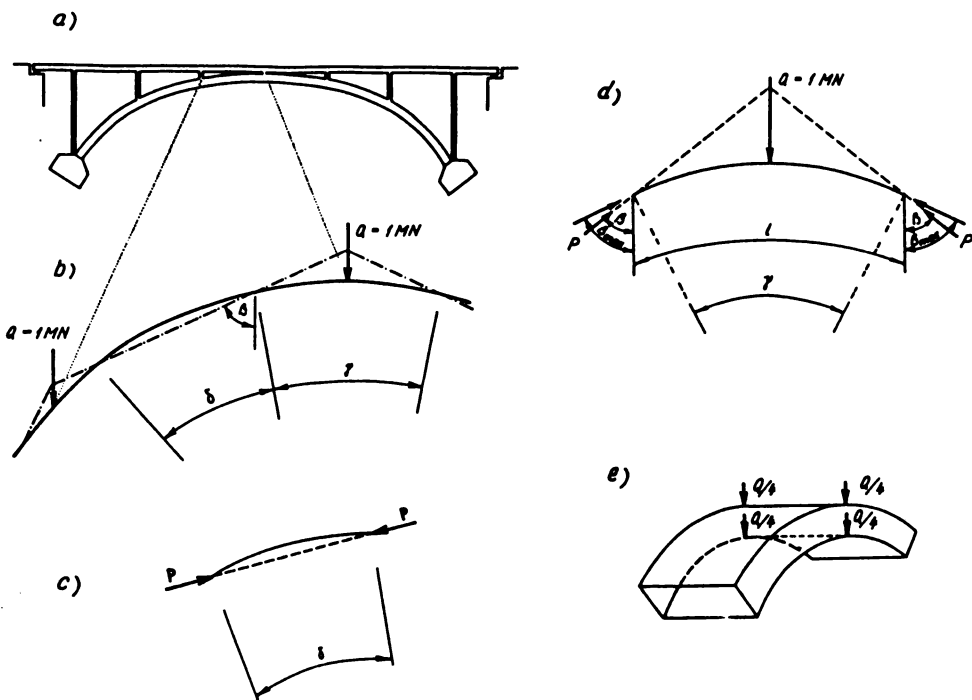


Fig. 1

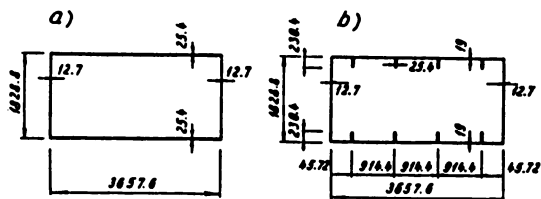


Fig. 2

In the intersections of the thrust line with the median line of the arch (Fig.1b), the bending moments are nil. Therefore, in an approximate solution, the shear lag analysis can be carried out independently for such individual portion of the arch between the adjacent points of zero bending moments. It is seen in Fig.1b that there are two kinds of segments in the arch. The first kind (Fig.1c), which can be termed a secant segment, is loaded only by two opposite forces  $P$  acting at its ends and having the direction of the chord of the segment. The intermediate segment (Fig.1d), on the other hand, is loaded by a mid-span vertical force  $Q$  and, at its ends, by two forces  $P$ , their inclination from the vertical being denoted as  $\beta$ . It follows from the above definitions of secant and intermediate segments that the angle  $\beta$  cannot surpass the angle  $\beta_{max}$ , between the vertical and the arch tangent at the segment end points.

The arch bridge studied was of box girder construction, two cases being considered in the investigation:

- (i) A box girder with longitudinally unstiffened flanges (Fig.2a).
- (ii) A box girder with longitudinally stiffened flanges (Fig.2b).

The main objective of the investigation was to look into the effect of girder curvature upon the distribution of longitudinal normal stresses in the upper and lower flanges of the girders and, consequently, on the intensity of the shear lag phenomenon present in them.

The investigation was performed via the finite strip method. In the numerical analysis and the evaluation of results, also Z. Kovanicova, a Ph.D. post-graduate student of the second author, took a significant part.

As it is beyond the scope and means of this short publication to present all data obtained (they are going to be published soon in a paper to appear in the journal "Acta technica" of the Czech. Academy of Sciences), we shall deal herebelow only with the results related to the behaviour of vertically curved girders having no diaphragm and no transverse stiffener at the section under the vertical load.

In this case, diaphragms are then placed only at the end sections.

The mid-span radial load  $Q$  is assumed to be split into four equal forces  $Q/4$  acting at the four corners of the box cross-section (Fig.1e).

## 2. THE SECANT SEGMENT

### 2.1 A BOX GIRDER WITH LONGITUDINALLY UNSTIFFENED FLANGES (Fig.2a) - Type 1

In the case of a straight girder, the secant forces  $P$  induce merely a state of axial compression and, therefore, uniformly distributed compressive normal stresses in the upper and lower flanges. (See the straight lines in Figs.3a and b, related to  $\delta = 0.015' \pm 0'$ . In order to avoid any misunderstanding, it should be noted at this juncture that in all figures giving stresses the scale of the vertical axis is such that the stresses

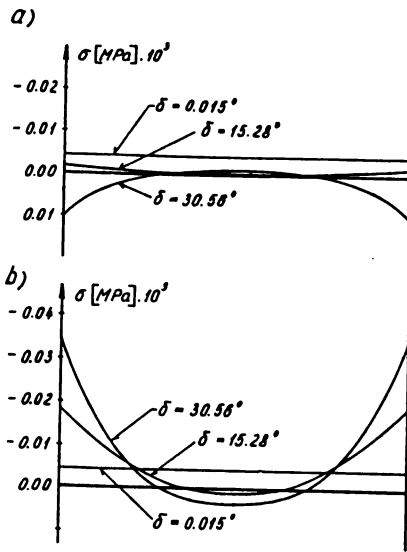


Fig. 3

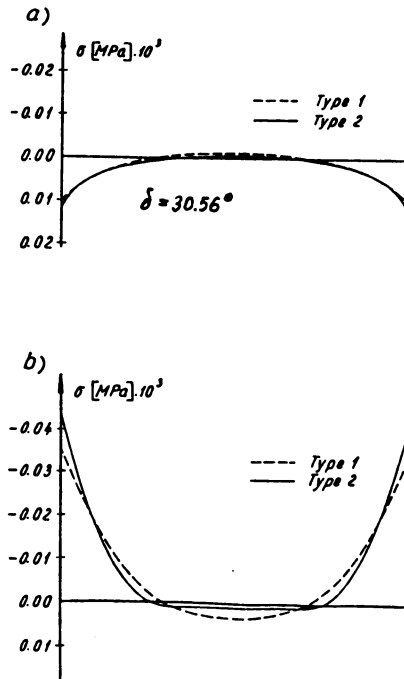


Fig. 4

are plotted in thousands of MPa .) When the girder curvature grows, the significance of bending enlarges. Thus the originally compressive stresses in the upper flange gradually change into tensile ones, which are non-uniformly distributed over the flange breadth ( as is typical of a shear lag phenomenon ) and attain their maximum values at the flange edges, i.e. at the junction of the flange with the vertical webs (Fig.3a). In the lower flanges of curved segments , the stresses remain mostly compressive; but as the eccentricity of the forces P increases, the non-uniformity of stress distribution (due to the shell action of the flange, flange , inclusive the effect of shear lag) grows, the maximum values occurring again at the junction of the flange plate with the webs (Fig.3b).

## 2.2 A BOX GIRDER WITH LONGITUDINALLY STIFFENED FLANGES (Fig.2b) - Type 2

To start with , let us mention at this juncture that the area of the cross-section studied with longitudinal ribs (see Fig.2b) was the same as the area of the cross-section of the longitudinally unstiffened box girder (Fig.2b) , which was investigated in the previous section.

This was achieved by using a thinner flange sheet than in the preceding case , in order to balance out the area of the longitudinal stiffening .

The results of the analysis are plotted in Fig.4. An inspection of the figure indicates that the non-uniformity of longitudinal normal stress distribution in longitudinally stiffened flanges ( i.e. the effect of shear lag ) is similarly to straight beams - more pronounced than that in flanges without longitudinal ribs (see nec.2.1 above). The reason for this observation can be attributed to the reduction of the flange sheet thickness described above, since it is merely the flange sheet that takes over the effects of shear and of transverse flexure.

## 3. THE INTERMEDIATE SEGMENT

As already said above, the intermediate segment is subject to a vertical , radial load Q , acting at mid-span of the segment, and to two skew forces P, acting at the end sections of the girder . The forces P can again be split into two states according to Fig.5 , viz. (i) the effect of the radial reactions  $Q_1$  ( Fig.5a ) and (ii) the effect of the tangent forces S and of the reactions  $Q_2$  related to them (Fig.5b). The latter case (Fig.5b) is quite identical with the performance of a secant segment described above, since - for the reasons of equilibrium - the resultant of the forces S and  $Q_2$  is bound to have the direction of the segment chord.

It is worth noting at this moment that the radial load Q, representing the compression transmitted via the stanchion into the arch girder (Fig.1a), is materialized in this study by four separate loads  $Q/4$  positioned at the corners of the box cross-section of the girder (Fig.1e).



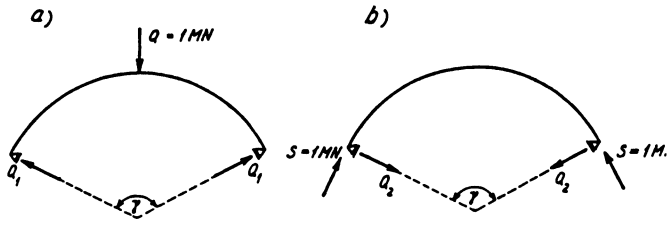


Fig. 5

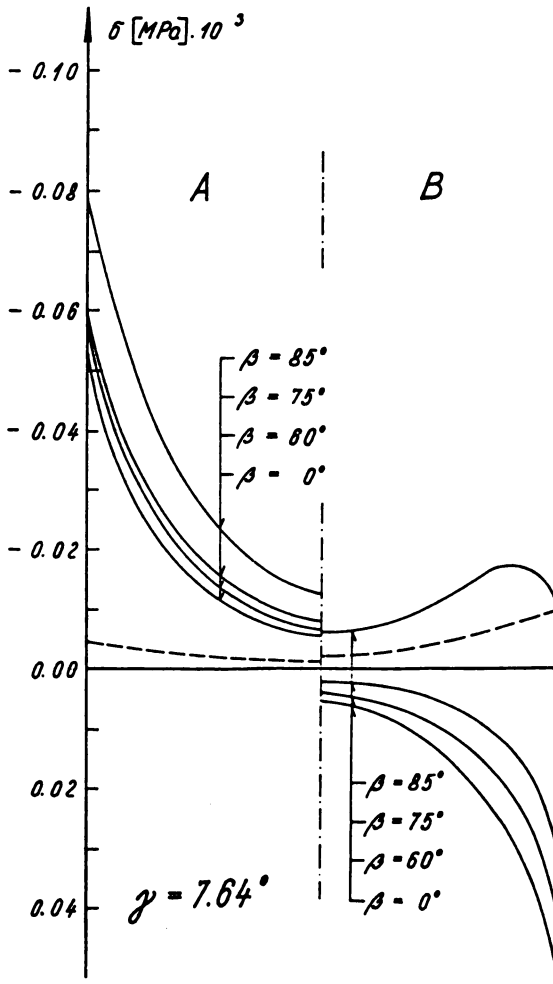


Fig. 6

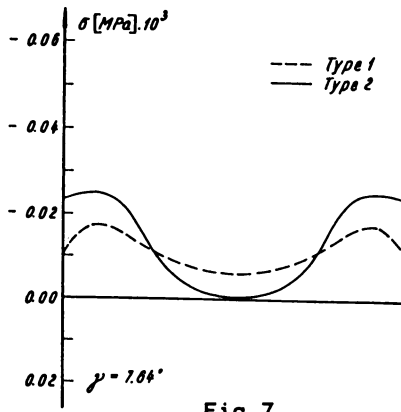
### 3.1 A BOX GIRDER WITH LONGITUDINALLY UNSTIFFENED FLANGES (Fig.2a) - Type 1

In the context of what was said above, the longitudinal normal stresses brought about by the action of the forces  $S$  and  $Q_x$  are necessarily identical with those occurring in the secant segment subjected to the secant forces  $P$  and portrayed in Figs. 3a and b. This implies that, with increasing girder curvature, the originally compressive stress in the upper flange gradually changes into a tensile one, which is non-uniformly distributed across the flange breadth and attains the maximum value on the flange boundary (Fig.3a). In terms of girder curvature, even the non-uniformity of the compressive stress distribution in the lower flange grows, the maximum value of the stress being again at the flange/web junction (Fig.3b).

The behaviour of the intermediate segments is governed by the effect of the inclination (denoted as  $\beta$  in Fig.1d) of the trust line on the longitudinal stress distribution, which can be studied by combining the stress states corresponding to Figs.5a and b. An analysis of the results related to a number of selected curvatures and various thrust line inclinations shows that for  $\beta = 0^\circ - 60^\circ$  the stress distribution is approximately the same. If the inclination  $\beta$  approaches to the angle between the longitudinal force and the vertical, the magnitude and distribution of the stress drastically change, the stress distribution in the lower flange even losing its parabolic character (see Fig.6). This is due to the interaction between (i) the non-uniformly distributed compressive stress induced by the longitudinal force (portrayed in the figure by a dashed line) and (ii) the non-uniformly distributed tensile stress brought about by the action of the radial load

### 3.2 A BOX GIRDER WITH LONGITUDINALLY STIFENED FLANGES (Fig.2b) - Type 2

Fig.7 shows the distribution of the longitudinal normal stresses in the intermediate segment of a vertically curved girder



der with  $\gamma = 7.64^\circ$ , i.e. in the case where the character of the distribution was out of the ordinary. Namely, in this case the maximum value of the stress  $\sigma$  did not occur at the flange / web junction, but at an inner point of the flange breadth, which is another difference from the shear lag behaviour of the flanges of straight box girders. The solid line gives the stress distribution in a girder with longitudinally stiffened flanges (type 2) and the dashed line that in a girder without longitudinal ribs (type 1). The shape of both curves is similar, but an examination of the figure reveals that with longitudinally stiffened flanges the effect of shear lag is more pronounced.

## SUMMARY

The objective of the paper is to study the effect of shear lag in vertically curved box girders (Fig.1), such as are encountered, for example, in the case of arch bridges and similar structures.

As a direct application of the theory of elasticity to the solution of the problem concerned would be very complex, the authors used the finite strip method in their analysis.

The vertically curved girder studied was of box girder construction, two cases being considered in the analysis:

- (i) A box girder with longitudinally unstiffened flanges (Fig.2a).
- (ii) A box girder with longitudinally stiffened flanges (Fig.2b).

An analysis of the results obtained shows that:

(a) The effect of shear lag in the flanges of vertically curved box girders subject to point loads is usually more significant than that in the flanges of straight box girders, the difference growing with girder curvature.

(b) Unlike the flanges of straight box girders, where the maximum longitudinal stress always occurs at the junction of the girder flange with the girder web, in the case of vertically curved girders this maximum stress value can develop at another point of the flange.

**A CONTRIBUTION TO THE SOLUTION OF ULTIMATE  
CARRYING CAPACITY OF POLYGONAL SLABS**

**Professor MILIĆ MILIĆEVIĆ**  
Structural Engineer, Dr. Sc.  
NiS Univ., Civil Eng. Faculty

**SUMMARY**

In this work a procedure for determination the lower bound of ultimate carrying capacity of polygonal slabs using nonlinear programming is presented. At first, the solution for trapezoidal slabs is given. After that, this solution is extended for polygonal slabs and for slabs with openings as well.

\* \* \* \*

As it is known, exact solutions of the problem of a slab ultimate carrying capacity could not be found in an closed form (except in some very specific cases). Therefore, approximate solutions are sought by application of known theorems on the upper and lower bounds. Whereas it is rather easy to find the upper bound by using the Theory of Fracture Lienes (Johansen), the lower bound of loading is calculated by detrmning statically and plastically admissible stress field which meets: the conditions of equilibrium (1), namely (2) boundary conditions regarding the forces (3) and the adopted yield condition (for illustration sake Johansen's yield condition of the orthotropic slab (5) was used).

As a rule, the herebelow presented procedur gives good solution for the upper bound.

$$M_{x,x} + M_{xy,y} - Q_x = 0 \quad \dots \dots \dots (1.a)$$

$$M_{xy,x} + M_{y,y} - Q_y = 0 \quad \dots \dots \dots (1.b)$$

$$Q_{x,x} + Q_{y,y} + q_{(x,y)} = 0 \quad \dots \dots \dots (1.c)$$

or:

$$M_{x,xx} + 2M_{xy,xy} + M_{y,yy} + q_{(x,y)} = 0 \quad \dots \dots \dots (2)$$

$$M_n = c^2 * M_x - d^2 * M_y + 2 * cd * M_{x,y} = M_{n0} \dots \dots \dots (3.a)$$

$$Q_n = Q_n - M_{nt,n} = Q_{n0} \dots \dots \dots (3.b)$$

$$M_{nt} = cd * (M_y - M_x) + (c^2 - d^2) M_{xy} \dots \dots \dots (4)$$

$$(1 - m_x) (k - m_y) - m_{xy}^2 = F(m_x, m_y, m_{xy}) \geq 0 \dots \dots \dots (5)$$

where:

$c = \cos(\text{ALFA}), d = \sin(\text{ALFA})$  (acc.Fig.1)

$M_0 = M_{px}, k = M_{py}/M_0; m_i = M_i/M_0$  ( $i=x,y,xy$ )

$$x = \frac{\lambda}{l}, \quad y = \frac{Y}{l}, \quad l = AD$$

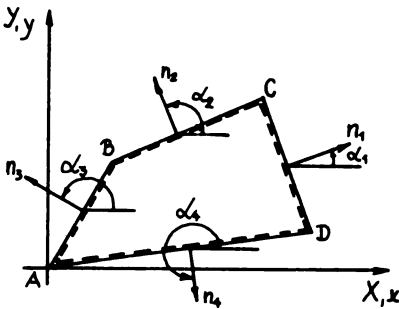


Fig. 1

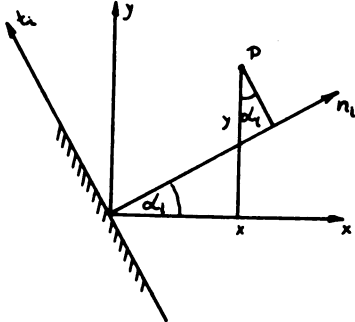


Fig 2

Let's assume that the state of stress could be presented in the form

$$\begin{bmatrix} m_x \\ m_y \\ m_{xy} \end{bmatrix} = \begin{bmatrix} A \\ B \\ C \end{bmatrix} * \vec{F} \dots \dots \dots (6)$$

where:

$$A = (A_0, A_1, A_2 \dots A_9); B = (B_0, B_1 \dots B_9); C = (C_0, C_1 \dots C_9) \dots (7)$$

$$\vec{F}^T = (1, x, y, x^2, xy, y^2, x^3, x^2y, xy^2, y^3) \dots \dots \dots (8)$$

If the equation of the boundary, whose normal makes the angle (ALFA)<sub>i</sub> with the x-axis, is given with  $x = a_i + b_i y$ , and the loading  $q(x,y)$  in the field, and  $M_{n0}$  and  $Q_{n0}$  on the boundary by:

$$q(x,y) = q_0 (1 + q_1 x + q_2 y) \dots \dots \dots (9)$$

$$M_n^{0(i)} = /M_0^i, M_1^i, M_2^i, M_3^i/ * /1, y, y^2, y^3/^T \dots \dots \dots (10.a)$$

$$Q_n^{0(i)} = /P_0^i, P_1^i, P_2^i/ * /1, y, y^2/^T \dots \dots \dots (10.b)$$

then the equilibrium conditions (2), boundry conditions (3) and yield condition (5) (after several transformations) could be given in the following form:

$$/N_A/ * A^T + /N_B/ * B^T + /N_C/ * C^T = - \frac{q_0}{2M_0} * \begin{bmatrix} 1 \\ q_1 \\ q_2 \end{bmatrix} \dots \dots (11)$$

$$/c_i^2, d_i^2, 2c_i d_i/ * /A, B, C/^T * /S_i/ = [M_0^i, M_1^i, M_2^i, M_3^i]^T \dots \dots (12)$$

$$/c_i^2, d_i^2, 2c_i d_i/ * /A, B, C/^T * /T_i/ + /-c_i d_i, c_i d_i, c_i^2 - d_i^2/ * /A, B, C/^T * /Q_i/ = /P_0^i, P_1^i, P_2^i/^T \dots \dots (13)$$

$$\begin{bmatrix} A_0 - 1 \\ A_1 \\ \vdots \\ A_9 \end{bmatrix} * F * F^T \begin{bmatrix} B_0 - k \\ B_1 \\ \vdots \\ B_9 \end{bmatrix} - C * F * F^T * C \geq 0 \dots \dots (14)$$

The introduced matrices  $S_i$ ,  $T_i$ ,  $Q_i$ ,  $N_a$ ,  $N_b$  and  $N_c$  are given by expressions (15), (16) and (17).

$$S_i = \begin{bmatrix} 1 & 0 & 0 & 0 \\ a_i & b_i & 0 & 0 \\ 0 & 1 & 0 & 0 \\ a_i^2 & 2a_i b_i & b_i^2 & 0 \\ 0 & a_i & b_i^2 & 0 \\ 0 & 0 & 1 & 0 \\ a_i^3 & 3a_i^2 b_i & 3a_i b_i^2 & b_i^3 \\ 0 & a_i^2 & 2a_i b_i & b_i^2 \\ 0 & 0 & a_i & b_i \\ 0 & 0 & 0 & 1 \end{bmatrix} \dots \dots \dots (15)$$

$$/T_i/T = \begin{bmatrix} 0 & 1 & 0 & 2a_i & 0 & 0 & 3a_i^2 & 0 & 0 & 0 \\ 0 & 0 & 0 & 2b_i & 1 & 0 & 6a_i b_i & 2a_i & 0 & 0 \\ 0 & 0 & 0 & 0 & 0 & 0 & 3b_i^2 & 2b_i & 1 & 0 \end{bmatrix} \dots \dots \dots (16.d)$$

$$/Q_i/T = \begin{bmatrix} 0 & 0 & 1 & 0 & a_i & 0 & 0 & a_i^2 & 0 & 0 \\ 0 & 0 & 0 & 0 & b_i & 2 & 0 & 2a_i b_i & 2a_i & 0 \\ 0 & 0 & 0 & 0 & 0 & 0 & 0 & b_i & 2b_i & 3 \end{bmatrix} \dots \dots \dots (16.e)$$

$$/N_A/ = \begin{bmatrix} 0 & 0 & 0 & 1 & 0 & 0 & 0 & 0 & 0 & 0 \\ 0 & 0 & 0 & 0 & 0 & 0 & 3 & 0 & 0 & 0 \\ 0 & 0 & 0 & 0 & 0 & 0 & 0 & 1 & 0 & 0 \end{bmatrix} \dots \dots \dots (17.a)$$

$$/N_B/ = \begin{bmatrix} 0 & 0 & 0 & 0 & 0 & 1 & 0 & 0 & 0 & 0 \\ 0 & 0 & 0 & 0 & 0 & 0 & 0 & 0 & 1 & 0 \\ 0 & 0 & 0 & 0 & 0 & 0 & 0 & 0 & 0 & 3 \end{bmatrix} \dots \dots \dots (17.b)$$

$$/N_C/ = \begin{bmatrix} 0 & 0 & 0 & 0 & 1 & 0 & 0 & 0 & 0 & 0 \\ 0 & 0 & 0 & 0 & 0 & 0 & 0 & 2 & 0 & 0 \\ 0 & 0 & 0 & 0 & 0 & 0 & 0 & 0 & 2 & 0 \end{bmatrix} \dots \dots \dots (17.c)$$

In a scalar notation, the condition (11) is transformed in there scalar equations, the condition (12), each of them in 4.

However, the condition (14) would have to be satisfied in all points of the field. In order to the problem solved in practice, we will require, in the first stage, that the condition (14) is satisfied in a certain series of points, whose coordinates are known. Parameter q from (11) could be expressed in the form:

$$q = f(A, B, C, x, y) = f(z, x, y) \dots \dots \dots (18)$$

where the vector z is denoted with A, B, C components.

The problem could be formulated as follows: to maximize the condition (19) (i.e. to define max q), however, provided that the conditions (20) have been fulfilled.

$$q = f(z, x, y) \dots \dots \dots (19)$$

$$h_j(z) = 0 \quad (j=1, 2, \dots, U_j) \dots \dots \dots (20.a)$$

$$q_k(z, x, y) \geq \quad (k=1, 2, \dots, U_T) \dots \dots \dots (20.b)$$

$$\min z_i \geq z_i \leq \max z_i \dots \dots \dots (20.c)$$

The problem defined in this way is a problem typical for non-linear programming (NPL) and could be solved by one of the wellknown procedures (the author has used the already prepared programmed package of Commet - R.L. Stah, 1973 and GAPFQL - J. S. Newel, 1974 of Texas University in Austin). In addition to the values for q, the solution of NPL problem gives also all components of the vector z i.e. of the A, B, C vectors. However, the solution meets the yield condition only in the chosen series of points, which does not still represent a strict proof that it had been satisfied on the entire surface of the slab. In order to eliminate this problem, one should solve the following:

$$\min g(z_0, x, y) = ?$$

$$\min x \leq x \leq \max x \quad \dots \text{ (NLP) '}$$

$$\min y \leq y \leq \max y$$

giving  $\min g = -a^2 \dots \dots \dots (21)$

$$x = x_0, \quad y = y_0 \dots \dots \dots (22)$$

The corrective factor GAMA could be obtained from the following expression:

$$GAMA = \frac{(kM_x + M_y) + \sqrt{(kM_x + M_y - 2k)^2 - 4ka^2}}{2 * (kM_x + M_y - k - a^2)} \dots \dots \dots (23)$$



leading to

$$q = \text{GAMA} * q' \leq q \quad \dots \dots \dots (24)$$

In the expression (21)  $M_x$  and  $M_y$  as well as  $M_{xy}$  are the values of moments in the point with  $x_0$  and  $y_0$  coordinates.

The proposed procedure, including the associated upper bound, gives the complete solution of the ultimate carrying capacity of trapezoidal slabs.

The table given together with Fig. 3 shows the results of the analysis of the upper and lower bounds, as well as of the experimental tests for the trapezoidal slab. The afore-described procedure was used for the lower bound, whereas the Theory of Fracture Lines together with the optimum of the fracture figure for the upper bound, Fig. 3. As the table shows, the differences expressed in percentage are not big. The discrepancies of both the upper and lower bounds amount to 5 to 6%.

TABLE

SLAB TYPE	k	$Q_e$	$Q^+$	$Q^-$	$\frac{Q^+ - Q_e}{Q^+ / 100}$	$\frac{Q^+ - Q^-}{Q^+ / 100}$	$\frac{Q_e - Q^-}{Q_e / 100}$
1	1,000	-	8,982	8,466	-	+ 5,75	-
2	0,640	7,705	8,086	7,660	+ 4,71	+ 5,27	+ 0,58
3	0,814	8,335	8,544	7,997	+ 2,45	+ 6,40	+ 4,06
4	0,363	6,966	7,354		+ 5,28		
5	1,280	10,005	9,649	9,115	- 3,69	+ 5,53	+ 8,90
6	2,131	12,819	11,866	11,250	- 8,03	+ 5,19	+12,24

$$k = M_{px} / M_{py}$$

$$M_0 = M_{py}$$

$$Q = q l^2 / 2 M_0$$

$$Q = \text{GAMA} * Q_{\text{calculated}}$$

When slabs of more complex boundaries are in question (polygonal slabs, slabs with holes, etc.) the proposed procedure could be generalized in two ways.

The first one is when a full polynomial of the fourth or higher power is used for the function. In that case  $A, B$  and  $C$  vectors have 15 or more elements each, which in some cases could give good results, however, this increases the (NLP) problem.

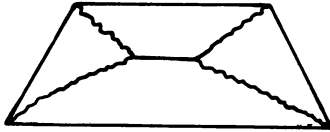


Fig. 3

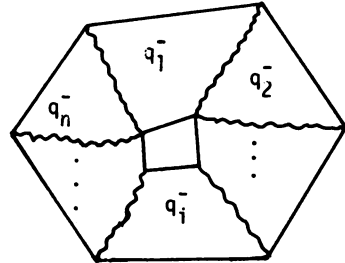


Fig. 4.

The second one is when the entire surface of the slab is divided into sections, and previously described procedure of optimization applied on these sections in succession, provided that the transition conditions on boundaries of the sections have been satisfied. Application of this procedure in a general form is the subject of a particular study.

However, if the fracture lines of the slab are taken as boundaries of the sections, obtained by optimization of the kinematic solution, the procedure could be simplified considerably. In that case, along the slab boundaries (Fig.4) the conditions (12) are valid, namely (13), the equilibrium (11) over the entire surface of the slab, and the conditions (12) along the fracture lines between adjacent sections of the slab.

After that, one could define the lower bounds  $q_1, \dots, q_i, \dots, q_n$  for each section in the identical way as for the previously described trapezoidal slab. The smallest of these values will represent the lower bound for the slab as a whole, whereas the upper bound had been previously determined during optimization of the kinematic solution.

#### REFERENCES

1. Hill, R.: *Mathematical Theory of Plasticity*, Oxford University Press, Ch 3 (1950).
2. Drucker, D. C.: *Variational Principles in the Mathematical Theory of Plasticity*, Proc. Symp. Appl. Math. 8 (1958)
3. Jaeger, T.: *Fligelenklientheorie*, Berlin (1962).
4. Sawczuk, A.: *Grenztragfahigkeitstheorie der Platen* (1963)
5. Save, M. et Massonet, C.: *Calcul plastic des structures spatiales (Vol 2)* Centre Belgo-Luxembourgeois de l'inform. de l'acier, Bruxelles (1963)
6. Bareš, R.: *Proračun ploča i zidnih platana prema graničnoj nosivosti* (Serbo-Croat), (1972).
7. Miličević, M.: *Jedan postupak granične analize transverzalne opterećenih poligonalnih ploča sa posebnim osvrtom na trapezoidne ploče* (Serbo-Croat), PHD Thesis (1980).



## ON TORSIONAL BUCKLING OF THIN-WALLED CONTINUOUS MEMBERS

Z. Cywiński

Technical University of Gdańsk -  
Majakowskiego 11/12  
80-952 Gdańsk, Poland

University of Tokyo  
Bunkyo-ku  
Tokyo, 113, Japan

### SUMMARY

In the paper certain research has been presented, aimed on the extension of the conventional method of displacements into the sphere of the technical theory of thin-walled bars. For the torsion problem the warping-twist equations of this method have been derived, suitable for the analysis of torsional buckling of thin-walled systems with open section, continuous members in particular. Simplifications of those equations characteristic for their classic slope-deflection forms have been demonstrated. A numerical example shows the application details of the procedure established. Possible development perspectives have been specified.

### 1. INTRODUCTION

It is well known that the displacement method is one of the most general and effective methods of structural mechanics. Presently it is classic as far as members of solid sections are concerned, but appears to be still insufficiently developed concerning those with thin-walled section.

It seems that the general principles of the displacement method related to thin-walled members have been first presented in monographs [19] and [2]; little later also in [13] outlines of this method have been given. Author of this paper, basing upon earlier Polish editions of [1], generalized the correlated conventional method of Cross for the requirements of the theory of thin-walled members [20], - in [3], [4], [6], [7], [9]. Other contributions in that field are referred to in [10]. Adequate force method is shown in [19], [2] and [14], but it is out of the scope of this paper.

A particular problem of that topic was the treatment of thin-walled frames. Corresponding references are presented in [7], [8], and [9]; author wishes to point only at [12] and [18], probably little known outside Poland, as well as at recent publication [16], characteristic for up-to date trends in that field.

For finite element procedures based upon the matrix displacement method proper stiffness matrices have been, already, settled; author mentions only [11] where the corresponding development and the actual state of this question have been shown.

Present paper refers closely to author's earlier contribution [5] and is aimed on the extension of the displacement method on the title problem.

## 2. WARPING-TWIST EQUATIONS OF THE GENERALIZED DISPLACEMENT METHOD FOR SINGLE MEMBERS

Since Wagner's classic research performed in the thirties it is known that the buckling problem of centrally compressed thin-walled member of bisymmetric section, practically - I-section as in Fig. 1, is governed by three uncoupled differential equations of the following shape:

$$\left. \begin{aligned} EJ_x \xi'''' + P \xi'' &= 0, \\ EJ_y \eta'''' + P \eta'' &= 0, \\ EJ_\omega \theta'''' + (r^2 P - GJ_d) \theta'' &= 0, \end{aligned} \right\} \quad (1)$$

where E and G are Young's and shear moduli,  $J_x$ ,  $J_y$  - moments of inertia of cross-section about x, y axes, respectively,  $J_\omega$  - is its sectorial moment of inertia,  $J_d$  - torsion constant, and  $r^2 = (J_x + J_y)/F$ , with F being the section area. The remaining notations result from Fig. 1 but ( )' stands for d/dz.

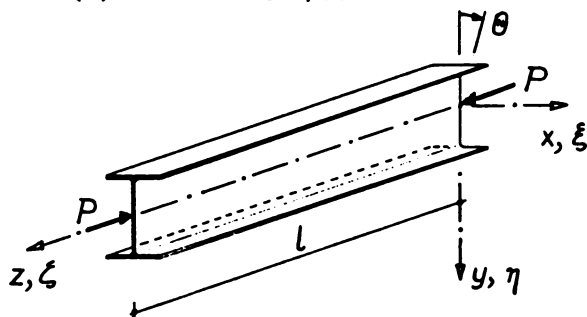


Fig. 1. Bisymmetric I-beam considered

The first and second of equations (1) describe the conventional bending buckling of Euler, respectively along the x- and y-direction, whereby the corresponding slope-deflection equations are well known [1], [15]. On the contrary, similar equations for the torsional buckling of Wagner, resulting from the third of equations (1), have been shown probably only by author in [5]; author suggests to call them "warping-twist equations". Their derivation is demonstrated underneath.

The differential equation of torsional buckling can be transformed to the following nondimensional form:

$$\theta'''' + 12 \frac{r^2 P - GJ_d}{EJ_\omega} \theta'' = 0, \quad (2)$$

whereby the differentiation refers to variable  $\zeta = z/l$ . Using the notation

$$\lambda = 1 \sqrt{\frac{r^2 P - EJ_d}{EJ_\omega}}, \quad (3)$$

one obtains equation (2) in its classic appearance

$$\theta'''' + \lambda^2 \theta'' = 0. \quad (4)$$

The general integral of equation (4) and its derivatives can be expressed by the following relations:

$$\left. \begin{aligned} \theta &= C_1 + C_2 \lambda \zeta + C_3 \cos \lambda \zeta + C_4 \sin \lambda \zeta, \\ \theta' &= C_2 \lambda - C_3 \lambda \sin \lambda \zeta + C_4 \lambda \cos \lambda \zeta, \\ \theta'' &= -C_3 \lambda^2 \cos \lambda \zeta - C_4 \lambda^2 \sin \lambda \zeta, \\ \theta''' &= C_3 \lambda^3 \sin \lambda \zeta - C_4 \lambda^3 \cos \lambda \zeta, \\ \theta'''' &= C_3 \lambda^4 \cos \lambda \zeta + C_4 \lambda^4 \sin \lambda \zeta, \end{aligned} \right\} \quad (5)$$

where the constants  $C_1, \dots, C_4$  depend upon the boundary conditions, i.e. - on the type of member supports.

First the axially compressed fixed-fixed member is being considered. Its ends  $i$  and  $k$  are assumed to undergo imposed rotations  $\theta_i$  and  $\theta_k$ , as well as - warpings  $\theta'_i$  and  $\theta'_k$ . These displacements are associated with the occurrence of support reactions: torsional moments  $H_{ik}^x, H_{ki}^x$ , and bimoments  $B_{ik}^x, B_{ki}^x$ . The original compression forces  $P$  are still there, exerting  $k$  within the 2-nd order theory - an additional effect on the expressions of  $\theta$  and of its derivatives along the member span. The graphical illustration of that situation is given in Fig. 2. To simplify the problem interpretation the illustration corresponds to the conventional one applied in bending, and used by author already in [3] - [7] and [9].

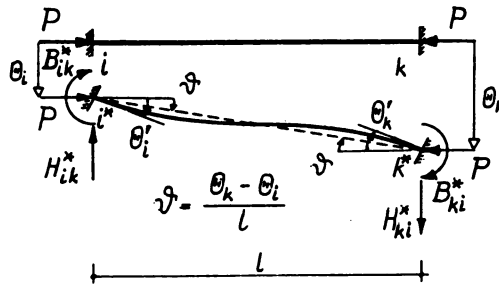


Fig. 2. Force-displacement illustration for fixed-fixed member

Constants  $C_1, \dots, C_4$  result from the governing boundary conditions:

$$\left. \begin{aligned} \theta(0) &= \theta_i, & \theta(1) &= \theta_k, \\ \theta'(0) &= \theta'_i, & \theta'(1) &= \theta'_k, \end{aligned} \right\} \quad (6)$$

and are expressed, as follows:

$$\left. \begin{aligned}
 C_1 &= \theta_1 + \frac{1}{\lambda} \frac{(\theta'_1 - \theta'_k)(\lambda - \sin\lambda) - (\theta'_1 - \phi)\lambda(1 - \cos\lambda)}{2(1 - \cos\lambda) - \lambda \sin\lambda}, \\
 C_2 &= \frac{1}{\lambda} \frac{(\theta'_1 + \theta'_k)(1 - \cos\lambda) - \phi\lambda \sin\lambda}{2(1 - \cos\lambda) - \lambda \sin\lambda}, \\
 C_3 &= -\frac{1}{\lambda} \frac{(\theta'_1 - \theta'_k)(\lambda - \sin\lambda) - (\theta'_1 - \phi)\lambda(1 - \cos\lambda)}{2(1 - \cos\lambda) - \lambda \sin\lambda}, \\
 C_4 &= \frac{1}{\lambda} \theta'_1 - \frac{1}{\lambda} \frac{(\theta'_1 + \theta'_k)(1 - \cos\lambda) - \phi\lambda \sin\lambda}{2(1 - \cos\lambda) - \lambda \sin\lambda},
 \end{aligned} \right\} (7)$$

Introducing the relations (7) into the first of equations (5) one obtains the general integral of the fundamental equation (4) in the following form:

$$\begin{aligned}
 \theta &= \theta_1 - \frac{21}{\lambda^2} [\bar{\alpha}(1 - \zeta - \cos\lambda\zeta + \frac{\sin\lambda\zeta}{\lambda}) + \bar{\beta}(-\zeta + \frac{\sin\lambda\zeta}{\lambda}) - \frac{\lambda}{2} \sin\lambda\zeta] \theta'_1 - \\
 &- \frac{21}{\lambda^2} [\bar{\beta}(1 - \zeta - \cos\lambda\zeta + \frac{\sin\lambda\zeta}{\lambda}) + \bar{\alpha}(-\zeta + \frac{\sin\lambda\zeta}{\lambda})] \theta'_k + \\
 &+ \frac{21}{\lambda^2} [(\bar{\alpha} + \bar{\beta})(1 - 2\zeta - \cos\lambda\zeta + 2\frac{\sin\lambda\zeta}{\lambda}) + \frac{\lambda^2}{2} (\zeta - \frac{\sin\lambda\zeta}{\lambda})] \phi,
 \end{aligned} \quad (8)$$

where the coefficients  $\bar{\alpha}$ ,  $\bar{\beta}$  and  $(\bar{\alpha} + \bar{\beta})$  are expressed by the following equivalent formulas:

$$\left. \begin{aligned}
 \bar{\alpha} &= \frac{1}{2} \frac{\lambda(\sin\lambda - \lambda\cos\lambda)}{2(1 - \cos\lambda) - \lambda \sin\lambda}, & \bar{\alpha} &= \frac{\lambda}{2 \tan\lambda} \frac{\tan\lambda - \lambda}{2 \tan\frac{\lambda}{2} - \lambda}, \\
 \bar{\beta} &= \frac{1}{2} \frac{\lambda(\lambda - \sin\lambda)}{2(1 - \cos\lambda) - \lambda \sin\lambda}, & \bar{\beta} &= \frac{\lambda}{2 \sin\lambda} \frac{\lambda - \sin\lambda}{2 \tan\frac{\lambda}{2} - \lambda}, \\
 \bar{\alpha} + \bar{\beta} &= \frac{1}{2} \frac{\lambda^2(1 - \cos\lambda)}{2(1 - \cos\lambda) - \lambda \sin\lambda}, & \bar{\alpha} + \bar{\beta} &= \frac{1}{2} \frac{\lambda^2 \tan\frac{\lambda}{2}}{2 \tan\frac{\lambda}{2} - \lambda}.
 \end{aligned} \right\} (9)$$

The approached warping-twist equations base upon the obvious differential relations

$$\left. \begin{aligned}
 B_{1k}^* &= -\frac{EJ\omega}{1^2} [\theta''']_{\zeta=0}, \\
 B_{ki}^* &= \frac{EJ\omega}{1^2} [\theta''']_{\zeta=1}, \\
 H_{1k}^* = H_{k1}^* &= -\frac{EJ\omega}{1^3} [\theta'''' + \lambda^2 \theta']_{\zeta=0}.
 \end{aligned} \right\} (10)$$

Taking advantage of (5), together with (7), one can express (10) in the particular forms

$$\left. \begin{aligned}
 B_{1k}^* &= \frac{2EJ\omega}{1} [\bar{\alpha}\theta'_1 + \bar{\beta}\theta'_k - (\bar{\alpha} + \bar{\beta})\phi], \\
 B_{k1}^* &= \frac{2EJ\omega}{1} [\bar{\beta}\theta'_1 + \bar{\alpha}\theta'_k - (\bar{\alpha} + \bar{\beta})\phi], \\
 H_{1k}^* = H_{k1}^* &= -\frac{EJ\omega}{1^2} \lambda^2 \phi - \frac{2EJ\omega}{1^2} (\bar{\alpha} + \bar{\beta}) (\theta'_1 + \theta'_k - 2\phi).
 \end{aligned} \right\} (11)$$

Applying the rule of d'Hospital the proof can be given that for  $\lambda=0$

$$\bar{\alpha} = 2, \quad \bar{\beta} = 1, \quad \bar{\alpha} + \bar{\beta} = 3, \quad (12)$$

and the warping-twist equations (11) reduce to

$$\left. \begin{aligned} B_{ik}^* &= \frac{2EJ\omega}{l}(2\theta_1' + \theta_k' - 3\vartheta), \\ B_{ki}^* &= \frac{2EJ\omega}{l}(\theta_1' + 2\theta_k' - 3\vartheta), \\ H_{ki}^* &= -\frac{6EJ\omega}{l^2}(\theta_1' + \theta_k' - 2\vartheta), \end{aligned} \right\} \quad (13)$$

which shapes are, formally, identic with the slope-deflection equations concerning the conventional bending problem.

Secondly, the axially compressed fixed-hinged member is being considered (Fig. 3). Required warping-twist equations can be found from (11), respecting  $B_{ki} = 0$ . Here the following relations hold:

$$\left. \begin{aligned} B_{ik}^* &= \frac{EJ\omega}{l}\bar{\gamma}(\theta_1' - \vartheta), \\ H_{ik}^* = H_{ki}^* &= -\frac{EJ\omega}{l^2}\lambda^2\vartheta - \frac{EJ\omega}{l^2}\bar{\gamma}(\theta_1' - \vartheta), \end{aligned} \right\} \quad (14)$$

where the coefficient  $\bar{\gamma}$  is given by equivalent formulas, as follows:

$$\bar{\gamma} = 2\frac{\bar{\alpha}^2 - \bar{\beta}^2}{\bar{\alpha}}, \quad \bar{\gamma} = \frac{\lambda^2 \sin \lambda}{\sin \lambda - \lambda \cos \lambda}, \quad \bar{\gamma} = \frac{\lambda^2 \tan \lambda}{\tan \lambda - \lambda}. \quad (15)$$

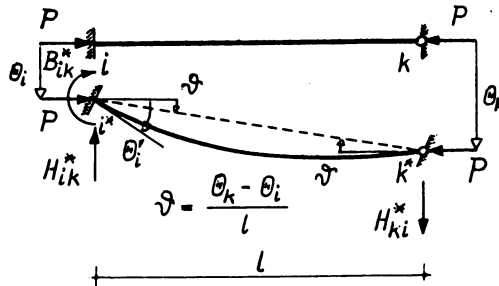


Fig. 3. Force-displacement illustration for fixed hinged member

Applying substitutions of type (12) it is visible that for  $\lambda=0$

$$\bar{\gamma} = 3 \quad (16)$$

and the warping-twist equations (14) become

$$\left. \begin{aligned} B_{ik}^* &= \frac{3EJ\omega}{l}(\theta_1' - \vartheta), \\ H_{ik}^* = H_{ki}^* &= -\frac{3EJ\omega}{l^2}(\theta_1' - \vartheta). \end{aligned} \right\} \quad (17)$$



The third and last case represents the axially compressed fixed-free member (Fig. 4). Proper warping-twist equations result from (14) taking  $H_{ki}^* = 0$ , as follows:

$$\left. \begin{aligned} B_{ik}^* &= \frac{EJ\omega}{l} \bar{\delta} \theta_1' \\ H_{ik} &= H_{ki} = 0. \end{aligned} \right\} \quad (18)$$

whereby

$$\bar{\delta} = -\lambda \tan \lambda. \quad (19)$$

For  $\lambda=0$  also  $\bar{\delta}=0$  what means that the support displacements undergo, obviously, reactionless.

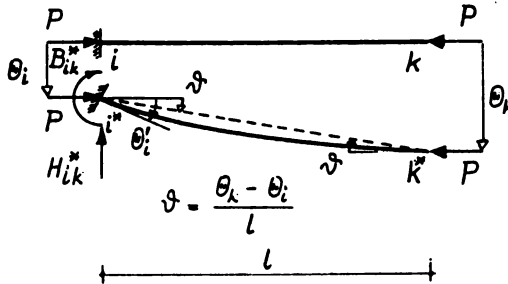


Fig. 4. Force-displacement illustration for fixed-free member

It is evident that the functions  $\alpha$ ,  $\bar{\delta}$ ,  $(\alpha + \bar{\delta})$ ,  $\bar{\gamma}$  and  $\bar{\delta}$ , specified by (9), (15) and (19), are - as far as their shapes are concerned - identical with those characteristic for the problem of bending with compression [1]; only the substance of  $\lambda$  is mutually different. Relevant tables of  $\lambda$  can be found in [1], [15].

### 3. PROCEDURE FOR CONTINUOUS MEMBERS

The developed warping - twist equations of the generalized displacement method can be utilized in the determination of the critical load of torsional buckling in case of systems composed out of thin-walled members. Because of the decisive effect of joint configuration on the distribution of cross-sectional forces [3], [12], [18], presently continuous member systems are considered only.

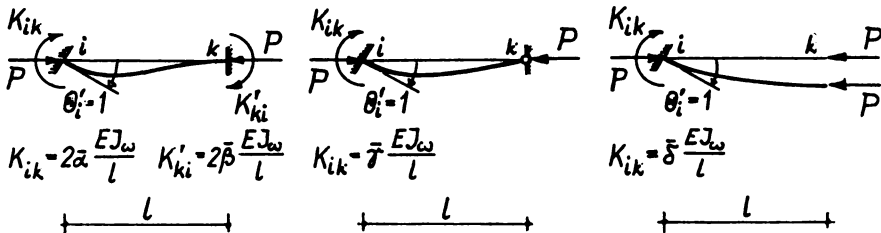


Fig. 5. Stiffness relations in thin-walled members: fixed-fixed, fixed-hinged, fixed-free

Within the conventional bending problem mentioned systems can be analysed, effectively, by a special procedure shown in [1]; for the case of torsion it must be generalized. According to that generalization first the flexural-torsional bar stiffnesses  $K_{ik}$  and bar restraints  $K'_{ki}$  for the basic support conditions must be settled, whereby  $K_{ik}$  is meant to be the bimoment at i-end which develops a unit warping of this end, and  $K'_{ki}$  - the associated bimoment occurring simultaneously at k-end (when fixed-fixed member is concerned)

For the case of fixed-fixed member,  $K_{ik}$  and  $K'_{ki}$  result from two first equations of (11):

$$K_{ik} = 2\alpha \frac{EJ\omega}{l}, \quad K'_{ki} = 2\beta \frac{EJ\omega}{l}. \quad (20)$$

For the member fixed at i and hinged at k,  $K_{ik}$  follows from the first of equations (14), taking  $\theta'_i=1$  and  $\delta=0$ :

$$K_{ik} = \gamma \frac{EJ\omega}{l}. \quad (21)$$

At last, for the member fixed at i and free at k,  $K_{ik}$  is a consequence of the first equation of (18), with  $\theta'_i=1$ :

$$K_{ik} = \delta \frac{EJ\omega}{l}. \quad (22)$$

The problem of flexural-torsional stiffnesses and restraint, for the discussed three cases of member supports, is illustrated in Fig. 5.

It can be easily noticed that for  $\lambda=0$  the quantities specified by the formulas (20) and (21) become identic with those governing the bending problem, what follows directly from the results (12) and (16); in that case  $K_{ik}$  corresponding to (22) is equal zero.

All the other items of the procedure applied in the determination of torsional buckling loads are identic with those concerning the bending problem.

#### 4. NUMERICAL EXAMPLE

The details of the discussed procedure will be shown on the example of a continuous member, analysed for flexural buckling in [1]; it is illustrated in Fig. 6.

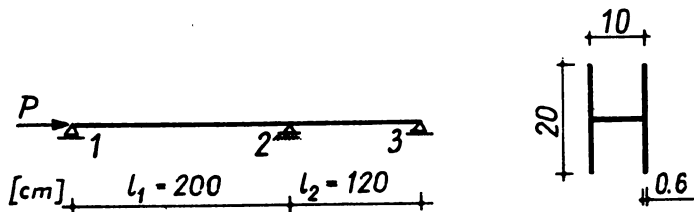


Fig. 6. Continuous member analysed

The member cross-sectional properties are the following:

$$\left. \begin{aligned} F &= 30 \text{ cm}^2, & r^2 &= \frac{J_x + J_y}{F} = \frac{145}{3} \text{ cm}^2, & E &= 2.6 G = \\ J_x &= 800 \text{ cm}^4, & J_d &= 3.6 \text{ cm}^4, & &= 21000 \text{ kNcm}^{-2}, \\ J_y &= 650 \text{ cm}^4, & J_w &= 20000 \text{ cm}^6, & k &= \sqrt{\frac{GJ_d}{EJ_w}} = 0.008325 \text{ cm}^{-1}. \end{aligned} \right\} (23)$$

The bimoment required to develop a unit warping at joint 2, i. e. - the joint stiffness  $K_2$ , is equal to the sum of stiffnesses  $K_{21}$  and  $K_{23}$  of both bars meeting at that joint:

$$K_2 = K_{21} + K_{23} = \bar{\gamma} \frac{EJ_w}{l_1} + \gamma \frac{EJ_w}{l_2}. \quad (24)$$

The stiffness  $K_{21}$  results from (21), since the member 1-2, at the initial stage, is hinged at 1 and fixed at 2. On the contrary, the stiffness  $K_{23}$  can not be settled on the basis of formula (21), although both members, 1-2 and 2-3, are identically supported, because the last one is not under compression. Therefore, the corresponding bar stiffness  $K_{23}$  must be calculated according to principles set in [3], [6]. The required  $\gamma$ -coefficient depends upon the flexural-torsional bar parameter  $\kappa_2$  of the second member:

$$\kappa_2 = l_2 \sqrt{\frac{GJ_d}{EJ_w}} = 0.99846 \quad (25)$$

which is associated with  $\gamma=3.1944$  determined by linear interpolation from tables shown in [3], [8]; the coefficient  $\bar{\gamma}$  depends on  $\lambda_1$ , competent for the first member and specified by formula (3).

In case that the axial thrust  $P$  becomes the continuous member critical load of torsional buckling  $P_\theta$ , the unit warping  $\theta'_2=1$  can be exerted without the bimoment itself; therefore, the stiffness of joint 2 must be equal zero:

$$\bar{\gamma} \frac{EJ_w}{l_1} + \gamma \frac{EJ_w}{l_2} = 0, \quad (26)$$

or

$$\bar{\gamma} = -\gamma - \frac{l_1}{l_2} = -3.1944 \frac{200}{120} = -5.3240. \quad (27)$$

Now, for instance, taking advantage of the third formula of (15), one obtains the following transcendental equation

$$\lambda_1^2 \tan \lambda_1 + 5.324 \tan \lambda_1 - 5.324 \lambda_1 = 0, \quad (28)$$

wherefrom, by trials, one can find  $\lambda_1=3.931$ . Having that, it is very easy to determine  $P_\theta$ , properly transforming the expression (3):

$$\begin{aligned} P_\theta &= P_d + P_w = \frac{GJ_d}{r^2} + \frac{EJ_w}{r^2} \frac{\lambda_1^2}{l_1^2} = \\ &= \frac{21000 \cdot 3.6}{2.6 \cdot \frac{145}{3}} + \frac{21000 \cdot 20000 \cdot 3.931^2}{\frac{145}{3} \cdot 200^2} = \\ &= 601.59 + 3356.98 = 3958.57 \text{ kN} \approx 3959 \text{ kN}. \end{aligned} \quad (29)$$

The Eulerian buckling loads  $P_x$  and  $P_y$  have been calculated, in line with [1], according to the following general expression:

$$P_{cr} = \frac{3.902 \cdot EJ}{l^2} = \frac{3.902 \cdot 21000}{200^2} J = 7.98525 \text{ J [kN]}. \quad (30)$$

Substituting for J, in sequence,  $J_x$  and  $J_y$ , one obtains:

$$\left. \begin{aligned} P_x &= 7.98525 \cdot 800 \approx 6388 \text{ kN}, \\ P_y &= 7.98525 \cdot 650 \approx 5190 \text{ kN}. \end{aligned} \right\} \quad (31)$$

It can be noticed that  $P_\theta$ , compared with  $P_x$  and  $P_y$ , is the smallest critical load.

Analysing the stiffening effect of the intermediate support 2, additionally two other bounding cases of that support have been studied: hinged and fixed ends. For the hinged end at 2, it is:

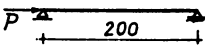
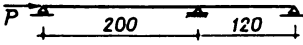
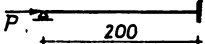
$$\left. \begin{aligned} P_\theta &= \frac{GJ_d}{r^2} + \frac{EJ\omega}{r^2} \cdot \frac{\pi^2}{l^2} \approx 2746 \text{ kN}, \\ P_x &= \frac{\pi^2 EJ_x}{l^2} \approx 4145 \text{ kN}, \quad P_y = \frac{\pi^2 EJ_y}{l^2} \approx 3368 \text{ kN}, \end{aligned} \right\} \quad (32)$$

and for the fixed one, respectively:

$$\left. \begin{aligned} P_\theta &= \frac{GJ_d}{r^2} + 2.092 \frac{EJ\omega}{r^2} \cdot \frac{\pi^2}{l^2} \approx 5087 \text{ kN}, \\ &\text{with } 2.092 \text{ taken from [19],[20];} \\ P_x &= 2 \cdot 4145 = 8290 \text{ kN}, \quad P_y = 2 \cdot 3368 = 6736 \text{ kN}. \end{aligned} \right\} \quad (33)$$

Full set of results is given in Table 1. They are characterized, on the one hand, by smaller values of  $P_\theta$  against  $P_x$  and  $P_y$  for any kind of member support at 2, and - by an  $\theta$  increase of all critical loads together with the stiffening of that support, on the other. It should be added that the critical loads calculated develop very high critical stressed lying outside the elastic range of common steel. Nevertheless, particular situations could bring up a more real danger of elastic buckling just through torsional instability.

Table 1. Confrontation of critical loads

Type of system	Critical load [kN]		
	$P_x$	$P_y$	$P_\theta$
	4145	3368	2746
	6388	5190	3959
	8290	6736	5087

## 5. FINAL REMARKS

Paper shows the possibilities of the generalized displacement method in handling the most simple buckling problem associated with torsion. It is thought to create a basis for the analysis of more complex stability problems of thin-walled systems, especially continuous members with monosymmetrical cross-sections treated in [17]. Presented method can be adapted for cases of closed sections.

## REFERENCES

1. BŁASZKOWIAK, S. and KĄCZKOWSKI, Z. - Iterative Methods in Structural Analysis, Pergamon Press/Państwowe Wydawnictwo Naukowe, Oxford/Warszawa, 1966.
2. Byehkov, D.W. - Structural Mechanics of Thin-Walled Bar Systems (in Russian), Gosstroilzdat, Moscow, 1962.
3. Cywiński, Z. - "The Cross Method Applied to the Solution of Plane, Thin-Walled Frame Systems of Open Cross-Sections" (in Polish). *Zeszyty Naukowe Politechniki Gdańskiej*, 1962, 32, 89-107.
4. Cywiński, Z. - "Determination of Influence Lines of Bimoments in Continuous Beams by Means of the Generalized Method of Cross-Błaszkwiaak" (in Polish), *Zeszyty Naukowe Politechniki Gdańskiej*, 1975, 231, 65-79.
5. Cywiński, Z. - "Warping-Twist Equations of the Displacement Method for the Torsional Buckling Problem" (in Polish). *Zeszyty Naukowe Politechniki Gdańskiej*, 1977, 257, 83-95.
6. Cywiński, Z. - "Bimoment Distribution Method for Thin-Walled Beams", *Der Stahlbau*, 1978, 47, 106-113, 152-157.
7. Cywiński, Z. - "On Torsion Design of Thin-Walled Frames", *Structural Engineering & Construction*, Ed. Kanok-Nukulchai, W., Pergamon Press, Oxford, 1986, 1019-1028.
8. Cywiński, Z. - "On Buckling of Thin-Walled Frames", *Sec. Reg. Coll. Stability of Steel Structures, Hungary 1986*, *Fin. Rep.* 157-160.
9. Cywiński, Z. - "Thin -Walled Frames under Moving Torques: Iterative Approach", *Int. Conf. Steel Structures, Budva 1986, Proceedings, Part II*, 451-458.
10. Cywiński, Z. - Discussion on "Warping Moment Distribution", *J. Struct. Engrg.* 1987, 113, 172-173.
11. Cywiński, Z. and Nishino, F. - "On Element Stiffness Matrices in the Matrix Displacement Analysis of Thin-Walled Frames", *J. of the Fac. of Engrg., The Univ. of Tokyo*, to be published.
12. Czapliński, K. - "Distortion Angles and Equilibrium of Bimoments in Rigid Joint of a Certain Type" (in Polish), *Archiwum Inżynierii Ładowej* 1970, 16, 301-313.
13. Klöppel, K. and Friemann, H. - "Erweiterung des Formänderungsgrößen-Verfahrens auf die Theorie der Wölbkrafttorsion", *Der Stahlbau* 1966, 35, 365-372.
14. Kollbrunner, C.F. and Hajdin, N. - Dünnwandige Stäbe, Bd. 1, Springer-Verlag, Berlin/Heidelberg/New York 1972.
15. Kollbrunner, C.F. and Meister, M. - Knicken, Biegedrillknicken, Kippen, Springer-Verlag, Berlin/Göttingen/Heidelberg 1961.
16. Krayterman, B.L. and Krayterman, A.B. - "Generalized Nonuniform Torsion of Beams and Frames", *J. Struct. Engrg.* 1987, 113, 1772-1787.
17. Schardt, R. - "Die genaue Ermittlung der Biegedrillknicklasten mehrfeldriger mittig gedrückter Stäbe mit einfach symmetrischem offenem dünnwandigem Querschnitt und beliebiger Lagerung an den Knoten nach dem Formänderungsgrößenverfahren", *Der Stahlbau*, 1966, 35, 365-372.
18. Szmidt, J.K. - "The Analysis of Frames Made Up of Thin-Walled Elements" (in Polish), *Rozprawy Inżynierskie - Engineering Transactions* 1975, 23, 447-472.
19. Urban, I.V. - Theory of Design of Thin-Walled Bar Structures (in Russian), *Tsanzheldorizdat, Moscow*, 1955.
20. Vlasov, V.Z. - Thin-Walled Elastic Beams, *Israel Program for Scientific Translations, Jerusalem*, 1961.

ON NONLINEAR FUNCTIONALS FOR SHALLOW SHELLS AND GEOMETRICALLY IMPERFECT PLATES (I)

R. Dąbrowski  
Technical University  
of Gdańsk, Poland

**SUMMARY** - Formal identity of equilibrium and compatibility equations in terms of normal displacement  $w$  and stress function  $F$  in the nonlinear theory of a shallow shell and that of an initially deformed plate is demonstrated; this is so despite of differences in underlying strain-displacement relations (initial twist curvature in the shallow shell is duly accounted for). Nonlinear functionals for both systems are derived.

1 INTRODUCTION

The topic goes back to problems and methods dealt with in the fifties [1]. Nonlinear equilibrium and compatibility equations with respect to normal displacement  $w$  and stress function  $F$  for a shallow shell, inclusive of residual stresses expressed in terms of initial stress function  $F_0$ , are well known. Analogous known equations apply to a plate with initial deflection  $w_0$  [2] - also inclusive of residual stresses as well [3].

However, one difference in both approaches should be pointed out. Whereas displacements  $u, v, w$  in a shell are measured in a plane tangential to the shell surface and normal to it, respectively, those in an imperfect plate are measured in initial reference system  $x, y, z$ ,  $xy$  being plate middle plane. Consequently, strain-displacement relations ought to appear differently.

(I) Originally submitted in Polish to Scientific Papers of Tech. University Gdańsk in June 1985. Publication pending.

## 2 EQUILIBRIUM AND COMPATIBILITY EQUATIONS IN GEOMETRICALLY NONLINEAR THEORY

### 2.1 Shallow shell

As an example, a shallow shell with initial twist curvature given by the equation

$$z = \frac{x^2}{2r_x} + \frac{y^2}{2r_y} + \frac{xy}{r_{xy}} \quad (1)$$

is considered (two special cases are shown in Fig.1a,b) where the curvatures are constant:

$$\begin{aligned} \kappa_x &= 1/r_x \approx z_{,xx} \\ \kappa_y &= 1/r_y \approx z_{,yy} \\ \kappa_{xy} &= 1/r_{xy} = z_{,xy} \end{aligned} \quad (2)$$

(indices following a comma denote differentiation).

Displacement components  $u, v, w$  are measured as indicated in Fig.1a,b. It is implied that normal displacement  $w$  is, in technical applications, markedly greater than tangential displacements  $u, v$ . The strain-displacement relations read [1], Eq.(5.4),

$$\begin{aligned} \epsilon_x &= u_{,x} - \frac{w}{r_x} + \frac{1}{2} (w_{,x})^2 \\ \epsilon_y &= v_{,y} - \frac{w}{r_y} + \frac{1}{2} (w_{,y})^2 \\ \gamma_{xy} &= u_{,y} + v_{,x} - 2 \frac{w}{r_{xy}} + w_{,x} w_{,y} \end{aligned} \quad (3)$$

Shear strain  $\gamma_{xy}$  has been supplemented by the twist-curvature term  $(1/r_{xy} + 0)$ .

One notices that for rigid-body translation  $\bar{w}$  in the direction of  $z$ -axis the corresponding displacement components read

$$w \approx \bar{w}, \quad u = \bar{w} z_{,x}, \quad v = \bar{w} z_{,y} \quad (4)$$

and, in accordance with Eqs (3), all strains vanish:

$$\epsilon_x = \bar{w} z_{,xx} - \bar{w}/r_x = 0, \quad \dots \quad \gamma_{xy} = 2\bar{w} z_{,xy} - 2\bar{w}/r_{xy} = 0 \quad (5)$$

Membrane forces are defined by means of stress function  $F$ :

$$n_x = F_{,yy}, \quad n_y = F_{,xx}, \quad n_{xy} = -F_{,xy} \quad (6)$$

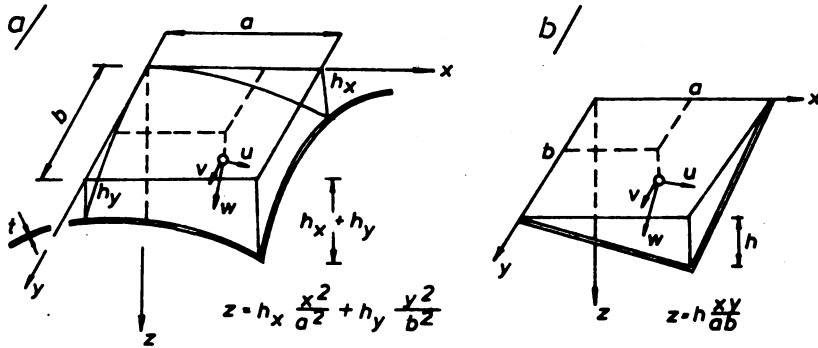


Fig. 1

Donnell-type equilibrium and compatibility equations for shallow shells have been derived by V.Z. Vlasov and subsequently by A.S. Volmir [1], Eqs (5.27) and (5.28),

$$K \nabla^4 w - \nabla_c^2 P = q + L(w, P) \quad (7)$$

$$\frac{1}{Et} \nabla^4 P + \nabla_c^2 w = -\frac{1}{2} L(w, w) \quad (8)$$

in which  $K = Et^3/12(1-\nu^2)$ ,  $E$  and  $\nu$  are denoting modulus of elasticity and Poisson coefficient, respectively;  $q$  is the normal load, and

$$\begin{aligned} \nabla^2 &= ( )_{,xx} + ( )_{,yy} \\ \nabla_c^2 &= \frac{1}{r_x} ( )_{,yy} - \frac{2}{r_{xy}} ( )_{,xy} + \frac{1}{r_y} ( )_{,xx} \end{aligned} \quad (9)$$

$$L(w, P) = w_{,xx} P_{,yy} - 2w_{,xy} P_{,xy} + w_{,yy} P_{,xx}$$

(in the operator  $\nabla_c^2$  twist curvature is duly presented).

Inclusion of residual stresses can proceed as done subsequently under 2.2 for an imperfect plate.

## 2.2 Imperfect plate with residual stresses

A simply supported rectangular plate is considered, with initial stress-free deformation given by (Fig.2)

$$w_0 = -f \sin \frac{\pi x}{a} \sin \frac{\pi y}{b} \quad (10)$$

and (variable) curvatures



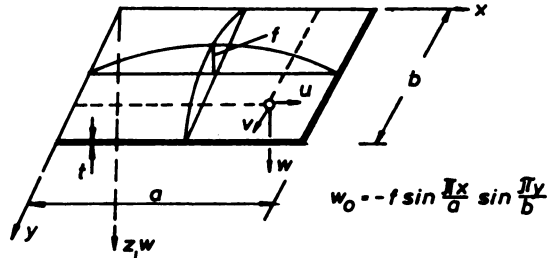


Fig.2

$$\begin{aligned}
 \kappa_x &\approx w_0'_{xx} = \frac{f\pi^2}{a^2} \sin \frac{\pi x}{a} \sin \frac{\pi y}{b} \\
 \kappa_y &\approx w_0'_{yy} = \frac{f\pi^2}{b^2} \sin \frac{\pi x}{a} \sin \frac{\pi y}{b} \\
 \kappa_{xy} &= w_0'_{xy} = -\frac{f\pi^2}{ab} \cos \frac{\pi x}{a} \cos \frac{\pi y}{b}
 \end{aligned}
 \tag{11}$$

Displacement components  $u, v, w$  are measured strictly along the coordinates  $x, y, z$  (Fig.2). Strain-displacement relations due to Marguerre [2] read now, see e.g. [1], Eqs (45):

$$\begin{aligned}
 \epsilon_x &= u_{,x} + w_{,x}w_0'_{,x} + \frac{1}{2}(w_{,x})^2 \\
 \epsilon_y &= v_{,y} + w_{,y}w_0'_{,y} + \frac{1}{2}(w_{,y})^2 \\
 \gamma_{xy} &= u_{,y} + v_{,x} + w_{,x}w_0'_{,y} + w_{,y}w_0'_{,x} + w_{,x}w_{,y}
 \end{aligned}
 \tag{12}$$

One notices that for rigid-body translation along  $z$ -axis equal  $\bar{w}$  a strain-free state of deformation is a priori secured. One also notices that derivatives of  $u$  and  $v$  appearing in Eqs (3) and (12) - identically written - have different meaning. Also corresponding terms like  $w/r_x$  and  $w_{,x}w_0'_{,x}$  are not necessarily identical.

The residual stresses are defined as follows:

$$n_{x0} = F_0'_{yy}, \quad n_{y0} = F_0'_{xx}, \quad n_{xy0} = -F_0'_{xy} \tag{13}$$

Combined with initial deflection  $w_0$ , they constitute a self-contained system without any external forces required for equilibrium.

Equilibrium and compatibility equations assume final form

$$K \nabla^4 w = q + L(w_0 + w, F) + L(w, F_0) \quad (14)$$

$$\frac{1}{Et} \nabla^4 F = -L(w_0, w) - \frac{1}{2} L(w, w) \quad (15)$$

in which  $q$  is the load acting in  $z$ -direction. Herewith the known Marguerre equations [2] have been supplemented by the effect of residual stresses, see also [3].

Let now the effect of residual stresses in Eq.(14) be suppressed,  $L(w, F_0) = 0$ . Assuming for small curvatures the following relations:

$$w_0'_{xx} \approx 1/r_x, \quad w_0'_{yy} \approx 1/r_y, \quad w_0'_{xy} = 1/r_{xy} \quad (16)$$

one obtains from definitions of  $\nabla_c^2$  and  $L$  according to (9) the following correspondencies:

$$L(w_0, F) \approx \nabla_c^2 F \quad \text{and} \quad L(w_0, w) \approx \nabla_c^2 w \quad (17)$$

and thus formal identities of Eqs (14) and (15) for an imperfect plate with Eqs (7) and (8) for a "pretwisted" shallow shell. This is so despite of differences in underlying strain-displacement relations according to Eq.(12) and Eq.(3), respectively, and despite, or rather because, of disparity in definition of displacement components (Fig.1 as opposed to Fig.2).

### 3 FUNCTIONALS

In the case under consideration, a functional  $\Pi$  constitutes an area integral of a function  $f(\dots)$  expressed by  $w(x,y)$  and  $F(x,y)$  an their first and second derivatives:

$$\Pi = \iint f(w, w_x, w_y, w_{xx}, w_{xy}, w_{yy}; F_x, F_y, F_{xx}, F_{xy}, F_{yy}) dx dy \quad (18)$$

Stationarity of functional  $\Pi$  corresponds to vanishing of the first variation:  $\delta\Pi = 0$ . From this condition the following Eulerian equation with respect (firstly) to displacement  $w$  and its derivatives results [4]:

$$\frac{\partial^2}{\partial x^2} \frac{\partial f}{\partial w_{xx}} + \frac{\partial^2}{\partial y^2} \frac{\partial f}{\partial w_{yy}} + \frac{\partial^2}{\partial x \partial y} \frac{\partial f}{\partial w_{xy}} - \frac{\partial}{\partial x} \frac{\partial f}{\partial w_x} - \frac{\partial}{\partial y} \frac{\partial f}{\partial w_y} + \frac{\partial f}{\partial w} = 0 \quad (19)$$

Analogous Eulerian equation applies to derivatives of the stress function  $F$ . Equation (19) is valid over the whole shell or plate surface and, in general, is supplemented by appropriate boundary conditions with respect to displacement  $w$  and derivatives of the stress function  $F$ .

From Eq. (19) equilibrium equation (7) ought to follow, from another one - the corresponding compatibility equation (8), or Eqs (14) and (15), respectively.

### 3.1 Functional for shallow shell

The functional  $\Pi$  constitutes strain energy of the structure due to bending, membrane strains and is completed by the potential of external forces:

$$\Pi = V_b + V_m + V_1 \quad (20)$$

In order to arrive at postulated equilibrium and compatibility equations, the membrane strain energy  $V_m$  is expressed in the form of a total energy (the sum of strain and complementary energies) from which the complementary energy is subtracted:

$$V_m = \iint (n_x \epsilon_x + n_y \epsilon_y + n_{xy} \gamma_{xy}) dx dy - \frac{1}{2Et} \iint [(F_{,xx})^2 + (F_{,yy})^2 - 2\nu F_{,xx} F_{,yy} + 2(1+\nu)(F_{,xy})^2] dx dy \quad (21)$$

The total-energy expression is integrated by parts; the resulting new integral is accompanied by the boundary term

$$\left[ \int (F_{,yy} u - F_{,xy} v) dy \right]_{x=0}^{x=a} + \left[ \int (F_{,xx} v - F_{,xy} u) dx \right]_{y=0}^{y=b} \quad (22)$$

which is cancelled by similar negative term of the edge load potential in  $V_1$ .

Under the assumption that at the boundaries the normal displacement  $w$  vanishes (Fig.1) the following functional is obtained:

$$\begin{aligned} \Pi = & \frac{K}{2} \iint [(\nabla^2 w)^2 - (1-\nu) L(w, w)] dx dy \\ & - \frac{1}{2Et} \iint [(\nabla^2 F)^2 - (1+\nu) L(F, F)] dx dy \\ & + \iint \left[ \frac{1}{r_x} F_{,y} w_{,y} + \frac{1}{r_y} F_{,x} w_{,x} - \frac{1}{r_{xy}} (F_{,y} w_{,x} + F_{,x} w_{,y}) \right] dx dy \\ & + \frac{1}{2} \iint [F_{,yy} (w_{,x})^2 + F_{,xx} (w_{,y})^2 - 2F_{,xy} w_{,x} w_{,y}] dx dy - \iint q w dx dy \quad (23) \end{aligned}$$

(Attention is drawn to the minus sign before the second integral.) Thus Broude's functional given recently [3] has been confirmed and extended to account for initial twist curvature.

It can be checked that for this functional from Eulerian equation (19) the equilibrium equation (7), as should be, is obtained; in similar way the compatibility equation (8) is confirmed. Functional and equations are valid for constant curvatures.

### 3.2 Functional for imperfect plate

Nonlinear functional for a bend and stretched plate - without imperfections of geometry and residual stresses - has been derived in the early fifties by A.S. Volmir [1], Eq.(1.116). Supplemented by both mentioned effects it reads in terms of displacement  $w$  along  $z$ -axis (Fig.2) and stress function  $F$  as follows:

$$\begin{aligned}
 \Pi = & \frac{K}{2} \iint [(\nabla^2 w)^2 - (1-\nu)L(w,w)] dx dy \\
 & - \frac{1}{2EF} \iint [(\nabla^2 F)^2 - (1+\nu)L(F,F)] dx dy \\
 & + \frac{1}{2} \iint \left\{ F_{,yy} [2w_{,x} w_{0,x} + (w_{,x})^2] + F_{,xx} [2w_{,y} w_{0,y} + (w_{,y})^2] \right. \\
 & \quad \left. - 2F_{,xy} (w_{,x} w_{0,y} + w_{,y} w_{0,x} + w_{,x} w_{,y}) \right\} dx dy \\
 & + \frac{1}{2} \iint [F_{0,yy} (w_{,x})^2 + F_{0,xx} (w_{,y})^2 - 2F_{0,xy} w_{,x} w_{,y}] dx dy \\
 & - \iint q w dx dy \qquad (24)
 \end{aligned}$$

Functional (24) is valid for variable curvatures  $w_{0,xx}$ ,  $w_{0,yy}$  and  $w_{0,xy}$ , and  $w = 0$  at the boundaries. (In a functional given for the case under consideration by B.M. Broude [3] a slight correction regarding the effect of initial deflection  $w_0$  had to be introduced, as done here in the third and fourth line of functional (24). The author of [3] has subsequently corrected his functional in another paper published in No 4/86 of the same journal.) Functional (24) is congruent with former Eqs (14) and (15).

The following observation is worth noticing. If the functional (24) is devoid of residual stresses (derivatives of  $F_0$  vanish) and constant curvatures are assumed, integration by parts of (24) yields its formal identity with functional (23).

### 3.3 Final remark

In numerical computations of stresses and deformations of steel-plated structures, more expedient than functional (24) can turn out to be an alternative functional in which all three displacement components  $u, v, w$  and the membrane forces  $n_x, n_y, n_{xy}$  are the unknowns [5], instead of  $w$  and  $F$ . The condition  $\delta\Pi = 0$  yields three equilibrium equations and three nonlinear compatibility relations, and boundary conditions as well.

Interesting is the application of the new functional to an approximate analysis of postcritical behavior of a rib-stiffened plate forming a compressed lower box-girder flange (as happens to be at intermediate supports in continuous girder bridges). Application is limited to (physically linear) elastic behavior. However discretely stiffened plate is treated as an doublelayered continuum. Shear lag is intrinsically accounted for.

#### REFERENCES

1. VOJMIR A.S. - Gibkie plastinki i oboločki, Gos.izdat.tech-teoret.lit., Moskva, 1956.
2. MARGUERRE K. - "Zur Theorie der gekrümmten Platte grosser Formänderung". Jahrbuch der deutschen Luftfahrtforschung, 1939, 413-418.
3. BROUDE B.M. - "Nelinejnye razrešajuščije uravnenia dla pologich oboloček s načalnymi napriženiami". Stroitenaja Mehanika i Rasčet Sooruženij, 1983, no 3, 60-61.
4. (Ed. by W. FLÜGGE) - Handbook of engineering mechanics, Chapter 16. Calculus of variations. McGraw-Hill, New York, 1962.
5. JETTEUR P., MAQUOI R., ŠKALOU M., ŽÖRNEROVA M. - "Interaction of shear lag with plate buckling of longitudinally stiffened compression flanges". Acta Technica ČSAV, 1984, no 3, 376-397.

**THE GENERAL NUMERICAL SOLUTION  
OF THE LAME'S EQUATIONS BY HAJDIN'S METHOD**

**Petar S. Petrović**

Civil Engineering Faculty, University of Beograd  
Bulevar Revolucije 73, Beograd 11000, Yugoslavia

**SUMMARY**

The three-dimensional state of stresses and deformations of an elastic, homogeneous and isotropic rectangular plate with constant thickness, described by the equilibrium equations of the Theory of elasticity expressed only with displacements and body forces, is determined. These Lamé's partial differential equations, together with arbitrary boundary conditions on any of the plate's surfaces, are solved by application of Hajdin's method of integral equations [1], [4], [5]. As an illustration of the obtained solution, the results for a simply supported square plate subjected to a sinusoidal transverse load on the upper surface, is presented. The results for a rough mesh  $3 \times 3$  placed on horizontal plane of a quarter of a plate, and 5 horizontal planes across the thickness of a plate, show very good agreement with exact solution [7].

**INTRODUCTION**

The basic problem of the linear Theory of elasticity - determination of state of stresses and deformations of an elastic body for the prescribed boundary conditions, has been focusing the attention of scientists for many years now. And while some of problems of the Theory of elasticity, which can be simplified to one-dimensional or two-dimensional problems, are solved, the three-dimensional solutions are very rare, being only given for the simplest forms of elastic bodies with the simplest boundary conditions.

Navier in 1821 was the first one who derived the equilibrium equations of an isotropic elastic body expressed through displacements, but containing only one

constant for description of elastic properties of an elastic body. In such a way the three-dimensional problem of the Theory of elasticity was for the first time reduced to solution of differential equations containing only displacements  $U$ ,  $V$  and  $W$  as unknowns. In the present form the equilibrium equations were derived by G. Lamé in 1852, and they comprehend two constants for description of elastic properties of an elastic body ( $G = E/(2+2\cdot\mu)$  and Poisson's ratio  $\mu$ ).

The general solution of these three Lamé's equations:

$$(a+1) \cdot \frac{\partial^2 U}{\partial x^2} + \frac{\partial^2 U}{\partial y^2} + \frac{\partial^2 U}{\partial z^2} + a \cdot \left( \frac{\partial^2 V}{\partial x \partial y} + \frac{\partial^2 W}{\partial x \partial z} \right) + \frac{X}{G} = 0 \quad (1)$$

$$\frac{\partial^2 V}{\partial x^2} + (a+1) \cdot \frac{\partial^2 V}{\partial y^2} + \frac{\partial^2 V}{\partial z^2} + a \cdot \left( \frac{\partial^2 U}{\partial x \partial y} + \frac{\partial^2 W}{\partial y \partial z} \right) + \frac{Y}{G} = 0 \quad (2)$$

$$\frac{\partial^2 W}{\partial x^2} + \frac{\partial^2 W}{\partial y^2} + (a+1) \cdot \frac{\partial^2 W}{\partial z^2} + a \cdot \left( \frac{\partial^2 U}{\partial x \partial z} + \frac{\partial^2 V}{\partial y \partial z} \right) + \frac{Z}{G} = 0 \quad (3)$$

( $E$  = modulus of elasticity,  $a = 1/(1-2\cdot\mu)$ ;  $X$ ,  $Y$ ,  $Z$  = body forces,  $U$ ,  $V$ ,  $W$  = displacements in  $x$ ,  $y$  and  $z$  directions respectively) in the form of three biharmonic functions was given by Boussinesq in 1885, and in the form of four harmonic functions - by P.F.Papkovich in 1932. Two years later H.Neuber arrived at the same solution. In 1959 V.M.Deyev developed the general solution of Lamé's equations - a class of functions which has infinite number of mutually different general solutions in form, in function of three arbitrary constants; for determined values of these constants his solution equals to Papkovich's solution.

Many scientists were engaged to solve Lamé's equations, presenting either "general solution" or "solution" of concrete problem: G.Lamé (1852), P.A.Schiff (1891), Kelvin (1863), O.Tedon (1904), P.Burgatti (1926), B.G.Galerkin (1930), G.D.Grodskij (1935), M.G.Slobodjanskij (1938), L.N.Ter-Mkrtichjan (1944), M.M.Filonenko-Borodich (1951), L.P.Vinokurov (1951), F.S.Churikov (1953), M.Mischonov (1960), V.V.Vischnjakov (1963), S.M.Saakjan (1966), A.B.Zolotov (1971), B.M.Lisicin (1971), N.A.Telegina (1972), B.F.Vlasov (1974), A.A.Rogovoj (1976), Isamura Okomura (1976), S.M.Hazardzan (1978), E.Bajda (1983), N.Bojko (1983) and others.

## TRANSFORMATION OF LAMÉ'S EQUATIONS

Consider a homogeneous, isotropic and elastic rectangular plate (parallelepiped - Fig.1) which has: four lateral surfaces denoted with  $A$ ,  $B$ ,  $C$  and  $D$ ; the upper surface is  $E$ , and the lower surface is  $F$ . The  $x$  and  $y$  axes of rectangular coordinate system lie in the surface  $E$  and intersection of the surfaces  $E$  and  $A$ , and  $E$  and  $C$  respectively. The  $z$  axis, intersection of the surfaces  $A$  and  $C$ , points downwards to form a left coordinate system. Each of the edges ( $d_x$ ,  $d_y$ ,  $d_z$ ) of a rectangular parallelepiped is divided into a certain number of parts, and the planes parallel to coordinate planes are placed through the points obtained in such a way. Intersections of these planes produce mutually orthogonal lines  $x_i$ ,  $Y_j$ ,  $z_k$ , along which the Lamé's equations are transformed into a system of algebraic equations [1]. Calculating points of a parallelepiped are in intersections of these lines. Position of calculating points is as follows:

- in a parallelepiped: points of parallelepiped (total of  $m$  points)  $i=1,2,$

..., l; j=1,2,...,J and k=1,2,...,k;

- on surfaces of a parallelepiped - boundary points (total of n points): polyhedral angles (ACE, BCE, ADE, BDE, ACF, BCF, ADF and BDF), edges without polyhedral angles (CE, DE, CF, DF, AE, BE, AF, BF, AC, BC, AD and BD), and surfaces without edges and polyhedral angles (A, B, C, D, E and F).

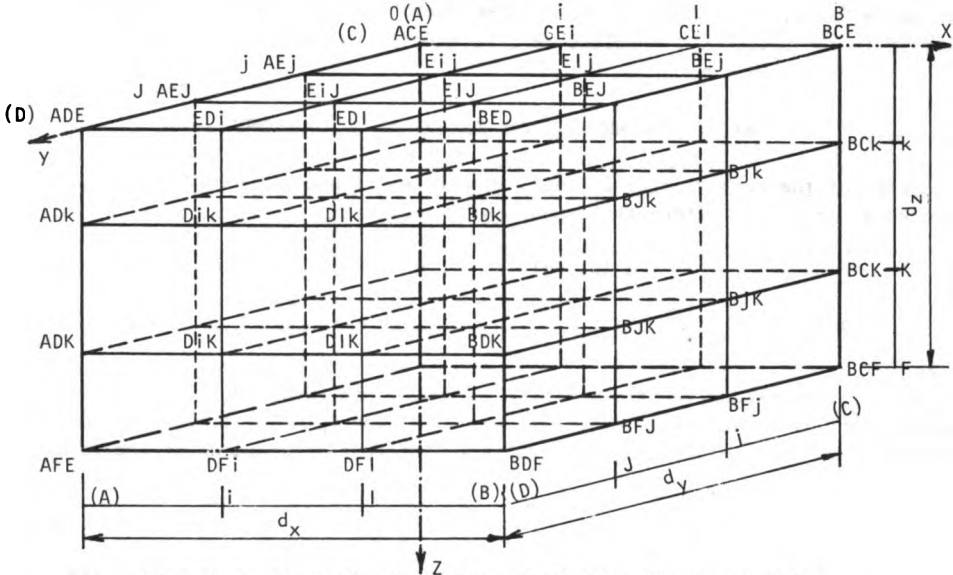


Fig. 1 A parallelepiped with calculating lines and points.

With denotations

$$\frac{\partial^2 S}{\partial x^2} = -p_s, \quad \frac{\partial^2 S}{\partial y^2} = -q_s, \quad \frac{\partial^2 S}{\partial z^2} = -r_s \quad (4,5,6)$$

$$\frac{\partial^2 S}{\partial x \partial y} = \alpha_s, \quad \frac{\partial^2 S}{\partial x \partial z} = \beta_s, \quad \frac{\partial^2 S}{\partial y \partial z} = \gamma_s, \quad (7,8,9)$$

where  $p_s, q_s, \dots, \gamma_s$  are "fictive loads", and  $S=U, V, W$ , equations (1) to (3) become a system of three algebraic equations. Let us write this system of algebraic equations for each of calculating points of a parallelepiped ( $m+n$ ). Let us form a system of matrix equations from the systems of algebraic equations obtained in such a way:

- for m calculating points in a parallelepiped:

$$c \cdot p_u + q_u + r_u = a \cdot (\alpha_v + \beta_w) + \frac{1}{G} \cdot x \quad (10)$$

$$p_v + c \cdot q_v + r_v = a \cdot (\alpha_u + \gamma_w) + \frac{1}{G} \cdot y \quad (11)$$

$$p_w + q_w + c \cdot r_w = a \cdot (\beta_u + \gamma_v) + \frac{1}{G} \cdot z \quad (12)$$

$$(c = a + 1)$$

- for n calculating points on the surfaces of a parallelepiped:

$$c \cdot p_{u*} + q_{u*} + r_{u*} = a \cdot (\alpha_{v*} + \beta_{w*}) \quad (13)$$



$$P_{v*} + c \cdot q_{v*} + r_{v*} = a \cdot (\alpha_{u*} + \gamma_{w*}) \quad (14)$$

$$P_{w*} + q_{w*} + c \cdot r_{w*} = a \cdot (\beta_{u*} + \gamma_{v*}) \quad (15)$$

These two systems have to be solved satisfying prescribed boundary conditions at each of calculating boundary points (n). It is very clear that solution of these systems of matrix equations can be obtained only by introducing expressions for fictive loads ( $p_s, \dots, \gamma_s$ ) resulted as solutions of (4) to (9) equations.

#### HAJDIN'S METHOD OF INTEGRAL EQUATIONS

Each of the members of the Lamé's equations - expressions (4) to (9), considered as a partial differential equation of the form

$$\frac{\partial^2 S(x, y, z)}{\partial \alpha^2} = -p_s(x, y, z) \quad (16)$$

or

$$\frac{\partial^2 S(x, y, z)}{\partial \alpha \partial \beta} = r_s(x, y, z) \quad (17)$$

( $p_s$  and  $r_s$  are unknown functions - fictive loads, and  $S=U, V, W$ ;  $\alpha, \beta=x, y, z$ ) along the straight lines  $x_i$  ( $i=1, \dots, M$ ),  $y_j$  ( $j=1, \dots, N$ ) and  $z_k$  ( $k=1, \dots, K$ ) (always two coordinates are constant) represents ordinary differential equation of the form

$$y''(x) = -p(x) \quad (18)$$

or

$$y'(x) = r(x) \quad (19)$$

If solutions of these two ordinary differential equations are known, then the solutions to the equations (4) to (9) can be obtained.

A method of numerical solution of boundary value problems of ordinary linear differential equations and of partial differential equations, was developed by Nikola Hajdin [1] in 1956.

According to the analogy with differential equations of linear systems of the Theory of structures, equation (18) is a differential equation of bending moments  $Y$  of a simple beam, loaded with  $p(x)$  along its span  $d$  and with bending moments  $Y_A$  and  $Y_B$  at the supports A and B. The equation (19) is a differential equation of shear forces. The kernels of the integral equations - Green's functions  $a(x, \xi)$  and  $a'(x, \xi)$  respectively, which appear in solution of these equations, represent the influence lines (functions) of the bending moments and shearing forces respectively, of a simple beam of a span  $d$ .

Numerical solutions of equations (18) and (19), defined in the interval  $[0, d]$ , with prescribed boundary conditions at the ends  $x=0$  and  $x=d$ , applying anyone of the methods of numerical integration, at the points  $x_i$  ( $i=1, 2, \dots, M$ ) and in matrix form, are as follows [1], [4], [5]:

$$Y = A \cdot P + A_A \cdot p_A + A_B \cdot p_B + E_A \cdot Y_A + E_B \cdot Y_B \quad (20)$$

$$r = Y' = A' \cdot P + A'_A \cdot p_A + A'_B \cdot p_B + E'_A \cdot Y_A + E'_B \cdot Y_B \quad (21)$$

It is supposed that equation (18) is the first derivative in respect to  $x$  of the equation (19), and that the boundary conditions for both of these equations are

the same. In the papers [1] to [6] and [8] definition and procedure for obtaining a Green's function (influence functions for: shear force, bending moment, tangent on elastic line and elastic line) is shown in detail, including general form of: matrices  $\mathbf{Q}$  and  $\mathbf{Q}'$  (for a simple beam - ordinates of a Green's function ( $a(x, \xi)$  and  $a'(x, \xi)$  respectively) - influence line of bending moment and of shear force respectively) for arbitrary, symmetric and antisymmetric loads; matrices of numerical integration ( $\mathbf{d}$ ) and interpolation of load  $p(x)$  ( $\mathbf{L}$ ), and product of matrices  $\mathbf{A} = \mathbf{Q} \cdot \mathbf{d} \cdot \mathbf{L}$  and  $\mathbf{A}' = \mathbf{Q}' \cdot \mathbf{d} \cdot \mathbf{L}$ .

In the equations (20) and (21) unknowns are:  $\mathbf{Y}$ ,  $\mathbf{Y}'$ ,  $\mathbf{p}$ ,  $p_A$  and  $p_B$ , where  $\mathbf{p}$  matrix represents ordinates of unknown load  $p(x)$  at calculating points  $i$  ( $i=1, 2, \dots, M$ ), and  $p_A$  and  $p_B$  are ordinate of the same load, but above supports A and B respectively. From these two equations may be expressed matrices  $\mathbf{p}$  and  $\mathbf{Y}'$  with  $\mathbf{Y}$ ,  $p_A$  and  $p_B$ ; so, there is a surplus of two unknowns:  $p_A$  and  $p_B$ . There are two possibilities to find them:

- the first one: by extrapolation of neighbouring ordinates ( $p_1, p_2, p_3$  and  $p_{M-2}, p_{M-1}, p_M$  respectively) from matrix  $\mathbf{p}$ :

$$p_A = C_{1A} \cdot \mathbf{p} \quad (22)$$

$$p_B = C_{1B} \cdot \mathbf{p} \quad (23)$$

In this case equations (20) and (21) become

$$\mathbf{Y} = \mathbf{B} \cdot \mathbf{p} + \mathbf{E}_A \cdot Y_A + \mathbf{E}_A' \cdot Y_A \quad (24)$$

$$\mathbf{r} = \mathbf{Y}' = \mathbf{B}' \cdot \mathbf{p} + \mathbf{E}_A' \cdot Y_A + \mathbf{E}_B' \cdot Y_B \quad (25)$$

This way is simple and easy (error is small), but when is applied in solving of equations (4) to (9), Lamé's equations are not satisfied on the surface of a parallelepiped.

- the second one: the correct way is to look for new two equations for  $p_A$  and  $p_B$ , as it is done in [8]; using prescribed boundary conditions it is obtained:

$$p_A = \beta_{Ap} \cdot \mathbf{p} + \beta_{Ay} \cdot \mathbf{Y} + \beta_{Ao} \quad (26)$$

$$p_B = \beta_{Bp} \cdot \mathbf{p} + \beta_{By} \cdot \mathbf{Y} + \beta_{Bo} \quad (27)$$

With these values of  $p_A$  and  $p_B$  Lamé's equations are satisfied on the surface of a parallelepiped. Exact values of  $p_A$  and  $p_B$  depend only from selected: interpolation of loads, way of numerical integration and mesh density of calculating lines (for rough mesh also depend from loads).

## SOLUTIONS OF EQUATIONS WITH FICTIVE LOADS

We shall consider that logical sequence of the elements in a column matrix is realised if:

- all the elements with values of displacements U, then V, then W, are placed in order; and

- all the elements with values of each of said displacements are arranged at the increasing indexes  $i$ , followed by  $j$ , and then  $k$ , i.e.  $i, j, k$ .

While forming some of column matrices with displacements U, V and W, due to

the procedure of numerical integration, the sequence of elements at the increasing indexes  $i, j, k$  could not be written directly. The combinations of these sequences are:  $k, i; k, j; j, i$  and  $j, k, i$ . Such column matrices need to be transformed at the increasing indexes:  $i, k; j, k; i, j$  and  $i, j, k$  respectively  $|1|, |4|, |8|$ .

Along the straight lines  $y_1 = \text{const.}$  and  $z_k = \text{const.}$  the equation (4) becomes ordinary differential equation

$$\frac{d^2}{dx^2} S(x, y_j, z_k) = -p_s(x, y_j, z_k), \quad (28)$$

which in its form resembles the equation (18). According to the expressions (24) and (25) at the points  $x_i$ , it follows ( $i=1, 2, \dots, l; q=A, B$ ):

$$P_{sjk} = A_{sjk}^{-1} \cdot S_{jk} - E_{Asjk}^* \cdot S_{Ajk} - E_{Bsjk}^* \cdot S_{Bjk} \quad (29)$$

$$S'_{jk} = L_{sjk} \cdot S_{jk} + L_{Asjk} \cdot S_{Ajk} + L_{Bsjk} \cdot S_{Bjk} \quad (30)$$

$$S'_{qjk} = q L_{sjk} \cdot S_{jk} + q L_{Asjk} \cdot S_{Ajk} + q L_{Bsjk} \cdot S_{Bjk} \quad (31)$$

Let us solve the equation (4) for each of calculating lines  $y_j (j=1, 2, \dots, J)$  (then, it is a solution for planes  $XY$  - for  $z_k = \text{const.}$ ) also, and write  $J$  expressions (29) to (31):

$$P_{sk} = A_{sk}^{-1} \cdot S_k - E_{sAk}^* \cdot S_{Ak} - E_{sBk}^* \cdot S_{Bk} \quad (32)$$

$$S'_k = L_{sk} \cdot S_k + L_{sAk} \cdot S_{Ak} + L_{sBk} \cdot S_{Bk} \quad (33)$$

$$S'_{qk} = q L_{sk} \cdot S_k + q L_{sAk} \cdot S_{Ak} + q L_{sBk} \cdot S_{Bk} \quad (34)$$

Finally, let us solve the equation (4) for each of calculating lines  $z_k (k=1, 2, \dots, K)$  also, and write  $K$  expressions (32) to (34), and then all necessary first derivatives in respect to  $x$ , at the calculating points of:

- a parallelepiped:

$$P_s = A_s^{-1} \cdot S - E_{As}^* \cdot S_A - E_{Bs}^* \cdot S_B \quad (35)$$

$$S' = L_s \cdot S + L_{As} \cdot S_A + L_{Bs} \cdot S_B \quad (36)$$

- surfaces:

$$S'_q = q L_s \cdot S + q L_{As} \cdot S_A + q L_{Bs} \cdot S_B \quad (37)$$

$$S'_r = L_{sj} \cdot S_r + L_{Asj} \cdot S_{Ar} + L_{Bs_j} \cdot S_{Br} \quad (38)$$

$$S'_t = L_{sk} \cdot S_t + L_{Ask} \cdot S_{At} + L_{Bsk} \cdot S_{Bt} \quad (39)$$

- edges:

$$S'_{rt} = L_{sjk} \cdot S_{rt} + L_{Asjk} \cdot S_{Art} + L_{Bs_jk} \cdot S_{Brt} \quad (40)$$

$$S'_{qt} = q L_{sk} \cdot S_t + q L_{Ask} \cdot S_{At} + q L_{Bsk} \cdot S_{Bt} \quad (41)$$

$$S'_{qr} = q L_{sj} \cdot S_r + q L_{Asj} \cdot S_{Ar} + q L_{Bs_j} \cdot S_{Br} \quad (42)$$

- polyhedral angles:

$$S_{qrt}^{-1} = q_{Lsjk} \cdot S_{rt} + q_{LAsjk} \cdot S_{Art} + q_{LBsjk} \cdot S_{Brt} \quad (43)$$

$$(s=U,V,W \quad S=U,V,W \quad q=A,B \quad r=C,D \quad t=E,F)$$

Solutions to the equations (5) and (6) will be obtained in a similar way to that described for the equation (4). Applying the transformation matrices, we finally obtain:

$$q_s = B_s^{-1} \cdot S - F_{Cs}^* \cdot S_C - F_{Ds}^* \cdot S_D \quad (44)$$

$$\dot{S} = M_s \cdot S + M_{Cs} \cdot S_C + M_{Ds} \cdot S_D, \text{ and so on.} \quad (45)$$

$$r_s = C_s^{-1} \cdot S - G_{Es}^* \cdot S_E - G_{Fs}^* \cdot S_F \quad (46)$$

$$\ddot{S} = N_s \cdot S + N_{Es} \cdot S_E + N_{Fs} \cdot S_F, \text{ and so on.} \quad (47)$$

Along the straight lines  $y_j = \text{const.}$  and  $z_k = \text{const.}$ , the equation (7) becomes ordinary differential equation

$$\frac{d}{dx} \dot{S}(x, y_j, z_k) = \alpha_s(x, y_j, z_k), \quad (48)$$

which in its form resembles the equation (19). According to the expression (25) at the points  $x_i$  ( $i=1,2,\dots,l$ ), it follows:

$$\alpha_{sjk} = L_{sjk} \cdot \dot{S}_{jk} + L_{sAjk} \cdot \dot{S}_{Ajk} + L_{sBjk} \cdot \dot{S}_{Bjk} \quad (49)$$

Let us solve the equation (48) also for each of the calculating lines  $y_j$  ( $j=1,2,\dots,J$ ), and then, also, for each of the calculating lines  $z_k$  ( $k=1,2,\dots,K$ ):

$$\alpha_s = L_s \cdot \dot{S} + L_{sA} \cdot \dot{S}_A + L_{sB} \cdot \dot{S}_B \quad (50)$$

or

$$\alpha_s = X_s \cdot S + X_{sA} \cdot S_A + X_{sB} \cdot S_B + X_{sC} \cdot S_C + X_{sD} \cdot S_D + X_{sAc} \cdot S_{Ac} + X_{sBc} \cdot S_{Bc} + X_{sAd} \cdot S_{Ad} + X_{sBd} \cdot S_{Bd} \quad (51)$$

Solutions to the equations (8) and (9) will be obtained in a similar way to that described for the equation (7). Applying the transformation matrices, we finally obtain:

$$\beta_s = Y_s \cdot S + Y_{sA} \cdot S_A + Y_{sB} \cdot S_B + Y_{sE} \cdot S_E + Y_{sF} \cdot S_F + Y_{sAE} \cdot S_{AE} + Y_{sBE} \cdot S_{BE} + Y_{sAF} \cdot S_{AF} + Y_{sBF} \cdot S_{BF} \quad (52)$$

$$\gamma_s = Z_s \cdot S + Z_{sC} \cdot S_C + Z_{sD} \cdot S_D + Z_{sE} \cdot S_E + Z_{sF} \cdot S_F + Z_{sCE} \cdot S_{CE} + Z_{sDE} \cdot S_{DE} + Z_{sCF} \cdot S_{CF} + Z_{sDF} \cdot S_{DF} \quad (53)$$

#### BOUNDARY CONDITIONS

The boundary value problems of the Theory of elasticity are classified according to boundary conditions into problems for which:

- displacements are prescribed everywhere on the boundary;
- stresses (surface forces) are prescribed everywhere on the boundary; and
- displacements are prescribed over a portion of the boundary, stresses are prescribed over the remaining part of the boundary.

At each of  $n$  boundary calculating points:

$$n = 2 \cdot [1 \cdot J + 1 \cdot K + J \cdot K + 2 \cdot (1 + J + K) + 4] \quad (43)$$

(on the surfaces:  $2 \cdot (1 \cdot J + 1 \cdot K + J \cdot K)$ ; edges:  $4 \cdot (1 + J + K)$  and at the polyhedral angles: 8) three boundary conditions are to be satisfied.

Let us denote matrices of displacements at calculating points in a parallelepiped with

$$\mathbf{h} = \left\| \mathbf{u} \mid \mathbf{v} \mid \mathbf{w} \right\|^T, \quad (44)$$

and on the boundary - surfaces, edges and polyhedral angles with similar matrices:  $\mathbf{h}_*$ ,  $\mathbf{h}_{**}$  and  $\mathbf{h}_{***}$  respectively. Matrices of surface forces we may denote with

$$\mathbf{p}_* = \left\| \mathbf{p}_{x*} \mid \mathbf{p}_{y*} \mid \mathbf{p}_{z*} \right\|^T \quad (45)$$

if they are on the surfaces, and with  $\mathbf{p}_{**}$  and  $\mathbf{p}_{***}$  - if they are at calculating points of edges and polyhedral angles, respectively.

For those problems in which boundary displacements components are given everywhere ( $\mathbf{h}^*$ ,  $\mathbf{h}^{**}$  and  $\mathbf{h}^{***}$ ) on the boundary, these displacements

$$\mathbf{h}_* = \mathbf{h}^*, \quad \mathbf{h}_{**} = \mathbf{h}^{**}, \quad \mathbf{h}_{***} = \mathbf{h}^{***} \quad (46 \text{ a,b,c})$$

have to be introduced directly into the Lamé's equations.

For those problems in which surface forces are prescribed everywhere on the boundary, have to be used relation between surface forces and displacements:

$$\frac{1}{G} \cdot p_x = (c \cdot U' + b \cdot \dot{V} + b \cdot \ddot{W}) \cdot \cos \phi_x + (\dot{U} + V') \cdot \cos \phi_y + (\ddot{U} + W'') \cdot \cos \phi_z \quad (47)$$

$$\frac{1}{G} \cdot p_y = (\dot{U} + V') \cdot \cos \phi_x + (c \cdot \dot{V} + b \cdot \ddot{W} + b \cdot U') \cdot \cos \phi_y + (\dot{W} + \ddot{V}) \cdot \cos \phi_z \quad (48)$$

$$\frac{1}{G} \cdot p_z = (\ddot{U} + W'') \cdot \cos \phi_x + (\dot{W} + \ddot{V}) \cdot \cos \phi_y + (c \cdot \ddot{W} + b \cdot U' + b \cdot \dot{V}) \cdot \cos \phi_z \quad (49)$$

$$a = 1/(1-2\mu) \quad b = a-1 \quad c = a+1 \quad G = E/(2+2\mu), \quad (50)$$

where  $\phi_x$ ,  $\phi_y$  and  $\phi_z$  are angles between the normal on the surface and  $x$ ,  $y$  and  $z$  coordinate axes respectively. The first derivative in respect to  $x$  with a dash ( $'$ ) is denoted, the first derivative in respect to  $y$  - with a dot ( $\dot{\phantom{x}}$ ), and in respect to  $z$  - with two dots ( $\ddot{\phantom{x}}$ ).

Let us write these three equations for each of boundary calculating points, and then let us form a system of matrix equations:

$$\frac{1}{G} \cdot \mathbf{p}_x = \varphi_x \cdot (c \cdot U' + b \cdot \dot{V} + b \cdot \ddot{W}) + \varphi_y \cdot (\dot{U} + V') + \varphi_z \cdot (\dot{W}' + \ddot{U}) \quad (51)$$

$$\frac{1}{G} \cdot \mathbf{p}_y = \varphi_x \cdot (\dot{U} + V') + \varphi_y \cdot (b \cdot U' + c \cdot \dot{V} + b \cdot \ddot{W}) + \varphi_z \cdot (\ddot{V} + \dot{W}) \quad (52)$$

$$\frac{1}{G} \cdot \mathbf{p}_z = \varphi_x \cdot (\dot{W}' + \ddot{U}) + \varphi_y \cdot (\ddot{V} + \dot{W}) + \varphi_z \cdot (b \cdot U' + b \cdot \dot{V} + c \cdot \ddot{W}) \quad (53)$$

By introducing matrix expressions for the first derivative of boundary displacements in calculating points in respect to x, to y and to z, obtained in the part SOLUTION OF EQUATIONS WITH FICTIVE LOADS, into the equations (51) to (53), bearing in mind equations (44) and (45), we shall obtain next three matrix equations for calculating points of:

- surfaces:

$$\frac{1}{G} P^* = D \cdot h + D_* \cdot h_* + D_{**} \cdot h_{**} \quad (54)$$

- edges:

$$\frac{1}{G} P^{**} = K_* \cdot h_* + K_{**} \cdot h_{**} + K_{***} \cdot h_{***} \quad (55)$$

- polyhedral angles:

$$\frac{1}{G} P^{***} = H_{**} \cdot h_{**} + H_{***} \cdot h_{***} \quad (56)$$

For those problems having "mixed" boundary conditions, for surface forces prescribed over a portion of the boundary, we have to use equations (54) to (56), and for displacements prescribed over the remaining part of the boundary - equations (46 a,b,c).

"Mixed" boundary conditions are the general form of the boundary conditions for a parallelepiped. There are  $3 \cdot n$  boundary conditions. Let us denote with e and f number of prescribed displacements and surface forces respectively:

$$e + f = 3 \cdot n \quad (57)$$

and with ep and fp number of prescribed displacements and surface forces respectively, which are on the surfaces, with ei and fi - on edges, and with er and fr - at polyhedral angles; then exist next equations:

$$ep + ei + er = e \quad (58)$$

$$fp + fi + fr = f \quad (59)$$

$$ep + fp = 6 \cdot (1 \cdot J + 1 \cdot K + J \cdot K) \quad (60)$$

$$ei + fi = 12 \cdot (1 + J + K) \quad (61)$$

$$er + fr = 24 \quad (62)$$

If we take out those rows, from matrices in the equations (54) to (56), which correspond to prescribed displacements, and then solve in such a way obtained matrix equations, we shall have:

$$h_{*fp} = -H_3 \cdot h + \frac{1}{G} \cdot H_5 \quad (63)$$

$$h_{**fi} = H_6 \cdot h + \frac{1}{G} \cdot H_7 \quad (64)$$

$$h_{***fr} = H_8 \cdot h + \frac{1}{G} \cdot H_9 \quad (65)$$

In that way unknown displacements of calculating points on the surfaces ( $h_{*fp}$ ), edges ( $h_{**fi}$ ) and polyhedral angles ( $h_{***fr}$ ) are expressed with displacements of calculating points in a parallelepiped ( $h$ ), and equations (63) to (65) are the general form of boundary conditions for a parallelepiped.

#### SOLUTION OF THE LAMÉ'S EQUATIONS

The matrix form of the Lamé's equations are equations (10) to (12) (there are

3·m equations) and (13) to (15) (there are 3·n equations). These two systems represent a system of 3·m + 3·n linear algebraic equations with total of 15·m + 15·n unknown fictive loads  $p_u, \dots, \gamma_w$  at all of the calculating points.

#### SOLUTION WITH EXTRAPOLATED VALUES OF "p<sub>A</sub>" and "p<sub>B</sub>"

The Lamé's equations (13) to (15) are not satisfied with extrapolated values of "p<sub>A</sub>" and "p<sub>B</sub>".

In the Lamé's equations (10) to (12) there are 3·m algebraic equations with 15·m unknown loads  $p_u, \dots, \gamma_w$ . By introducing matrix expressions for fictive loads, obtained in the part SOLUTION OF EQUATIONS WITH FICTIVE LOADS (3·m + 3·n displacements in 15 m algebraic equations), into a system of matrix equations (10) to (12), it is obtained a matrix equation

$$\mathbf{R} \cdot \mathbf{h} = \mathbf{R}_* \cdot \mathbf{h}_* + \mathbf{R}_{**} \cdot \mathbf{h}_{**} + \frac{1}{G} \cdot \mathbf{Z}_a \quad (66)$$

where matrix  $\mathbf{Z}_a$  represents a matrix of body forces:

$$\mathbf{Z}_a = \left\| \mathbf{X} \mid \mathbf{Y} \mid \mathbf{Z} \right\|^T \quad (67)$$

Each of the matrices  $\mathbf{h}_*$  and  $\mathbf{h}_{**}$  has two column matrices of:

- prescribed displacements:  $\mathbf{h}_e^*$  and  $\mathbf{h}_e^{**}$
- unknown displacements:  $\mathbf{h}_{*f}$  and  $\mathbf{h}_{**f}$

and equation (66) may be written as follows:

$$\mathbf{R} \cdot \mathbf{h} = \mathbf{R}_{*f} \cdot \mathbf{h}_{*f} + \mathbf{R}_{**f} \cdot \mathbf{h}_{**f} + \frac{1}{G} \cdot (\mathbf{Z}_a + \mathbf{R}_{O*}) \quad (68)$$

This matrix equation represents a system of 3·m linear algebraic equations with 3·m + fp + fi unknown displacements of calculating points.

By introducing matrix expressions (63) and (64) ( $\mathbf{h}_{*f} = \mathbf{h}_{*fp}$ ,  $\mathbf{h}_{**f} = \mathbf{h}_{**ff}$ ; fp + fi algebraic equations with 3·m unknown displacements) into the equation (68) it is obtained the general numerical solution of the Lamé's equations for a parallelepiped:

$$\mathbf{h} = \frac{1}{G} \cdot \mathbf{R}_1 \cdot \mathbf{R}_2 \quad (69)$$

$$\mathbf{h}_{*f} = \frac{1}{G} \cdot (\mathbf{H}_3 \cdot \mathbf{R}_1 \cdot \mathbf{R}_2 + \mathbf{H}_5) \quad (70)$$

$$\mathbf{h}_{**f} = \frac{1}{G} \cdot (\mathbf{H}_6 \cdot \mathbf{R}_1 \cdot \mathbf{R}_2 + \mathbf{H}_7) \quad (71)$$

$$\mathbf{h}_{***f} = \frac{1}{G} \cdot (\mathbf{H}_8 \cdot \mathbf{R}_1 \cdot \mathbf{R}_2 + \mathbf{H}_9) \quad (72)$$

#### SOLUTION WITH CORRECT VALUES OF "p<sub>A</sub>" AND "p<sub>B</sub>"

For the fictive load  $p(x, y, z)$  we may write two equations of the type (26) and (27) for fictive loads "p<sub>A</sub>" and "p<sub>B</sub>" on the ends of the line connecting boundary calculating points A and B, taking into account boundary conditions at A and B:

$$p_x = \beta_p \cdot p + \beta_y \cdot y + \beta_{O*} \quad (73)$$

In this equation there are no boundary displacements. In that way, instead of the equations (24) and (25) we have to use equations (20) and (21), by introducing into them the expression (73) for p<sub>A</sub> and p<sub>B</sub>:

$$Y = \bar{A} \cdot p + E_A \cdot Y_A + E_B \cdot Y_B + E_O \quad (74)$$

$$r = Y' = \bar{A}' \cdot p + E_A' \cdot Y_A + E_B' \cdot Y_B + E_O' \quad (75)$$

Now, for example, solution of the equation (28) is not the equation (29), but

$$P_{sjk} = \bar{A}_{sjk}^{-1} \cdot S_{jk} - E_{Asjk}^* \cdot S_{Ajk} - E_{Bsjk}^* \cdot S_{Bjk} - E_{osjk}^* \quad (29 a)$$

and so on.

In that way we shall get in a matrix form solution for each of fictive loads in a form:

- for calculating points in a parallelepiped:

$$P_s = \bar{A}^{-1} \cdot S - E_{*s}^* \cdot S_* - E_{os}^* \quad (76)$$

- for boundary calculating points:

$$P_{*s} = \beta_{ps} \cdot P_s + \beta_s \cdot S + \beta_{os} \quad (77)$$

For all fictive loads ( $T_s = p_u, \dots, y_w$ ;  $T_{*s} = p_{*u}, \dots, y_{*w}$ ) equations (76) and (77) become equations of the next type:

$$T_s = Y_s \cdot S + Y_{*s} \cdot S_* + Y_{os} \quad (78)$$

$$T_{*s} = X_{Ts} \cdot T_s + X_{*s} \cdot S + T_{os} \quad (79)$$

The equation (78) has  $15 \cdot m$  algebraic equations with  $3 \cdot m + 3 \cdot n$  displacements, and the equation (79) has  $15 \cdot n$  equations with  $3 \cdot m + 3 \cdot n$  displacements.

The Lamé's equations (10) to (12) may be written in a form

$$R \cdot T_s = \frac{1}{G} \cdot Z_a \quad (80)$$

and the equations (13) to (15) in a form:

$$R_* \cdot T_{*s} = 0 \quad (81)$$

By introducing matrices  $T_s$  and  $T_{*s}$  in these two equations, it is obtained

$$R_1 \cdot S + R_{1*} \cdot S_* = \frac{1}{G} \cdot (Z_a + R_{10*}) \quad (82)$$

$$R_2 \cdot S + R_{2*} \cdot S_* = R_{20*} \quad (83)$$

Two systems of matrix equations (82) and (83) have  $3 \cdot m + 3 \cdot n$  linear algebraic equations and  $3 \cdot m + 3 \cdot n$  unknown displacements. Solution of these two equations

$$S = (R_1 - R_{1*} \cdot R_{2*}^{-1} \cdot R_2)^{-1} \cdot \frac{1}{G} \cdot [(Z_a + R_{10*}) - R_{1*} \cdot R_{2*}^{-1} \cdot R_{20*}] \quad (84)$$

$$S_* = R_{2*}^{-1} \cdot (R_{20*} - R_2 \cdot S) \quad (85)$$

is the general solution of the Lamé's equations for prescribed arbitrary boundary conditions, which satisfied the Lamé's equations on the boundary also.

## NUMERICAL EXAMPLE AND RESULTS

As an illustration of the obtained solution (69) to (72), the results for a simply supported square plate subjected to sinusoidal transverse load on the



upper surface  $p = p_0 \cdot \sin \frac{\pi x}{d} \cdot \sin \frac{\pi y}{d}$  is presented. Calculation is carried out for value of Poisson's ratio  $\mu = 0,30$  and a plate lateral dimension to thickness (h) ratio  $d/h = 3$ :  $d_x = d_y = 3 \cdot d_z = 3 \cdot h$ . ( $s = d/6$ ,  $s_1 = h/6 = s/3$ ).

Boundary conditions for a simply supported plate are taken as follows:

$$\begin{aligned} x = A, B: & \quad V = 0 \quad W = 0 \quad \sigma_x = 0 \\ y = C, D: & \quad U = 0 \quad W = 0 \quad \sigma_y = 0 \\ z = E: & \quad \tau_{xz} = 0 \quad \tau_{yz} = 0 \quad \sigma_z = -p \\ z = F: & \quad \tau_{xz} = 0 \quad \tau_{yz} = 0 \quad \sigma_z = 0 \end{aligned}$$

Displacements are calculated at the points on one sixth of each of dimensions of a plate. With horizontal and vertical planes a plate is divided on 216 small parallelepipeds with total 343 calculatin points and 1029 displacements.

Due to symmetric loads and symmetric boundary conditions only a quarter of plate is taken into consideration, and a rough mesh is placed on it:  $3 \times 3$  in a horizontal plane and 5 horizontal planes across the thickness of a plate (Fig.2). Symmetry of loads and boundary conditions reduced number of unknown displacements on 60.

Coefficients  $K_w$  of a plate's middle plane vertical displacements are presented (at the points denoted with : 19, 20, 21, 22, 23, 24, 25, 26 and 27, which

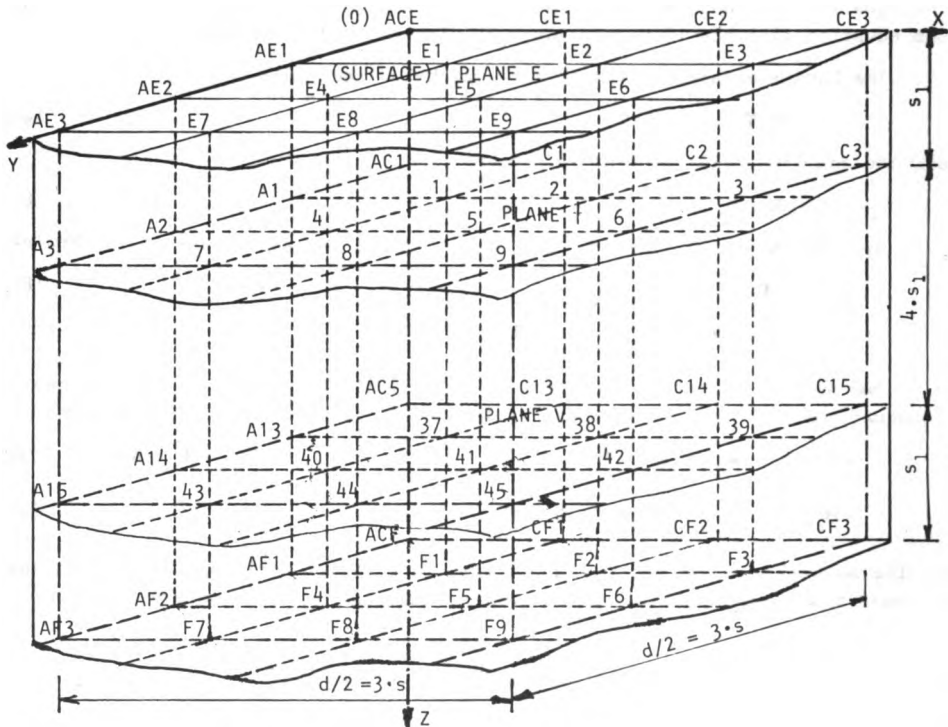


Fig..2 A quarter of plate with meshes at horizontal and vertical planes,

are on the same vertical calculating line with: 1, 2, 3, 4, 5, 6, 7, 8 and 9 respectively) in Table 1 ( $W = K_w \cdot p_0 \cdot 10^{-5} \cdot d/E$ ) together with exact solution of:

- theory of thin plates [9];
- Reissner's theory of plates [9]; and
- Lamé's equations [7],

and solution of the equations of Reissner's theory of plates by Hajdin's method [10].

Value of $K_w$ in vertical displacements $W = K_w \cdot p_0 \cdot 10^{-5} \cdot d/E$							
calculating points	Solution of equations					error in %	
	e x a c t			Hajdin's method		(5)-(2)	(6)-(3)
	Lamé	Reissner	thin plates	Lamé	Reissner	(2)	(3)
1	2	3	4	5	6	7	8
(19) 1	29089	28994	18918	29294	29018	0,70	0,08
(20) 2	50383	50219	32766	50764	50254	0,76	0,07
(21) 3	58177	57988	37835	58629	58016	0,76	0,05
(22) 4	50383	50219	32766	50764	50254	0,76	0,07
(23) 5	87266	86981	56753	87945	87055	0,78	0,08
(24) 6	100766	100438	65532	101568	100512	0,80	0,07
(25) 7	58177	57988	37835	58629	58016	0,76	0,05
(26) 8	100766	100438	65532	101568	100512	0,80	0,07
(27) 9	116355	115976	75670	117308	116053	0,82	0,07

Table 1 Coefficients  $K_w$  ( $W = K_w \cdot p_0 \cdot 10^{-5} \cdot d/E$ ) for sinusoidal load;  $d_x = d_y = 3 \cdot d_z = 3 \cdot h$ ;  $\mu = 0,30$

### CONCLUSION

The general numerical solution of the Lamé's equations (including body forces) for an elastic, homogeneous and isotropic rectangular plate with constant thickness, is presented. These equations are solved by application of Hajdin's method of integral equations on two ways:

- the first one: with extrapolation of values of fictive loads on the boundary, Lamé's equations are not satisfied on the boundary; calculation is not extensive, and error is small; and

- the second one: with exact values of fictive loads on the boundary, Lamé's equations are satisfied on the boundary also; calculation is extensive, and may be expected very small error (calculation in this paper is carried out using the first way).

Calculation of a plate's middle plane vertical displacements, for the same

rough mesh  $3 \times 3$  on a quarter of a plate, show:

- excellent agreement with exact solution ( $< 0,08\%$ ), when Hajdin's method is applied to problems in the plane (Reissner's theory of plates - even better than Finite element method - with same number of unknown displacements - see [5]),
- good agreement with exact solution ( $< 0,82\%$ ) when Hajdin's method is applied to three-dimensional problems (Lamé's equations).

Similar to the other numerical methods employed in solving problems of the Theory of elasticity, the accuracy depends on number of calculating points, namely, on density of mesh of calculating lines applied, but also from: selected method of numerical integration and interpolation of loads, and of wished extent of calculations - with or without accurate values for fictive loads on the boundary.

To get excellent agreement with exact solution of the Lamé's equations - let's say  $< 0,1\%$ , calculation should be carried out on the second way and with fine meshes in horizontal and vertical planes.

#### REFERENCES

1. HAJDIN, N. - "A Method for Numerical Solution of Boundary Value Problems and its Application to certain Problems of the Theory of Elasticity", Proc. of Civil Eng. Faculty, Vol. 4, 1958, Beograd (in Serbian).
2. HAJDIN, N. - "A contribution to the analysis of arch dams". Comm. inter. des grands barrages, Bul. 12, Paris, 1958.
3. HAJDIN, N. - "An integral equation method for arch dam analysis", Int. Symposium on the Theory of Arch Dams, Pergamon Press, Southampton, 1964.
4. HAJDIN, N. and KRAJČINOVIĆ, D. - "Integral equation method for solution boundary value problems of structural mechanics", Part I and Part II, Int. J. num. Meth. Engng., 1972, 4, 509-539.
5. PETROVIĆ, P. - "Solution of Equations of Reissner's Theory of Plates by Application of Hajdin's Method", Var. Meth. Eng. Southampton, 1973, 2, 9/57-9/75
6. PETROVIĆ, P. - "A contribution to the bending analysis of clamped rectangular plates", Int. symp. on Innov. num. anal. in applied eng. science, 1977, Paris
7. VLASOV, B.F. - "Bending of rectangular thick plate", Vestnik Univ. of Moskva, 1957, 2, pp.25 (in Russian)
8. PETROVIĆ, P. - "Numerical solution of the Lamé's equations of the Theory of elasticity by integral equations method", Doc. thesis, Civil Eng. Faculty, Beograd, 1985 (in Serbian).
9. PETROVIĆ, P. - "A contribution to the theory of thick plates", M. techn. sciencé thesis, Civil Eng. Faculty, Beograd, 1969 (in Serbian).
10. PETROVIĆ, P. - "Analysis of thick homogeneous plates applying the method of the integral equations", Proc. of 10th Yugoslav Con. of Rat. and Appl. Mech., 1970, pp.393-407, Baško Polje (in Serbian).
11. HAJDIN, N. - "Ein Verfahren zur numerischen Lösung der Randwertaufgaben von elliptischen Typus", Inst. mat. de l'Acad. Serbe des Sciences, 1956, IX, Beograd
12. HAJDIN, N. - "Une methode pur la solution numerique des problemes de valeurs aux limites et son application a certain problems de la theorie de l'elasticite", IX Con. int. de Mech. appli. Actes, Bruxelles, 1956, t.V.

## A RAYLEIGH ESTIMATE OF THE FUNDAMENTAL FREQUENCY OF SIMPLY SUPPORTED SLABS WITH INTERMEDIATE COLUMN SUPPORTS

M.N. Pavlović

Department of Civil Engineering, Imperial College of Science and Technology, University of London

### SUMMARY

A simple method for estimating the lowest natural frequency of boundary-supported slabs with additional interior supports is presented through the use of Rayleigh's quotient, in which the assumed vibrating shape is obtained by superimposing known statical solutions. While the proposed technique is illustrated chiefly by reference to simply supported, isotropic, rectangular slabs with single internal point support, the possibility of its extension to more general systems is also discussed.

### 1. INTRODUCTION

The natural response of rectangular plates with point supports along its *edges* has been the subject of a considerable number of studies [1-10]. On the other hand, the related problem when these supports are located throughout the *span* has received much less attention. This is somewhat surprising, since edge-supported plates having additional point supports elsewhere have, besides their intrinsic mechanics interest, a wide field of practical application. An obvious example is that of simply supported plates such as the slabs frequently encountered in civil engineering construction, where the element sides are often stiffened by edge beams possessing high flexural - but relatively low torsional - properties.

The main contribution to the free-vibration problem of a plate hinged along its contour and having point supports inside its span appears to be that of Nowacki, whose early work [11] was later incorporated into his classic textbook [12]. Nowacki only deals with one point support and even this leads to a cumbersome characteristic equation. Its awkwardness is apparent from the fact that the value of fundamental frequency calculated for a square plate with a central point support shows considerable disagreement with the corresponding result stemming from the more general computation in which the support is allowed to relocate along the centreline; this was already noted by Leissa [13], who summarized the seven

values of lowest frequency for plates with point supports worked out by Nowacki (one of which is, as just pointed out, incorrect). It is clear, therefore, that in view of the cumbersome nature of the characteristic condition, Nowacki's method requires considerable care even in the case of a single point support while its use becomes far too cumbersome for practical application if more than one support is present (unless all the supports lie on a line parallel to either pair of sides). The reason for this is that the method is based, essentially, on Levy's technique, so that additional points will, in general, require a larger number of regions (and associated integration constants) to be matched, leading to very lengthy and awkward algebraic and numerical work.

An even more involved analytical investigation of the free transverse vibrations of rectangular slabs simply supported along the periphery and resting on interior (supporting) columns was carried out by Lynn and Kumbasar [14]. Their study was aimed primarily at achieving a more realistic modelling of actual column behaviour and thus improving on Nowacki's method. This was to be done by taking into account the size of the column and by imposing this element's restraining forces on the plate so as to preserve the continuity of the plate-column system. However, the compatibility equation used was not exact since the continuity of the system was satisfied only at the centre of the column heads. More important still is the fact that the stress distribution adopted does not appear to conform to that expected to occur in a rigid plate-to-column joint [15]. Therefore, it is difficult to judge the accuracy of the results of the two numerical examples presented in Ref. 14. (These refer to a square plate with one and four (symmetric) interior supports respectively.)

In the course of estimating the probable dynamic response of suspended floors, it is often sufficient to carry out the necessary computations based on an approximate value of the lowest frequency of natural vibration. Such an estimate would provide adequate data for the various simplified methods used to predict the dynamic response of flat slabs, at least for purposes of preliminary design (see, for example, Refs. 16 and 17). It is the aim of the present paper to show that approximate values for the natural frequencies of simply supported slabs with interior columns can easily be obtained through the application of Rayleigh's quotient and the use of readily available deflected shapes for statically loaded systems. The proposed scheme is much simpler than the techniques of Nowacki, and Lynn and Kumbasar, while it retains the key feature common to both these methods, namely the fact that the axial deformations of the supporting columns are negligible compared to the overall (bending) deformation of the slab.

## 2. ANALYTICAL FORMULATION AND EXAMPLES

### 2.1 Simply supported rectangular slab with a single intermediate column

The Rayleigh quotient is such an universally used concept and tool that it needs no introduction. As has recently been remarked [18, 19], despite more refined and accurate techniques, Rayleigh's method has retained its appeal and usefulness, at least as a first estimate. For the problem under investigation, the quotient formula may be written as

$$\omega^2 = \frac{D \int_0^a \int_0^b \left( \frac{\partial^2 W}{\partial x^2} + \frac{\partial^2 W}{\partial y^2} \right)^2 dx dy}{\mu \int_0^a \int_0^b W^2 dx dy} \quad (1)$$

where  $\omega$  is the fundamental circular frequency, and the plate is rectangular (with dimensions  $a$ ,  $b$ ), simply supported, isotropic, and having uniform flexural rigidity  $D$  and mass per unit area  $\mu$ . Expression (1) is a simplified version of the more general formula, since zero-deflection conditions apply throughout the boundaries [20]. Therefore, the assumed deflected shape  $W(x,y)$  must satisfy this condition for expression (1) to be used, and since this constraint also describes the geometric boundary conditions for the problem, such a function  $W$  will automatically comply with the basic requirements of Rayleigh's technique [18].

In the present scheme for estimating the lowest frequency of slabs with intermediate supports, Navier's closed-form solution for the deflected shape of simply supported plates subject to arbitrary loading conditions will be used [21]. The basic idea is to superimpose the deflection shape for a slab without intermediate columns on those due to point (or patch) loads which represent the effects of column supports. Consider the case of a rectangular plate with a single support located at the point  $x = \xi a$ ,  $y = \eta b$ . (The origin is at one of the corners, and the positive directions of the axes  $x$ ,  $y$  run along its edges; the plan dimensions along  $x$  and  $y$  are  $a$  and  $b$  respectively. The shape  $W$  for the actual problem (with the point  $(\xi a, \eta b)$  prevented from deflecting) is split into two components: (i) that of the edge-supported slab under a uniformly distributed load (per unit area)  $q$ , and (ii) that of the edge-supported slab under a point load  $P$  acting at the column location (and opposing  $q$ ). The continuity requirement at the point of intermediate support is then met by computing the force  $P$  necessary to cancel out the deflection produced at this point by the loading  $q$ .

The deflected shape of the slab under the action of the uniformly distributed load  $q$  is given by

$$w_q = \frac{4q}{D\pi^6} \sum_{m=1}^{\infty} \sum_{n=1}^{\infty} \frac{(1 - \cos m\pi)(1 - \cos n\pi)}{mn \left(\frac{m^2}{a^2} + \frac{n^2}{b^2}\right)^2} \sin \frac{m\pi x}{a} \sin \frac{n\pi y}{b} \quad (2)$$

while that due to the point load acting at  $x = \xi a$ ,  $y = \eta b$  is

$$w_P = \frac{4P}{D\pi^4 ab} \sum_{m=1}^{\infty} \sum_{n=1}^{\infty} \frac{\sin m\pi\xi \sin n\pi\eta}{\left(\frac{m^2}{a^2} + \frac{n^2}{b^2}\right)^2} \sin \frac{m\pi x}{a} \sin \frac{n\pi y}{b} \quad (3)$$

The imposition of the compatibility condition at  $x = \xi a$ ,  $y = \eta b$  such that the total deflection  $w(t)$  is zero at this point leads to

$$P = \frac{qa^2}{\pi^2 \phi} \frac{\sum \frac{(1 - \cos m\pi)(1 - \cos n\pi) \sin m\pi\xi \sin n\pi\eta}{mn (m^2 + n^2\phi^2)^2}}{\sum \frac{\sin^2 m\pi\xi \sin^2 n\pi\eta}{(m^2 + n^2\phi^2)^2}} \quad (4)$$

where  $\phi$  ( $= a/b$ ) is the aspect ratio, and the summation limits (always understood to extend from 1 to  $\infty$ ) have been dropped for convenience. The total deflected shape for the actual problem of the simply supported plate with additional internal point support then becomes:

$$w(t) = \sum W_{mn} \sin \frac{m\pi x}{a} \sin \frac{n\pi y}{b} \quad (5)$$

where

$$W_{mn} = \frac{4qa^4}{D\pi^6} \frac{(1 - \cos m\pi)(1 - \cos n\pi)}{mn (m^2 + n^2\phi^2)^2} - \frac{4Pa^2\phi}{D\pi^4} \frac{\sin m\pi\xi \sin n\pi\eta}{(m^2 + n^2\phi^2)^2} \quad (6)$$

subject, of course, to condition (4). Clearly, the natural frequency is independent of the magnitude of the loading  $q$  which appears in both the numerator and denominator of the Rayleigh quotient and hence eventually cancels out. This may be anticipated by defining *a priori* a non-dimensional shape, and one obvious way of achieving such a result is to divide the terms of the deflection series by  $W_{11}$ , i.e.

$$C_{mn} = \frac{W_{mn}}{W_{11}} \quad (7)$$

so that  $C_{11} = 1$ . It is then easy to show that the fundamental frequency, as obtained from expression (1), becomes

$$\omega = \left( \frac{\pi}{a} \right)^2 \left( \frac{D}{\mu} \right)^{0.5} \left( \frac{\sum E D_{mn}^2}{\sum E C_{mn}^2} \right)^{0.5} \quad (8)$$

where

$$D_{mn} = C_{mn} (m^2 + n^2 \phi^2) \quad (9)$$

Before embarking upon the computation of expression (8) for various aspect ratios and column locations, it is important to recall that, in its usual form, Rayleigh's method, when used with a shape function that satisfies at least the geometric boundary conditions, always provides an overestimate to the natural frequency of a system (unless, of course, the true vibrating shape has been guessed, in which case the answer is exact). This is a result of the artificial stiffening which stems from the need to constrain the system into the assumed shape, leading to an overestimate of the strain energy of the system. The present scheme, however, does not quite conform to this general picture. For a start, it will be seen that the assumed 'shape' consists of a series rather than the usual single-term function. (This series, of course, has a single undefined coefficient,  $W_{11}$ , and hence should not be confused with the series one associates with Ritz's method.) By limiting the series to a single term, one obtains the frequency corresponding to the plate without the support; such a drastic underestimate of  $\omega$  is due to the fact that a single series term does not allow for the shape change due to the column, but simply gives the single half-wave mode (along both  $x$  and  $y$ ) corresponding to the free vibration of an edge-suspended slab. Additional terms are needed to impose the zero-deflection condition at the intermediate support but, as the number of terms increases, the higher mode shapes must perforce cause an overestimate in the fundamental-frequency value. At first sight, it might appear that the results are highly dependent on the number of series terms retained. It turns out, however, that as soon as the second term is considered, the calculated frequency experiences a sudden increase which brings it up to a value close to that corresponding to the plate with intermediate support. Moreover, the effect of the higher mode shapes upon the fundamental frequency that is being sought is found to be very small: thus, once the true frequency value is exceeded (and this is usually achieved with a small number of terms), its overestimates increase very slowly with  $m$  and  $n$ . The above effects will be illustrated subsequently in Table 1.

For purposes of checking the accuracy of the present method against existing benchmarks, it is necessary to ensure that sufficient terms have been included in the series so as to approach the condition of zero deflection at the intermediate supports (say, the deflection at the interior support should be less than one-hundredth of the value at that location

corresponding to the suspended-slab case). Typically, this can usually be achieved with  $m, n < 20$ , although in some cases one may have to truncate the series at  $m, n \sim 30$ . Once the interior-support deflection becomes negligible, the satisfaction of all the geometric boundary conditions has been achieved to a sufficiently close degree for the method to yield an overestimate of  $\omega$ , and hence no further terms should be considered as the value of the calculated frequency will further overshoot the true value (albeit, very slowly). As an example, consider a square plate with a centrally located column support. Table 1 gives the results for the non-dimensional frequency parameter

$$\Omega = \omega a^2 \left( \frac{\mu}{D} \right)^{0.5} \quad (10)$$

for increasing values of  $m$  and  $n$  up to and including  $m, n = 21$ . (Note that, for this case, the only non-zero terms correspond to both  $m$  and  $n$  being simultaneously odd.) The criterion that the total deflection at the support,  $w(s)$ , should be approximately one-hundredth of the value of the edge-supported slab case is attained at  $m, n = 19$ . The corresponding  $\Omega$

$m, n$	$w(s)$	$\Omega$
1	0.000566	19.7392
3	0.000128	48.5729
5	0.000063	50.6009
7	0.000035	51.6251
9	0.000023	52.0220
11	0.000016	52.2650
13	0.000012	52.4004
15	0.000009	52.4937
17	0.000007	52.5549
19	0.000006	52.6003
21	0.0000045	52.6329

Table 1. Square slab with a central column support. Convergence of  $w(s)$  and  $\Omega$  with the number of terms in the series for the shape function.

coincides with the exact value of 52.6 (as reported by Nowacki [11, 12]). Table 1 also illustrates the fact that, for practical purposes, the number of terms may be less than that suggested for accurate estimates; a reasonable value of  $\Omega$  is achieved as soon as the values of  $m, n$  are incremented beyond the clearly inaccurate case,  $m, n = 1$ , and once  $m, n \sim 5$  has been reached the error in the calculated  $\Omega$  is less than 4%. To give an idea of the overestimate rate beyond the exact value  $\Omega = 52.6$ , it is sufficient to point out that, for  $m, n = 101$ ,  $\Omega$  has only increased to 52.78. Finally, one might mention that, if an automatic check on  $w(s)$  is not included in the calculations, the optimum accuracy may be taken to occur for  $m, n \sim 20$ .

The values of  $\Omega$  corresponding to a centrally situated column are listed in Table 2 for several aspect ratios. Three of these values have theoretically exact counterparts which also appear in Table 2, showing the proposed scheme to be accurate to within 1%. It may be interesting to check also the behaviour of the system for long plates. As  $\phi \rightarrow \infty$ , the plate becomes a long thin strip, in which case the column support at its mid-length can be



expected to provide effectively a fixed-end condition. Several frequencies for the case of a rectangular plate with three edges simply supported and the fourth side clamped are listed in Ref. 13; the corresponding value of  $\Omega$

$\phi$	$\Omega$				
	1.0	1.5	2.0	2.5	3.0
Present method	52.6	73.6	91.9	113.4	139.7
Exact (Nowacki [10, 11])	52.6	73.1	91.1	-	-

Table 2. Rectangular slab with a central column support. Calculated values of  $\Omega$  for various  $\phi$ 's and comparison with the available corresponding exact values.

is given as 9.869 for  $\phi = 0$ , which is also the asymptotic value  $\pi^2$  for a simply supported plate since, clearly, an increase in restraint at the short edges becomes negligible when the ratio of the sides is large. The use of the Rayleigh quotient (8) for  $\phi = 6.0$  and  $\phi = 10.0$  gave values of  $\Omega$  of 406.4 and 1,040 respectively. When these values are converted to the non-dimensional frequency  $\Omega^*$  ( $= \Omega/\phi^2$ ), one obtains 11.2 ( $\phi = 6.0$ ) and 10.4 ( $\phi = 10.0$ ), showing that, as in the case of a hinged plate,  $\Omega^*$  converges to its asymptotic value  $\pi^2$  as  $\phi \rightarrow \infty$ .

Consider next the case of an eccentrically located column. Before presenting some of the results for various values of coordinates ( $\xi, \eta$ ), it is important to remark that the assumed deflected shape is still made up by combining expressions (2) and (3). The use of the uniformly distributed load in conjunction with the non-symmetric shape for the point load when  $\xi, \eta \neq 0.5$  might, at first sight, appear to be a somewhat poor choice for the first component of the shape function. Nevertheless, the results of an extensive investigation, which was conducted for a wide variety of non-symmetric loadings, have shown that, while other shapes may sometimes prove superior to that corresponding to the uniform load, the latter was always within 5% of the best frequency estimate, and was often the most suitable choice even in those cases of marked column eccentricity. In view of the approximate nature of the method adopted, it is clear that the shape for the uniformly distributed load may be used irrespective of the column location since it constitutes the simplest general shape while, at the same time, providing results which are well within engineering accuracy. Table 3 illustrates this, showing the predicted frequency for a square slab as the column location is moved along the centreline  $\eta = 0.5$ . The approximate results obtained through formula (8) compare quite well with their exact counterparts, these also appearing in Table 3. (The slight underestimate in  $\Omega$  at  $\xi = 0.125$  is either due to the criterion for  $w(s)$  not being stringent enough for this case, or it may be a result of a possible inaccuracy in the 'exact' value quoted in Ref. 12, which certainly gives an incorrect  $\Omega (= 49.3)$  for  $\xi = 0.5$  in the same figure.) It will be noticed that the frequency decreases steadily as the column is moved from the centre to the edge of the plate, the last point corresponding to a hinged slab without internal point support ( $\Omega = 19.7$ ). The same effect is observed when the column is moved from the centre to the corner of the square slab (i.e. along the line  $\xi = \eta$ ), the relevant results for  $\Omega$  being 52.6, 28.7, 20.7, 19.7.

which correspond to  $\xi = \eta$  having the values 0.5, 0.3, 0.1, 0 respectively. Thus, the method correctly predicts the loss in stiffness of the plate system as the point support nears an edge. (This, of course, would not be

$\xi$	$\Omega$				
	0	$1/8$	$1/4$	$3/8$	$1/2$
Present method	19.7	25.4	30.9	41.0	52.6
Exact (Nowacki [10, 11])	19.7	25.5	30.4	38.9	52.6

Table 3. Square slab with a column support situated at various locations along the centreline  $\eta = 0.5$ . Calculated values of  $\Omega$  and comparison with the available corresponding exact values.

the case in the one-dimensional instance of a beam, since then the intermediate support would effectively produce a clamped end as it approaches the support.)

## 2.2 Extension of the method to various other types of slab

So far, consideration has only been given to slabs that are simply supported, rectangular and isotropic, and which are stiffened by a single point support. While these conditions are often relevant in practice, especially in floor slabs, the aim of this section is to explore whether the present approximate method can be extended to cases of material anisotropy (e.g. such as reinforced concrete floors with non-isotropic reinforcement), multiple internal supports, and to plates that are non-rectangular and which may be subjected to boundary conditions other than those corresponding to hinged supports.

First, it is evident that the proposed Rayleigh quotient should readily be applicable to anisotropic plates. Of practical relevance are simply supported orthotropic slabs for which deflected shapes are available in the form of Navier's solutions. In fact, the previously derived expressions for transverse deflections are applicable upon modifying  $D(m^2/a^2 + n^2/b^2)^2$  in the denominator to  $(D(x)m^4/a^4 + 2Hm^2n^2/a^2b^2 + D(y)n^4/b^4)$ , where  $D(x)$ ,  $H$ ,  $D(y)$  are the relevant orthotropic constants [20].

Another potential extension of the approximate method outlined in this paper is to cases involving several intermediate supports. There are no apparent conceptual difficulties since the deflected shape can be made up of a number of Navier-solution components which, when superimposed, give zero deflection at the column location as well as, of course, satisfying the boundary conditions at the edges of the slab. Such problems, however, require an increasing amount of computational effort, especially if accurate estimates of the fundamental frequency are to be obtained. In the case of a large number of internal supports, there is a proportionally high number of simultaneous linear equations that must be solved so as to adjust the values of the various column reactions. (However, multiple interior columns within a slab are often placed on a regular grid, and the ensuing symmetry then permits some of the columns to be grouped as a single variable, thus decreasing the numerical effort in solving for the various interior support

reactions.) On the other hand, a small number of interior columns may cause the lowest-mode shape of a slab to exhibit a 'chequer-board' pattern so that similar (i.e. 'chequer-board') loading patterns provide a better approximation than the uniformly distributed load case used so far, and then more complicated series coefficients are needed.

The above remarks on multiple interior columns may be illustrated by means of the following three examples. The first of these refers to a slab with four internal supports situated symmetrically with respect to the centrelines  $x = a/2$ ,  $y = b/2$  (i.e. forming a rectangular pattern analogous to the rectangular boundaries of the system). While this symmetry obviates the need to solve any simultaneous equations, it is found that, when the distance between two columns that is parallel to one of the edges of the slab exceeds about one-tenth of the size of this edge, the uniformly distributed load used to initiate the computational process begins to lose accuracy (unless, conversely, the columns approach a position close to the boundaries). To obtain a more accurate answer, a 'chequer-board' pattern of patch loads is required. However, even the uniformly distributed load case is adequate for purposes of reaching an important conclusion regarding the effect of column size (a parameter hitherto ignored). Namely, if one considers the four point supports to represent the corners of a single column, it appears that there is no need to allow for the latter's size provided its dimensions do not exceed approximately one-tenth of the dimensions of the slab itself, a finding consistent with that of related work [14]. For instance, for a square plate, with a square column arrangement in which the distance between columns is set at one-tenth of the sides, one obtains  $\Omega = 59.6$ , i.e. a difference of 13% from the value corresponding to the point-support case. Similar conclusions are reached by studying the second example, which consists of a rectangular plate with four internal supports located symmetrically on the centrelines  $x = a/2$ ,  $y = b/2$  (i.e. forming a rhomboidal pattern with the rectangular boundaries of the system). Once again, a 'chequer-board' pattern of loading should be used for high accuracy unless the columns are either close to each other or near the edges. Furthermore, the effect of column size for this interior-support arrangement is even less marked than in the previous case since, for a square column, one obtains  $\Omega = 55.9$  when the distance (measured along the centrelines) between each pair of columns is one-tenth the side of the (square) slab; this represents an increase of only 6% over the single central-support case. The third example consists of a rectangular slab with  $\phi = 2$  and having six interior columns: four of these are located symmetrically with respect to both centrelines, the distance between each pair of columns being  $0.4a$  and  $0.4b$  respectively; the remaining two columns have coordinates  $(0.2a, 0.55b)$  and  $(0.9a, 0.45b)$ . The fundamental-frequency value obtained by using the uniformly distributed load shape for the first deflection component is  $\Omega \sim 150$ , as compared with the 'exact' value of  $\Omega \sim 125$  (obtained by means of the finite element method). With increasing number of interior supports it appears that the accuracy in  $\Omega$  improves, and hence it would seem that the increasingly difficult alternative of adopting more and more complex patch-load patterns for obtaining reasonably accurate  $\Omega$  estimates is then not needed.

Finally, although the present paper has concentrated on rectangular slabs with hinged external boundaries, there are no conceptual difficulties in envisaging its extension to other contours and/or boundary conditions provided the statical solutions for uniformly distributed and point loads are readily available or derivable. (In this respect, the system ALTRAN could prove of use in providing explicit closed-form solutions [22].) As a

tentative example, consider a circular plate of radius  $a$ , with the origin at its centre  $r = 0$ , and clamped along its circumference. The deflections under a uniform load  $q$  and a centrally applied point load  $P$  are, respectively [20, 21]:

$$w_q = \frac{q}{64D} (a^2 - r^2)^2 \quad (11)$$

$$w_p = \frac{P}{8\pi D} \left[ r^2 \ln \frac{r}{a} + \frac{1}{2} (a^2 - r^2) \right] \quad (12)$$

The condition that the combined deflections should satisfy  $w = 0$  at  $r = 0$  leads to

$$P = \frac{\pi q a^2}{4} \quad (13)$$

Rayleigh's quotient formula in polar coordinates (assuming axisymmetric loading and clamped edges [20]) can be written as:

$$\omega^2 = \frac{D \int_0^{2\pi} \int_0^a \left( \frac{\partial^2 W}{\partial r^2} + \frac{1}{r} \frac{\partial W}{\partial r} \right)^2 r \, dr \, d\theta}{\mu \int_0^{2\pi} \int_0^a W^2 r \, dr \, d\theta} \quad (14)$$

When the shapes (11) and (12) are combined in accordance to (13) and the result substituted into (14), one obtains  $\Omega = 22.88$  (with  $\Omega$  as defined by (10) but with  $a$  now denoting the radius - rather than the side along  $x$  - of the plate). This result compares rather well with the exact value  $\Omega = 22.7$ , as quoted in Ref. 13 (taken from the work of Sakharov [23], based on the formal use of Bessel functions), the error being less than 1%.

### 3. CONCLUDING REMARKS

The present article has explored the possibility of obtaining quick Rayleigh estimates of the fundamental frequency of slabs with interior (as well as boundary) supports. The key requirement is the ready availability of statical solutions which, when superimposed, satisfy at least the geometric boundary conditions at both edge and internal points. In this respect, Navier's solution provides the means for tackling simply supported rectangular slabs. Both isotropic and orthotropic plates can be dealt with and, in principle, any number of internal supports may be present. However, the latter instance may require a more accurate visualization of the vibrating system (with consequent increase in the complexity of the loading pattern) unless the number of interior columns be large but, then, this case leads to what is possibly too large a number of simultaneous equations for a programmable calculator and the method soon becomes one of rapidly diminishing returns when compared, say, to finite elements. Otherwise, the method is amenable to other plate contours and/or boundary supports provided, again, statical deflected shapes be known. As regards this aspect, the potential use of the system ALTRAN might, in the future, not only increase the range of analytical expressions available, but it should also provide the means for performing the tedious integrations associated with energy methods (especially in the case of non-orthogonal functions).

### ACKNOWLEDGEMENTS

The author is grateful to K. Coffin, S.A.G. Hajjar, S.K.S. Hui and S.C. Lee who helped at various stages of the research described in this paper.

## REFERENCES

1. NISHIMURA, T. - 'Studies on Vibration Problems of Flat Plates by Means of Difference Calculus'. Proc. 3rd Jap. Nat. Congr. Appl. Mech., 1955, 417.
2. COX, H.L. - 'Vibration of a Square Plate, Point-Supported at Midpoints of Sides'. J. Acoust. Soc. Am., 1955, 27, 791.
3. COX, H.L. - 'Vibration of Certain Square Plates Having Similar Adjacent Edges'. Quart. J. Mech. Appl. Math., 1955, 2, 454.
4. PLASS, H.J. - 'Application of Reissner's Variational Principle to Cantilever Plate Deflection and Vibration Problems'. Report DRL-418/CM-921, Def. Res. Lab. Univ. Texas, 1958.
5. COX, H.L. and BOXER, J. - 'Vibration of Rectangular Plates Point-Supported at the Corners'. Aeron. Quart., 1960, 11, 41.
6. JANICH, R. - 'The Approximate Calculation of the Eigenfrequencies of Rectangular Plates with Various Edge Conditions' (in German). Die Bautechnik, 1962, 3, 93.
7. KIRK, C.L. - 'A Note on the Lowest Natural Frequency of a Square Plate Point-Supported at the Corners'. J. Roy. Aeron. Soc., 1962, 66, 240.
8. REED, R.E. - 'Comparison of Methods in Calculating Frequencies of Corner-Supported Rectangular Plates'. Technical Note D-3030, NASA, 1965.
9. GORMAN, D.J. - 'Free Vibration Analysis of Rectangular Plates with Symmetrically Distributed Point Supports along the Edges'. J. Sound & Vibr., 1980, 73, 563.
10. SALIBA, H.T. - 'Free Vibration Analysis of Rectangular Cantilever Plates with Symmetrically Distributed Point Supports along the Edges'. J. Sound & Vibr., 1984, 94, 381.
11. NOWACKI, W. - 'Vibration and Buckling of Rectangular Plates Simply Supported at the Periphery and at Several Points inside' (in Polish). Arch. Mech. Stosow., 1953, 5, 437.
12. NOWACKI, W. - Dynamics of Elastic Systems, Chapman and Hall, London, 1963.
13. LEISSA, A.W. - Vibration of Plates, NASA SP-160, NASA, 1969.
14. LYNN, P.P. and KUMBASAR, N. - 'Free Transverse Vibration of Flat Slabs'. J. Engg Mech. Div. (Proc. ASCE), 1969, 95, 255.
15. PAVLOVIC, M.N. and POULTON, S.M. - 'On the Computation of Slab Effective Widths'. J. Struct. Engg (Proc. ASCE), 1985, 111, 363.
16. JEARY, A.P. - 'Determining the Probable Dynamic Response of Suspended Floors'. Information Paper IP17/83, Build. Res. Establ., 1983.
17. WYATT, T.A. - 'Floor Excitation by Rhythmic Vertical Jumping', Engg Struct., 1985, 7, 208.
18. WARBURTON, G.B. - 'Rayleigh's Contribution to Modern Vibration Analysis'. J. Sound & Vibr., 1983, 88, 163.
19. JOHNSON, D.A. - 'Rayleigh Revisited'. J. Appl. Mech. (Proc. ASME), 1985, 52, 220.
20. TIMOSHENKO, S.P. and WOINOWSKY-KRIEGER, S. - Theory of Plates and Shells, McGraw-Hill, New York, 1959.
21. HAJDIN, N. - Theory of Plates (in Serbo-Croat), Gradjevinski Fakultet Univerziteta u Beogradu, Belgrade, 1984.
22. PAVLOVIC, M.N. and SAPOUNTZAKIS, E.J. - 'Computers and Structures: Non-Numerical Applications'. Comp. & Struct., 1986, 24, 455.
23. SAKHAROV, I.E. - 'Dynamic Stiffness in the Theory of Axisymmetric Vibrations of Circular and Annular Plates'. Izv. An. SSSR (OTN, Mekh. i Mashin.), 1959, 2, 90.

# LINEAR PROGRAMMING APPROACH TO LIMIT ANALYSIS OF THIN-WALLED STRUCTURES

Š. Dunica

University of Belgrade, Faculty of Civil Engineering  
11 000 Belgrade, Yugoslavia

## SUMMARY

The paper presents a procedure for plastic analysis of thin-walled structures subjected to bending and torsion. The static theorem of limit analysis is used, which, in general, involves the following conditions:

- Equilibrium conditions, expressed by equations corresponding in number to the degrees of freedom of the structure, and
- Plasticity conditions, expressed by inequalities to guarantee that the yield conditions are respected.

The plasticity conditions for three different cross-sections (I, [-sections and rectangular box) subjected to warping torsion and bending are derived. These conditions are then linearized in such a form which is convenient for plastic analysis of structural systems by using the linear programming.

On the bases of the proposed algorithm the computer program is developed and the results of a numerical example solved using that program are presented.

## 1. INTRODUCTION

The study of the behaviour of thin-walled structures, particularly their plastic strength is of great importance in design, especially of steel structures. Their complex behaviour including warping has obtained an interest of many authors. The plastic behaviour of thin-walled beams has been particularly thoroughly studied by Kollbrunner and Hajdin [8].

This paper outlines a method for plastic analysis of thin-walled frames introducing the following assumptions:

- The frame is composed only of straight members.
- The dimensions of the cross-sections are small in

- comparison with the member length.
- The equilibrium conditions are formulated on the undeformed system (first order theory).
- The cross-sectional shape remains unchanged.
- A rigid-perfectly plastic behaviour of the material is assumed.
- The structure is subjected to constant loading and proportional loading defined by the load factor, acting only at the joints of the system.

Existing methods for plastic analysis are based on either the kinematic or static approach. A corresponding solution of the problem has to satisfied the following conditions:

- Equilibrium conditions.
- Plasticity conditions, which imply that the sectional forces exceed nowhere the plastic resistance of the cross-section.
- Mechanism condition, which is satisfied when sufficient plastic hinges are developed forming a collapse mechanism.

If the static theorem of limit analysis is used, the solution is reduced to determination of the greatest value of the load factor, satisfying the equilibrium and plasticity conditions.

The most suitable approach for computer application is based on the fact that the plastic analysis problem can be cast in a linear programming form.

Firstly, the plasticity conditions for tree different cross-sections ( I, [-sections and rectangular box) subjected to warping torsion and bending are derived, and then, the linear programming approach of the problem is presented.

## 2. CROSS-SECTIONAL RESISTANCE - PLASTICITY CONDITIONS.

Now, the plasticity conditions for tree different cross-sections subjected to warping torsion and bending are derived. In order to simplify the mathematical approach the effect of shear stress in yield condition is neglected.

### 2.1 I-section

Consider the beam of a symmetrical I-section subjected to warping torsion and bending about y axis (Fig. 1.a). The diagrams of the coordinate z, sectorial coordinate  $\omega$  and longitudinal normal stress  $\sigma_x$  for fully plastic section are shown in

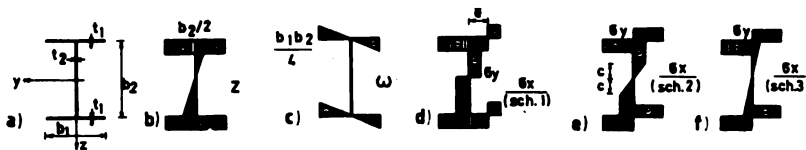


Fig. 1

Fig. 1.b-d. For the stress distribution shown in Fig. 1.d, the bending moment  $M$  and warping moment  $M_\omega$  can be expressed in the following form:

$$\left. \begin{aligned} M_y &= \int_F \sigma_x z \, dF = \sigma_y b_2 \left( 2et_1 + \frac{1}{4} b_2 t_2 \right) \\ M_\omega &= \int_F -\sigma_x \omega \, dF = \sigma_y b_2 t_1 \left( \frac{1}{4} b_1^2 - e^2 \right) \\ (0 \leq e \leq \frac{1}{2} b_1) \end{aligned} \right\} \dots\dots\dots(1)$$

where  $\sigma_y$  is the yield stress for uniaxial tension. Eliminating the parameter  $e$  from these equations we obtain the relation

$$\left[ (1+\alpha) \frac{M_y}{M_y^*} - \alpha \right]^2 + \frac{M_\omega}{M_\omega^*} = 1 \dots\dots\dots(2)$$

where

$$\left. \begin{aligned} M_y^* &= (1+\alpha) \sigma_y b_1 b_2 t_1 \\ M_\omega^* &= \frac{1}{4} \sigma_y b_1^2 b_2 t_1 \end{aligned} \right\} \dots\dots(3)$$

are the values of plastic bending moment and plastic warping moment, and

$$\alpha = \frac{1}{4} \frac{b_2 t_2}{b_1 t_1} \dots\dots\dots(4)$$

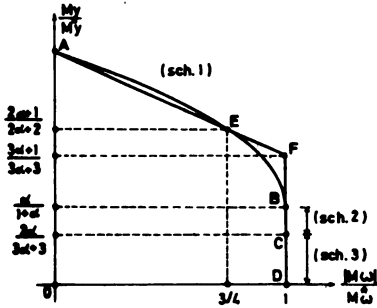


Fig. 2

plastification of the flanges only occurs ( $e=0$  in Fig. 1.d), so that the section is still capable to carry the bending moment. The state of stress in the web, then, can be elasto-plastic (Fig. 1.e) - line BC in Fig. 2, or elastic (Fig. 1.f) - line CD in Fig. 2. The linearized form of plasticity conditions is presented in Fig. 2 by bold lines.

2.2 [-section

Consider now a beam of [-section (Fig. 3.a). The diagrams of the coordinate  $z$ , sectorial coordinate  $\omega$  and stress  $\sigma_x$  for fully

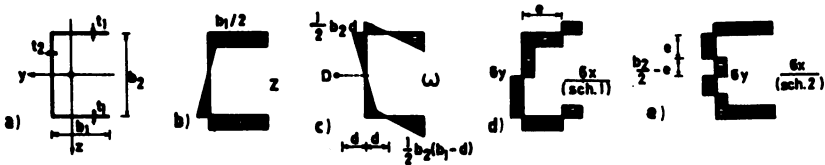


Fig. 3

plastic section are presented in Fig. 3.b-d. The position of the shear centre D is defined by



$$d = \frac{1}{2(1+\alpha)} b_1 \dots\dots\dots(5)$$

where

$$\alpha = \frac{1}{4} \frac{b_2 t_2}{b_1 t_1} \dots\dots\dots(6)$$

According to stress distribution shown in Fig. 2.d we have

$$\left. \begin{aligned} M_y &= \sigma_y [b_2 t_1 (2e - b_1) + \frac{1}{4} b_2^2 t_2] \\ M_\omega &= \sigma_y b_2 t_1 (\frac{1}{2} b_1^2 - e^2) + M_y d \\ (0 \leq e \leq b_1) \end{aligned} \right\} \dots\dots\dots(7)$$

Eliminating the parameter e from these equations we obtain

$$\left[ (1+\alpha) \frac{M_y}{M_y^*} + 1 - \alpha \right]^2 + 4(1+\alpha) \frac{M_\omega - M_y d}{b_1 M_y^*} - 2 = 0 \dots\dots\dots(8)$$

where  $M_y^*$  is the plastic bending moment given by

$$M_y^* = (1+\alpha) \sigma_y b_1 b_2 t_1 \dots\dots\dots(9)$$

Graphic presentation of equation (8) is given in Fig. 4.a by curve ABD for  $\alpha \leq 1$ , or in Fig. 4.b for  $\alpha > 1$ .

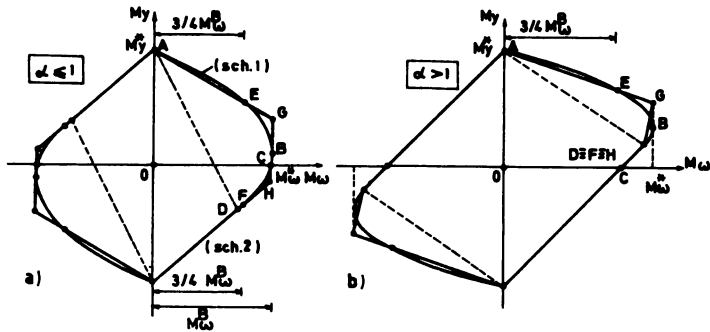


Fig. 4

For stress distribution according to Fig. 3.e we obtain the following expressions

$$\left. \begin{aligned} M_y &= -\frac{1}{1+\alpha} \left\{ 1 - \alpha \left[ 1 - 8 \frac{e}{b} \left( 1 - \frac{e}{b} \right) \right] \right\} M_y^* \\ M_\omega &= \frac{\alpha}{(1+\alpha)^2} \left[ 1 - 4 \frac{e}{b} \left( 1 - \frac{e}{b} \right) \right] b_1 M_y^* \\ (0 \leq e \leq \frac{b^2}{2}) \end{aligned} \right\} \dots\dots\dots(10)$$

which, after elimination of parameter e become

$$2(1+\alpha) \frac{M_\omega}{b_1 M_y^*} - \frac{M_y}{M_y^*} = 1 \dots\dots\dots(11)$$

Equation (11) in Fig. 4.a and Fig. 4.b is presented by line DA'. The linearized form of plasticity conditions in Fig. 4.a,b is presented by bold lines.

### 2.3 Rectangular box section

Fig. 5 presents a rectangular box section with corresponding diagrams of coordinates  $z$  and  $\omega$  and stress  $\sigma_x$  for fully plastic section.

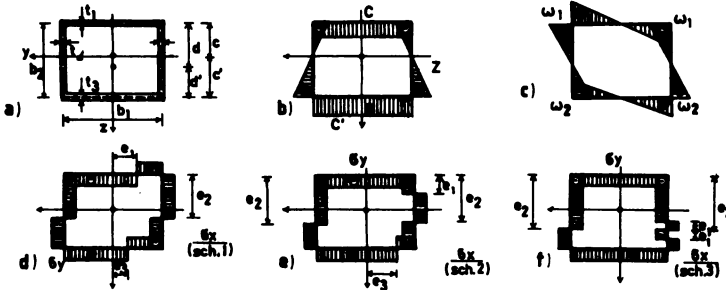


Fig. 5

For stress distribution according to Fig. 5.d, using the conditions  $N=0$  and  $M_z=0$  we obtain

$$\left. \begin{aligned} M_y &= 2\sigma_y b_2 t_1 e_1 \\ M_\omega &= \sigma_y \left\{ \frac{1}{2b_1} [\omega_1 t_1 (b_1^2 - 4e_1^2) - \omega_2 t_2 (b_1^2 - 4e_2^2)] + \right. \\ &\quad \left. + \frac{t}{b_2} [\omega_1 (4b_2 e_2 - 2e_2^2 - b_2^2) + \omega_2 (2e_2^2 - b_2^2)] \right\} \dots\dots\dots (12) \end{aligned} \right\}$$

$(0 \leq e_1 \leq \frac{b_1}{2})$

where

$$e_2 = \frac{1}{2} b_2 + \frac{1-\theta_1}{8\theta_2} b_1 + \frac{t_1(1-\theta_1)}{2t_2 b_1} e_1^2, \quad e_3 = \theta_1 e_1 \dots\dots\dots (13)$$

and

$$\theta_1 = \frac{t_1}{t_2}, \quad \theta_2 = \frac{t_2}{t_2} \dots\dots\dots (14)$$

Similarly, for stress scheme given in Fig. 5.e we have

$$\left. \begin{aligned} M_y &= \sigma_y [b_1 t_1 e_2 + 2e_3 t_2 (b_2 - e_2) + e_1 t_2 (2e_2 - e_1)] \\ M_\omega &= \sigma_y \left\{ \frac{\omega_2 t_2}{2b_1} (4e_2^2 - b_1^2) + \frac{t}{b_2} (e_2 - e_1) [2\omega_1 b_2 - (\omega_1 - \omega_2) (e_1 + e_2)] - \right. \\ &\quad \left. - \frac{t}{t_1} (b_2 - e_2) [b_2 (\omega_1 + \omega_2) - e_2 (\omega_1 - \omega_2)] \right\} \dots\dots\dots (15) \end{aligned} \right\}$$

$(0 \leq e_1 \leq \frac{1-\theta}{2\theta_2} b_1)$

where

$$e_2 = \frac{1}{2} b_2 + \frac{b_1}{8\theta_2} (1-\theta_2^2) + \frac{1}{2} e_1 (1-\theta_1 - \theta_2 \frac{e_1}{b_1}), \quad e_3 = \frac{1}{2} \theta_1 b_1 + \theta_2 e_1 \quad (16)$$

Finally, for stress scheme according to Fig. 5.f we have

$$\left. \begin{aligned}
 M_y &= \sigma_y \{ b_1 [ t_2 b_2 - e_2 (t_2 - t_1) ] + t_2 [ b_2^2 - 2e_2 (b_2 - e_2) - 2e_1^2 ] \} \\
 M_{\omega} &= 2\sigma_y \frac{\omega_1 - \omega_2}{b_2} t_2 e_1^2 \\
 (0 \leq e_1 \leq \frac{1}{2} b_2 - \frac{1 - \theta_1}{4\theta_2} b_1)
 \end{aligned} \right\} \dots (17)$$

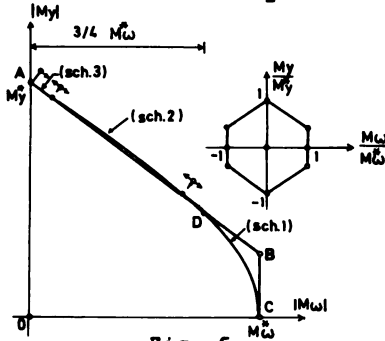


Fig. 6

where

$$e_2 = \frac{1}{2} b_2 + \frac{1 - \theta_1}{4\theta_2} b_1 \dots (18)$$

The graphic presentation of equations (12), (15) and (17) is given in Fig. 6, where the linearization of the plasticity conditions is also performed.

### 3. EQUILIBRIUM CONDITIONS

Fig. 7 shows an arbitrary member *m* in local coordinate system *xyz* with corresponding member end forces.

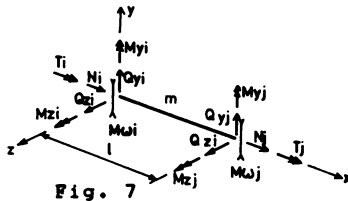


Fig. 7

Equilibrium conditions for element *m* are

$$\left. \begin{aligned}
 Q_{yi} &= -Q_{yj} = \frac{1}{l} (M_{zi} + M_{zj}) \\
 Q_{zi} &= -Q_{zj} = -\frac{1}{l} (M_{yi} + M_{yj}) \\
 N_j &= -N_i
 \end{aligned} \right\} (19)$$

Using the solution of differential equation of thin-walled beam due to warping torsion given in textbook [7] we can write the following relations:

$$\left. \begin{aligned}
 \varphi_j &= \varphi_o + \frac{T_{\omega o}}{GK} \frac{1}{k} \operatorname{sh} kl + \frac{M_{\omega o}}{GK} (\operatorname{ch} kl - 1) + \frac{T_o}{GK} (1 - \frac{1}{k} \operatorname{sh} kl) \\
 M_{\omega j} &= T_{\omega o} \frac{1}{k} \operatorname{sh} kl + M_{\omega o} \operatorname{ch} kl - T_o \frac{1}{k} \operatorname{sh} kl \\
 T_j &= T_o
 \end{aligned} \right\} \dots (20)$$

where  $\varphi_o$  is the rotation around the beam axis *x*,  $T_o$  is the St. Venant's part of torsional moment,  $M_{\omega o}$  is the warping moment and  $T_o$  is the total torsional moment at the end *i* of element *m*, noting that the sign convention for  $M_{\omega}$  is taken opposite than in work [7].

The conditions  $\varphi_o = 0$  and  $\varphi_j = 0$  give

$$T_i = T_j = \frac{1}{l} (M_{\omega i} + M_{\omega j}) \dots (21)$$

where, according to sign convention for member end forces shown in Fig. 7, we have taken

$$\left. \begin{aligned} T_o &= -T_i \\ M_{\omega\omega} &= -M_{\omega i} \end{aligned} \right\} \dots\dots\dots(22)$$

Equations (19) and (21) can be written in matrix form

$$Q_n = A_n \cdot S_n \dots\dots\dots(23)$$

where  $A_n$  is the force matrix, and

$$\left. \begin{aligned} Q_n^T &= [N_i \ Q_{y_i} \ Q_{z_i} \ T_i \ M_{y_i} \ M_{z_i} \ M_{\omega_i} \ N_j \ Q_{y_j} \ Q_{z_j} \ T_j \ M_{y_j} \ M_{z_j} \ M_{\omega_j}] \\ S_n &= [N_i \ 0 \ 0 \ 0 \ M_{y_i} \ M_{z_i} \ M_{\omega_i} \ 0 \ 0 \ 0 \ 0 \ M_{y_j} \ M_{z_j} \ M_{\omega_j}] \end{aligned} \right\} \dots\dots(24)$$

**3.1 Modification of the force matrix due to member releases**

Let write the matrices  $Q_n$ ,  $S_n$  and  $A_n$  in the form

$$Q_n^T = [Q_1 \ Q_2 \ \dots \ Q_{14}], \quad S_n^T = [S_1 \ S_2 \ \dots \ S_{14}], \quad A_n = [A_{ij}]_1^{14} \dots\dots(25)$$

If member end force  $Q_k = 0$ , the matrix equation (23) can be written in a modified form

$$\bar{Q}_n^{(1)} = \bar{A}_n^{(1)} \cdot S_n \dots\dots\dots(26)$$

where  $\bar{A}_n^{(1)} = [\bar{A}_{ij}^{(1)}]_1^{14}$  is the modified force matrix due to member release  $Q_k = 0$ , which elements are given by

$$\bar{A}_{ij}^{(1)} = A_{ij} - A_{ik} \frac{A_{kj}}{A_{kl}}, \quad A_{kl} \neq 0, \quad (i, j = 1, 2, \dots, 14) \dots\dots(27)$$

If more than one member release exists, this procedure can be repeated unless the final form of the matrix relation (23) is obtained, i.e.

$$\bar{Q}_n = \bar{A}_n \cdot S_n \dots\dots\dots(28)$$

where  $\bar{A}_n$  is the modified force matrix due to all member releases.

**3.2 Transformation of the force matrix with respect to global coordinate system**

Denoting by  $Q_n^g$  the force vector in global coordinate system XYZ, we can express this vector by vector  $\bar{Q}_n$  in the following form:

$$Q_n^g = T_n \cdot \bar{Q}_n \dots\dots\dots(29)$$

where  $T_n$  is a quasideagonal transformation matrix depending on the directions cosines of the individual axes of local coordinate system with respect to the global system.

Substituting (28) in (29) follows

$$Q_n^g = A_n^g \cdot S_n \dots\dots\dots(30)$$

where

$$A_n^g = T_n \cdot \bar{A}_n \dots\dots\dots(31)$$

**3.3 Transformation of the force matrix with respect to master nodes**

The ends of the beam can be geometrically constrained to a master or slave nodes. Slave degrees of freedom at the end of the

beam are eliminated from the formulation and replaced by the transformed degrees of freedom of the master node. This technique reduces the total number of joint equilibrium equations of the system. Two master nodes  $r$  and  $j$  and a slave node  $i$  are shown in Fig. 8.

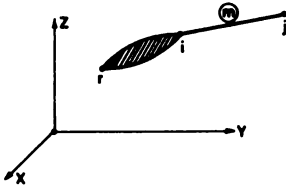


Fig. 8

The equilibrium conditions of the rigid part  $r-i$  give

$$Q_m^{**} = B_m \cdot Q_m^* \dots\dots\dots(32)$$

or using (30)

$$Q_m^{**} = A_m^{**} \cdot S_m \dots\dots\dots(33)$$

where

$$A_m^{**} = B_m \cdot A_m^* \dots\dots\dots(34)$$

is the force matrix in global coordinate system with respect to master nodes  $r$  and  $j$ .

### 3.4 Joint equilibrium equations

Equilibrium equations of whole system can be written in the form

$$\sum_{m=1}^M Q_m^{**} = P \dots\dots\dots(35)$$

where  $M$  is the total number of members.

If we present the load vector as

$$P = P_0 + \lambda P_1 \dots\dots\dots(36)$$

where  $\lambda$  is the load factor, using the relation (34), the joint equilibrium equations (35) can be written in the following form

$$\sum_{m=1}^M A_m^{**} \cdot S_m - \lambda P_1 = P_0 \dots\dots\dots(37)$$

or briefly

$$A \cdot S - \lambda P_1 = P_0 \dots\dots\dots(38)$$

### 4. PLASTICITY CONDITIONS OF WHOLE SYSTEM

In paragraph 2. we derived the linearized plasticity conditions for three different cross-sections.

Writing the force vector  $S_m$  in equation (37) as

$$S_m = \begin{bmatrix} S_m^{(i)} \\ S_m^{(j)} \end{bmatrix} \dots\dots\dots(39)$$

where  $(i)$  and  $(j)$  indicate the end joints of member  $m$ , the plasticity conditions of whole system can be written in the following form

$$\left. \begin{aligned} C_m^{(i)} \cdot S_m^{(i)} &\leq D_m^{(i)} \\ C_m^{(j)} \cdot S_m^{(j)} &\leq D_m^{(j)} \\ (m = 1, 2, \dots, M) \end{aligned} \right\} \dots\dots\dots(40)$$

or briefly

$$C \cdot S \leq D \dots\dots\dots(41)$$

**5. SOLUTION BY LINEAR PROGRAMMING**

Formulation of plastic analysis problem is based on the static theorem giving the lower bound of the load factor  $\lambda$ .

Based on equations (38) and (39), the following Linear Programming (LP) problem is formulated: find  $\lambda$  and  $S$  such that

$$\left. \begin{aligned} (\max) f &= \lambda \\ A \cdot S - \lambda P_1 &= P_0 \\ C \cdot S &\leq D \end{aligned} \right\} \dots\dots\dots(42)$$

If we represent the force vector  $S$  by difference of two nonnegative variables  $\bar{S}$  and  $S^*$ , i.e.

$$S = \bar{S} - S^* \dots\dots\dots(43)$$

where  $S^*$  is the vector of limit values of member forces, the LP problem (40) becomes

$$\left. \begin{aligned} (\max) f &= \lambda \\ A \cdot \bar{S} - \lambda P_1 &= P_0 \\ C \cdot \bar{S} &\leq D \\ \bar{S} &\geq 0 \end{aligned} \right\} \dots\dots\dots(44)$$

The Solution of this LP problem can be significantly simplified by using the decomposition method; where, the member forces are expressed as linear combinations of extreme points of plasticity conditions.

**6. NUMERICAL EXAMPLE**

On the basis of the presented procedure the computer program is written. Using that program the limit value of the load eccentricity  $e$  in the numerical example shown in Fig. 9.a is obtained. The eccentricity  $e$  can be considered here as a load factor (Fig. 9.b). For given geometry of the system the limit

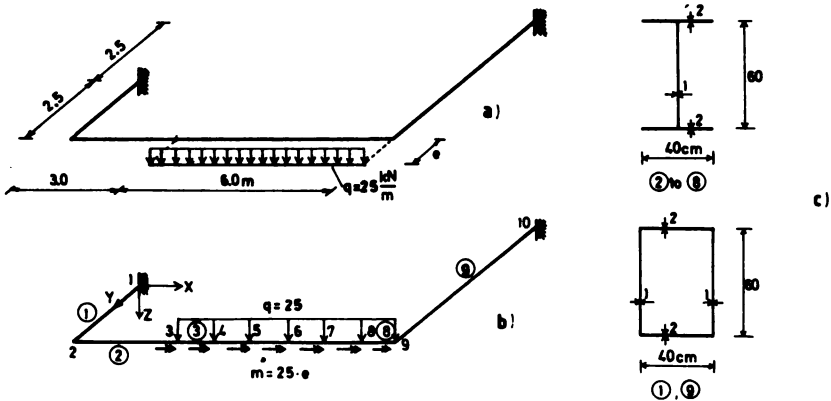


Fig. 9

value of  $e$  is  $e = 1.08$  m, and the corresponding diagrams of member forces are presented in Fig. 10. The plastic hinges are formed in joints 1, 2, 5 and 9.

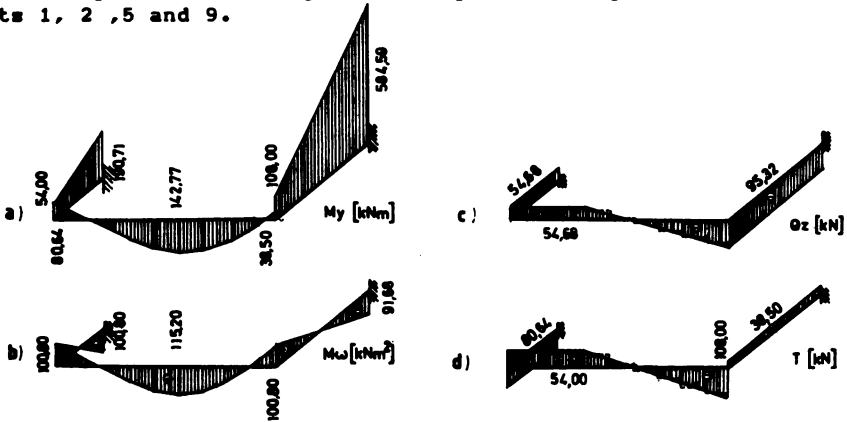


Fig. 10

#### REFERENCES

1. DUNICA, Š. - 'Contribution to the Plastic Analysis of Space Frames Composed of Truss, Beam and Thin-walled Elements'. Ph. D. thesis (in Serbo-Croat), Građevinski fakultet, Belgrade, 1979.
2. DUNICA, Š. - 'Plasticity Conditions of Thin-walled Structures Subjected to Warping Torsion and Bending' (in Serbo-Croat), Proc. of the 15. Yugoslav Cong. of Theor. and Appl. Mech., Kupari, 1981.
3. DUNICA, Š. - 'Plastic Analysis of Thin-walled Frames by Linear Programming' (in Serbo-Croat), Proc. of the 15. Yugoslav Cong. of Theor. and Appl. Mech., Kupari, 1981.
4. GASS, S. I. - Linear Programming, McGraw-Hill Book Co., ed. 3, New York, 1969.
5. GAVARINI, C. - 'L'analyse limite des structures au moyen de la programmation mathématique', Symp. on Theory of Plasticity, Niš, 1974.
6. GROB, J. - 'Plastic Strength of Steel Beams with Thin-walled Open Cross Sections', Proc. of the Inter. Conf. on Steel Structures, part II, Budva, 1986.
7. KOLLBRUNNER, C. F. and HAJDIN, N. - Dünnwandige Stäbe, Band I, Springer-Verlag, Berlin-Heilderberg-New York, 1972.
8. KOLLBRUNNER, C. F. and HAJDIN, N. - Dünnwandige Stäbe, Band II, Springer-Verlag, Berlin-Heilderberg-New York, 1975.
9. KOLLBRUNNER, C. F., HAJDIN, N. and ĆORIĆ, B. - 'Elastic-Plastic Thin-walled I-section Beam Subjected to Bending and Warping Torsion', Verlag Schulthess AG, Zürich, 1978.
10. MASSONNET, Ch. and SAVE, M. - Calcul plastic de construction, Vol. I, ed. II, Bruxelles, 1967.
11. NEAL, B. G. - The Plastic Method of Structural Analysis, Chapman and Hall, ed. 2, London, 1963.
12. STRELBIZKAJA, A. I. - Investigation on the Strength of Thin-walled Beams Beyond the Elastic Range (in Russian), Kiev, 1985.
13. ZAVELANI - ROSSI, A. - 'A New Linear Programming Approach to Limit Analysis', Inter. Symp. on Variational Methods in Engineering, Southampton, 1972.

## COLLAPSE OF PLATE GIRDERS SUBJECTED TO PATCH LOADING

T.M. Roberts

University College, Department of Civil and Structural Engineering  
Cardiff, Great Britain.

B.Čorić

University of Belgrade, Faculty of Civil Engineering  
Belgrade, Yugoslavia.

### SUMMARY

The paper describes theoretical and experimental study of behaviour of slender plate girders subjected to localised edge loading to investigate the influence of co-existent bending stresses on the collapse load. Simple closed form equations for predicting the collapse load, based on a mechanism solution, are presented together with a reduction factor to allow for the influence of co-existent bending stresses.

The relationship between the collapse load and the elastic critical load of the web is also investigated.

### NOTATIONS

- b width of web panel
- $b_f$  width of flange
- c loaded length
- d depth of web panel
- s standard deviation
- $t_w$  thickness of web
- $t_f$  thickness of flange
- E Young's modulus
- K buckling coefficient



- P load
- $P_{cr}$  elastic critical load
- $P_{ex}$  experimental collapse load
- $P_u$  predicted collapse load
- $P_{uo}$  collapse load for  $\sigma_b = 0$
- $\nu$  Poisson's ratio
- $\sigma_b$  bending stress
- $\sigma_f$  flange yield stress
- $\sigma_w$  web yield stress

## 1. INTRODUCTION

The problem of increasing practical importance is that of determining the collapse load of plate girders subjected to patch loading.

This paper describes tests on two girders [1] carried out as part of a continuing investigation at University College Cardiff and University of Belgrade into a collapse of plate girders subjected to localised edge loading.

The purpose of the tests was to investigate the influence of co-existent bending stresses on the collapse load.

For slender plate girders, where failure is induced by bending of the web, the relationship between the collapse load and the elastic critical load of the web is also investigated.

## 2. DESCRIPTION OF TESTS

Details of the girders tested are shown in Fig.1.

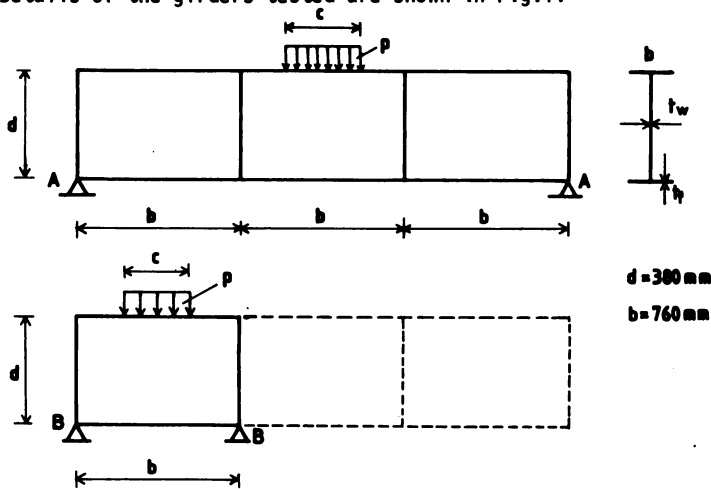


Fig. 1. DETAILS OF TEST GIRDERS

Each girder comprised three panels with aspect ratios  $b/d=2$ . In the first test, the girders were simply supported at A-A and the middle panel was loaded by a concentrated load  $P$  applied through a 50 mm wide bar at the centre of the panel. The load was then increased up to failure.

The girder was then simply supported at B-B and the end panel tested in the same way.

In each test the girder was restrained laterally (Fig.2) so that it did not become laterally unstable. Varying the span induced different values of the co-existent bending stress  $\sigma_b$  at collapse. The typical mode of failure is shown in Fig.3 and the test data is given in TABLE 1.

GIRDER	SUPPORT	$t_w$ mm	$b_f$	$t_f$	$c$	$\sigma_w$ N/mm <sup>2</sup>	$\sigma_f$	$P_{ex}$ N	$\sigma_b/\sigma_w$
D2-3S	B-B	1.96	80	3.05	50	178	272	33550	0.26
"	A-A	"	"	"	"	"	"	32000	0.77
D3-6S	B-B	3.0	"	6.25	"	245	298	84100	0.25
"	A-A	"	"	"	"	"	"	84000	0.74

TABLE 1. DETAILS OF TESTS

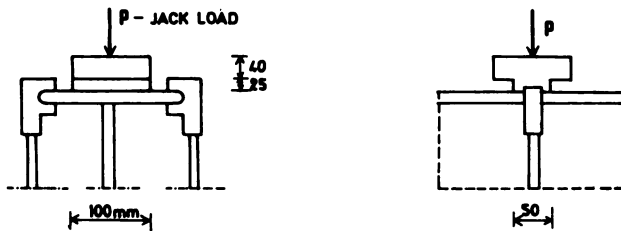


Fig. 2. DETAILS OF LOADING MEMBERS

### 3. THEORY

In [2] Roberts and Rockey presented a mechanism solution for predicting the collapse load of plate girders subjected to localised edge loading. Two alternative forms of the mechanism solution were presented, one considering failure to occur due to web bending and the other considering failure to be initiated by direct yielding of the web.

In [3] the mechanism solutions have been slightly modified and reduced to simple closed form equations. For web bending, the collapse load  $P_u$  is given by

$$P_U = 0.5 t_w^2 [E \sigma_w t_f/t_w]^{1/2} [1 + \frac{3c}{d} (\frac{t_w}{t_f})^{1.5}] \quad (1)$$

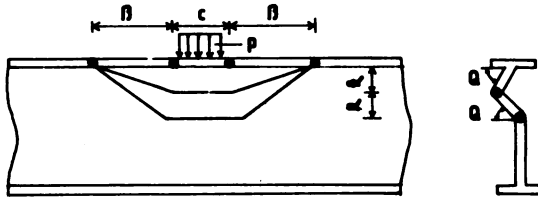


Fig.3. TYPICAL MODE OF FAILURE

where an upper limit of 0.2 is imposed on the value of  $c/d$  and a lower limit of 3 is imposed on the value of  $t_f/t_w$  used in equation (1). For web yielding the collapse load is given by

$$P_U = 2 [\sigma_f b_f t_f^2 \sigma_w t_w]^{1/2} + \sigma_w t_w c \quad (2)$$

The collapse load is taken as the lesser of the values given by equations (1) and (2).

When failure results from web bending, it can be deduced theoretically that a conservative estimate of the effect of co-existent bending stresses  $\sigma_b$  is to reduce the collapse load given by equation (1) by a factor

$$[1 - (\sigma_b/\sigma_w)^2]^{1/2} \quad (3)$$

and it is recommended that this factor be used for web yielding also.

If the last term in equation (1), which defines the influence of the loaded length  $c$ , is omitted (this term is of only minor significance) equation (1) reduces to

$$P_U = 0.5 t_w^2 [E \sigma_w t_f/t_w]^{1/2} \quad (4)$$

Equation (4) has been shown to provide a lower bound solution for over one hundred tests on slender plate girders giving a mean value of  $P_{ex}/P_U$  of 1.54 and a coefficient of variation  $V$  of 17.8%. If therefore equation (4) is modified to

$$P_U = 0.77 t_w^2 [E \sigma_w t_f/t_w]^{1/2} \quad (5)$$

equation (5) would give a mean value of  $P_{ex}/P_u$  of unity.

The elastic critical load  $P_{cr}$  of a web panel subjected to localised edge loading, assuming all edges of the panel to be simply supported (Fig.4) is given by [Ref. 4]

$$P_{cr} = K \frac{\pi^2 E t_w^3}{12(1-\nu^2)d} \quad (6)$$

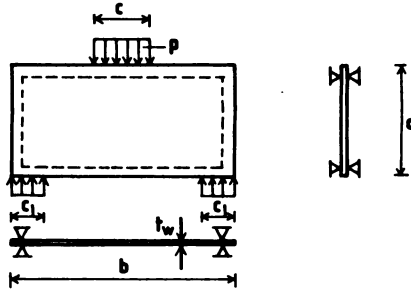


Fig. 4. WEB PANEL WITH SIMPLY SUPPORTED EDGES.

where  $K$  is a factor which depends on the girder dimensions and the loaded length  $c$ . If  $K$  is taken as 3.5 which is the value for a panel having  $b/d = 1$  and  $c/d = 0.25$ , and typical values of  $E$ ,  $\nu$  and  $\sigma_w$  are assumed to be  $210000 \text{ N/mm}^2$ ,  $0.3$  and  $250 \text{ N/mm}^2$  respectively, equations (5) and (6) give,

$$\frac{P_u}{P_{cr} (t_f/t_w)^2} = 0.0077 \frac{d}{t_w} \quad (7)$$

The implication of equation (7) is that if  $P_{ex}/P_{cr} (t_f/t_w)^2$  is plotted against  $d/t_w$ , all experimental results should be distributed about a mean line, having a gradient of 0.0077 and passing through the origin, with a standard deviation relative to the mean line of 17.8%.

#### 4. RESULTS AND CONCLUSIONS

The test results given in TABLE 1 are plotted in Fig. 5.  $P_{u0}$  is the value of the collapse load for  $\sigma_b = 0$  which is deduced from the test results when the girder was simply supported at B-B. It can be seen that the reduction factor  $[1 - (\sigma_b/\sigma_w)^2]^{1/2}$  provides a conservative estimate of the influence of co-existent bending stresses.

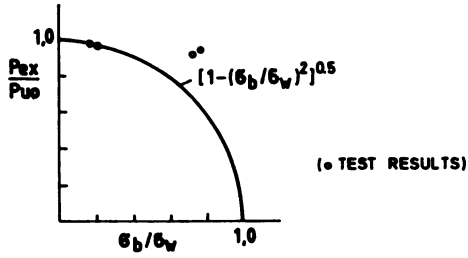


Fig. 5. INFLUENCE OF CO-EXISTENT BENDING STRESS

In Fig. 6 over one hundred test results from various sources are compared with equation (7). The test girders had  $t_w$  varying from 1 to 5 mm,  $t_f$  varying from 3 to 20 mm,  $b/d$  varying from 0.6 to 8 and  $d/t_w$  varying from 75 to 500. In Fig. 6, the mean line is shown together with two other lines, spaced at two standard deviations on each side of the mean line, which define the 95% confidence limits. There is good agreement between theory and experiment

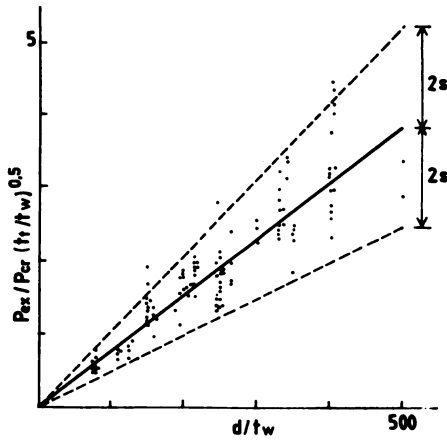


Fig. 6. COMPARISON OF TEST DATA WITH EQUATION (7)

## REFERENCES

- |1| CORIC, B. and ROBERTS, T.M. Test results. Department of Civil and Structural Engineering, University College, Cardiff, U.K.
- |2| ROBERTS, T.M. And ROCKEY, K.C. A mechanism solution of predicting the collapse load of slender plate girders when subjected to in-plane patch loading. Proc. Instn. Civ. Engrs. Part 2, 1979, 67, Mr., p. 167-185.
- |3| ROBERTS, R.M. Experimental and theoretical studies on slender plate girders subjected to edge loading. Department of Civil and Structural Engineering, University College, Cardiff, Departmental Report, July 1980.
- |4| KHAN, M.Z., and JOHNS, K.C. Buckling of web plates under combined loadings. Proc. ASCE, ST10, Oct. 1975., p. 231-237.



**RISIKOANALYSE ÜBER DEN BETRIEBZUSTAND  
DER 109-JÄHRIGEN SCHWEISSEISERNEN  
WETTSTEINBRÜCKE IN BASEL (SCHWEIZ)**

J. GROB  
Universal Ingenieur AG  
Zürich, Switzerland

**ZUSAMMENFASSUNG**

Das aus dem Jahre 1879 stammende schweisseiserne Bogentragwerk der Basler Wettsteinbrücke weist gravierende Schäden auf. Selbst unter den heute zugelassenen, reduzierten Verkehrslasten mit Gewichtsbeschränkungen für Strassenfahrzeuge ergeben sich lokal sehr hohe Beanspruchungswerte und Sicherheitsmargen unterhalb der verlangten Normwerte. Deshalb und, weil Uebertretungen der Gewichtsbeschränkungen vorkommen, wurde eine Risikoanalyse über den Betriebszustand der Wettsteinbrücke durchgeführt. Die Risikobeurteilung wurde aufgrund rechnerischer Sicherheitsmargen und Eintretenswahrscheinlichkeiten vorgenommen.

**1. AUFGABENSTELLUNG**

Im Auftrag des Tiefbauamtes Basel-Stadt führte die Arbeitsgemeinschaft der Ingenieurbüros Jean Gut, Künsnacht ZH und A. Aegerter & Dr. O. Bosshardt AG, Basel, eine Risikoanalyse über den Betriebszustand der Basler Wettsteinbrücke durch.

Ein Grossteil der dreifeldrigen Flussbrücke und der beiden Vorlandbrücken stammt aus dem Jahre 1879. In den Jahren 1936 bis 1939 wurde die ursprüngliche Bogenbrücke umgebaut und durch den Anbau von zwei getrennten seitlichen Balkenbrücken im Fluss- und von massiven Stahlbeton-Konstruktionen im Vorlandbereich verbreitert. Dabei wurde auch die ursprüngliche Zoresseisen-Platte im Flussbereich durch eine massive Stahlbetonplatte ersetzt. Bild 1 zeigt einen Querschnitt der heutigen Flussbrücke. Bemerkenswert ist, dass Strassenfahrzeuge und Tramzüge über den alten Brückenteil fahren, die neueren seitlichen Anbauten jedoch nur den Fussgänger- und Veloverkehr aufnehmen.

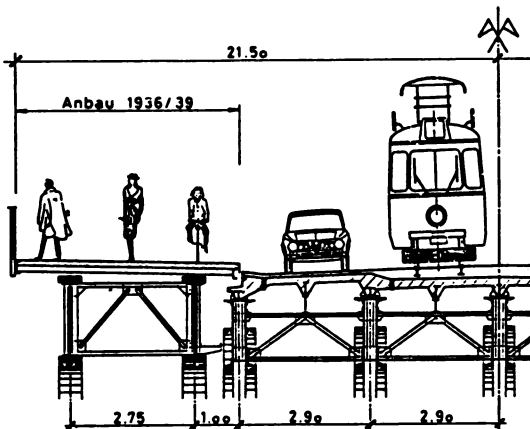


Bild 1: Brückenquerschnitt

Während die Vorlandbrücken sowie die Pfeiler, Widerlager und seitlichen Balkenbrücken des Flussbereichs eine ausreichende Tragfähigkeit aufweisen, genügen die Tragreserven der alten schweisseisernen Bogenbrücke mit Ausnahme der Fahrbahnplatte den Normlasten bei weitem nicht mehr. Die hier vorgestellte Risikoanalyse beinhaltet aus diesem Grunde nur eine Untersuchung der 109 Jahre alten Schweisseisen-Konstruktion. Bild 2.



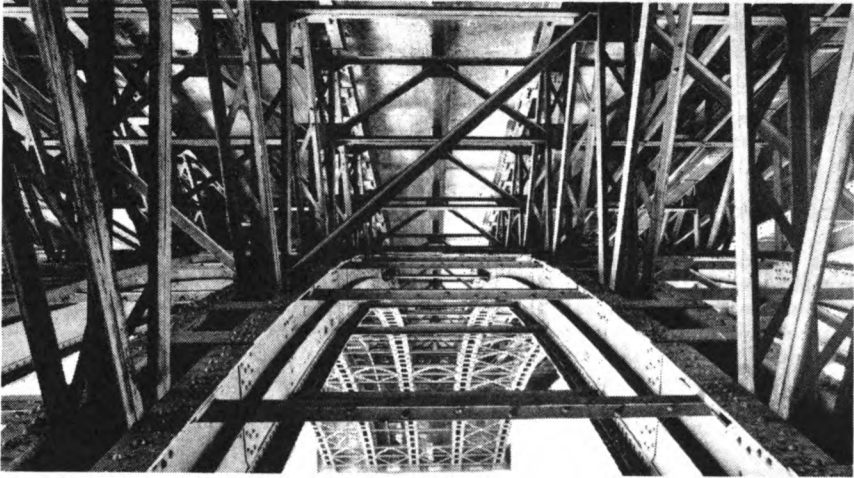


Bild 2: Schweisseisen-Konstruktion

## 2. UEBERBAU DER BOGENBRUECKE

### 2.1 Tragwerk

Der Ueberbau der dreifeldrigen Bogenbrücke ist ein komplexes räumliches Tragwerk mit einer Fachwerk-Konstruktion aus Schweisseisen und einer im Verbund hergestellten Fahrbahnplatte aus Stahlbeton. Die Schweisseisen-Konstruktion besteht aus fünf Fachwerk-Bogenträgern, Bild 3, die ihrerseits durch Fachwerk-Querträger in Abständen von 3,20 m und durch die aufbetonierte Fahrbahnplatte relativ steif miteinander verbunden sind. Somit weist die Bogenbrücke ein gekoppeltes Tragverhalten der fünf Hauptträger auf.

### 2.2 Schweisseisen-Konstruktion

Entsprechend dem damaligen Stand der Technik ist die Schweisseisen-Konstruktion genietet. Die aus kontinuierlich gekrümmten Untergurten, Pfosten, Streben und Obergurten bestehenden Fachwerkbögen sind aus Breitflachstahl und Winkeln zusammengesetzt, zweiteilig ausgebildet und durch Bindebleche oder Vergitterungen ausgesteift. Pfosten und Streben sind ohne Knotenbleche an den Bögen und Obergurten angenietet, wobei die Obergurtnoten sehr kurze Anschlusslängen aufweisen. Als Bogenlager sind Keil-Stemmlager aus Grauguss eingebaut. Die Bögen können, solange die Bogenresultierenden zwischen den Lagerkeilen liegen, als eingespannt betrachtet werden.

Aufgrund der vorgenommenen Untersuchungen an Ort und von Materialprüfungen kann der Zustand der Schweisseisen-Konstruktion wie folgt beschrieben werden:

Im Grundmaterial der Schweisseisen-Konstruktion konnten von Auge keinerlei Anrisse entdeckt werden. Sämtliche Querträger-Diagonalen, die ursprünglich nur an die Knotenbleche angenietet waren, wurden beim Umbau 1936/39 zusätzlich durch Kehlnähte mit den Knotenblechen verschweisst. Trotzdem konnten im Bereich dieser nicht materialgerechten Schweissnähte visuell keine Anrisse entdeckt werden. Die Nietverbindungen sind auch heute noch einwandfrei; alle 1984 ausgebauten Niete  $\varnothing 25$  mm befanden sich in einem erstaunlich guten Zustand und waren nur leicht angerostet.

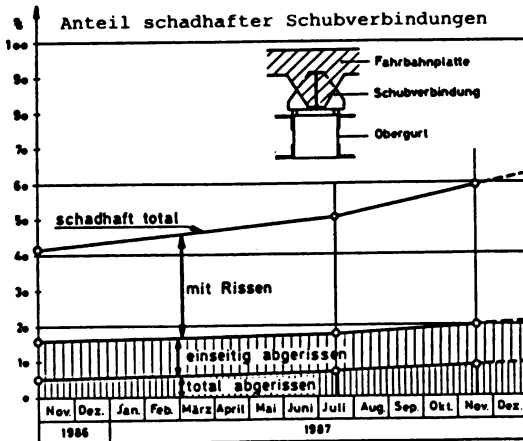


Die im Jahre 1984 durchgeführte Untersuchung hat im Vergleich zur Kontrolle des Jahres 1975 eine fortschreitende Verschlechterung des Bauzustandes der Schweisseisen-Konstruktion als Folge von verschiedenartigen Korrosionserscheinungen ergeben. Nebst anderen Faktoren hat auch das durch die undicht gewordene Fahrbahn dringende Wasser zu dieser Entwicklung beigetragen. Die kritischen Stellen der Schweisseisen-Konstruktion wurden aus diesem Grunde im Rahmen der konservierenden Sofortmassnahmen 1985 gereinigt und mit einem neuen Korrosionsschutz versehen. Seitdem konnten an der Schweisseisen-Konstruktion infolge Korrosion keine weiteren bedrohlichen Schadenentwicklungen mehr festgestellt werden.

### 2.3 Schubverbindungen

Die Schubverbindungen sind über paarig angeordnete Stahlklötze mit Kehlnähten auf den Obergurten angeschweisst. Sie sind unzweckmässig konstruiert und könnten die Schubkräfte bei voller Verbundwirkung nicht aufnehmen. Durch Schwinden des Betons und durch Temperatureinwirkungen sowie durch die verminderte Bewegungsmöglichkeit der Fahrbahnlager infolge Verschmutzung und Rostbildung entstanden durchgehende Querrisse in der Fahrbahnplatte. Diese verminderten die Verbundwirkung und damit auch die Beanspruchung der Schubverbindungen in starkem Ausmass.

An diesen Schubverbindungen treten seit wenigen Jahren und in beschleunigtem Masse Schweissnaht-Risse auf. Die Ursache für diese Risse liegt nicht in der Schubübertragung, sondern in Zwangsbeanspruchungen, die durch das unterschiedliche Verformungsverhalten von Fahrbahnplatte und Schweisseisen-Konstruktion bedingt sind. Die massgebenden Zwängungen sind durch Temperaturunterschiede sowie durch lokale Plattendeformationen verursacht, welche infolge der fortgeschrittenen Schadenentwicklung (lokal verminderte Steifigkeit der Fahrbahnplatte in Querrichtung) zugenommen haben.



Sobald eine Schubverbindung infolge Reissen der Schweissnähte ausgefallen ist, werden die benachbarten Schubverbindungen stärker beansprucht, was zu einem beschleunigten Aufreissen der Schweissnähte an diesen Schubverbindungen führt. Die entsprechende Schadenentwicklung geht aus Bild 5 hervor.

Bild 5: Schweissnaht-Risse an den Schubverbindungen

## 3. BERECHNUNGSGRUNDLAGEN

### 3.1 Statisches System

Das Tragsystem der alten Bogenbrücke ist in Bild 3 schematisch dargestellt. Eine ausführliche Berechnung dieses räumlichen Tragsystems wurde in den

Jahren 1980/81 mittels des Computer-Programmes NASTRAN durchgeführt. Bei der Nachrechnung konnte auf diese Berechnung zurückgegriffen werden, die auf folgenden grundlegenden Annahmen beruht:

- Räumliches Fachwerk mit fünf auf Zweipunktlagern abgestützten Bogenträgern und Fachwerk-Querträgern im Abstand von 3,20 m
- Biegesteife Knotenverbindungen
- Zusammenwirken Stahlkonstruktion/Fahrbahnplatte:  
Kein Verbund für Eigengewicht und ständige Lasten;  
für Verkehrslasten jeweils der ungünstigere Fall aus 0%-igem bzw. 50%-igem Verbund (100%-iger Verbund bedeutet elastische Schubverbindungen und unge-rissene Fahrbahnplatte)
- Fahrbahnplatte als biegeeweiche Scheibe
- Linear elastisches Materialverhalten

Die Schnittkräfte in der Schweisseisen-Konstruktion und in der Stahlbeton-Fahrbahnplatte sind in bestimmtem Umfang von der Verbundwirkung zwischen der Stahlkonstruktion und der Fahrbahnplatte abhängig. Im heutigen Zustand der Fahrbahnplatte mit den vielen Querrissen ist diese Verbundwirkung stark reduziert. Die Verbundwirkung der Fahrbahnplatte liegt aufgrund der Kräfte in den Schubverbindungen irgendwo zwischen 0% und 50%. Für die Nachrechnung wurden deshalb die jeweils ungünstigeren Beanspruchungswerte für 0%-igen bzw. 50%-igen Verbund verwendet.

Es wurde angenommen, dass die Rostschäden zu lokaler Schwächung der Stahlquerschnitte führen, die Steifigkeitsverhältnisse im Brückentragwerk jedoch nicht wesentlich beeinflussen. Somit konnten die Schnittkräfte von der früheren räumlichen NASTRAN-Berechnung übernommen werden.

### 3.2 Bauteile

Die Ueberprüfung der Tragfähigkeit der Fachwerkstäbe erfolgt näherungsweise durch einen Vergleich der rechnerisch vorhandenen Stahlspannungen mit dem Rechenwert der Streckgrenze, Grenz- oder Knickspannung. Die Pfosten, Streben und Obergurte der Bogenträger sowie die Querträger werden ohne Berücksichtigung der sekundären Biegemomente überprüft, für die biegesteiferen Untergurte hingegen werden die Biegemomente berücksichtigt.

Die Obergurtknoten sind ohne Knotenbleche ausgeführt, Pfosten und Streben sind exzentrisch am Stegblech des Obergurtes angenietet. Im Kräfteinleitungsbereich des Stegbleches wird das lokal vorhandene Schubfeld durch Vergleich mit jener Grenzspannung überprüft, die sich aus der Fließbedingung nach v.Mises ergibt.

Während die gemessenen Rostkerben an den Streben und Pfosten eine direkte Bestimmung der entsprechenden effektiv wirksamen Stahlquerschnitte ermöglichen, konnte die Wirkung der Rostschäden an den Untergurten nur über umfangreiche Berechnungen erfasst werden. Die Verformung der Gurt- und Stegbleche der Untergurte wurde rechnerisch mit Verformungsansätzen erfasst, die mit den Konstruktionsdetails geometrisch verträglich sind und mit den gemessenen Rost-Abträgen und Rost-Auftreibungen übereinstimmen. Die Mitwirkung der verformten und teilweise abgerosteten Bleche am Tragwiderstand wurde mittels dieser Verformungsansätze aus der Fließfigur für exzentrisch beanspruchte Rechteckquerschnitte abgeleitet.

### 3.3 Materialkennwerte des Schweisseisens

Die Festigkeitswerte des Schweisseisens sind, abgesehen von den bekannten anisotropen Eigenschaften, mit dem heutigen Baustahl Fe 360 vergleichbar. In Walzrichtung können aufgrund der Untersuchungen [1] folgende rechnerische Streck- bzw. Fließgrenzen angenommen werden:

- Streckgrenze für Querträger:  $\sigma_{0,2} = 210 \text{ N/mm}^2$
- Streckgrenze für übrige Bauteile:  $\sigma_{0,2} = 220 \text{ N/mm}^2$

In Anlehnung an die Versuche [2] und [3] wurde für eine Abschätzung der Ermüdungswirkung infolge Verkehrslasten folgender Vergleichswert der Ermüdungsfestigkeit für die genietete Schweisseisen-Konstruktion der Wettsteinbrücke angenommen:

- Ermüdungsfestigkeit:  $\Delta\sigma_R = 60 \text{ N/mm}^2$

Eine Ausnahme bilden die stark gekerbten Pfosten und Streben der Randträger. Für ihre Ueberprüfung wurde der Vergleichswert der rechnerischen Ermüdungsfestigkeit vorsichtigerweise reduziert auf:

- Ermüdungsfestigkeit:  $\Delta\sigma_R = 50 \text{ N/mm}^2$

### 3.4 Annahmen für Lasten und Zwängungen

Eigengewicht und ständige Lasten:

- Stahlkonstruktion:  
Gewicht für theoretische Abmessungen nach Plan. Keine Zuschläge für Verbindungsmittel, Knotenbleche, Vergitterungen usw.
- Fahrbahnplatte, Geleisebett:  
Gewicht für theoretische Abmessungen nach Plan.
- Isolation, Strassenbelag:  
Gewicht für Abmessungen nach Plan und Zuschlag von 2 cm Belagsstärke zur Berücksichtigung von Ausführungsungenauigkeiten.

Reduzierte Verkehrslasten (entsprechend dem heute zugelassenen Betriebszustand):

- Strassenfahrzeuge mit 3,5 t Maximalgewicht:  
Gleichmässig verteilte Last von 0,135 t/m<sup>2</sup> pro 3,00 m-Fahrspur (gemäss Unterlagen von Herrn Prof. Dr. M. Hirt, EPFL).
- Tramzüge:  
Kreuzungs- und Folgeverbot für sämtliche Tramzüge.  
Schwerster vorkommender Tramzug (Gesamtgewicht 76 Tonnen):  
Linienlast von 1,90 t/m auf 40 m Länge.

Sonder-Verkehrslasten (unerlaubte, aber möglicherweise vorkommende Strassenfahrzeuge):

- Einzelnes Schwerfahrzeug:  
Fahrzeug mit 28 bzw. 38 t Gesamtgewicht:  
Zwei Lastpaare von je 14 bzw. 19 t im Abstand von 1,30 m (Annahme auf sicherer Seite).

#### Zwängungen aus Temperaturänderungen:

- Temperaturunterschied Beton/Stahl von  $+ 10^{\circ}\text{C}$
- Gleichmässige Temperaturänderungen von  $+ 20^{\circ}\text{C}$   
(Diese Zwängungen sind im wesentlichen gleichbedeutend mit Widerlager- bzw. Pfeilerverschiebungen).

#### 4. GEFAHRDUNGSBILDER

Den Tragfähigkeitsnachweisen sind folgende Gefährdungsbilder A bis D für die heute zugelassenen, reduzierten Verkehrslasten sowie für nicht erlaubte, aber nicht völlig auszuschliessende Lastfälle zugrunde gelegt:

##### A: Grundlast:

- Eigengewicht und ständige Lasten
- reduzierte Verkehrslasten, d.h. ein schwerer Tramzug und Strassenfahrzeuge von max. 3,5 t Gesamtgewicht auf beiden Fahrspuren.

Zwängungen aus Temperaturänderungen je nach Fall.

B: Grundlast und zusätzlich ein trotz Verbot kreuzender schwerer Tramzug auf der Brücke.

C: Grundlast und zusätzlich ein unerlaubtes Strassenfahrzeug von 28 t Gesamtgewicht.

D: Grundlast und zusätzlich ein unerlaubtes EG-Strassenfahrzeug von 38 t Gesamtgewicht.

Bei den Gefährdungsbildern B bis D werden die Zwängungen infolge Temperaturänderungen nicht berücksichtigt. Ebenso spielt die Ermüdung für diese Fälle keine Rolle, weil sie nur sehr selten auftreten.

Die Risikobeurteilung der Gefährdungsbilder erfordert ausser der Kenntnis der Tragsicherheitsreserven auch eine Abschätzung der Eintretenswahrscheinlichkeiten, welche auf folgenden Annahmen beruhen:

- Täglich eine Nichtbeachtung (Vergessen) des Tram-Kreuzungsverbot auf der Wettsteinbrücke.
- Ein Strassenfahrzeug von 28 Tonnen pro Woche auf der Wettsteinbrücke trotz Gewichtsbeschränkung.
- Ein EG-Strassenfahrzeug von 38 Tonnen alle drei Monate auf der Wettsteinbrücke trotz Gewichtsbeschränkung. Bei der Ueberlagerung mit der Grundlast, Fall D, wird vorausgesetzt, dass jeder vierte Tramzug ein schwerer, die anderen leichte Tramzüge sind.

#### 5. HAUPTERGEBNISSE

##### 5.1 Schweisseisen-Konstruktion

Die Sicherheitsmargen, die sich aus Vergleich der rechnerischen Stahlspannungen mit den Rechenwerten der Streckgrenze, Grenz- oder Fliessspannung ergeben, wurden für alle Bauteile vorerst als Gesamtfaktoren ermittelt. Dabei wurde die durch Rostabtrag und Rostauffreibung erfolgte Schwächung der Stahlquerschnitte berücksichtigt. Bild 6 gibt einen Auszug der wichtigsten Ergebnisse für das Gefährdungsbild A mit den heute zugelassenen, reduzierten Verkehrslasten.

Bauteil	Sicherheitsmargen $\gamma^*$	Ort	Versagensart
Bogen	1,62	I / X, 42-43	Plastifizierung der Gurtungen durch Druck und Biegung
	1,74	II / IX, 42-43	
	1,75	III, 42-43	
Pfosten	2,43	I / X, 43	Plastifizierung des Kerbbereichs Knicken
	2,39	II / IX, 43	
	2,39	III, 43	
Streben	2,65	I / X, 45-46	Plastifizierung des Kerbbereichs Ermüdung des Kerbbereichs (Zug)
	4,66	I / X, 45-46	
	3,07	II / IX, 44-45	
	3,07	III, 43-44	
Obergurt-knoten	1,56	I / X, 46	Lokale Plastifizierung des Obergurt-Stegbleches
	1,47	II / IX, 46	
	1,52	III, 46	

\* mit Zwängungen aus Temperaturänderungen

Bild 6: Sicherheitsmargen als Gesamtfaktoren für Gefährdungsbild A

Gefährdungsbild	Sicherheitsmargen $\gamma^*$	$\gamma_{QS}^*$	Obergurt-Knoten	Eintretenswahrscheinlichkeit
A	2,06	9,40	II / IX, 46	mehrmals täglich
B	1,53	7,50	III, 46	alle 4 Monate
C	1,46	1,49	II / IX, 46	alle 2 Jahre
			I / X, 46	
D	1,32	1,15	II / IX, 46	alle 100 Jahre
			I / X, 46	

\* ohne Zwängungen aus Temperaturänderungen

Bild 7: Minimale Sicherheitsmargen als Gesamt- und Teilfaktoren

Für die massgebenden Bauteile berechnete man die Sicherheitsmargen zusätzlich als Teilfaktoren, um aussagekräftigere Ergebnisse zu erhalten. Dabei wurde folgender Vergleich der Stahlspannungen durchgeführt:

$$\sigma_G \cdot \gamma_G + \sigma_{QT} \cdot \gamma_{QT} + \sigma_{QS} \cdot \gamma_{QS} = \sigma_R / \gamma_R$$

mit:  $\sigma_G$  : Spannung infolge Eigengewicht und ständigen Lasten

$\sigma_{QT}$  : Spannung infolge Tramlasten

$\sigma_{QS}$  : Spannung infolge Strassenlasten

$\sigma_R$  : Rechenwert der Streckgrenze, Grenz- oder Knickspannung

$\gamma_G$  : Lastfaktor für Eigengewicht = 1,20 (Annahme)

$\gamma_{QT}$  : Lastfaktor für Tramlasten = 1,00 (Annahme)

$\gamma_{QS}$  : grösstmöglicher Lastfaktor für Strassenlasten; wird rechnerisch aus obiger Gleichung ermittelt

$\gamma_R$  : Materialfaktor = 1,15 (Annahme)

Die Abschätzung der Eintretenswahrscheinlichkeit erfolgte mit den im Abschnitt "Gefährdungsbilder" getroffenen Annahmen.

Bild 7 zeigt die Hauptergebnisse für das Gefährdungsbild A mit den heute zugelassenen, reduzierten Verkehrslasten sowie für die Gefährdungsbilder B bis D mit nicht erlaubten, aber nicht völlig auszuschliessenden Sonderlasten. Interessant ist, dass die Obergurtnoten bei allen Gefährdungsbildern die geringsten Sicherheitsmargen aufweisen.

## 5.2 Schubverbindungen

Die Schubverbindungen wurden nicht nachgerechnet. Ihr Totalausfall führt zu Kräfteumlagerungen, welche die Schweisseisen-Konstruktion ohne weiteres verkraften kann. Dagegen werden durch das sukzessive Abreissen der Schubverbindungen die von Fahrzeugen stammenden Schläge auf die Schweisseisen-Konstruktion verstärkt. Dies ergibt eine Vergrösserung der Sprödbruchgefahr in unbekanntem Ausmass.

## 6. RISIKOBEURTEILUNG

Die Ueberwachung des Brückentragwerks lässt eine von Jahr zu Jahr beschleunigte Schadenentwicklung, insbesondere an der Fahrbahnplatte und den Schubverbindungen, erkennen. Deshalb geht die Risikobeurteilung von der Annahme aus, dass das alte Bogentragwerk der Wettsteinbrücke bis um das Jahr 1990 ersetzt sein wird. Eine Weiterbenützung der Brücke über diesen Zeitpunkt hinaus würde zusätzliche Ueberlegungen und möglicherweise weitere Kostenaufwendungen und sogar Lastbeschränkungen oder ein Fahrverbot für Tramzüge erfordern. Die bisher angeordneten Massnahmen sind notwendig und auch ausreichend, um die Funktionstüchtigkeit der Wettsteinbrücke bis um das Jahr 1990 sicherzustellen.

Für Lastwagen bis 28 Tonnen kann die Uebertretung der Gewichtsbegrenzung mit der bisher festgestellten geringen Häufigkeit noch toleriert werden. Die Ueberfahrt eines EG-Fahrzeuges mit über 28 bis 38 Tonnen Gesamtgewicht ist in Kombination mit den erlaubten Verkehrslasten jedoch kritisch. Bei Auftreten dieses Gefährdungsbildes D sind lokale Schäden an den Obergurtnoten nicht mehr auszuschliessen. Die minimale Teil-Sicherheitsmarge für die Strassenlasten beträgt in diesem Falle gemäss Bild 7 nur noch 1,15. Wegen der möglichen Kräfteumlagerungen muss bei Auftreten eines derartigen lokalen Schadens noch kein Totaleinsturz der Brücke befürchtet werden. Dagegen könnten örtlich die Fahrbahn einbrechen sowie einzelne Stäbe und eventuell ein einzelner Bogenträger der Schweisseisen-Konstruktion in einem Masse verformt werden, so dass die betroffene Fahrspur ohne vorgängige Reparatur nicht mehr gebrauchstauglich wäre.

Die Eintretenswahrscheinlichkeit, dass trotz Lastbeschränkung ein EG-Fahrzeug mit 38 Tonnen gleichzeitig mit einem Tram die Brücke befährt, ist jedoch sehr gering (ca. einmal in 100 Jahren). Dabei ist zu beachten, dass dieser kritische Lastfall nur eintritt, wenn ein vollbeladenes EG-Fahrzeug in gleicher Richtung und neben einem vollbeladenen Tramzug die Brücke befährt, was allein schon wegen der knappen Platzverhältnisse (schmale Fahrbahn neben dem Tramtrasse) eher unwahrscheinlich ist.

Das geringe Restrisiko für diesen kritischen Sonderfall mit einem EG-Strassenfahrzeug von 38 Tonnen scheint angesichts der Feststellung, dass ein Totaleinsturz nicht befürchtet werden muss, und angesichts der sehr geringen Eintretenswahrscheinlichkeit für die Bauherrschaft als durchaus tragbar.

## 7. LITERATURVERZEICHNIS

- [1] EMPA-Untersuchungsbericht Nr. 50'568 vom 19. November 1984 betreffend Schweisseisen-Konstruktion, EMPA Dübendorf ZH
- [2] ICOM (EPFL)-Untersuchungsbericht "Ermüdungsversuche an genieteten Blechträgern der Zürich Quaiabücke" vom Dezember 1984, EPF Lausanne
- [3] ICOM (EPFL)-Untersuchungsbericht "Essais de fatigue sur des poutres a treillis double en fer puddle" vom März 1986, EPF Lausanne





## Schrägkabelbrücken mit Paralleldrahtkabeln

Hans Rudolf Müller, dipl. Ing. ETH      Bureau EBR Ltd. / Stahlton AG, Zürich

Unter der Leitung von Prof. Dr. N. Hajdin, Belgrad, wurden zwei Schrägkabelbrücken von europäischer Bedeutung projektiert und ausgeführt. Bei beiden Brücken kamen Paralleldrahtkabel zur Anwendung. 1979 wurde die erste Eisenbahnbrücke mit Schrägkabeln für zwei Vollgeleise als Weltpremiere über die Save in Belgrad erstellt [1]. Ihre Mittelspannweite von 254 m wurde bis heute bei reinen Eisenbahnbrücken in Europa nicht überschritten (Bild 1).

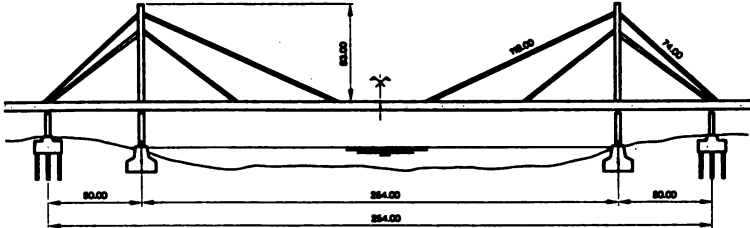


Bild 1 Eisenbahnbrücke über die Save, Belgrad.

Die Brückenkonstruktion hat sich als ein hervorragendes Bauwerk bestens bewährt. Zur Zeit steht eine weitere Eisenbahnbrücke mit grosser Spannweite kurz vor der Vollendung. Es handelt sich um die Brücke über den Frazer in Vancouver (Spannweite 340 m) [2].

Eine zweite Brücke, die Strassenbrücke über die Donau in Novi-Sad, genannt die "Brücke der Freiheit" wurde am 23. Oktober 1981, einem historischen Datum, dem Betrieb übergeben [3] [4]. Mit einer Mittelspannweite von 351 m zählt diese Schrägseilbrücke zu den weitgespanntesten Europas und übertrifft die repräsentativen Rheinbrücken Deutschlands. Sie zeichnet sich besonders aus durch die ästhetisch ansprechende Formgebung mit der Kabelanordnung in der Mittelebene (Bild 2).



Bild 2 Strassenbrücke über die Donau, Novi-Sad.

## 1. HiAm-Kabel

Die Bereitstellung von grossen Paralleldrahtkabeln hoher Schwingweite, wie sie die in der Schweiz entwickelten und hergestellten HiAm-Kabel (high amplitude) und -Verankerungen darstellen, hat dazu geführt, dass Schrägkabelbrücken bei Spannweiten ab 200 m solchen vom Hängebrückentypus wirtschaftlich überlegen sind. Es ist heute möglich auch Eisenbahnbrücken, also Brücken mit hohem Anteil an Nutzlast, als Schrägkabelbrücken zu verwirklichen.

Die im Bereich der Gebrauchsspannung (0.45 fu) ertragbare Schwingweite von HiAm-Kabeln beträgt etwa 200 bis 250 N/mm<sup>2</sup>, bei einer Lastwechselzahl von  $2 \cdot 10^6$  (Schwellfestigkeit).

Kritisch bezüglich wechselnder Lasten sind bei allen als Zugelemente verwendeten Draht- oder Litzen-Bündeln die Ankerzonen.

Unterwirft man ein mit einer guten Vorspannverankerung ausgerüstetes Kabel einem Ermüdungsversuch, so wird es in der Ankerzone zu Bruche gehen. Dies gilt auch für die mit Zamak (flüssiges Metall) warm vergossenen Seilverankerungen. Die erwähnte HiAm-Verankerung (Bilder 3 und 4) an Paralleldraht- oder Litzen-Bündeln erreicht die Schwellfestigkeit des Bündels, d.h. die Drähte des Bündels gehen im Ermüdungsversuch nicht an der Ankerzone, sondern irgendwo, statistisch verteilt, in der freien Länge zu Bruch. (Bild 5)

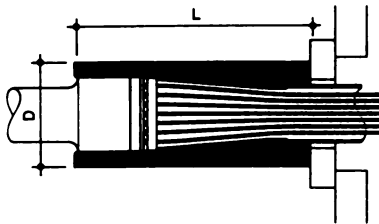


Bild 3  
HiAm-Anker im Längsschnitt.

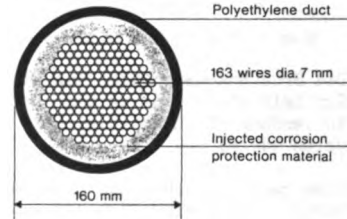


Bild 4  
Querschnitt durch Paralleldrahtbündel mit 163 # 7 mm.

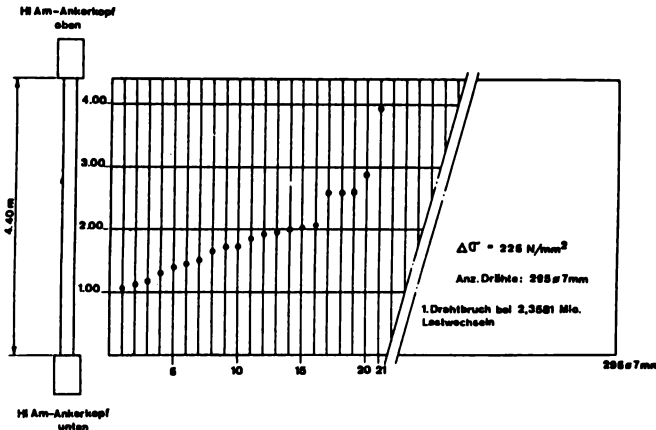


Bild 5  
Lage der Drahtbrüche beim Ermüdungsversuch an einem Paralleldrahtbündel mit 295 # 7 mm. (EMPA Bericht Nr. 73844)

versehenen Ankerkopf. Das Kabel selbst besteht aus einer beliebigen Anzahl (bis etwa 400) paralleler Drähte, versehen mit einem äusseren Polyäthylenmantel. Es wird nach der Montage und dem Spannen mit Injektionsmörtel oder anderen korrosionshemmenden Materialien verfüllt. (Bild 6)

Die Dauerfestigkeit des Bündels selbst kann also ausgenützt und als Dimensionierungsgrundlage verwendet werden. 250 N/mm<sup>2</sup> als Amplitude entsprechen ungefähr der 1 %-Fraktile der Dauerfestigkeit eines patentiert kaltgezogenen Drahtes.

Die HiAm-Verankerung besteht aus einer Kombination von endgestauchten BBRV-Köpfchen mit Stahlplatte und einem Kaltverguss mit Epoxid-Harz, gefasst in einem mit konischer Bohrung

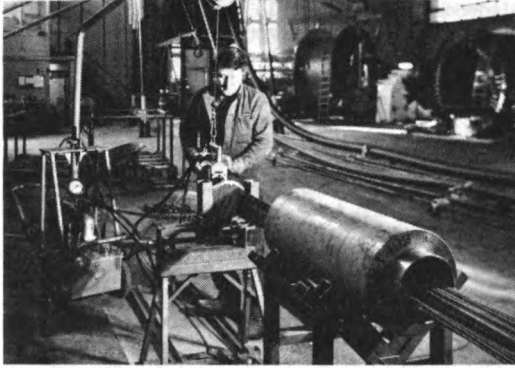


Bild 6  
Zusammenbau einer HiAm-  
Verankerung im Werk.  
Montage der BBRV-Köpfchen.

## 2. Beurteilungskriterien für Paralleldrahtkabel

Für die Beurteilung der Güte von Paralleldrahtkabeln sind folgende Kriterien massgebend:

- statische und dynamische Festigkeit
- Herstellungsprozess und Korrosionsschutz
- mechanischer Schutz

Für die Beurteilung der Dauerhaftigkeit während des Betriebes ist der Korrosionsschutz von ausschlaggebender Bedeutung. Dies ist beim Herstellungsprozess gebührend zu berücksichtigen.

### Statische und dynamische Festigkeit

Paralleldrahtkabel bestehen aus einer den erforderlichen Kräften entsprechenden Anzahl von hochwertigen, kaltgezogenen und thermisch behandelten Stahl-drähten mit der Normfestigkeit von 1670 N/mm<sup>2</sup> bei blanker Ausführung. Bei verzinkter Ausführung werden ca. 1600 N/mm<sup>2</sup> erreicht.

Die Ausnützung bei Schrägkabeln liegt bei 0.45 ftk als Obergrenze. In diesem Bereich ist das Drahtmaterial wenig empfindlich auf Spannungsrisse. Die Ermüdungsfestigkeit der blanken Drähte liegt bei etwas 300 N/mm<sup>2</sup> (gültig für  $\sigma_{max.} = 0.45 ftk$  und Probenlängen von 1.00 m und darüber). Erfahrungsgemäss liegt die entsprechende Schwingweite für verzinkte Drähte ca. 10 bis 20 % höher.

Als weiteres Kriterium für das Paralleldrahtkabel ist der hohe und mit kleiner Toleranz garantierte E-Modul anzuführen, welcher für die Verformungen unter den nicht ständigen Lasten günstige Bedingungen schafft. Dies gilt ebenso bei der Montage, die meistens vor Aufbringen der gesamten ständigen Last ausgeführt wird. Auch hier erlaubt der klar bestimmte E-Modul die zuverlässige Berechnung von erforderlichen Ueberhöhungen.

### Sicherheit gegen Korrosion

Die Sicherheit gegen Korrosion ist zu gewährleisten durch den Herstellungsprozess für die Kabel sowie durch den Aufbau des gesamten Kabels (Korrosionsschutz-System).

### Herstellungsprozess

Es ist ein Verfahren zu wählen, bei dem die fertigen Paralleldrahtkabel in einer Fabrik hergestellt werden, wo sowohl alle Einrichtungen zur laufenden Qualitätskontrolle bestehen sowie gewährleistet ist, dass während der Fabrikation keine korrosionsfördernden Einwirkungen bestehen.

Durch einen Schutzfilm aus Korrosionsschutzöl, der während der Fabrikation auf die blanken Drähte aufgebracht wird, ist der Schutz der Drähte innerhalb des PE-Rohres bis zur Injektion der Kabel gewährleistet.

Es wird immer ein System verschiedener Komponenten als Korrosionsschutz verwendet. Diese ergänzen sich in ihren Funktionen gegenseitig. Ihre Verträglichkeit muss gewährleistet sein. Neben dem klassischen Korrosionsschutz-System (A) für Paralleldrahtkabel sind auch in einzelnen Fällen Varianten bekannt und auch angewendet worden. In der untenstehenden Tabelle sind die bei HiAm-Paralleldrahtkabeln verwendeten Korrosionsschutz-Systeme zusammengestellt. Als wirtschaftlichstes System ist nach wie vor der Schutz mit Mörtel und PE-Rohr zu bezeichnen (A). Neuerdings finden auch Fettfüllungen Eingang (B). Als sehr hochwertig und entsprechend mit hohen Kosten verbunden gilt System (C), welches insbesondere in Belgien zur Anwendung gelangte. Die ersten Anwendungen gehen auf das Jahr 1961 (Schillersteg) zurück, wobei der Zustand dieser nunmehr 27 Jahre in Betrieb stehenden Kabel vom Otto-Graf-Institut im Jahre 1973 eingehend untersucht wurde. Die Feststellungen dieser Ueberprüfung sind: "Die augenscheinliche Untersuchung an zwei Stellen der Haupttragkabel ergab, dass innerhalb der Langzeitbewitterung von rund 12 Jahren seit der Erstellung des Bauwerkes keine Korrosion an den Spanndrähten eingetreten ist und der aktive Korrosionsschutz durch den Einpressmörtel noch wirksam ist".

Korrosionsschutz-System

Typ	Draht	Temporärer Schutz	Zwischenraum	Hüllrohr
A	blank	Motorex	spezieller Portland-Zement-Mörtel	PE
B	blank	---	Fett	PE
C	verzinkt	---	Teer-Epoxy oder Fett	PE

Die Verfüllung des Zwischenraumes zwischen Hüllrohr und Drahtbündel bei verzinkten Drähten kann nicht mit Portland-Zementmörtel erfolgen, weil die Bildung eines galvanischen Elementes zwischen den einzelnen Drähten und dem noch nicht vollständig ausgetrockneten Mörtel befürchtet werden muss. Die Verfüllung muss daher mit einem chemisch neutralen Stoff erfolgen. Vereinzelt sind in Japan auch andere Stoffe (Polybutadien) verwendet worden. Diese Verfüllungen sind sehr teuer (10- bis 20-fache Kosten der Mörtelinjektion), so dass sie nur bei speziellen Voraussetzungen in Betracht gezogen werden können. Erfahrungen bei der Anwendung von Teer-Epoxy liegen seit 10 Jahren vor.

#### Verankerung

Die Verankerung von blanken und verzinkten Drähten mit Kunststoff-Verguss (beim Verfahren HiAm mit Zinkstaub und Stahlkugeln angereichert) unterbindet die Anwesenheit von Feuchtigkeit vollständig und gewährleistet einen einwandfreien Korrosionsschutz im Ankerbereich für beide Drahtsorten.

Bei Ausföhrung mit verzinktem Draht ist die Möglichkeit eines metallischen Kontaktes ausserhalb des Kunststoff-Vergusses zu vermeiden.

#### Massnahmen bei der Montage von Paralleldrahtkabeln

Die bei der Montage vorzusehenden Massnahmen bestehen im allgemeinen darin, Knicke der Kabel zum Schutz der PE-Hüllrohre und der Drähte durch geeignete Umlenkkonstruktionen auszuschliessen.

Dabei besteht kein Unterschied zwischen blanken oder verzinkten Drähten. Wesentlich ist, dass es sich bereits bei der Anlieferung um ein geschlossenes System handelt.

### 3. Qualitätskontrollen

Neben dem Brückenträger und seinen Fundationen gehören die Tragkabel zu den wichtigen Bauelementen der Schrägkabelbrücken. Die Gewährleistung ihrer Tragfunktion ist entscheidend für die Gebrauchsfähigkeit und Lebensdauer der Gesamtkonstruktion. Die sorgfältige Abklärung der technologischen Eigenschaften der Abspannungen mittels Bruch- und Ermüdungsversuchen an ganzen Kabeln ist wohl eine der Voraussetzungen zur Bewertung der Gebrauchseigenschaften, entscheidend aber ist die Auswahl und Prüfung der Komponenten der eigentlichen Kabellieferung und die Ueberwachung und Kontrolle der Herstellung.

Für den Nachweis der geforderten Eigenschaften ist vom Kabelhersteller ein umfangreiches Kontrollsystem-Verfahren anzuwenden.

#### Ankerköpfe und Stützmuttern

Jede Charge des geschmiedeten Materials ist mit Festigkeits- und Zähigkeitsproben zu überprüfen. Ermittelt werden:

- Zugfestigkeit
- Streckgrenze
- Dehnung nach Bruch
- Einschnürung
- Kerbschlagzähigkeit bei  $-20^{\circ}$

Die Probenentnahme erfolgt an den bereits geschmiedeten Rohlingen. Die Ankerhülsen und Stützmuttern werden nach der mechanischen Vorbearbeitung mit Ultraschall auf Ungängen überprüft.

#### Draht

Sämtliche Drahtringe werden sowohl beim Drahtlieferanten als auch beim Kabelhersteller untersucht und die erhaltenen Resultate pro Charge statistisch ausgewertet und verglichen.

Bei Schrägkabeln ist der Schwingfestigkeit besonderes Augenmerk zu schenken. Diese bildet bei Brückenkonstruktionen das wichtigste Dimensionierungskriterium. Die Ueberprüfung ist so zu planen, dass auf verschiedenen vorgewählten Spannungsniveaus die Anzahl der Brüche und Durchläufer (für 2 Mio. Lastwechsel) bestimmt werden kann. Die im Wahrscheinlichkeitsnetz eingetragenen Bruchwahrscheinlichkeiten gestatten dann die Bestimmung ausgewählter Fraktillenwerte der Schwingweite (Bild 7). [5]

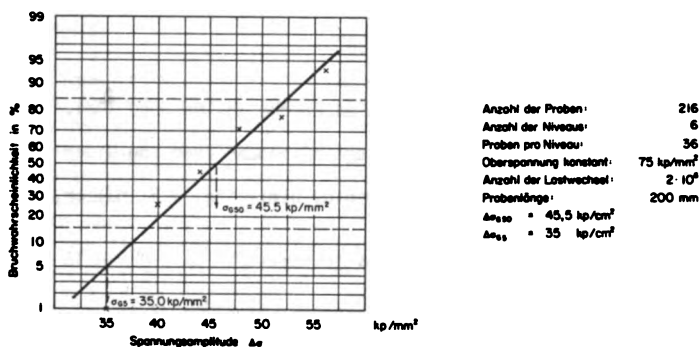


Bild 7 Ermittlung des Ermüdungswiderstandes des Drahtmaterials für die Save-Brücke.

#### HiAm-Kugelkunststoffverguss

In der Regel werden pro Verguss zwei Ankerköpfe verfüllt. Die einzelnen Vergusskomponenten, bestehend aus Epoxidharz und Härter, Zinkstaub und Stahlkugeln, sind mit Werksattesten von den Lieferanten ausgewiesen. Für jeden Verguss wird ein Protokoll erstellt, in welchem die angewandten Temperaturen und die Aushärtungszeit aufgezeichnet sind. Die Gewichtsbilanz der Zuschlagstoffe gibt Auskunft über die genaue Zusammensetzung der einzelnen Vergussstufen. An separat vergossenen Probeprismen wird die Druck- und Biegezugfestigkeit ermittelt.

#### PE-Rohre

Jede Rohrcharge wird mit Zeitstandindruckversuchen überprüft. Zudem werden der Schmelzindex bestimmt und die Masshaltigkeit untersucht.

#### Injektionsmörtel

Vorversuche haben Aufschluss über die zu wählende Rezeptur des Mörtels zu geben. Dabei sind Zementqualität, Anmachwasser und Kunststoffzusätze sorgfältig gegeneinander abzustimmen. Die Viskosität der Mörtelmischung wird mit dem Fließkorus überwacht und die Druckfestigkeiten an separat abgefüllten Proben bestimmt.

#### 4. Schlussbemerkung

Schräggabelbrücken gehören heute zu den meist angewandten Brückentypen im Spannweitenbereich von 200 m bis 800 m. Es ist das Verdienst von Prof. Dr. N. Hajdin, Entwurf, Berechnung und Konstruktion der Schräggabelbrücken nachhaltig gefördert zu haben. Die von ihm entworfenen Bauwerke zeichnen sich aus durch Wirtschaftlichkeit, Aesthetik und Dauerhaftigkeit.

#### Literaturnachweis

- [1] Eisenbahnschrägseilbrücke über die Save in Belgrad.  
Prof. Dr. N. Hajdin und Prof. L. Jeftović.  
"Der Stahlbau", 47. Jahrg. April 1976, Heft 4.
- [2] New Angle on BC Bridge, BC Transit Sky Bridge.  
George A. Peer.  
"Heavy Construction News", May 18, 1987.
- [3] Most Slobode.  
Festschrift zur Einweihung der Novi-Sad Brücke 23. Oktober 1981.
- [4] Construction of the cable-stayed bridge "Sloboda" over the River Danube, Novi-Sad.  
Prof. Dr. N. Hajdin, Dipl. Ing. S. Dinic, Dipl. Ing. H.R. Müller,  
10th FIP-Congress 1982, Stockholm.
- [5] Die Anwendung der Vorspanntechnik bei Schräggabeln an Brücken in Belgrad und Novi-Sad.  
"Vorgespannter Beton in der Schweiz", T.F.B. Wildegg, 1982.

## FATIGUE CRACK GROWTH AT LARGE DEFLECTIONS OF WEB LOADED IN SHEAR

Jozef Djubek

Assoc. Prof., DrSc., Head of Department

Institut of Construction and Architecture of SAS, 842 20 Bratislava  
Czechoslovakia

### SUMMARY

The fatigue crack growth is plotted in the form  $da/dN = B(\Delta S)^m$  and the number of cycles is considered in (5.4). Conditions of crack growth are described in chapt. 5 and the stress  $\sigma_1$  at the stable crack growth is obtained in (5.3).

Before the crack propagation the large web deflections or the maximum tensile stresses (membrane and bending) are calculated. The differential Kármán-Marguerre's equation are used. To the solution of the system (1.1) Galerkin method of high number of  $w_{mn}$  and  $\phi_{mn}$  members is solved. The coefficients  $\sigma_m$  and  $\sigma_{m+b}$  for membrane and bending stresses are obtained. The unrestrained and restrained edges are discussed. For cyclic plasticity the uniaxial and multiaxial case of deformations is considered.

### INTRODUCTION

Fatigue crack growth considered historically as an empirical discipline by the mechanical engineers, meanwhile stability of members loaded in shear or of compression members has been solved by structural engineers.

The problem of large deflections of elastic isotropic or elasto-plastic webs is usually solved in static loading e.g. solution of the system Kármán-Marguerre's differential equations, ultimate load theories of web loaded in shear, etc. In the paper the effect of shear stresses is considered and the first attention is focused to the maximum tensile stresses on the opposite web corners or generally on the web boundary. The crack initiation starts at the points of maximum tensile stresses. Stability of web in cyclic loading at global instability sinks that means the structure reaches the limit state. At maximal loading stresses, the residual stresses do not reach, as a rule, the maximal value of tensile stresses.

The crack growth rate, denoted as the slope of crack growth curve  $da/dN$  is considered as extension of a crack occurring in one cycle.

The fatigue crack growth is plotted in the form

$$da/dN = B(\Delta S)^m$$



where  $\Delta S$  is the range of strain energy density factor, B and m are constants.

### 1. LARGE DEFLECTIONS OF WEB

For large web deflections we suppose that the load history may be the kind of structural and geometrical imperfections. For an elastic range the differential Kármán-Marguerre's equations

$$\begin{aligned}
 D \Delta \Delta (w-w_0) = t & \left[ \frac{\partial^2(\varphi+\varphi_0)}{\partial y^2} \frac{\partial^2 w}{\partial x^2} + \frac{\partial^2(\varphi+\varphi_0)}{\partial x^2} \frac{\partial^2 w}{\partial y^2} - \right. \\
 & \left. - 2 \frac{\partial^2(\varphi+\varphi_0)}{\partial x \partial y} \frac{\partial^2 w}{\partial x \partial y} \right], \\
 \Delta \Delta \varphi = E & \left\{ \left( \frac{\partial^2 w}{\partial x \partial y} \right) - \frac{\partial^2 w}{\partial y^2} \frac{\partial^2 w}{\partial x^2} - \right. \\
 & \left. - \left[ \left( \frac{\partial^2 w_0}{\partial x \partial y} \right)^2 \frac{\partial^2 w_0}{\partial y^2} \frac{\partial^2 w_0}{\partial x^2} \right] \right\}
 \end{aligned} \tag{1.1}$$

can be used, if satisfactorily large number of cycles is occurred. In the equations  $\varphi$  being the stress function,  $w_0$  and  $w$  the initial and additional deflections,  $D = \frac{E t^3}{12(1-\nu^2)}$  the flexural rigidity,  $E$  the Young's modulus,  $t$  the web thickness and  $\nu$  the Poisson ratio.

Let us have the simply connected domain  $\Omega = (0,a) \times (0,b)$ . The crack is supposed to be on the boundary of the domain where the maximal values of tensile stresses occur.

For the web loaded in shear, which example for the web of  $a/b = 2$  is given in the paper, the unrestrained edges solved by Galerkin method are discussed. To obtain an overall picture of the problem the influence of restrained edges in the webplate plane is shortly described.

It is necessary to distinguish the low and high width-to-thickness ratio of the web. In the case of lower width-to-thickness ratio the deflections of the web are distributed relatively uniformly and the influence of membrane stresses on the edges is negligible. For lower width-to-thickness ratio there is no difference between flexible and inflexible edges in the web plate plane.

If the web slenderness increases the position of maximum membrane web stress for flexible edges is changed. For inflexible web edges maximum membrane stresses are at the web corners  $x = 0, y = 0$ , or  $x = a, y = b$ . For flexible (unrestrained) edges the maximum membrane stresses are concentrated (except for the small slendernesses) at  $x = 0, 4a - 0,6a$  for  $y = 0, b$ , respectively. Maximum membrane and bending stresses for unrestrained edges are at  $x = 0, y = 0$  or  $x = a, y = b$ . The maximum difference of membrane stresses for restrained or for unrestrained web edges is at the critical loading. At the web loaded in shear for  $w_0/t = 0,7$  the difference is 17%, for  $w_0/t = 1,05$  is 19%.

In the solved example the homogeneous boundary conditions were used, e.g.

$$w = w_0 = 0/\Gamma, \quad \frac{\partial^2 w}{\partial n^2} = \frac{\partial^2 w_0}{\partial n^2} = 0 \tag{1.2}$$

where  $\Gamma$  is the boundary of the orthogonal domain and  $n$  is the independent variable in the direction of the normal to the domain boundary.

The biharmonic function  $\phi_0$  is chosen in the form

$$\phi_0 = -\lambda \alpha_E xy \tag{1.3}$$

where  $\lambda$  is the load parameter and  $\alpha_E = \frac{E t^2}{12(1-\nu^2)b^2}$ . In the web plate plane the conditions

$$\frac{\partial^2 \phi}{\partial y^2} = 0 /_{x=0,a}, \quad \frac{\partial^2 \phi}{\partial x^2} = 0 /_{y=0,b}, \quad \frac{\partial^2 \phi}{\partial x \partial y} = 0 /_{\Gamma} \tag{1.4}$$

are used.

## 2. SOLUTION TO THE SYSTEM (1.1)

The Papkovitch or Galerkin method is successfully used in a solution to the formulated problem. In the former case it is the differential equation of deformation compatibility that is solved exactly, while the differential equation of equilibrium is solved approximately. In the latter case both equations are solved approximately. In both cases, however, the problem leads to a solution of a system of nonlinear algebraic equations. Further we will use the Galerkin method of high number of  $w_{mn}$  and  $\phi_{mn}$  members.

The functions of the initial and total deflections are considered in the form

$$w = \sum_m \sum_n w_{mn} \sin \frac{m\pi x}{a} \sin \frac{n\pi y}{b} \tag{2.1}$$

$$w_0 = \sum_m \sum_n w_{0mn} \sin \frac{m\pi x}{a} \sin \frac{n\pi y}{b}$$

The stress function is assumed as follows

$$\phi = \sum_{r=2} \sum_{s=2} \phi_{rs} \left[ \cos \frac{r\pi x}{a} - \cos (1-(-1)^r) \frac{r\pi x}{2a} \right] \left[ \cos \frac{s\pi y}{b} - \cos (1-(-1)^s) \frac{s\pi y}{2b} \right] \tag{2.2}$$

The nonlinear algebraic equations (1.1) as Euler equations are computed from the functional

$$Q(\lambda, \phi, w) = \int \left\{ \frac{D}{2} [\Delta(w-w_0)]^2 - \frac{t}{2E} (\Delta\phi)^2 + \frac{t}{2} \left[ \frac{\partial^2(\phi+\phi_0)}{\partial x^2} \left(\frac{\partial w}{\partial y}\right)^2 + \frac{\partial^2(\phi+\phi_0)}{\partial y^2} \left(\frac{\partial w}{\partial x}\right)^2 - 2 \frac{\partial^2(\phi+\phi_0)}{\partial x \partial y} \frac{\partial w}{\partial x} \frac{\partial w}{\partial y} \right] - \frac{t}{2} \left[ \frac{\partial^2(\phi+\phi_0)}{\partial x^2} \left(\frac{\partial w_0}{\partial y}\right)^2 + \frac{\partial^2(\phi+\phi_0)}{\partial y^2} \left(\frac{\partial w_0}{\partial x}\right)^2 - 2 \frac{\partial^2(\phi+\phi_0)}{\partial x \partial y} \frac{\partial w_0}{\partial x} \frac{\partial w_0}{\partial y} \right] \right\} d\Omega \tag{2.3}$$

The system of algebraic equations is obtained and the coefficients  $w_{mn}$  and  $\phi_{mn}$  for  $a/b = 1, 2, 3$  are solved in [1] (the author Sadovský, Z.). Numerical solution of algebraic equations is given in tables, from which as

Table 1. Web loaded in shear,  $a/b = 2$ ,  $|w_0| / t = 1,05$

$w_{mn}$	$w_0$	$\lambda$			$\psi_{mn}$	$\lambda$		
		3,27	6,54	9,81		3,27	6,54	9,81
$w_{12}$	-0.257105	-0.418517	-0.706628	-1.137978	$\psi_{22}$	-0.02697110	0.08520671	-0.18244752
$w_{14}$	-0.004171	-0.011280	-0.030877	-0.070992	$\psi_{24}$	-0.00164724	-0.00632372	-0.01593082
$w_{21}$	0.932341	1.348351	1.969763	2.669109	$\psi_{26}$	-0.00018651	-0.00080328	-0.00226820
$w_{23}$	-0.064905	-0.105133	-0.192290	-0.358193	$\psi_{28}$	-0.00006834	-0.00031561	-0.00094986
$w_{25}$	-0.004245	-0.007632	-0.016404	-0.036426	$\psi_{33}$	0.00409500	0.01008262	0.01322097
$w_{32}$	0.284098	0.479523	0.834216	1.343306	$\psi_{35}$	0.00071234	0.00198776	0.00253110
$w_{34}$	0.004652	0.009936	0.019875	0.027947	$\psi_{37}$	0.00020957	0.00056302	0.00062305
$w_{41}$	-0.109037	-0.131243	-0.134411	-0.106220	$\psi_{42}$	0.00806839	-0.02550077	-0.05485996
$w_{43}$	0.028743	0.053102	0.116385	0.240989	$\psi_{44}$	0.00092800	0.00398378	0.01005881
$w_{45}$	0.002369	0.004385	0.009904	0.021175	$\psi_{46}$	0.00022508	0.00114539	0.00332002
$w_{52}$	0.014507	0.027356	0.068229	0.166637	$\psi_{48}$	0.00004919	0.00024946	0.00072227
$w_{54}$	0.001802	0.003870	0.012753	0.041421	$\psi_{53}$	-0.00363025	-0.01066000	-0.01973441
$w_{61}$	-0.012337	-0.023840	-0.050986	-0.092121	$\psi_{55}$	-0.00051337	-0.00117047	-0.00079423
$w_{63}$	0.006536	0.010733	0.020919	0.051510	$\psi_{57}$	-0.00016872	-0.00044642	-0.00054543
$w_{65}$	0.000845	0.001613	0.004170	0.013893	$\psi_{62}$	-0.00113246	-0.00524039	-0.01400503
$w_{72}$	0.003634	0.007255	0.011331	0.009106	$\psi_{64}$	-0.00070142	-0.00298215	-0.00681017
$w_{74}$	0.000895	0.001601	0.002785	0.005293	$\psi_{66}$	-0.00020082	-0.00090219	-0.00211880
$w_{81}$	0.002890	-0.003934	-0.005657	-0.014941	$\psi_{73}$	-0.00043865	-0.00284891	-0.00907984
$w_{83}$	0.002155	0.004353	0.009353	0.013742	$\psi_{75}$	-0.00003755	-0.00070246	-0.00305404
$w_{92}$	0.001181	0.002462	0.006594	0.011936	$\psi_{82}$	-0.00010169	-0.00030269	-0.00058775
					$\psi_{84}$	-0.00008486	-0.00037096	-0.0002794
					$\psi_{86}$	0.00003456	-0.00004318	-0.00096569
					$\psi_{93}$	-0.00010589	-0.00040518	-0.00187269
					$\psi_{104}$	-0.00004839	-0.00025075	-0.00100253
					$\psi_{113}$	-0.00010061	-0.00045858	-0.00115453

an example the Table 1 for  $a/b = 2$ ,  $|w_0| / t = 1,05$  and  $\lambda = 3,27; 6,54$  and  $9,61$  is presented.

The stresses on digigraph DGF 1712 in Computer Centre of SAS were plotted according to which the coefficient

$$\rho = \frac{\tau_{xy} \sqrt{3}}{\sqrt{\sigma_x^2 + \sigma_y^2 - \sigma_x \sigma_y + 3\tau_{xy}^2}} \quad (2.4)$$

was calculated.

The stresses  $\sigma_x, \sigma_y, \tau_{xy}$  in (2.4) express either the membrane stresses

$$\begin{aligned} \sigma_{x,m} &= \frac{\partial^2(\varphi+\varphi_0)}{\partial y^2}, & \sigma_{y,m} &= \frac{\partial^2(\varphi+\varphi_0)}{\partial x^2} \\ \tau_{xy,m} &= - \frac{\partial^2(\varphi+\varphi_0)}{\partial x \partial y} \end{aligned} \quad (2.5)$$

or the membrane and bending stresses.

The bending stresses are written in the form

$$\begin{aligned} \sigma_{x,b} &= \pm \frac{Et}{2(1-\nu^2)} \left( \frac{\partial^2(w-w_0)}{\partial x^2} + \nu \frac{\partial^2(w-w_0)}{\partial y^2} \right) \\ \sigma_{y,b} &= \pm \frac{Et}{2(1-\nu^2)} \left( \frac{\partial^2(w-w_0)}{\partial y^2} + \nu \frac{\partial^2(w-w_0)}{\partial x^2} \right) \\ \tau_{xy,b} &= \pm \frac{Et}{2(1+\nu)} \frac{\partial^2(w-w_0)}{\partial x \partial y} \end{aligned} \quad (2.6)$$

where  $w$  is the total deflection function of the web.

The obtained results for  $a/b = 2$  ( $\tau_{cr} = 6,54 \sigma_E$ ) are shown in Fig. 1.

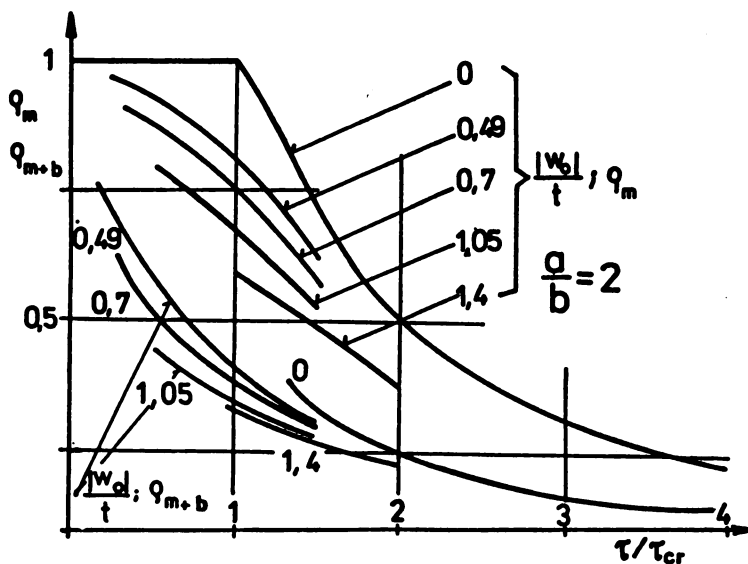


Fig. 1 Coefficients  $q_m$  and  $q_{m+b}$

In the solution the web flanges were not assumed, e.g. that the membrane and bending stresses are considered as maximum possible value of the web.

### 3. CYCLIC PLASTICITY

#### 3.1 Uniaxial case of deformation

The total strain can be decomposed into a plastic rate and elastic rate

$$\dot{\epsilon} = \dot{\epsilon}_e + \dot{\epsilon}_p, \quad (3.1)$$

where  $\epsilon$ ,  $\epsilon_e$ ,  $\epsilon_p$  are the total, elastic and plastic strain respectively and the dot over each one denotes the material time derivatives or rate. Since  $\epsilon = \sigma/E$ ,  $\epsilon_e = \sigma/E_e$  and  $\epsilon_p = \sigma/E_p$ , where  $\sigma$  is the stress rate,  $E_t$ ,  $E_e$  and  $E_p$  are the total, the elastic and the plastic moduli respectively.

From (3.1) we have

$$\frac{1}{E_t} = \frac{1}{E_e} + \frac{1}{E_p} \quad (3.2)$$

When the elastic deformation takes place, the value is infinite and from (3.2)  $E_t = E_e$ . When  $E_e$  is constant or changing continuously, the plastic modulus  $E_p$  at the onset of yielding must be infinite for such a smooth transition.

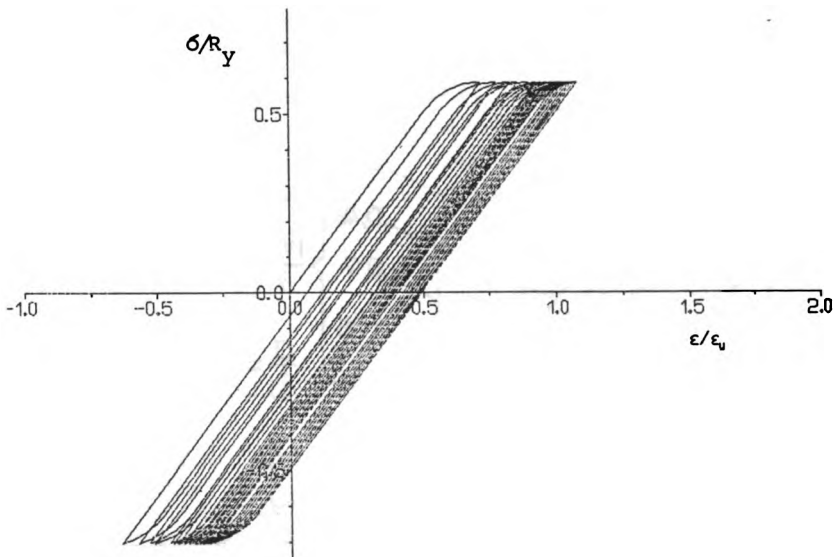


Fig. 2 Cyclic tensil and compressive stress of web

Numerous experimental investigations onto the behaviour of metals have been carried out. The experimental results frequently differ from each other and sometimes the results of various tests even seem contradictory. However, when taking account of different experimental conditions, we can conclude that there exist straininduced anisotropy of material in the domain beyond the yield limit.

As an example the numerical results for an onedimensional element in elasto-plastic cyclic loading are shown in Fig. 2.

The greatest buckling coefficient in compression  $\sigma/R_y = 0.6$  and that one in tension  $\sigma/R_y = 0.7$ . The total and the elastic modulus is considered in the form  $E_t = 9000$  MPa and  $E_e = 210\ 000$  MPa.

### 3.2 Multiaxial case of deformation

A basic relationship for the theory of elasto-plastic deformation is [2]

$$\sigma = F(\epsilon_e) \quad (3.3)$$

where the effective stress  $\sigma_e$  and the effective deformation  $\epsilon_e$  for two axial case is

$$\begin{aligned} \sigma_e &= (\sigma_x^2 + \sigma_y^2 - \sigma_x \sigma_y + 3 \tau_{xy}^2)^{1/2} \\ \epsilon_e &= \frac{\sqrt{2}}{3} \left[ (\epsilon_x - \epsilon_y)^2 + (\epsilon_y - \epsilon_z)^2 + (\epsilon_z - \epsilon_x)^2 + \frac{3}{2} \tau_{xy}^2 \right]^{1/2} \end{aligned} \quad (3.4)$$

The relationship (3.3) can be determined for every material, for example using a tensile test. Then

$$\begin{aligned} \sigma_y = \sigma_z = \tau_{xy} = 0, & \Rightarrow \sigma_e = \sigma_x, \\ \epsilon_y = \epsilon_z = -\nu' \epsilon_x, & \Rightarrow \epsilon_e = \frac{2(1+\nu')}{3} \epsilon_x \end{aligned}$$

When the dependance  $\sigma_x - \epsilon_x$  is obtained from tensile tests for the uniaxial case of a static and cyclic loading, the relationship  $\sigma_e - \epsilon_e$  is then found out by multiplying  $\sigma_x$  by the quantity  $2(1+\nu')/3$ .

The solution of a basic system of Kármán-Marguerre's differential equation, generalized for elasto-plastic web for one static loading can be found in [2], p. 178.

Generally speaking failure does not occur instantaneously. It initiates with subcritical crack growth prior to reach the unstable crack propagation. Before the unstable crack the web deflections or tensile stresses not connected else with macro- or micro crack may be calculated.

The limit state of the web for static loading is defined by that load under which the maximum membrane stress reaches the yield stress [2], p. 95. Elastic membrane and bending stress Fig. 1 which we use for cyclic loading would be very near to fatigue live stress  $\sigma_{fat}$ .

It is very important to know how much is the maximum tensile effective stress (membrane and bending) before the crack propagation.

## 4. RESIDUAL STRESSES

### 4.1 Welding residual stresses

First, the residual stresses developed as a result of the welding process are considered. Welds as well as their immediate vicinity are subjected to tension equal to the yield stress and the remainder of the cross-section is subjected to residual compression. As the web has been cooled the longitudinal stresses near the weld remain very close to the yield stress of the material.

It is advantageous to work with idealized rectangular residual stresses, which satisfactorily describe the stress distribution. In civil engineering structures, the tension zone is assumed to extend the distance  $c = 2t$  to  $c = 4t$ , where

$t$  is thickness of web sheet. The residual stress on loaded boundaries of the web is of the form  $n_r = R_y \times 2c/(b - 2c)$ , where  $n_r$  is the compressive residual stress and  $b$  is the web panel width. If we assume the value  $c = 3t$ , the yield stress of the material  $R_y = 230$  MPa, the geometrical imperfections  $w_0 = b/100$  and flexible in the web plane unloaded edges, the resulting maximum residual stresses  $n_r$  for width-to-thickness ratio of the web, calculated according large deflection theory, are as follows:

$b/t$	30	45	60	90
$n_r/R_y$ %	20.6	8.13	6.85	3.02

For lower  $w_0$  the residual stress would be smaller. So, for example, if  $w_0 = b/200$  and  $b = 30$ , the residual compressive stress  $n_r/R_y = 9.83\%$  and for  $b/t = 60$ ,  $n_r/R_y = 3.44\%$ .

These results for geometrical imperfection  $w_0 = b/200$  are in very good agreement with one of the conclusion of the international Task Group Tolerances in Steel Plated Structures [3]. It should be mentioned that the welding residual stress depends not only of the web slenderness but also from the geometrical imperfections.

#### 4.2 Compressive residual stresses and fatigue crack closure

Consider a plate with a central hole loaded in tension shown in Fig. 3. For technical material and sufficiently high load, plastic deformation occurs near the edge of the hole. The unloading will cause elastic deformation and compressive residual stress distribution exceeding the compressive yield limit will occur near the hole. The remainder of the cross-section is subject to residual tension.

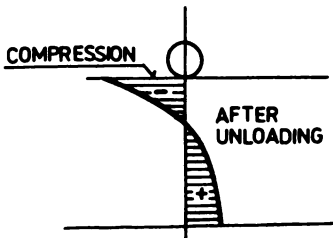


Fig. 3 Residual stress at fatigue crack closure

called crack closure and was first observed by Elber, W. [4]. The problem is how to calculate the stresses in the tension zone. Effective stress intensity factor of the crack arises and empirical results are used founded on crack closure measurements.

The same procedure could be used as in welding residual stresses where  $n_r$  would be the tensile residual stress. As in welding residual stresses, the maximum residual stresses  $n_r$  for width-to-thickness ratio of the web may be calculated.

It should be mentioned that tensile residual stresses in fatigue crack closure go to zero with increasing width-to-thickness ratio  $b/t$ .

### 5. STRAIN ENERGY DENSITY THEORY

#### 5.1 Conditions of crack growth

To study the problem of initiation, stable and unstable growth of crack the strain energy density function,  $\partial W/\partial V$ , is used. For continuum element we have

the relation

$$\frac{dW}{dV} = \int \epsilon_{ij} \sigma_{ij} d \epsilon_{ij} \quad (i, j = 1, 2, 3 \dots) \quad (5.1)$$

where  $\sigma_{ij}$  and  $\epsilon_{ij}$  are the stress and strain components, respectively. In the linear elastic range  $dW/dV = \sigma_{ij} \epsilon_{ij} / 2$ .

Material damage is time dependant. It can be expressed by the relation

$$\frac{dW}{dV} = \frac{S}{r} \quad (5.2)$$

where  $S$  is the strain energy density factor and  $r$  is the linear distance of studied crack growth. Once  $(dW/dV)_c$  and  $S_c$  are known from tests, the critical distance parameter  $r_c$  follows from equ. (5.2). According to (5.2) the stress at the beginning of stable growth is obtained [6.7]:

$$\sigma_1 = \frac{1}{F(a/b)} \left( \frac{2 E r_0 (dW/dV)^{1/2}}{(1+\nu)(1-2\nu)a_0} \right) \quad (5.3)$$

Example: Let us have a steel with the following properties :

$E = 210\,000 \text{ MPa}$ ,  $\nu = 0,3$ ,  $\sigma_Y = 520 \text{ MPa}$ ,  $(dW/dV) = 187.734 \text{ MJ/m}^3$ ,  
 $S_c = 13,485.10^3 \text{ N/m}$ .

The values  $r_c$  is calculated as  $r_c = S_c / (dW/dV)_c = 7,183.10^{-3}$ , in while  $r_0 = 3.10^{-3}$ , which is considered to be a material constant. Let us have  $F(b/h) = 1$  then the stress at crack initiation according to (5.3) is  $\sigma_1 = 427,62 \text{ MPa}$ . Critical stress at global instability at crack length  $a_0 = 2,5 \text{ cm}$  (for  $h = \infty$ )  $\sigma_s = 580 \text{ MPa}$  [5.7]. The difference  $\sigma_s - \sigma_1 = 165 \text{ MPa}$ .

## 5.2 Fatigue crack growth

The crack growth rate denoted as the slope of crack growth curve  $(da/dN)$  is considered as an extension of a crack occurring in one cycle. The crack growth is plotted in the form  $da/dN = B(\Delta S)^m$ , where  $\Delta S$  is the range of strain energy density factor,  $a$  is the crack length and  $N$  the number of cycles.

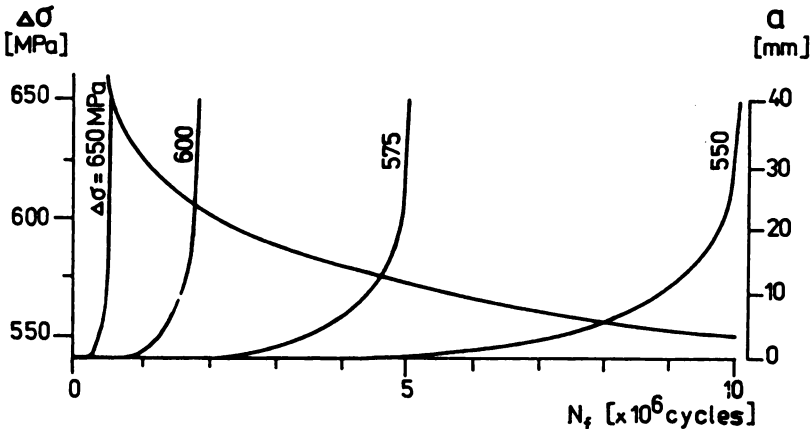


Fig. 4 Fatigue life curve for edge cracked web



It is supposed that the stable crack growth is not connected with the web deflection changes.

For simple solution we assume that the fatigue crack at the length  $2a_0$  (in the web thickness direction) on the web boundary grows in the direction to the web centre.

The number of cycles is considered in the form

$$N_f = \sum_{i=1}^j \frac{a_i - a_{i-1}}{B (\Delta S)^m} \quad (5.4)$$

The constant are as follows:  $B = 6181.10^{-11}$ ,  $m = 1,414$ , the number of elements  $j = 26$  and  $\Delta S = 50$  to  $8000 \text{ J/m}^2$ . The material properties are given by  $\sigma_{fl} = 517 \text{ MPa}$ ,  $(\partial W / \partial V)_C = 48,46 \text{ MJ/m}^3$ ,  $K_{1C} = 103,52 \text{ MPa } \sqrt{\text{m}}$ ,  $S_C = 13,485 \text{ kN/m}$ ,  $c = 2t$  and  $\Delta t = 1 \text{ mm}$ .

Some results are analysed in Fig. 4.

#### REFERENCES

1. DJUBEK, J. - SADOVSKÝ, Z. and RAVINGER, J.: Non-Linear Problems of Stiffened Webs and Shallow Shells. Report P-12-124-003-02/2d, Inst. of Construction and Architecture of SAS, 1975 (in Slovak).
2. DJUBEK, J. - KODNÁR, R. - ŠKALOUD, M.: Limit State of the Plate Elements of Steel Structures. Birkhäuser Verlag, Basel-Boston-Stuttgart, 1983.
3. MASSONNET, Ch.: IABSE TASK GROUP "Tolerances in Steel Plated Structures", IABSE Surveys, S-14/80, Zurich 1980, pp. 49-76.
4. ELBER, W.: Fatigue Crack Closure under Cyclic Tension. Engng. Fracture Mech. 2/1970/37. The significance of fatigue crack closure. ASTM STP 486, 1971, 230.
5. GDOUTOS, E.E. and SIH, G.C.: Crack Growth Characteristics Influenced by Load Time Record. Theor. and Appl. Fracture Mechanics 2, 1984, pp. 91-103.
6. DJUBEK, J.: Fatigue Crack Growth at Consideration of Material and Geometric Nonlinearity. Staveb. Čas. No.4, 1988 (in Slovak).

**New Lighting Technologies in TV and Film Studios and Their Reflexes to The Structural Steelwork**

Slobodan Cvetkovic  
Mostprojekt, Palmira Toljatija 11  
11070 Beograd, Yugoslavia

**Summary**

This paper gives the basic idea of structural steelwork for lighting grids in TV and film studios which ought to be assembled in very narrow tolerances even for 1000 sqm studio area.

The lighting must give an illusion of reality and spectator must enter without restraint into the screen of his receiver or of his cinema. Therefore to recreate this illusion it is necessary to place light sources around and above the sets so that they cannot be seen in the line of vision (always an illusion), and they must be independent of the work area in the stage.

In order to get the most economical use of expensive multipurpose studio space, it is very important to reduce the spotlight adjustment time. The new studio lighting technology developed by Telestage, practically was used first time in Belgrade Television about twelve years ago. It gives the opportunity to get flexible spotlight arrangement in very short time. The new technologic requirements need new type of lighting grid structure - ie. some kind of suspended ceiling. It is formed of numerous platforms (dimensions appr. 1,50 x 1,00 m) which cover the whole studio area of 300 to 1000 m<sup>2</sup>.

All these platforms are arranged in the way to get free space of 65 mm between each platform, forming orthogonal system of slots (figure 2). This slot system carries many telescope units for spotlights (figure 3).

Every new scene or stage in the studio has new requests for lighting arrangement, ie the spotlight shall be then rearranged. All light adjustments practically are carried out over grid platforms. During the light arrangements, each spotlight telescope unit which is properly positioned, is translatory transferred to the parking slot for further light focusing leaving the main slot for next telescope unit. This brilliant idea should be followed with adequate grid steelwork.

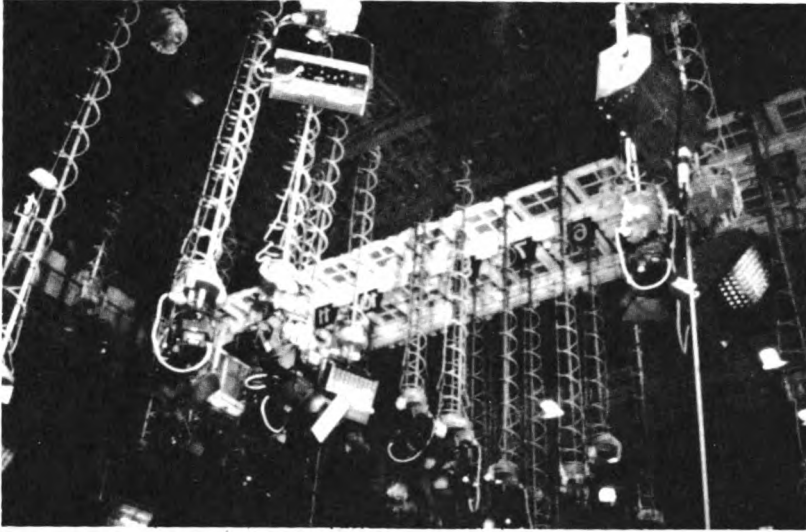


Figure 1. Spotlights in studio

The rigidity of whole grid structural system is necessary, together with requests for very narrow tolerances in slot assembling: distance between two platforms ought to be 65 mm +/- 1 mm followed with maximal differences in adjacent platform levels of 0,5 mm due to specific construction of spotlight units with telescope suspension length of appr. 10.000 mm.

The author's solution of grid steelwork for few TV studios which have been built in Yugoslavia (figure 1, 2), compromise necessary accuracy in grid steelwork assembling with tolerances in studio building structure. At the same time, the future reassembling of platform positions (each 5-10 years) is very easy and does not need long brakes in studio use.

The main elements of lighting grid are:

1. Grid overhead beams placed at the distances of 3-6 m; cross section two channels. They have rigid connections with roof supporting structure.
2. Grid hangers and grid supporting beams. The crosssection of these elements allows assembling of electric cables, contact sockets and lighting equipment. They are spaced at 1500 mm distances.
3. Grid cantilevers which supports the grid platforms. (figure 4).
4. Grid platforms formed of two parts:
  - a) frame - path for telescope units (as main part of grid structure) and
  - b) grating. (figure 5)

The templates and welding process control shall be used in frame fabrication in order to prevent shrinkage and distortion. The grating is connected to the frame by screws.

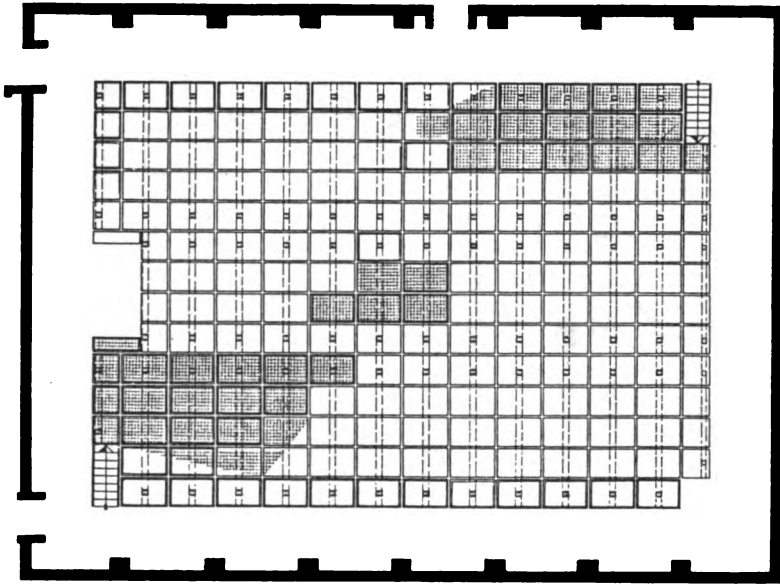


Figure 2. Plan view of lighting grid with parking slots

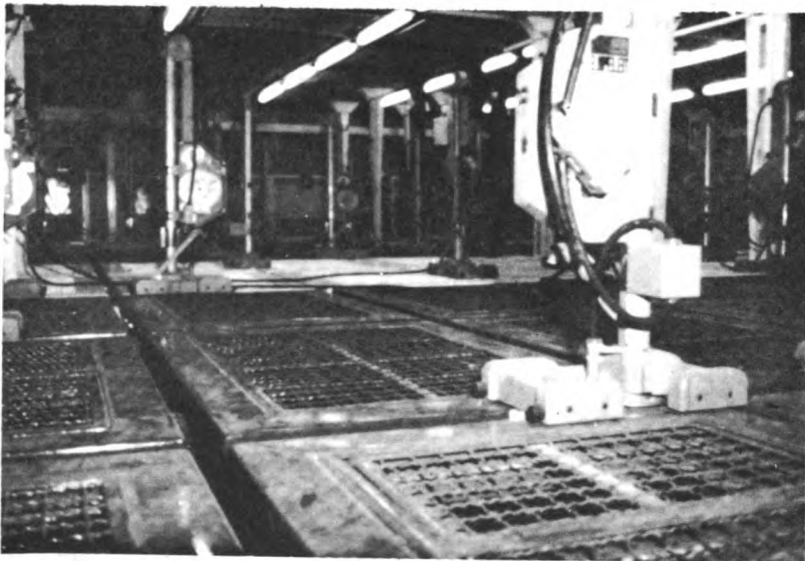


Figure 3. Trolley of telescope unit in parking slot

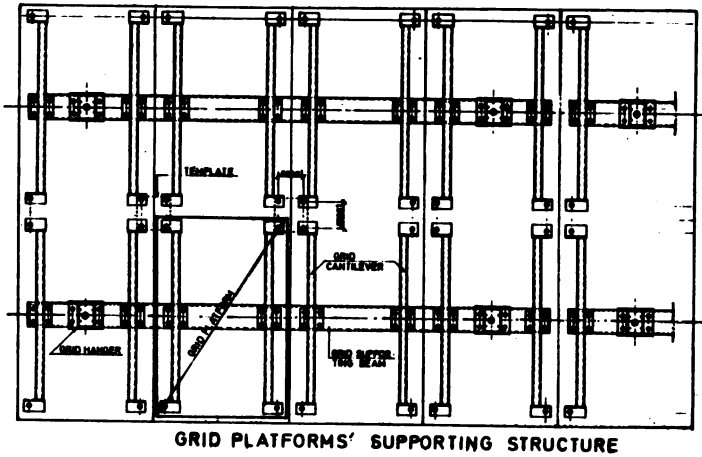


Figure 4.

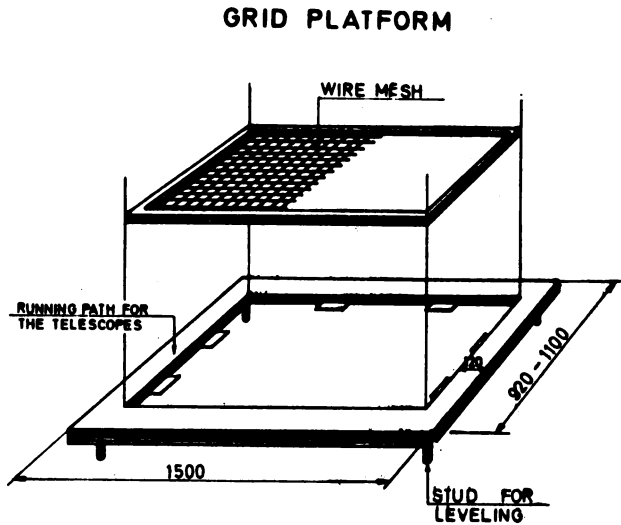


Figure 5.

The assembling of the lighting grid steelwork shall be done in following order:

- grid overhead beams, hangers and grid supporting beams are placed and properly adjusted. It is necessary supporting beams to be horizontal together with plan tolerances of  $\pm 2$  mm.
- Grid cantilevers assembling. Their adjusting in plan shall be done by means of templates in order to get proper accuracy in plan for grid platform supports. The final levelling of grid platforms shall be done over supporting threaded studs (each equipped with washers and nuts) which are welded in each corner of platform frame.

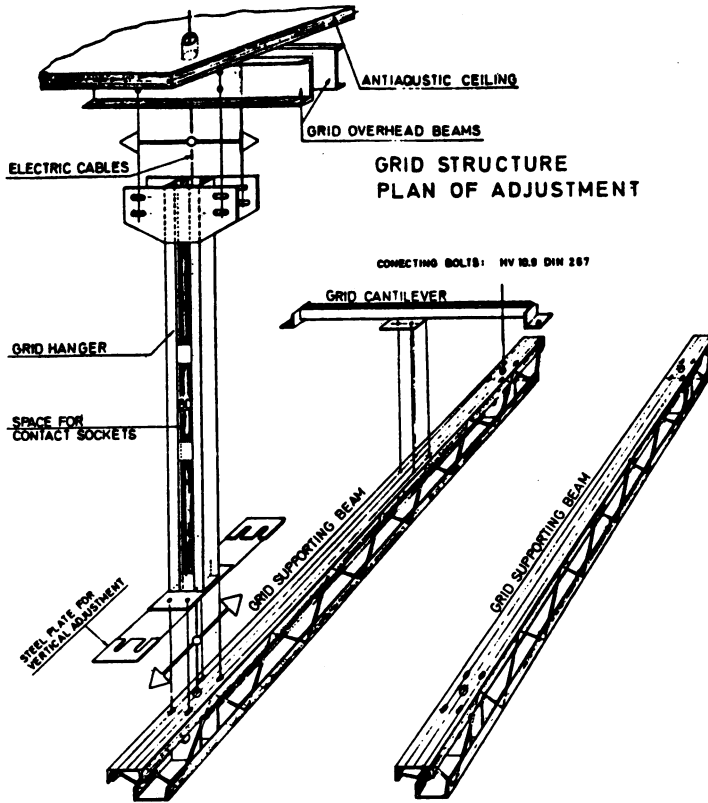


Figure 6.

\* \* \* \*

The film lighting technology and equipment are not the same as for TV, but the basic principles are similar. The new film studio of Jadran-film Zagreb are completely equipped according to the author's design which was based on the owner's requirements for modern and flexible lighting positioning. The studio is in use about one year and basic ideas for lighting grid and equipment are veified through more then six movies.

Along studio walls, the galleries are placed at levels +4.00 m and + 6.60 m. They are used ase "cat-walks" and their tube railings can carry spotlights and flood lights equipped with standard clips. The lighting grid structure consists of 7 pairs of rails (channels) going parallel to the longitudinal studio axis, cat-walks at the grid level and at level of + 11,0 m and one pair of transverse rails placed paralel to the gable wall (figures 6, 7, 8, 9, 10, 11).

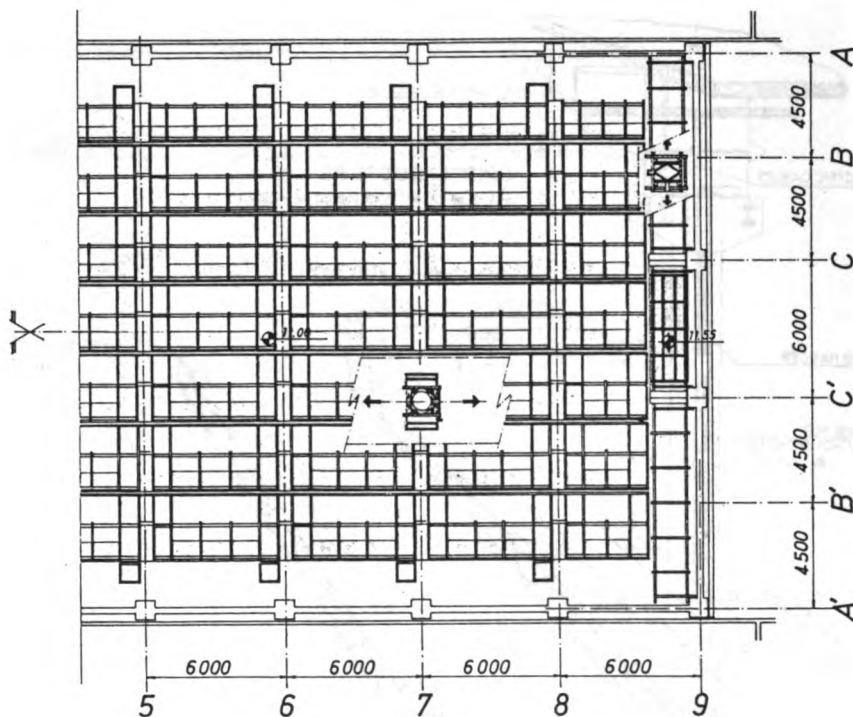


Figure 7. Grid layout

The rail system carries the number of platforms. There are two types of platforms:

A. TELESCOPE PLATFORM (cca 3.0 m<sup>2</sup> in plan) in form of rigid "cage" which is suspended on motorized trolley which is moving along the rails. The cage is formed as two-part telescope with two degrees of freedom: +/- 90 rotation in plan and platform lifting between + 4.00 m and + 6.70 m levels. If it is necessary to have some spotlights under + 4.00 m level, the platform may be equipped with hoist system - steel tube suspended by two cables and winch drums, lowering light sources at necessary level. The communication with platform is possible over grid cat-walks, either from the ladder or special giraffe platforms (standard studio equipment) from the floor level. Each platform is equipped with two remote control boxes:

- fixed remote control box on the platform level with commands: platform moving up and down, platform rotation and connection for hoist command system.
- portable remote control box at grid cat-walk level with commands: platform moving up and down, platform rotation, trolley moving. Trolley moving command is effective only when platform has no rotation.

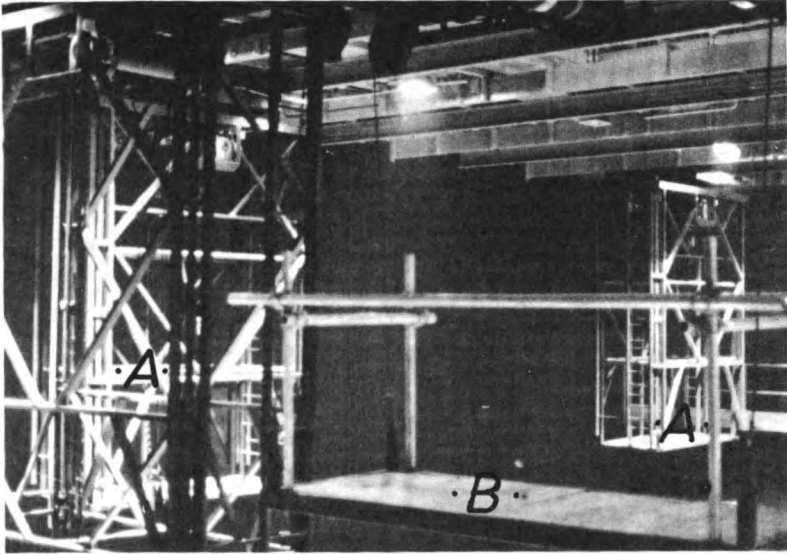


Figure 8. Platforms in studio

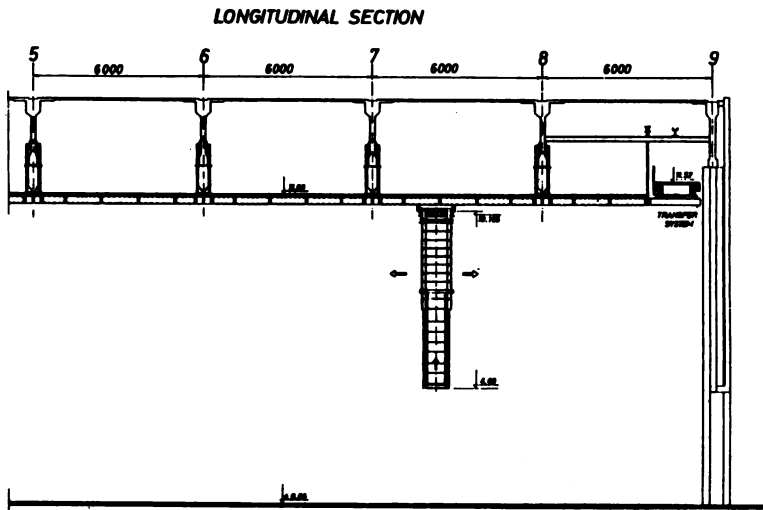


Figure 9.



### CROSS SECTION

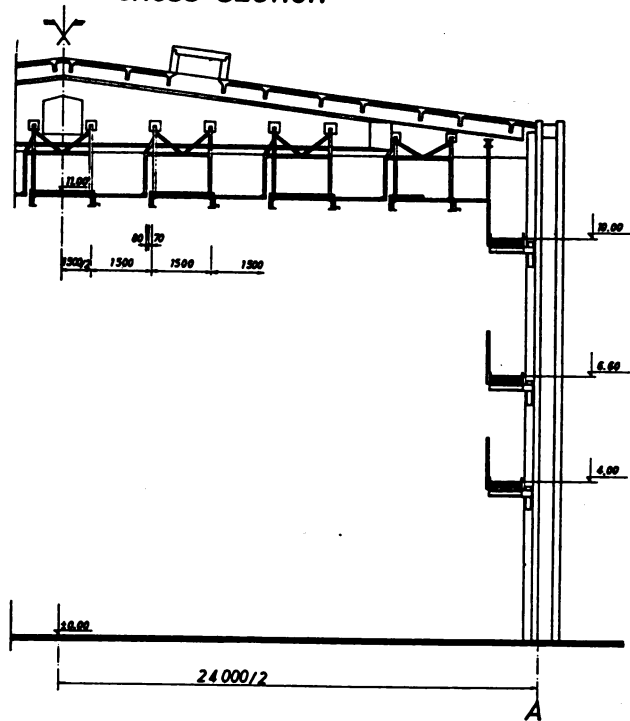


Figure 10.

**B. FLEXIBLE PLATFORM** - suspended by four cables (one in each corner) moving up and down by mean of pulleys fixed on the trolley, winding on winch drums. This type of platform has the same functions as first one. It may be lowered from + 10.0 m level to the floor level. When platform is properly positioned, it ought to be horizontally braced by means of ties or standard tube scaffolding elements. Few of this platforms may be connected in the way to form some kind of bridge. Communication with this type of platform is from floor level. This type of platforms is used when it's necessary to have high concentration of spotlights in limited space.

The transverse pair of rails, parallel to the gable wall, carries special trolley in order to have transfer system for units A and B. It allows to have full concentration of platform units along only one or two pairs of rails in very short time, which gives maximal flexibility to the lighting positioning according to the film director's requests. Parallel to the transfer system, just under the studio roof structure, the overhead single rail crane is assembled - it allows lowering whole platform units in case of repair.

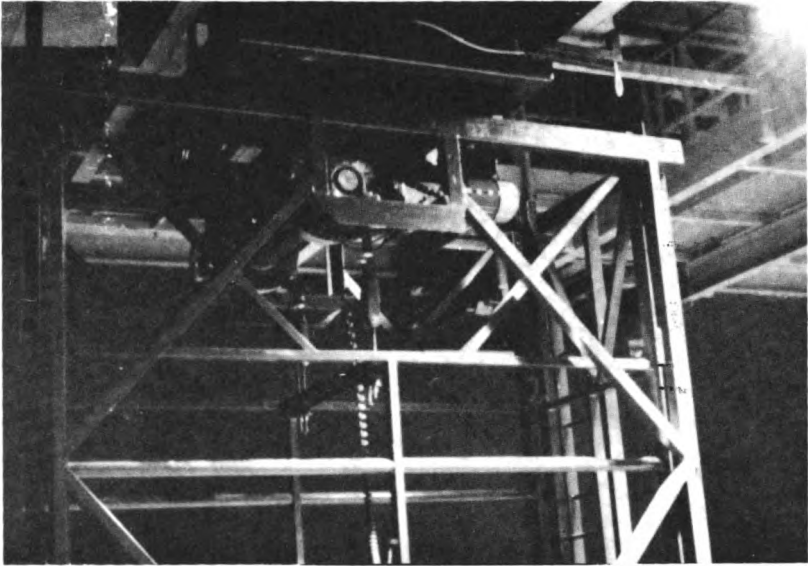


Figure 11. Detail of telescope platform-type A.



## CONTRIBUTION TO THE NUMERICAL SOLUTION OF THE CABLE

Dragoljub Grbić

Department of Applied Mechanics and Structural Analyses,  
Faculty of Civil Engineering, University of Belgrade

### SUMMARY

In the present paper the elastic cable subjected to its dead weight, following distributed and live distributed loading is investigated. Numerical solution for the displacement and forces is described using the integral matrix and Newton-Raphson's method. Finally, numerical example is presented.

### 1. EQUATIONS OF THE PROBLEM

Consider the catenary loaded with its dead weight only. Cartesian coordinate  $y(x)$  determinates position of arbitrary point of the catenary. The horizontal force  $H_0$  is given. Required boundary conditions for the inextensible chain are:  $x=0, y=0$  and for  $x=1, y=h$ .

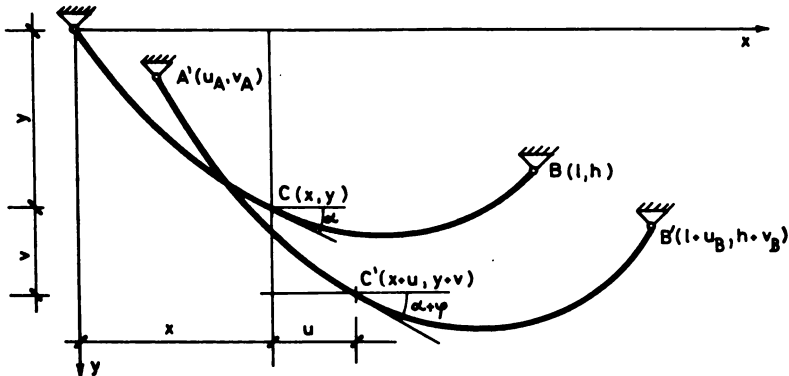


Fig. 1 Geometry of the catenary

Considered catenary is under the action of distributed loading: dead weight  $g_y$ , following forces  $p_\tau$  and  $p_n$  and live loading  $p_x$  and  $p_y$ , see Fig. 2.

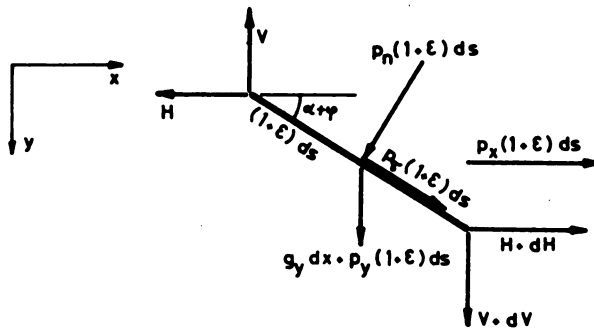


Fig. 2. Element of the cable

The equations that describe the problem are:

$$\frac{du}{dx} = (1 + \epsilon) \sec \alpha \cos(\alpha + \phi) - 1, \quad (1)$$

$$\frac{dv}{dx} = (1 + \epsilon) \sec \alpha \sin(\alpha + \phi) - \text{tg } \alpha, \quad (2)$$

$$\frac{dH}{dx} = - p_x^* \sec \alpha, \quad (3)$$

$$\frac{dV}{dx} = - p_y^* \sec \alpha, \quad (4)$$

$$S = \sqrt{H^2 + V^2}, \quad (5)$$

$$\epsilon = \frac{S}{EF} + \alpha_t \Delta t, \quad (6)$$

$$\text{tg } \alpha = \frac{V}{H}, \quad (7)$$

where:  $ds$  - differential length of the cable arc,  $\epsilon$  - dilatation,  $E$  - Young's modulus,  $F$  - cross sectional area,  $\alpha_t$  - temperature coefficient and  $\Delta t$  - temperature increment.

Boundary conditions are:

$$\text{for } x=0 \quad u=u_A \quad v=v_A$$

$$\text{for } x=1 \quad u=u_B \quad v=v_B,$$

where  $u_A, u_B, v_A, v_B$  are prescribed displacements of the catenary end sections.

The solution of the above described boundary-value problem represents the state of the stress and deformation of the catenary under prescribed geometrical and mechanical conditions, given loading, temperature increment and boundary conditions.

To the differential equations (1), (2), (3) and (4) the integral matrix is applied. Unknown end forces at  $x=0$  may be obtained from the boundary conditions. Loading  $p_T$  and  $p_n$  are applied in the increments from zero up to the final level. For any increment the iterative process is performed and for every iteration the corresponding partial derivatives are determined.

## 2. NUMERICAL EXAMPLE

The problem given in Fig. 3 for the following numerical data is investigated:

$$l = 400 \text{ m}$$

$$y(0) = 0 \text{ m}$$

$$y(1) = 100 \text{ m}$$

$$u(0) = u(1) = y(0) = y(1) = 0 \text{ m}$$

$$g = 0,03732 \text{ kN/m}$$

$$H_0 = 15,75 \text{ kN}$$

$$F = 1107,08 \times 10^{-6} \text{ m}^2$$

$$E = 68,65 \times 10^6 \text{ kN/m}^2$$

$$p = 0,001 (y + v) \text{ kN/m}$$

$$\text{calculated } H(0) = 50,15 \text{ kN}$$

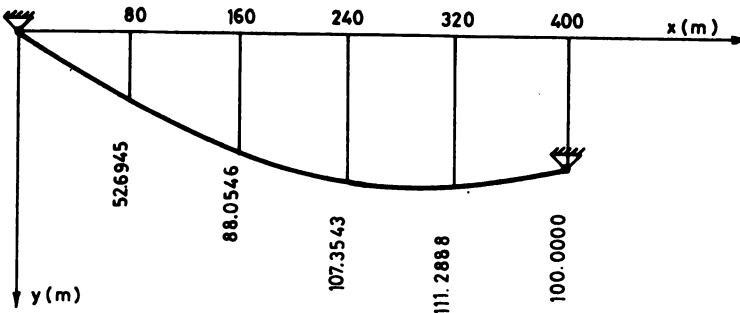


Fig. 3. Geometry of the inextensible catenary

Numerically, the problem is solved in the sequence of the cross sections. The ordinates  $y$  and angles  $\alpha$  for undeformed state and displacements and forces for the extensible catenary have been found. The results of the numerical solution are shown (diagram and Table) in Fig. 3.

$i$	$S_i \sin (\alpha_i + \phi_i)$ kN	$y_i$ m	$\alpha_i$
1	34.43377	0	.6588371
3	33.35758	14.89132	.6208327
5	32.03132	28.61738	.5817667
7	30.47433	41.20902	.5416706
9	28.70386	52.6945	.5005834
11	26.73587	63.09962	.4585516
13	24.58578	72.44774	.4156294
15	22.26905	80.75984	.3718785
17	19.80159	88.05461	.3273682
19	17.20001	94.34841	.2821749
21	14.48181	99.65537	.2363818
23	11.66537	103.9874	.1900779
25	8.769957	107.3543	.1433579
27	5.815592	109.7635	9.632075E-2
29	2.822878	111.2205	4.906888E-2
31	-.1871971	111.7286	1.707131E-3
33	-3.193484	111.2888	-4.565845E-2
35	-6.174906	109.9003	-9.292176E-2
37	-9.110691	107.5598	-.1399779
39	-11.98058	104.2622	-.1867241
41	-14.765	100	-.2330611

i	$S_i$ kN	$v_i$ m	$u_i$ m
1	60.83061	0	0
3	60.30945	-.9154845	.6756152
5	59.81629	-1.416977	1.034869
7	59.35332	-1.593342	1.16768
9	58.92233	-1.521466	1.147815
11	58.52486	-1.268099	1.034334
13	58.16221	-.8912464	.8731083
15	57.83545	-.4412184	.6983647
17	57.54553	3.858023E-2	.5341853
19	57.2932	.5110593	.3959539
21	57.07911	.9449963	.2917236
23	56.90377	1.314697	.2235014
25	56.76758	1.599733	.1884495
27	56.67084	1.784743	.1800079
29	56.61372	1.859279	.1889489
31	56.59633	1.817694	.2043755
33	56.61864	1.659068	.2146798
35	56.68057	1.387166	.208478
37	56.78189	1.010439	.1755409
39	56.92234	.5420595	.1077369
41	57.1015	-5.513895E-6	7.358612E-6

#### REFERENCES

1. Nikolić, D.S. - "Contribution to the solution of the curved beam according to the theory of large deformations" (In Serbo-Croatian), XII YU Congress of Theoretical and Applied Mechanics, Ohrid, 1974.
2. Grbić, D.G. - "Contribution to the solution of extensible chain" (In Serbo-Croatian), V YU Symposium on Plasticity, p. 90-94, Lipik, 1987.





## A FINITE ELEMENT SIMULATION OF 2D FLUID FLOW AROUND RIGID STRUCTURES - IBM PC/AT IMPLEMENTATION

Stanko Brčić

Faculty of Civil Engineering, University of Belgrade  
Bulevar revolucije 73, 11000 Belgrade, Yugoslavia

### SUMMARY

The paper presents a brief outline of the finite element solution of the Navier-Stokes equations in two dimensions. Some results of the stationary fluid flow around rigid circular cylinder are presented as numerical example.

Presented discussion is a part of a wider fluid-structure analysis which is not yet in its final stage. The particular goal is to utilize a small personal computer like an IBM PC/AT and to determine its possibilities and limits in the fluid-structure interaction analysis.

### 1. INTRODUCTION

One of the very important aspects of various fluid-structure interaction problems is the case of external fluid flow, i.e. the fluid flow around solid bodies. The presence of the structure in the fluid flow clearly imposes certain boundary conditions for the flow and is therefore affecting the flow. On the other hand, fluid flow imposes a loading onto the structure. If the structure is flexible enough it will deflect or rather move under the action of fluid loading. Such structural motion means the change of fluid boundary conditions and consequently, the change of the flow itself. Therefore, the fluid loading onto the structure is different then it was previously. As a consequence, the fluid and the structure are in the constant state of mutual interaction in the sense that motion of one medium is affecting and also dependant on the motion of the other one.

If the structure is relatively rigid, i.e. if its motion under the influence of surrounding fluid is negligible, previously discussed interaction does not take place now. Rigid structure represents fixed boundary conditions for the flow and any change in fluid flow is due to other reasons, not to the presence of the structure.

This paper is dealing with the finite element simulation of two-dimensional fluid flow around rigid structures. Basically, it represents the finite element solution of the Navier-Stokes equations in 2D. Corresponding computer code was developed, implemented and tested first on the medium sized computer such as DIGITAL DEC 20/40, and later on the personal computer IBM PC/AT. Mentioned computer code was developed to simulate 2D interaction between flexible structures (which are modelled as a rigid lamina undergoing planar motion with 3 DOF) and surrounding fluid flow. Therefore, presented numerical example is just a branch (an option) in the wider computer code.

## 2. GOVERNING EQUATIONS

The fluid is considered to be a constant property, incompressible Newtonian fluid. Consequently, its equations of motion may be expressed as:

$$u_{i,t} + u_j u_{i,j} = f_i - \frac{1}{\rho} p_{,i} + \nu u_{i,jj} \quad (1.1)$$

$$u_{i,i} = 0 \quad (i, j=1, 2) \quad (1.2)$$

These equations, the Navier-Stokes equations and the continuity equation, are written in the so-called primitive variables of velocity components  $u_1=u$  and  $u_2=v$ , and pressure  $p$ . The fluid properties of mass density and kinematic viscosity are denoted by  $\rho$  and  $\nu$ . The bounded domain  $\Omega$  of the fluid flow around rigid structure and corresponding boundary surfaces (i.e. lines) is represented in Fig.1.

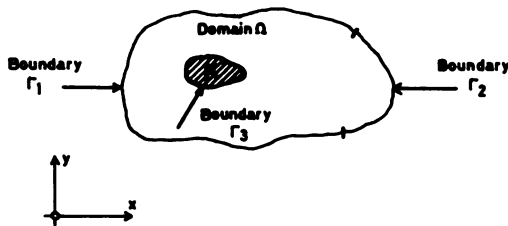


Fig. 1 Domain of the fluid flow around a structure

The boundary conditions associated with equations of motion (1) may be:

- essential (Dirichlet's)

$$u_i = \bar{u}_i \quad \text{boundaries } \Gamma_1, \Gamma_3 \quad (2)$$

- natural (Neumann's)

$$u_{i,n} = \gamma_i \quad \text{boundary } \Gamma_2 \quad (3)$$

where  $n$  is the outward normal on the boundary  $\Gamma_2$ .

In the case of a stationary (i.e. rigid) structure which is not changing its spatial position due to the flow, velocity components  $\bar{u}_i$  related to the boundary  $\Gamma_3$  fluid-structure contact surface, i.e. line in 2D) are equal to zero. Also, it is possible and sometimes usefull to define the natural boundary conditions in terms of traction force components.

If the fluid flow is considered as nonstationary, as presented in eqs. (1.1), initial velocity conditions are specified as:

$$u_i(t=0) = u_{i0} \quad (4)$$

where initial velocity field  $u_{i0}$  satisfies the continuity equation  $u_{i0,i} = 0$ .

### 3. FINITE ELEMENT APPROXIMATION

One of the most widely used approaches to obtain numerical solution of the Navier-Stokes equations is the so-called integrated primitive variable formulation in which the velocity components and pressure are solved simultaneously. Usually, the spatial finite element discretization of eqs. (1) is performed via the Galerkin weighted residual method (mainly in the weak formulation). This approach is used in this paper too.

It is possible to employ various types of elements, but whatever elements used, it is now the well known fact that the velocity shape functions are to be one degree higher than those for pressure approximation (in integrated velocity - pressure approach). In the numerical example presented here eight-noded parabolic elements are used: eight velocity and geometry nodes and four corner pressure nodes. However, the computer code supports four types of 2D elements.

Discretized form of eqs. (1) may be obtained as:

$$\{M\}\{\dot{a}\} + \{K(a)\}\{a\} + \{C\}\{p\} = \{d\} \quad (5.1)$$

$$\{D\}\{a\} = \{0\} \quad (5.2)$$

where the matrices  $M$ ,  $K(a)$ ,  $B$ ,  $C$ ,  $D$  are mass, convective, diffusive, pressure gradient and divergence matrices, respectively, while  $a$  and  $p$  are unknown nodal velocity and pressure vectors. Vector  $d$  is a load vector resulting from body forces (which were neglected in this work) and specified natural boundary conditions.

Obtained equations are nonlinear and nonsymmetric due to convective acceleration terms - matrix  $K(a)$ . The continuity equation (5.2) is actually the incompressibility constraint equation. Since it involves only velocity unknowns, integrated velocity - pressure approach becomes non-positive definite, thus adding a bit more to numerical difficulties. Furthermore, nonstationary fluid flow simulation expressed by eqs. (5) requires some implicit time integration, since there are no pressure time derivative terms.

At last, but not the least, the number of finite elements necessary for reasonable spatial approximation of the flow domain should be sufficient. Therefore, the number of unknown nodal quantities may be quite substantial - say, well over 1000 unknowns.

### 4. NUMERICAL SOLUTION

In the case of a stationary fluid flow the nodal accelerations vanish (local accelerations in the continuum are zero), so eqs. (5) may be represented in the form

$$\{K_1(a)\}\{a_1\} = \{d_1\} \quad (6)$$

The nonlinear nature of algebraic equations (6) requires some form of iterative solution. Various forms of successive substitution and Newton-Raphson's procedures are provided for in the computer code, together with the frontal method of assembly and solution.

In the case of transient (nonstationary) flow, implicit time integration is required. Computer code supports the Wilson  $\theta$  method or the predictor-corrector (Adams-Bashworth's) procedure. In either case, equations are reduced to nonlinear algebraic equations

$$(\hat{k}_j(a))\{\hat{a}_j\} = \{\hat{d}_j\} \quad (7)$$

for each time step.

### 5. NUMERICAL EXAMPLE

Laminar fluid flow around rigid circular cylinder is considered. Such an example was analyzed in literature (see, for example (2) or (3)), so it is convenient for comparison and verification purposes. Since the flow is stationary with small velocities, only symmetrical part of flow domain is considered, Fig. 2

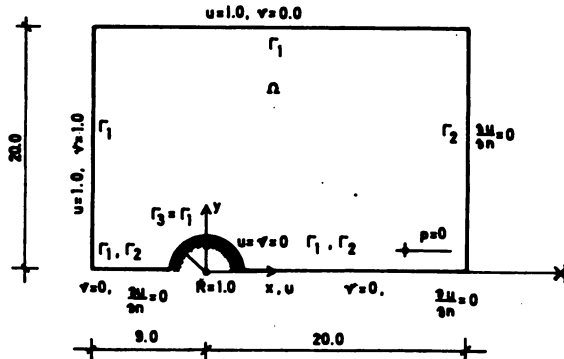


Fig. 2 Flow domain of laminar flow around circular cylinder and boundary conditions

Spatial discretization of the flow domain in Fig. 2 was adopted exactly the same as in (2): 73 eight-noded parabolic elements, see Fig. 3.

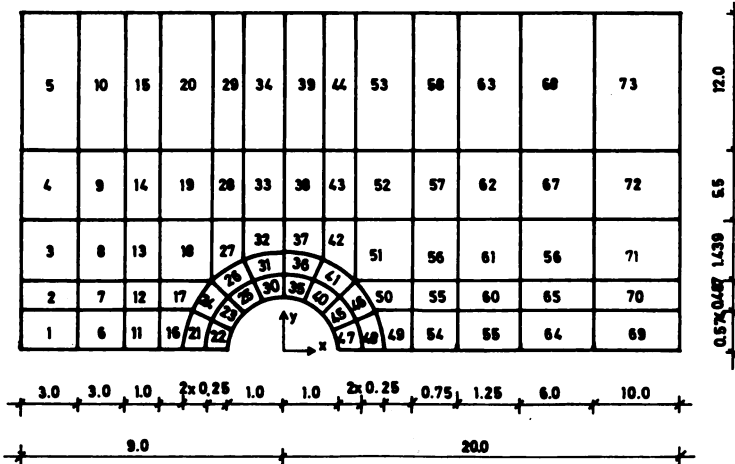


Fig. 3 Finite element mesh (8-noded parabolic elements)

For adopted finite element mesh the total number of unknown nodal values is 624, or rather 490 when essential boundary conditions are extracted.

Considered example is the main numerical example presented in (2), so it was well documented (complete input file and main part of output file were included). Consequently, it was very convenient for close comparison. In short, two identical results were obtained using two different and independent computer codes: in this work (or rather in (1)), and in (2).

Convergent flow field was obtained after five cycles of successive substitutions in nonlinear equations. The total run time on a 12 MHz IBM PC/AT compatible computer was about 24 minutes. Some of the results are presented in the following figures.

Velocity field in the vicinity of cylinder is presented in Figs 4 and 5. As may be observed especially from Fig. 5 (which is a close up of Fig. 4), two symmetrical stationary vortices (Föppl's vortices) are formed behind cylinder. Such vortices are formed in the flow regime characterized by Reynolds number:  $5-15 < Re < 40$ . In considered example was  $Re = 20$  (based on cylinder diameter).

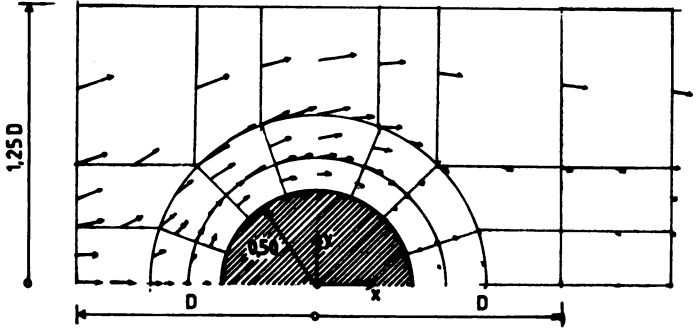


Fig. 4 Velocity field around circular cylinder ( $Re = 20$ )

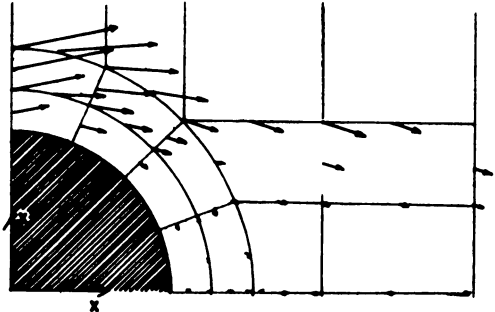


Fig. 5 Velocity field around cylinder (a close-up)

Obtained pressure coefficient distribution around the circular cylinder is presented in Fig. 6.

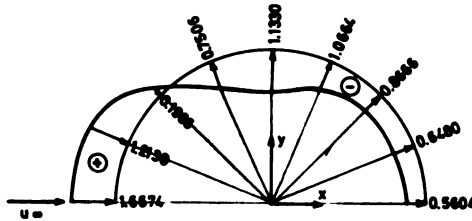


Fig. 6 Pressure coefficient distribution on circular cylinder ( $Re=20$ )

Obtained velocity and pressure fields in the vicinity of cylinder may be used to calculate, for instance, the drag coefficient  $C_D$ . Comparative values for circular cylinder drag coefficients (for  $Re < 100$ ) are presented in Table 1.

	REFERENCE	Drag Coeff. $C_D$
Numerical approach	S.Brčić (1) (also C.Taylor (2))	1.31
	P.Gresho (1980)	1.27
	Jordan and Framm (1972)	1.28
	Swanson and Spaulding (1978)	1.39
	Smith and Brebbia (1978)	1.43
Experimental	Tritton (1959)	1.27
	Tritton (1977)	1.33

Table 1. Various numerical and experimental values of circular cylinder drag coefficient (see (2), pp.27-81)

## LITERATURE

- (1) Brčić, S.: Dynamical Behaviour of Structures in Fluid Environment, Ph.D dissertation, University of Belgrade, Faculty of Civil Engineering, Belgrade, 1987.
- (2) Taylor, C., Hughes, T.G.: "Finite Element Programming of the Navier-Stokes Equations", Pineridge Press, 1981.
- (3) Taylor, C., Morgan, K. (editors): "Recent Advances in Numerical Methods in Fluids, Vol. 1, Pineridge Press, 1980.





## SOME ASPECTS OF NONLINEAR FINITE ELEMENT ANALYSIS OF WELDED GUSSET PLATES

Dj. Vuksanović and B. Pujević

Faculty of Civil Engineering, Belgrade, Yugoslavia

### ABSTRACT

The elastic and elastoplastic, finite element analysis of welded gusset plates is presented. Two basic states are considered: gusset plates in tension and gusset plates in compression. For gusset plates in tension an overview of some previous experimental and finite element investigations is presented. In finite element analysis for the nonlinear material response the material is assumed to obey an elastoplastic isotropic or a kinematic hardening material law based on the von Mises yield condition. For gusset plates in compression a buckling analysis based on the 9-node Lagrangian Mindlin plate element with enhanced shear interpolation is used.

### 1. INTRODUCTION

The gusset plate, which is one of the most commonly used connecting elements in a number of structural steel systems, has received relatively little attention over the years in terms of theoretical, experimental and design investigations. The current design procedures are essentially based on very limited research work and consist of simple methods of analysis based on strength of materials, appropriate specification rules, combined with the general practice and experience of the designer. These design methods for gusset plates are still in use because of their past satisfactory performance although they are based on linear elastic assumptions.

The extensive application of steel structures for heavy industrial buildings and large span bridges underlines the need for adequate design methods for gusset plates. From the standpoint of safety and economy the ultimate limit

design analysis of gusset plates is required. Due to the existence of powerful numerical tools, such as the finite element method, it is possible to obtain the reliable response of gusset plates which includes the required nonlinear effects.

Among some of the related research activities on the gusset plates are those of Vasarhelyi [1], who was probably the first to conduct experimental tests along with elastic finite element analysis. Bjorhovde [2] considered the behaviour and strength of gusset plates on the basis of an experimental investigation of full-scale diagonal bracing connections. Pujević and Vuksanović [7] studied the elastoplastic behaviour of gusset plates by the finite element method and in the elastic range they compared their results with experimental data obtained from photoelastic measurements. Results of these investigations showed that the finite element model of gusset plates provides reasonable results for elastic and elastoplastic material conditions and that agreement between the numerical and experimental results is quite satisfactory.

The structural elements that are connected to the gusset plate may be tension or compression members or a combination of both types of member. The object of this paper is to analyse, using the finite element method, two basic states: gusset plates in tension and gusset plates in compression. Since the thickness of the gusset plate is much smaller than its other dimensions, for gusset plates in tension we performed the elastoplastic analysis assuming a state of plane stress. For gusset plates in compression the stability phenomenon is of prime interest, especially the problem of inelastic buckling behaviour. In this paper we present only elastic buckling analysis of gusset plates using the finite element method, although we are aware that gusset plates in compression is still a subject that needs much more research.

## 2. GUSSET PLATES IN TENSION

In most large span steel truss structures, chord members are generally composed of welded box sections and two gusset plates are usually connected to the webs of these sections. In our investigations we consider the monolith-type of gusset plates, shown on Figure 1. With this kind of joint it is assumed that the gusset plate is an integral part of the chordmembers' web.

Gusset plates of this type are subjected to very high stresses because of the abrupt change of the cross section and because they transmit the entire chord-member forces. See Figure 2.

The geometry of the welded gusset plate is determined from the structural details of the truss joints. The main problem in achieving this continuity in welded structures is the design of this joint connection from the standpoint of security and reliability. Figure 3 shows the various types of welded gusset

plates which have been investigated.

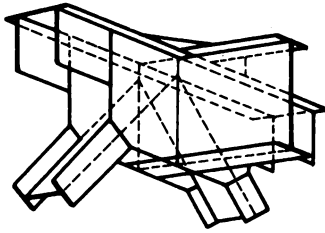


Figure 1 The monolith-type of truss joint

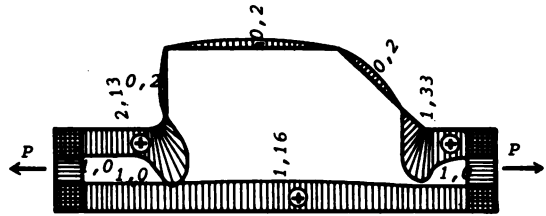


Figure 2 Stress distributions in a gusset plate

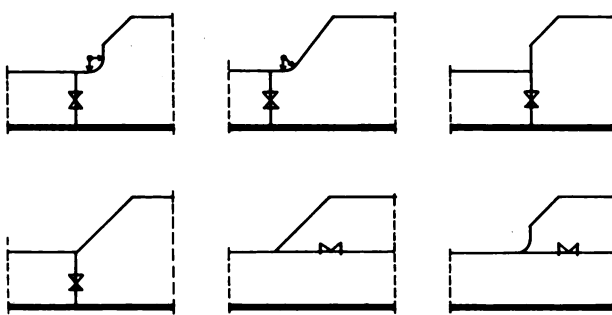


Figure 3 Various types of welded gusset plates

The stress distribution in a gusset plate under tension is primarily governed by axial forces. Bending moments sometimes produce high stress concentrations, especially on the curved corners of the gusset plate. These local peak stresses can be significant in relation to fatigue for cyclic load effects. (See Figure 4.)

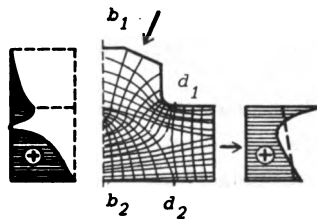


Figure 4 Stress distribution in a gusset plate under tension

Figure 5 shows the distribution of principal stresses and the local concentration areas in gusset plates with various shapes calculated using the

finite element method.

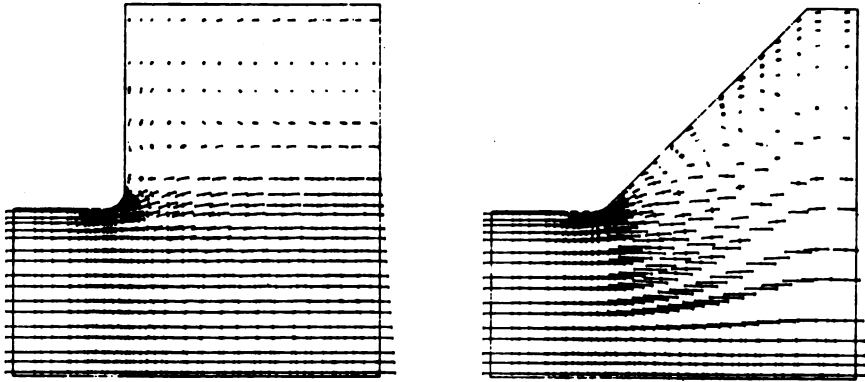


Figure 5 Principal stresses in gusset plates

From experimental data obtained from photoelastic measurements made by polarised light transmitted through transparent thin gusset plate models the same concentration of stresses can be observed. A fringe photograph of the stressed gusset plate model under tension loads is shown in Figure 6.

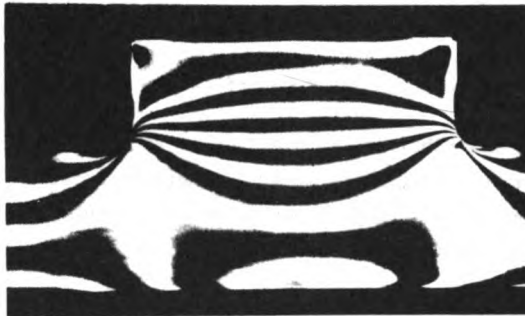


Figure 6 Fringe photograph of gusset plate model

From the experimental and numerical parametric studies it was found that certain geometrical properties of gusset plates are the most dominant factors in obtaining these local peak stresses [7].

To check the dependence of the stress concentration factor on the contour around point A and certain geometrical parameters mentioned above, several finite element models were analyzed [7]. Two kinds of round contours were examined: circular, with the radius of 100 mm, and elliptical, with the semi-axes 100/200 mm. The results obtained using finite element program were compared with the

experimental data in Table 1. As expected, the stress concentration factor is much greater for the circular contour  $K=1,92$  than for elliptical  $K=1,42$  and this fact must be considered in designing the gusset plates.

Table 1

	circular contour $\alpha=90^\circ$	elliptical contour $\alpha=90^\circ$	circular contour $\alpha=60^\circ$	circular contour $\alpha=45^\circ$
Ratio $a/\rho$	$\frac{2100}{2 \cdot 100} = 10.5$	$\frac{2100}{2 \cdot 400} = 2.63$	10.5	10.5
Experimental stress concen. faktor $K_e$	2.00 {3}	1.33	2.06	2.11
	2.13 {4}	1.53	2.04	2.07
Numerical stress concen. factor $K_n$ obtained using F.E.M	1.92	1.42	1.90	1.97

From an engineering analysis and design standpoint the complexity of the gusset plate in tension makes it infeasible to deal with anything but ultimate limit states. This is primarily due to the fact that serviceability criteria for such elements are extremely difficult to formulate. Taking into account previous considerations, our research effort was directed towards the development of an appropriate elastoplastic finite element model [6] for the determination of the static strength.

Based on the results obtained from linear analysis several models of gusset plates were used to perform the elastoplastic finite element analysis. The material was assumed to obey an elastoplastic isotropic and kinematic hardening material law, using the von Mises yield condition for infinitesimally small displacements and strains. For structural steels the yield surface described by the von Mises yield function was adopted

$$F(\sigma_{ij} - \bar{\alpha}_{ij}) = \frac{3}{2} (\sigma_{ij}' - \alpha_{ij})(\sigma_{ij}' - \alpha_{ij}) \tag{1}$$

where

$$\begin{aligned} \sigma_{ij}' &= \sigma_{ij} - \frac{1}{3} \sigma_{ii} \delta_{ij} & \delta_{ij} &= 0, \quad i \neq j \\ \alpha_{ij} &= \alpha_{ij} - \frac{1}{3} \alpha_{ii} \delta_{ij} & \delta_{ij} &= 1, \quad i = j \end{aligned}$$

and  $\sigma_{ij}$  are the components of the stress tensor, and  $\alpha_{ij}$  are the coordinates of the centre of the yield surface in stress space. Regarding the above equation, various criteria can be applied to hardening of the material, i.e. isotropic hardening, kinematic hardening and combined isotropic and kinematic hardening.

The total strain increment is regarded as the sum of its elastic and plastic components

$$d\epsilon = d\epsilon^e + d\epsilon^p \quad (2)$$

An associated flow rule is adopted

$$d\epsilon_{ij}^p = \frac{3}{2} \frac{\sigma_{ij}'}{\sigma_{ef}} d\bar{\epsilon}_{ef}^p \quad (3)$$

where

$$d\bar{\epsilon}_{ef}^p = \sqrt{\frac{2}{3} d\epsilon_{ij}^p d\epsilon_{ij}^p} \quad , \quad \sigma_{ef} = \sqrt{\frac{3}{2} \sigma_{ij}' \sigma_{ij}'}$$

The incremental stress-strain relationship may be written as

$$d\sigma = D^{ep} d\epsilon \quad (4)$$

where  $D^{ep}$  represents the instantaneous elastoplastic stress strain matrix.

All the parameters presented in the respective mathematical expressions were obtained from the stress-strain curves of the specific carbon steels in cold state. For the isothermal conditions the stress-strain curve has been approximated by three different stages: an elastic stage, a stage with constant hardening, and variable hardening stage.

The basic finite element equations regarding the constitutive equations are of incremental form. In Reference [8] we gave an overview of some recent developments we have pursued for the more effective solution of those nonlinear equations in solving the gusset plate problems. Also we considered the problem of convergence criteria and the accurate integration of stresses.

The displacement response of point A for increasing loads for various gusset plates is shown in Figure 7 for elastoplastic isotropic hardening.

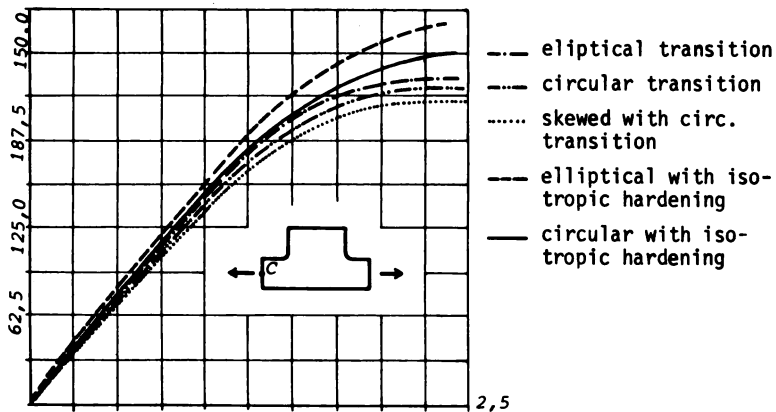


Figure 7 Elastoplastic displacement response for various gusset plates

The spread of plastic zones for a characteristic gusset plate for various load steps is shown in Figure 8.

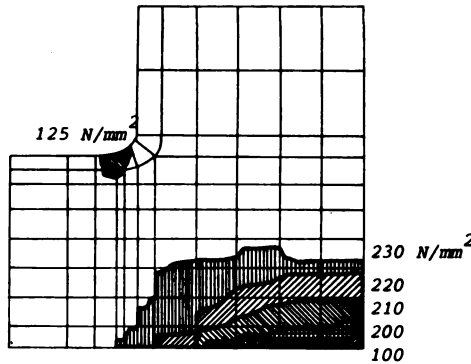


Figure 8 Spread of plastic zones for a typical gusset plate

### 3. GUSSET PLATE IN COMPRESSION

One of the most difficult problems in the design of gusset plates is that associated with the compression behaviour of the gusset plates. The determination of the plate buckling load is a difficult task due to the fact that plate buckling is influenced by many parameters such as: plate geometry, type of connections between members and gusset plate, type of boundary conditions for the gusset plate, the existence of stiffeners in the plates, etc. Gusset plate buckling can be tackled by treating the gusset as an initially stressed plate. This section presents a suitable finite element formulation for dealing with this problem.

#### Finite element formulation

In recent years considerable research effort has been directed towards the development of the ideal Mindlin plate element. It is well known that finite elements based on Mindlin's plate theory require only  $C(0)$  continuity of the lateral displacement and independent rotations. This provides an important advantage over finite elements based on classical thin plate Kirchhoff theory where  $C(1)$  continuity is required. Thus, it would appear that Mindlin plate elements are simpler to formulate and they have the added advantage of being able to model shear-weak as well as shear-stiff plates - of transverse shear effects are present in the plate they are automatically modelled with Mindlin elements. However, several difficulties can be encountered when Mindlin plate elements are used in plate situations. Full integration of the stiffness matrices leads to locking behaviour and while reduced or selective integration can often overcome



these difficulties, over stiff solutions may still occur in problems with highly constrained boundaries. On the other hand, when such elements are used in problems with lightly constrained boundaries the solutions may fail due to the formation of mechanisms or be polluted by oscillations caused by near mechanisms.

To overcome these difficulties we implemented the 9-node Lagrangian Mindlin plate element with enhanced shear interpolation developed by Huang and Hinton [9]. This element satisfies most of the requirements of the ideal Mindlin plate element, i.e. it does not lock, it passes the appropriate patch tests exactly and it has the requisite number of zero energy modes.

Following a finite element spatial discretisation, the stability problem of initially stressed Mindlin plates can be expressed in matrix form as

$$(\underline{K} - \lambda \underline{K}_G) \underline{a}^i = 0 \quad i = 1, 2, \dots, r \quad (5)$$

where  $\underline{K}$  is the global stiffness matrix,  $\underline{K}_G$  is the global geometric stiffness matrix and  $\lambda$  is a constant by which the chosen in-plane loads must be multiplied to cause buckling. Vector  $\underline{a}^i$  gives the  $i^{\text{th}}$  buckling mode and  $r$  is the total number of degrees of freedom. From (5) it follows that all the in-plane stresses must be simultaneously increased by a factor  $\lambda$  which will increase the geometric stiffness matrix proportionally. Thus, buckling loads can be found by solving the typical eigenvalue problem defined by (5).

The element stiffness matrix  $\underline{K}$  may be written in the following form

$$\underline{K}^e = \underline{K}_b^e + \underline{K}_s^e \quad (6)$$

The contributions to the submatrix of the element stiffness matrix linking nodes  $i$  and  $j$  are defined in the usual way

$$\begin{aligned} \underline{K}_{bij}^e &= \int_{-1}^{+1} \int_{-1}^{+1} \underline{B}_{bi}^T \underline{D}_b \underline{B}_{bj} \det \underline{J} \, d\zeta d\eta \\ \underline{K}_{sij}^e &= \int_{-1}^{+1} \int_{-1}^{+1} \underline{B}_{si}^T \underline{D}_s \underline{B}_{sj} \det \underline{J} \, d\zeta d\eta \end{aligned} \quad (7)$$

where  $\underline{B}_{bi}$  is the strain matrix associated with flexural deformation,  $\underline{B}_{si}$  is the strain matrix associated with shear strain, (the so called substitute strain matrix due to the existence of substitute shear strain fields in the element formulation see [10] for details) and the full integration scheme is used to evaluate  $\underline{K}_{bij}^e$ .  $\underline{D}_b$  and  $\underline{D}_s$  are matrices of flexural and shear rigidities respectively and  $\det \underline{J}$  is the determinant of the Jacobian matrix  $\underline{J}(\xi, \eta)$ .

If initial in-plane stresses  $\underline{\sigma}^0 = (\sigma_x^0, \sigma_y^0, \tau_{xy}^0)^T$  act on the second order strains in the Mindlin plate, then the geometric stiffness matrix  $\underline{K}_G^e$  may be

written as

$$\underline{K}_G^e = \underline{K}_{Gb}^e + \underline{K}_{Gs}^e \quad (8)$$

A typical submatrix of  $\underline{K}_{Gb}^e$  linking nodes  $i$  and  $j$  can be expressed as

$$\underline{K}_{Gb1j}^e = \int_{-1}^{+1} \int_{-1}^{+1} \underline{G}_{bi}^T \underline{\sigma}^0 \underline{G}_{bj} h \det \underline{J} d\xi d\eta \quad (9)$$

where

$$\underline{G}_{bi} = \begin{bmatrix} N_{i,x} & 0 & 0 \\ N_{i,y} & 0 & 0 \end{bmatrix} \quad \text{and} \quad \underline{\sigma}^0 = \begin{bmatrix} \sigma_x^0 & \tau_{xy}^0 \\ \tau_{xy}^0 & \sigma_y^0 \end{bmatrix}$$

A typical submatrix of  $\underline{K}_{Gs}^e$  linking nodes  $i$  and  $j$  can be expressed as

$$\begin{aligned} \underline{K}_{Gs1j}^e = & \int_{-1}^{+1} \int_{-1}^{+1} \underline{G}_{s1i}^T \underline{\sigma}^0 \underline{G}_{s1j} \frac{h^3}{12} \det \underline{J} d\xi d\eta + \\ & + \int_{-1}^{+1} \int_{-1}^{+1} \underline{G}_{s1i}^T \underline{\sigma}^0 \underline{G}_{s2j} \frac{h^3}{12} \det \underline{J} d\xi d\eta \end{aligned} \quad (10)$$

where

$$\underline{G}_{s1i} = \begin{bmatrix} 0 & N_{i,x} & 0 \\ 0 & N_{i,y} & 0 \end{bmatrix} \quad \text{and} \quad \underline{G}_{s2i} = \begin{bmatrix} 0 & 0 & N_{i,x} \\ 0 & 0 & N_{i,y} \end{bmatrix}$$

$\underline{K}_{Gs}^e$  is the part of the geometric stiffness matrix associated with shear deformations and in the case of thin plates can be omitted. However, its effect becomes significant for thick plate situations.

### Gusset plate buckling analysis

Using program VIBUK (which is well documented and listed in reference [10]) we performed a buckling analysis of the gusset plate of a bridge truss upper chord member joint, shown in Figure 1. Initial in-plane stresses  $\underline{\sigma}^0$  were obtained for plane stress conditions for the gusset plate loaded with dead and live load simultaneously.

The boundary conditions chosen for the buckling analysis adequately modelled the conditions of a real gusseted joint where, due to the existence of an upper chord bracing system, displacements along the web of the vertical member and along the upper edge are restrained. The first three buckling modes are shown in Figure 9.

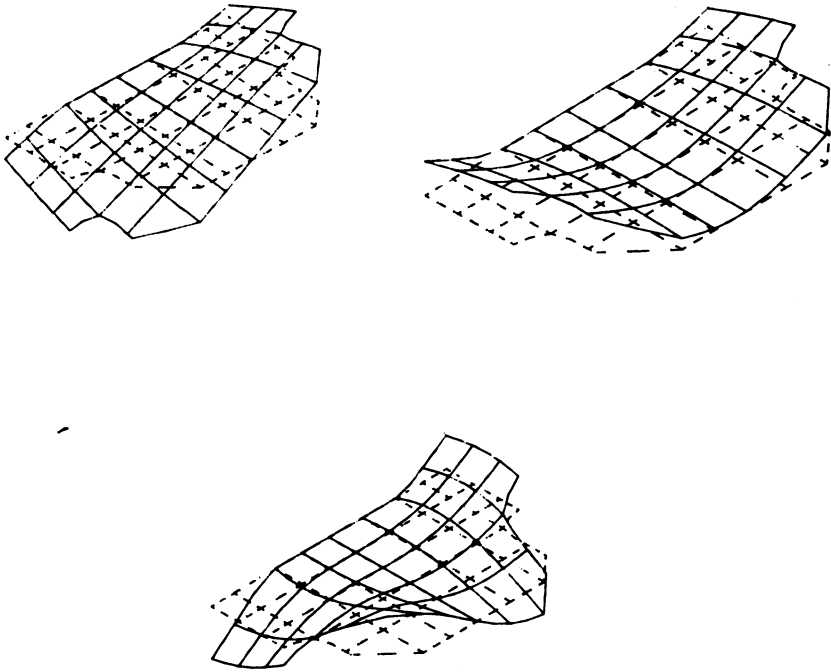


Figure 9 Buckling modes of the gusset plate

#### 4. CONCLUDING REMARKS

The objective of this paper was to present the behaviour of gusset plates in tension and compression. For tension applications it was shown from experimental and numerical finite element data that the limit state considerations using von Mises yield criteria may provide a means for establishing design criteria. The stability of gusset plates in compression can also be investigated using the finite element method.

Although this study was restricted to simple loading conditions and elastic plate buckling only, the results obtained can be used to provide some useful conclusions about gusset plate behaviour. It is clear that much research needs to be conducted to resolve the behaviour of gusset plates in more complex situations (i.e. inelastic buckling, cycle loading, etc.).

## REFERENCES

- |1| VASARHELYI, D.D. - Tests of Gusset plate Models, Journal of the Structural Division, ASCE, Vo. 97. No. ST2, February, 1971.
- |2| BJORHOVODE, R. and CHAKRABARTI, S.K. - Tests of Full-Size Gusset Plate Connections, Journal of Structural Engineering, ASCE, Vol. 111, No. ST3, March, 1985.
- |3| RADOJKOVIĆ, M and BRČIĆ, V. - Investigation of the gusset plates, (in Serbian). Zbornik 5, 197-210. Faculty of Civil Engineering (1962).
- |4| LESNIAK, Z. - Pregrand Spawaalnictwa 7, 160-165 (1965).
- |5| TESAR, A. - Czechoslovakian Academy of Sciences, REPORT 388/56.
- |6| PUJEVIĆ, B. - Elasto-plastic analysis using F.E.M., Ms. thesis presented on the. Faculty of Civil Engineering in Belgrade, In 1983.
- |7| PUJEVIĆ, B. and VUKSANOVIĆ, Dj. - Elastoplastic Analysis of the Concentration of Stresses in Welded Gusset Plates using ADINA, Computers and Structures, Vol. 21, No. 1/2, 1985. (Special Issue).
- |8| PUJEVIĆ, B. and VUKSANOVIĆ, Dj. - The Finite Element Analysis of the Concentration of Stresses in Welded Gusset Plates, Proceedings of 16th Yugoslav Congress of Theoretical and Applied Mechanics, Bečići, 1984. (In Serbian)
- |9| HUANG, H.C. and HINTON, E. - A Nine Node Lagrangian Mindlin Plate Element with Enhanced Shear Interpolation, Engineering Computations, Vol. 1, No. 4, 1984.
- |10| HINTON, E., VUKSANOVIĆ Dj. and HUANG, H.C. - Finite Element Free Vibration and Buckling Analysis of Initially Stressed Mindlin Plates, Pineridge Press, Swansea, (to be published).
- |11| VUKSANOVIĆ, Dj., PUJEVIĆ, B. and HINTON, E. - Nonlinear finite element analysis of welded gusset plates. Proceedings of the International Conference on Computational Plasticity held in Barcelona, Spain, 1987.



## NON-LINEAR ANALYSIS OF CABLE-STAYED BRIDGES

BRATISLAV STIPANIC  
Structural Engineer. MSc  
Belgrade Univ., Civil Eng. Faculty

### 1. SUMMARY

The non-linear analysis of cable-stayed bridges is considered. Special emphasis is given to the following actual problems: application of effective cable modulus of elasticity, second-order analysis of tower and second-order analysis of girder due to traffic load. The all three problems are illustrated by the corresponding numerical examples.

### 2. INTRODUCTION

The non-linearity in statical analysis of cable-stayed bridges is due to relatively large displacements of girder and towers combined with bending moment-axial force interaction and catenary action of the cables.

Because of the presence of high compressive forces in the slender girder and towers non-linear analysis should be done to assure that the cable-stayed bridge has the required safety against overstresses.

As the cable-stayed bridges are usually erected by free cantilevering from the towers, the bridge system should be analysed according to second-order theory in order to correct the bridge leveling that is changed during the erection by adding the new erection units and by introducing the new cable-to-girder attachments. For example, the registered deflections of girder during the free cantilever erection applied to bridge over Danube in Novi Sad /6/ were from 1,5 m up to 0,8 m down. Hence, the corresponding detailed second-order analysis was carried out.

The non-linear behaviour of stay cables due to changes of sag under various tensions (catenary action of the cables) is taken into account approximately by the effective cable modulus of elasticity.

### 3. EFFECTIVE CABLE MODULUS OF ELASTICITY

#### 3.1. Treatment of the problem

Effective cable modulus of elasticity is an equivalent cable modulus of elasticity for the substitute straight line chord member, which includes the material as well as geometrical elongation, and thus enables the elongation of the substitute member being nearly compatible with that of the real curved cable.

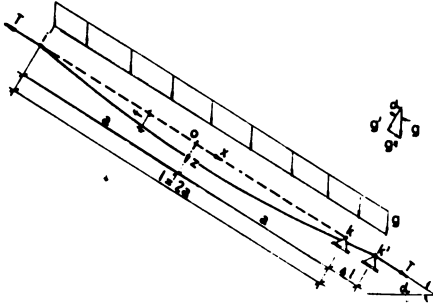


Fig. 1 Stay cable in deformed position ik'

If unstressed, stay cable of the original length  $l$  has the position  $ik$  ( $i$  marked as the fixed point, the angle of inclination  $\alpha$ ). If stressed, i.e. deformed by its own weight  $g$  and the end tensile forces  $T$ , the stay cable has the new position  $ik'$  (Fig. 1). The cable displacements, with reference to the unstressed position, are defined as  $u$ ,  $w$  ( $u$  - displacement in the direction of  $x$ -axis,  $w$  - displacement in the direction of  $z$ -axis). The displacement  $w$  of the middle cable point  $0$  is marked by  $f$ .

Uniformly distributed load - cable weight  $g$  can be divided in the components  $g'$ ,  $g''$  (with reference to the coordinate axes  $z$ ,  $x$ )

$$\begin{aligned} g' &= g \cdot \cos \alpha, \\ g'' &= g \cdot \sin \alpha. \end{aligned} \quad (3.1a,b)$$

The influence of component  $g''$  of self weight  $g$  on the tensile cable force  $T$  can be neglected.

As known, a hanging cable under its own weight has a catenary line. The cable line, with sufficient accuracy for a technical use, can be regarded as parabola (instead catenary). It can be proved that the error made by this approach is practically insignificant.

Thus the equation of the stay cable line can be presented in the form

$$w = f \cdot \left[ 1 - \left( \frac{x}{a} \right)^2 \right]. \quad (3.2)$$

Differentiating  $w$  with respect to  $x$  one obtains

$$\frac{dw}{dx} = - 2 \frac{f}{a} \cdot \frac{x}{a}. \quad (3.3)$$

From the equilibrium condition of the cable half part follows

$$f = g' \frac{a^2}{2T}. \quad (3.4)$$

Introducing the previous expression (3.4) into relation (3.3) one obtains

$$\frac{dw}{dx} = -\frac{g' \cdot a}{T} \cdot \frac{x}{a} \quad (3.5)$$

One considers now the differential element  $DD_1$  (of the cable  $ik$ ) of the initial length  $ds$ , that loaded by its own weight and by the tensile forces  $T$ , has the deformed position  $D'D'_1$  (cable position  $ik'$ ). Under deformation, the ends  $D$  and  $D_1$  of the differential element  $DD_1$  made the displacements  $u, w$  and  $u+du, w+dw$ ; the chord  $D'D'_1$  made the rotation  $\phi$  and the length  $ds$  of the differential element  $DD_1$  increased to  $(1+\epsilon) ds$  (Fig. 2).

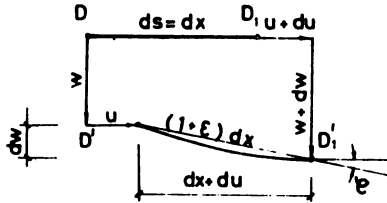


Fig. 2 Differential element  $DD_1$  of the cable in the deformed position  $DD'_1$

Having in mind that the unstressed cable line contains the  $x$ -axis, it is valid

$$ds = dx.$$

From Fig. 2 one follows

$$\begin{aligned} dx + du &= (1 + \epsilon) \cdot dx \cdot \cos \phi, \\ dw &= (1 + \epsilon) \cdot dx \cdot \sin \phi. \end{aligned} \quad (3.6a,b)$$

Applying the Maclorin's series to the functions  $\cos \phi$  and  $\sin \phi$ , where  $\phi$  is the infinitely small value, one gets

$$\cos \phi \approx 1 - \frac{\phi^2}{2}, \quad \sin \phi \approx \phi. \quad (3.7a,b)$$

Substituting  $\cos \phi$  and  $\sin \phi$  by the expressions (3.7a,b), Eqs. (3.6 a,b) become

$$\begin{aligned} dx + du &= (1 + \epsilon) \cdot dx \cdot \left(1 - \frac{\phi^2}{2}\right) \\ dw &= (1 + \epsilon) \cdot dx \cdot \phi \end{aligned} \quad (3.8a,b)$$

If the infinitesimal values of higher order are neglected than the relations (3.8a,b) are transformed as follows

$$du = -\frac{\phi^2}{2} \cdot dx + \epsilon \cdot dx, \quad dw = \phi \cdot dx \quad (3.9a,b)$$

From the expressions (3.9a,b), the normal strain  $\epsilon$  can be obtained in the form

$$\epsilon = \frac{du}{dx} + \frac{1}{2} \cdot \left(\frac{dw}{dx}\right)^2 \quad (3.10)$$



As known, for one-axial state of stress Hook's law is valid as

$$\epsilon = \frac{\sigma}{E}, \quad (3.11)$$

where  $\sigma$  is the normal stress (tensile stress in the cable) and  $E$  is the modulus of elasticity (Young's modulus).

Introducing the expression (3.10) into relation (3.11) and using the formula (3.5), one comes to the following expression for the tensile cable stress  $\sigma$ :

$$\sigma = E \left[ \frac{du}{dx} + \frac{1}{2} \left( \frac{g'a}{T} \right)^2 \cdot \left( \frac{x}{a} \right)^2 \right]. \quad (3.12)$$

Considering  $\sigma = \frac{T}{A}$  where  $A$  is the area of cable cross section, from the expression (3.12) one gets

$$\frac{du}{dx} = \frac{T}{EA} - \frac{1}{2} \left( \frac{g'a}{T} \right)^2 \cdot \left( \frac{x}{a} \right)^2. \quad (3.13)$$

The elongation  $\Delta l = kk'$  of the cable is defined as

$$\Delta l = \int_{-l/2}^{l/2} \frac{du}{dx} dx \quad (3.14)$$

Having introduced the expression (3.13) into the relation (3.14), after the integration one gets

$$\frac{\Delta l}{l} = \frac{T}{EA} - \frac{1}{24} \left( \frac{g'l}{T} \right)^2. \quad (3.15)$$

When the force  $T$  is changed for  $\Delta T$  and increased to  $\bar{T}$ , i.e.

$$\bar{T} = T + \Delta T, \quad (3.16)$$

the relation (3.15) is transformed in the form

$$\frac{\Delta \bar{l}}{l} = \frac{\bar{T}}{EA} - \frac{1}{24} \left( \frac{g'l}{\bar{T}} \right)^2, \quad (3.17)$$

where  $\Delta \bar{l}$  is the cable elongation due to the cable tensile force  $\bar{T}$ .

Suppose that the considered stressed cable  $ik'$  can be replaced by an equivalent, fictive straight member which system line is its chord.

The substitute equivalent straight member in the interval  $\Delta t$ , which corresponds to the change  $\Delta T$  of force  $T$ , has the approximately compatible elongation with that of the real curved cable. Thus it is valid

$$\tilde{\epsilon}(\Delta l) = \frac{\Delta \bar{l}(\bar{T}) - \Delta l(\sigma)}{l} \quad (3.18)$$

where  $\tilde{\epsilon}$  is the change of normal strain in the interval  $\Delta t$ .

Introducing the expressions (3.15) and (3.17) into the relation (3.18) one obtains

$$\frac{\tilde{\epsilon}}{\bar{T} - T} = \frac{1}{EA} + \frac{1}{24} (g'l)^2 \frac{\bar{T} - T}{T^2 - T^2} \quad (3.19)$$

The average modulus of elasticity  $\tilde{E}$  during the change of the tensile force from  $T$  to  $\bar{T} = T + \Delta T$  is named as the effective (equivalent, fictive, modified or apparent) cable modulus of elasticity and it is defined as follows

$$\tilde{E} = \frac{\bar{T}-T}{\bar{E}A} \quad (3.20)$$

Substituting the expression  $\frac{\bar{T}-T}{\bar{E}A}$  by  $\tilde{E}$  in the relation (3.19), one gets the effective cable modulus of elasticity in the form

$$\tilde{E} = \frac{E}{1 + \frac{1}{24}(g'l)^2 \frac{\bar{T}+T}{T^2\tau^2} E \cdot A} \quad \text{or} \quad E = \frac{E}{1 + \frac{1}{24}(\gamma'l)^2 \frac{\bar{\sigma} + \sigma}{\sigma^2\sigma^2} E} \quad (3.21a,b)$$

where  $\gamma' = \frac{g'}{A}$ ,  $\bar{\sigma} = \frac{\bar{T}}{A}$  (3.22a,b)

In the case when the change  $\Delta T = \bar{T} - T$  of the cable tensile force is small, the effective cable modulus of elasticity  $\tilde{E}$  with a sufficient accuracy can be determined as

$$\tilde{E} = \frac{E}{1 + \frac{1}{12} \frac{(g'l)^2}{T^3} EA} \quad \text{or} \quad \tilde{E} = \frac{E}{1 + \frac{1}{12} \frac{(\gamma'l)^2}{\sigma^3} E} \quad (3.23a,b)$$

Non-linear effect is relatively small for the considerably large values of cable stresses; therefore due to almost all variations of live load only one or two average stresses by the formulae (3.23a,b) can be considered.

### 3.2. Change of the effective cable modulus of elasticity during the bridge erection

The influence of the effective cable modulus of the elasticity on the exactness of bridge analysis during the erection is treated /1/. After the theoretical treatment of the problem, for the bridge erected on temporary piers it is shown how the effective cable modulus of elasticity (given by the expressions (3.22a,b) considerably changes from one to another erection phase. It can be seen (in this example) how the analysis correctness depends on the number of the calculation steps.

Cable-stayed bridge (Fig.3) during the erection on temporary piers (at the points 2,3,5 and 6) is considered.

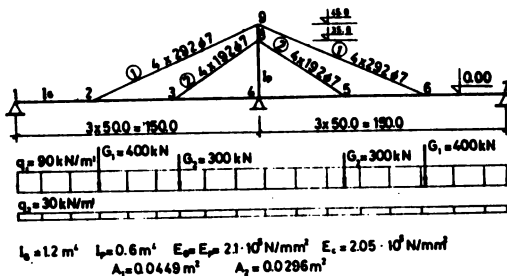


Fig. 3 Cable-stayed bridge analysed during the erection

Before cable adjustments the bridge girder is lifted by the jacks that are placed on the piers at the points 2,3,5,6. Having the bridge been jacked, the cables are adjusted so that the initial cable forces are due to cable self weights

only. After the cable adjustments, the bridge girder goes down by jacks on the piers and thus the reactions  $X_k(k=1,2)$  are decreased gradually. The analysis was carried out iteratively in four calculation steps. Some principal results of the analysis will be pointed out.

The reactions of piers  $X_k(k=1,2)$ , calculated in the calculation steps 0,1,2,3, are presented in Table 1.

k	$X_k^{(0)}$	$X_k^{(1)}$	$X_k^{(2)}$	$X_k^{(3)}$
	kN			
1	6820	6386	6212	6243
2	-3849	-3927	-3763	-3780

Table 1 Reactions of piers  $X_k(k=1,2)$

The changes of cable moduli of elasticity  $E_i(i=1,2)$  during the bridge erection depending on the number of calculation steps (numerical values from the first iteration are marked by +, from the second by ·, and the results of the third iteration are given by diagrams) are presented in Fig. 4a,b.

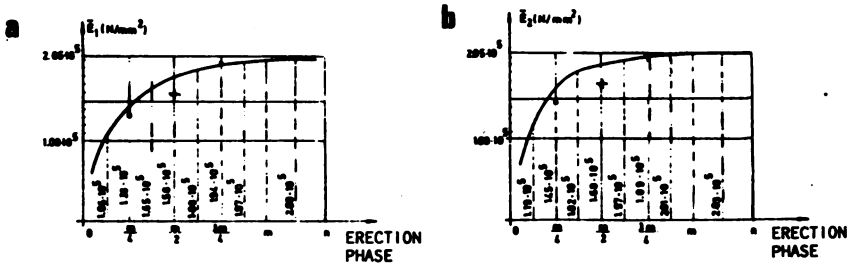


Fig. 4a,b Diagrams of the effective cable moduli of elasticity  $E_i(i=1,2)$

#### 4. SECOND-ORDER ANALYSIS OF TOWER

Tower should be designed as member subjected to axial compression and combined bending moments from longitudinal and transverse directions. The overall tower buckling in these both directions should be evaluated. The overall buckling in longitudinal direction may be treated by a stability analysis of the entire system.

The overall stability analysis of the tower can be carried out by approx. iterative calculations of deformations and internal forces according to second-order theory due to the action of an adequate load combination (cable forces resulting from dead and live loads and lateral wind) with the assumed eccentricities of cable forces (Fig. 5). The eccentricities should be taken as the sum of system eccentricities and the tolerated erection inaccuracy. As specified by German Code (DIN 4114) second-order analysis should be carried out with load factors: 1,71 (for dead load + live load) or 1,5 (for dead load + live load + wind + temperature...) and the obtained stresses should be below the yield point.

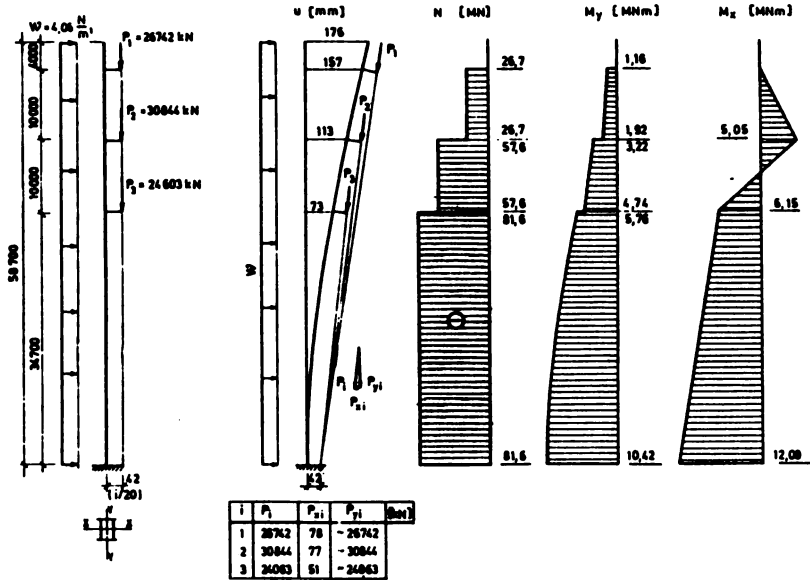


Fig. 5 Second-order analysis of the tower that was carried out in design of bridge over Danube in Novi Sad /6/

## 5. SECOND-ORDER ANALYSIS OF GIRDER DUE TO TRAFFIC LOAD

Setting up the equilibrium conditions of differential element of member in deformed position  $CC_1$  (Fig. 6) and introducing the relations between the deformations ( $\epsilon, \phi$ ) and displacements ( $u, v$ ) and applying Hook's law, one gets the following basic equations of member according to theory of large deformations:

$$\begin{aligned}
 dx + du &= (1 + \epsilon) \cdot ds \cdot \cos(\alpha + \phi), \\
 dy + dv &= (1 + \epsilon) \cdot ds \cdot \sin(\alpha + \phi), \\
 dH + p_x ds &= 0, \\
 dH + d_y ds &= 0, \\
 dM + H(dy + dv) - V(dx + du) &= 0,
 \end{aligned} \tag{4.1a-g}$$

$$\frac{d\phi}{ds} = -\frac{M}{EI} - \alpha_t \cdot \frac{\Delta t}{h},$$

$$\epsilon = \frac{N}{EF} + \alpha_t \cdot t^0 = \frac{1}{EF} \cdot H \cdot \cos(\alpha + \phi) + V \cdot \sin(\alpha + \phi) + \alpha_t \cdot t^0.$$

Substituting the second-order values of the internal forces by the adequate first-order values in member of Eqs. (4.1a-g) where they are multiplied by the values of deformations, neglecting the influence of normal strain  $\epsilon$  on deformation and utilizing the assumption of small deformation (but not the assumption of small displacements), the following basic equations of member according to second-order theory can be derived from Eqs (4.1a-g):

$$\begin{aligned}
 du &= -\phi \cdot ds \cdot \sin \alpha, \\
 dV &= \phi \cdot ds \cdot \cos \alpha, \\
 dH + p_x ds &= 0, \\
 dV + p_y ds &= 0.
 \end{aligned}
 \tag{4.2a-f}$$

$$dM + HdY - Vdx + N_0 \cdot \phi ds = 0.$$

$$\frac{d\phi}{ds} = -\frac{M}{EI} - \alpha_t \frac{\Delta t}{h}$$

Comparing the obtained system of Eqs. (4.2a-f) to the analogue system resulting from first-order analysis, one concludes that the considered member can be calculated according to first-order theory when besides the given loads  $p_x$  and  $p_y$  it is loaded by the fictive distributed moments  $m^f = N_0 \cdot \phi$  as well.

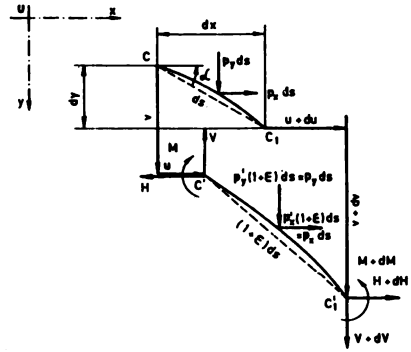


Fig. 6 Differential element of member in non-deformed (CC<sub>1</sub>) and deformed (CC'<sub>1</sub>) position

Introducing in the Eqs. (4.2a-f) the expressions for the internal forces (M,H,V) and rotation  $\phi$

$$\begin{aligned}
 M &= M_g + M_p, \\
 H &= H_g + H_p, \\
 V &= V_g + V_p, \\
 \phi &= \phi_g + \phi_p,
 \end{aligned}
 \tag{4.3a-f}$$

where the indexes g and p denote the effects of dead and traffic load, one derives the equation

$$dM_g + H_g \cdot dy - V_g \cdot dx + dM_p + H_p \cdot dy - V_p \cdot dx + (N_g + N_p) \cdot \phi_p = 0. \tag{4.4}$$

Setting up the above equation (4.4) that the values of internal forces and deformations of bridge system can be calculated by the superposition of the first-order values due to dead load and the values due to traffic load computed according to linearized second-order theory, i.e. according to first-order theory if besides the applied traffic load the girder is loaded by the distributed fictive moment

$$m^f = (N_g + N_p) \cdot \phi_p \tag{4.5}$$

The exposed theoretical approach was applied to design of bridge over Danube in Novi Sad /6/ (Fig. 7).

The values of bending moments in the girder sections were calculated (Table 2) iteratively. It can be noticed that the convergence of the applied iterative procedure requires only several iterations.

Iter.	max M	max M	min M	min M	min M	min M
	MNm	MNm	MNm	MNm	MNm	MNm
I	144.0	98.6	25.3	79.1	35.7	-43.0
II	149.3	101.9	-26.9	-85.1	-38.6	-44.8
III	150.1	103.7	-27.4	-85.9	-39.1	-45.3
IV	150.3	103.9	-27.5	-86.0	-39.3	-45.4

Table 2 Values of bending moment in girder sections obtained iteratively /6/

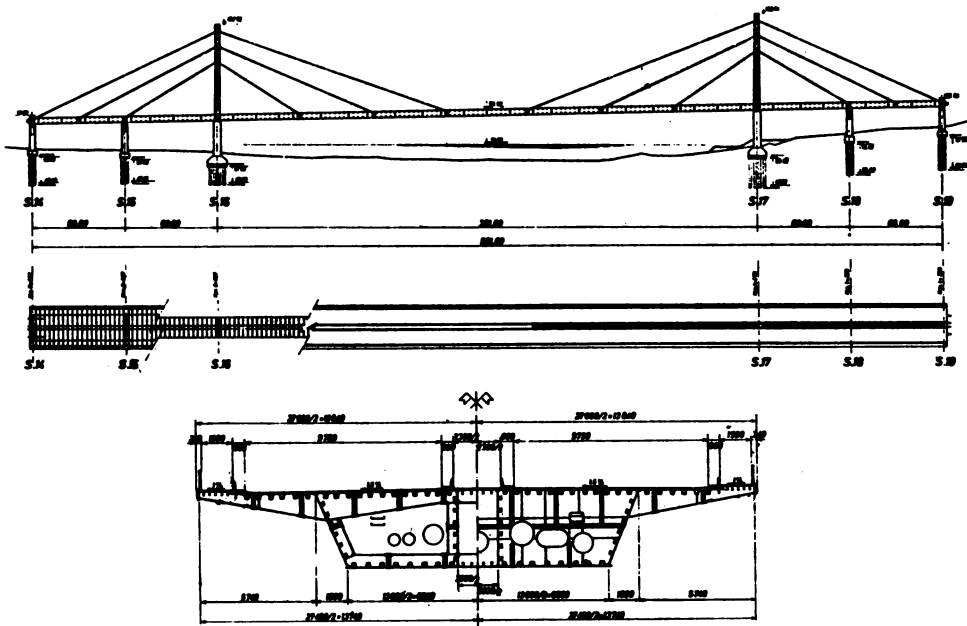


Fig. 7. Bridge over Danube in Novi Sad /5/

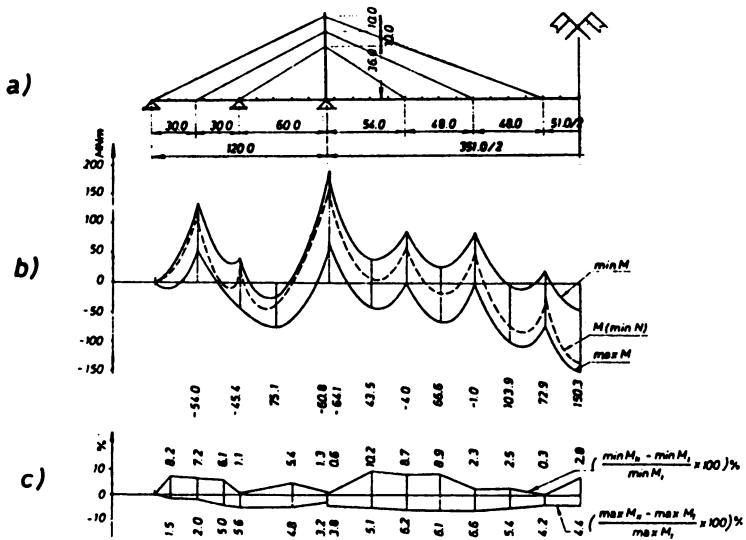


Fig. 8 a) Statical system of bridge over Danube in Novi Sad  
 b) Distribution of maximum and minimum design moments  
 c) Comparison between second-order and first-order values of moment /6/

It can be seen /6/ from Fig. 8c that the increase of absolute values of moment according to second-order theory in comparison with linear theory was (at the most) about 10%.

## 6. REFERENCES

1. KOLLBRUNNER, C.F., HAJDIN, N and STIPANIĆ, B.-Contribution to the Analysis of Cable-Stayed Bridges, Institute for Engineering Research (Foundation Kollbrunner/Rodio)H. 48, Verlag Schultness AG, Zurich (1980).
2. KOLLBRUNNER, C.F. HAJDIN, N and STIPANIĆ, B.- Contribution to the Analysis of Cable-Stayed Bridges (in Japanese), Bridge Engineering 19, Vol. 6 p. 16-19, Vol. 7 p. 20-28, Tokyo (1983).
3. STIPANIĆ, B.- Contribution to the Analysis of Steel Cable-Stayed Bridges I-V. Izgradnja 1-5, Belgrade (1982).
4. STIPANIĆ, B. - Some Specific Analysis Problems Related to Design of Cable-Stayed Bridges, Cable-Stayed Bridges-Experiences and Design, Proceedings of the International Conference on Cable-Stayed Bridges, Vol. 1, p. 150-163, Bangkok (1987.)
5. HAJDIN, N - Strassenbrücke "Sloboda" über die Donau in Novi Sad, Der Stahlbau 52, H. 4, 97-103, Berlin (1983).
6. Highway Bridge over Danube in Novi Sad - Design Books 14.1, 14.2, 19, 21.1 21.2, Owner: City of Novi Sad, Design: Kirilo Savić - Beograd, Designer: N. Hajdin, Belgrade (1978).

## ON THE DETERMINATION OF FINITE INCREMENTS IN PERFECT PLASTICITY

Ljubomir Savić

Civil Engineering Faculty, Belgrade, Yugoslavia

### SUMMARY

The paper is concerned with the calculation of finite increments in the implementation of perfectly-plastic material behaviour. The exact solution for finite plastic strain increments due to the given strain increment is outlined in the framework of the purely mechanical form of the general thermodynamical rate-type plasticity theory, proposed by Green and Naghdi [1] and formulated in the strain space. The approximate solution, based on the Taylor series expansion, as well as three common algorithms for perfect plasticity are evaluated by comparison with the exact solution. Special attention is paid to the approximate series solution and it is shown that relatively concise and high accurate expressions can be obtained in such a form. It is particularly important that similar solutions can be derived for the calculations with other constitutive models, where exact solutions for finite plastic strain increments, up to date, have not been found.

### 1. SOME BASIC RELATIONSHIPS BETWEEN INFINITESIMAL INCREMENTS

Denote the components of the Lagrangian strain, plastic strain and Piola-Kirchhoff stress tensors by  $e_{KL}$ ,  $e_{KL}^P$  and  $s_{KL}$ , respectively. Throughout the paper matrix notation will be used and the before mentioned tensor components will be stored in nine-vectors:

$$\begin{aligned} \{e\}^T &= \{e_{11} \ e_{12} \ \dots \ e_{33}\}, \quad \{e^P\}^T = \{e_{11}^P \ e_{12}^P \ \dots \ e_{33}^P\}, \\ \{s\}^T &= \{s_{11} \ s_{12} \ \dots \ s_{33}\}. \end{aligned} \quad (1)$$

The considerations will be confined to the constitutive equations appropriate for ductile metallic materials which are homogeneous and initially isotropic in their reference state. Assuming small deformations, the stress response will be adopted in the following form:



$$\{\sigma\} = [C_e^e] \{\epsilon^e\}, \quad (2)$$

where  $[C_e^e]$  is the symmetric constitutive matrix for the linearly elastic material and

$$\{\epsilon^e\} = \{\epsilon\} - \{\epsilon^p\}. \quad (3)$$

The yield (or loading) surface is given by the equation

$$g(\{\epsilon\}, \{\epsilon^p\}, k) = 0, \quad (4)$$

where  $k$  is a constant.

In what follows the attention will be confined to the special case where the equation (4) can be substituted by

$$G(\{\gamma\}, \{\gamma^p\}, k) = 2\mu^2 (\{\gamma\}^T - \{\gamma^p\}^T) (\{\gamma\} - \{\gamma^p\}) - k = 0. \quad (5)$$

In this equation the deviatoric parts of the vectors  $\{\epsilon\}$  and  $\{\epsilon^p\}$  are denoted by  $\{\gamma\}$  and  $\{\gamma^p\}$ , respectively and  $\mu$  stands for the shear modulus. The equation (5) represents the well known von Mises type yield surface in strain space.

The deviatoric part of the infinitesimal plastic strain increment will be denoted by  $\{\dot{\gamma}^p\}$ . Starting from the well known work postulate by Naghdi and Trapp [2] it is possible to show that the flow rule in the case of perfect plasticity can be expressed as

$$\{\dot{\gamma}^p\} = \{\bar{G}_\gamma\} \{\bar{G}_\gamma\}^T \{\dot{\gamma}\}, \quad G=0, \quad \{\bar{G}_\gamma\}^T \{\dot{\gamma}\} > 0, \quad (6)$$

where  $\{\dot{\gamma}\}$  is the infinitesimal strain increment and  $\{\bar{G}_\gamma\}$  stands for the unit outward normal on the yield surface (for further details see, for instance, the paper [3]).

The infinitesimal increment of the deviatoric stress vector  $\{\tau\}$ , can be determined on the basis of equations (2) and (6) as

$$\{\dot{\tau}\} = (\{\dot{\gamma}\} - \{\dot{\gamma}^p\}) 2\mu, \quad G=0, \quad \{\bar{G}_\gamma\}^T \{\dot{\gamma}\} > 0, \quad (7)$$

where can be noticed that the vector

$$\{\dot{\tau}^p\} = \{\dot{\gamma}^p\} 2\mu \quad (8)$$

is also directed along the outward normal  $\{\bar{G}_\gamma\}$ .

## 2. THE EXACT SOLUTION FOR FINITE INCREMENTS IN PERFECT PLASTICITY

The use of numerical techniques, such as the finite element method, is essential for solving plastic deformation problems which arise in a wide range of engineering disciplines. Finite element materially nonlinear structural analysis usually involve an incremental-iterative procedure whereby displacements, strains and stresses are gradually updated in order to trace out the response path. Each iteration comprises, as a rule, three main computational steps: linearization, equation solving and state determination. In the present paper, in what follows, the state determination step, a crucial one for the reliability and economy of the overall procedure will be concerned.

The main question within the scope of the state determination step is how to update the position of the loading surface at each numerical integration point.

The constitutive equations of the plasticity theory are given in an infinitesimal form and it follows that for a truly infinitesimal strain increment the motion of the loading surface, given by the equation (5), is parallel to the local normal. But as a matter of practicality in the implementation of elastic-plastic problems, it is hard to keep the strain increments very small. Strain increments are usually so large to cause a motion of the loading surface with a significant deviation from the local normal. Therefore, it is

necessary to express the unknown finite plastic strain increment and the finite stress increment as functions of the given independent strain increment.

In the case of perfect plasticity this problem can be solved exactly. In the paper [4] using the framework of the traditional stress-space theory of perfectly plastic material behaviour Krieg and Krieg derived this solution. In the present paper the exact solution will be outlined in the spirit of the strain space plasticity theory.

Consider an elastic-plastic state represented by the point O in the deviatoric strain space as given in Figure 1. Denote the unit normal on the yield surface in point O by  $\{\bar{G}_Y\}_O$ :

$$\{\bar{G}_Y\}_O = \{G_Y\}_O / m_G, \quad (9)$$

$$\{G_Y\}_O = (\{\gamma\}_O - \{\gamma^P\}_O)^2,$$

$$m_G = (\{G_Y\}_O^T \{G_Y\}_O)^{1/2},$$

where  $\{\gamma^P\}$  is the corresponding plastic strain vector.

Consider a given finite strain increment  $\{\Delta\gamma\}_O$  defined by

$$\{\Delta\gamma\} = \{\bar{r}\} z_1, \quad (10)$$

where  $\{\bar{r}\}$  and  $z_1$  denote the corresponding unit vector and the modulus of the vector  $\{\Delta\gamma\}$ , respectively. The vector  $\{\Delta\gamma\}$ ,

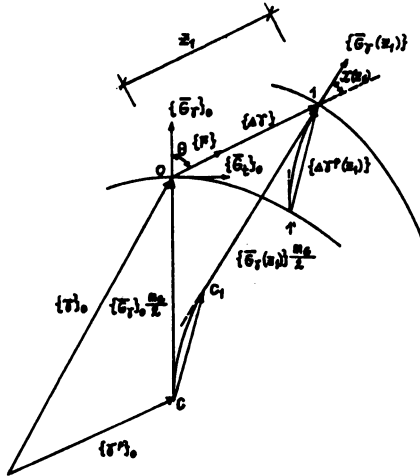


Figure 1 Geometrical interpretation of relationships between finite strain increments in perfect plasticity.

satisfies the loading condition (7)<sub>3</sub>, what can be expressed in the following form

$$\{\bar{r}\}^T \{\bar{G}_Y\}_O = \cos \theta > 0, \quad (11)$$

where the angle  $\theta$  between unit vectors  $\{\bar{r}\}$  and  $\{\bar{G}_Y\}_O$  is introduced.

The problem is how to determine the motion of the yield surface in strain space due to the given strain increment  $\{\Delta\gamma\}$ . In other words, the question is how to calculate the components of the finite increment  $\{\Delta\gamma^P\}$ , i.e. how to update the position of the center of the yield surface.

It follows at once from (6) that for  $\theta=0$  the increment  $\{\Delta\gamma^P\}$  is directed along the outward normal  $\{\bar{G}_Y\}_O$ :

$$\{\Delta\gamma^P\} = \{\bar{G}_Y\}_O z_1, \quad (12)$$

i.e. the considered direction of loading, according to developments given in [3], is critical.

Therefore, in what follows the attention will be focused to directions of loading specified by

$$0 < \theta < \pi/2. \quad (13)$$

During loading from point O to point 1, what is shown in Figure 1, the corresponding strain trajectory can be described by

$$\{\gamma(z)\} = \{\gamma\}_O + \{\bar{r}\} z, \quad 0 \leq z \leq z_1. \quad (14)$$

The corresponding unknown trajectory  $CC_1$  of the center of the yield surface, i.e. the trajectory of the vector  $\{\gamma^P\}$  can be expressed in the following way:

$$\{\gamma^P(z)\} = \{\gamma^P\}_0 + \{\Delta\gamma^P(z)\}, \quad 0 < z < z_1. \quad (15)$$

In an arbitrarily chosen point along this trajectory the tangent vector to this trajectory, in view of (6), can be defined as

$$\{\dot{\gamma}^P(z)\} = \{\bar{G}_Y(z)\} \cos \chi(z), \quad 0 < z < z_1, \quad (16)$$

where  $\{\bar{G}_Y(z)\}$  denotes the outward unit normal to the updated yield surface which corresponds to  $\{\gamma(z)\}$  and  $\chi(z)$  stands for the angle between the normal  $\{\bar{G}_Y(z)\}$  and the direction of loading:

$$\cos \chi(z) = \{\bar{G}_Y(z)\}^T \{\bar{r}\}. \quad (17)$$

According to (9) it follows that

$$\{\bar{G}_Y(z)\} = (\{\gamma(z)\} - \{\gamma^P(z)\}) / m_G. \quad (18)$$

Furthermore, taking the derivative of (17) and (14) with respect to  $z$  and using (16), we find that

$$\dot{\chi} = -2 \sin \chi / m_G. \quad (19)$$

The solution of this differential equation, taking into account the condition  $\chi(0) = \theta$ , is given in the form

$$\chi(z) = 2 \arctg(e^{-2z/m_G} \cdot \tg(\theta/2)). \quad (20)$$

Next, by a simple and purely geometrical analysis, the following expression for  $\{\Delta\gamma^P(z)\}$  can be obtained:

$$\{\gamma^P(z)\} = \{\bar{G}_{Y0}\} (m_G (1 - \cos(\theta - \chi(z))) / 2 + z \cos \theta) + \{\bar{G}_t\}_0 (z \sin \theta - m_G \sin(\theta - \chi(z))) / 2, \quad (21)$$

where the unit vector

$$\{\bar{G}_t\}_0 = \{\bar{r}\} / \sin \theta - \{\bar{G}_Y\}_0 \cot \theta, \quad \{\bar{G}_t\}_0^T \{\bar{G}_Y\}_0 = 0, \quad (22)$$

is introduced.

In closing this development it must be emphasized that the finite deviatoric stress increments can be calculated in a simple way according to

$$\{\Delta\tau\} = (\{\Delta\gamma\} - \{\Delta\gamma^P\}) / 2\mu, \quad (23)$$

when  $\{\Delta\gamma\}$  and  $\{\Delta\gamma^P\}$  are given.

### 3. SOME NUMERICAL SOLUTION METHODS FOR THE DETERMINATION OF FINITE INCREMENTS

Four approximate algorithms for implementing perfect plasticity will now be evaluated against the foregoing analytical solution which provides a useful benchmark.

In reference [5] some "closed" form formulas for  $\{\Delta\gamma^P(z)\}$  based on the Taylor series expansion are presented. Such expressions are particularly important when various hardening plasticity problems are to be handled. Naturally, in the case of perfect plasticity it is also possible to use such formulas and in what follows it will be shown to what extent some of these approximations can be used.

Omitting details of the derivation, the following approximate expression will here be quoted:

$$\{\Delta\gamma^P(z)\} \approx \{\bar{G}_Y\}_0 z (\cos \theta + z (1 - \cos 2\theta) / 2 + z^2 (\cos 3\theta - \cos \theta) / 2 + z^3 (-3 \cos 4\theta + 5 \cos 2\theta - 2) / 6 + z^4 (15 \cos 5\theta - 30 \cos 3\theta + 15 \cos \theta) / 30) + \quad (24)$$

$$\begin{aligned}
 & +\{\bar{G}_t\}_0 z (z \sin 2\theta / 2 + z^2 (-3 \sin 3\theta + 5 \sin \theta) / 6, + \\
 & + z^3 (3 \sin 4\theta - 5 \sin 2\theta) / 6 + z^4 (-15 \sin 5\theta + 30 \sin 3\theta - 19 \sin \theta) / 30),
 \end{aligned} \tag{24}$$

where

$$\bar{z} = z / m_G. \tag{25}$$

The foregoing expression for the power series of order 5 can be reduced to obtain more simple expressions for power series of lower orders, 1 to 4.

Let  $\{\Delta \tilde{\gamma}^p(z)\}$  be an approximation of the vector  $\{\Delta \gamma(z)\}$ . Then, the deviation of such an approximation from the exact solution can be represented by two quantities with obvious geometrical meaning. First, it can be observed that the exact radial vector of the updated yield surface

$$\{\bar{G}_Y(z)\} \bar{m}_G = (\{\bar{G}_Y\}_0 \cos(\theta - \chi(z)) + \{\bar{G}_t\}_0 \sin(\theta - \chi(z))) \bar{m}_G, \quad \bar{m}_G = m_G / 2, \tag{26}$$

will be substituted by the vector

$$\{\tilde{G}_Y^*(z)\} = \{\bar{G}_Y\}_0 \bar{m}_G + \{\bar{r}\} z - \{\Delta \tilde{\gamma}^p(z)\}. \tag{27}$$

The radius error can be calculated simple as

$$\Delta_m = \bar{m}_G^* - \bar{m}_G \tag{28}$$

where

$$\bar{m}_G^* = (\{\tilde{G}_Y^*\}^T \{\tilde{G}_Y^*\})^{1/2}. \tag{29}$$

This kind of error in working with power series expansion can easily be removed substituting  $\{\tilde{G}_Y^*\}$  with

$$\{\tilde{G}_Y(z)\} = \{\tilde{G}_Y^*(z)\} \bar{m}_G / \bar{m}_G^* \tag{30}$$

Furthermore, the vector  $\{\tilde{G}_Y(z)\}$  exhibits an additional deviation from the exact solution, represented by  $\{\bar{G}_Y\} \bar{m}_G$ . That can be measured by the angle

$$\psi = \arccos(\{\tilde{G}_Y(z)\}^T \{\bar{G}_Y(z)\} / \bar{m}_G). \tag{31}$$

The contour plots in Figure 2, a-e show how the angle of error varies for each of the five aforementioned simplest expressions based on Taylor series expansion. The angle  $\psi$  is chosen to be negative whenever the final radial vector  $\{\tilde{G}_Y(z)\}$  ends up lying more nearly parallel that it should to the initial one,  $\{\bar{G}_Y\} \bar{m}_G$ . The results are given for  $z/\bar{m}_G$ , ranging from 0 to 1. The horizontal axis corresponds to the normalized tangential component of the strain increment vector  $z \sin \theta / \bar{m}_G$  and consequently along the vertical axis the radial component  $z \cos \theta / \bar{m}_G$  should be given.

Three well known numerical algorithms will now be considered.

The so called tangent stiffness radial return method has been widely used in structural analysis programs [4,6] and it has been carried out in the stress space. It is, however, possible to consider this method in the framework of the strain space plasticity theory. The main results of such an analysis lead to the conclusion that this scheme is identical to the first order approximation in using Taylor series expansion.

The second scheme is called secant stiffness method [7] and is originally developed in a stress space plasticity theory. However, we can recast the method to the equivalent form which holds in a strain space plasticity theory, what is shown in the Figure 3. In the case of perfect plasticity, as observed in [5], the angular error,  $\psi_s$ , is to be determined by

$$\psi_s = \phi_\theta - \theta + \chi, \tag{32}$$

where



$$\phi_s = \theta_s^P - \arcsin(\sin\theta_s^P + z\sin(\theta_s^P - \theta)/\bar{m}_G),$$

$$\gamma_s^P = \arccos((1+z\cos\theta/2\bar{m}_G)/(1+z\cos\theta/\bar{m}_G + z^2/4\bar{m}_G^2)^{1/2}). \quad (33)$$

The contour plot is given in the Figure 4. By comparison between Figures 4, 2b) and 2c) it can be observed that the secant stiffness method is more accurate than the second order series approximation and less accurate than the third order power series approximation for  $z/\bar{m}_G$  ranging from 0 to 1.

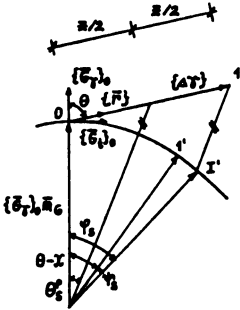


Figure 3 Secant stiffness method

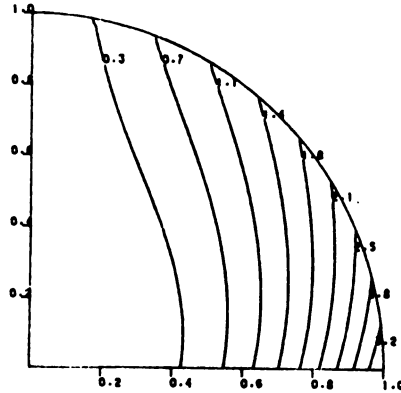


Figure 4 Contours of the angular error for the secant stiffness method

The third common algorithm is called radial return method. This oldest method [8] is shown in the Figure 5 by using the strain space formulation of the plasticity theory. As illustrated, in order to find the approximate increment of the plastic strain vector the so called trial state, represented by point 1, is pulled back to the yield surface by a simple reduction in magnitude. The angular error is, as shown in [5], given by

$$\psi_R = \phi_R - \theta + \chi, \quad (34)$$

where

$$\phi_R = \arccos((1+z\cos\theta/\bar{m}_G)/(1+2z\cos\theta/\bar{m}_G + z^2/\bar{m}_G^2)^{1/2}). \quad (35)$$

The corresponding contour plot of  $\psi_R$  is depicted in the Figure 6. Having in mind the results described by the Figure 2a) it becomes immediately clear that the radial return method has, roughly speaking, the same accuracy as the tangent stiffness radial return method for  $z/\bar{m}_G$  varying between the limits 0 and 1. However, it must be noticed that although the radial return method appears to be as crude as the tangent stiffness method when  $0 < z/\bar{m}_G < 1$ , the radial return method continues to stand out among the three widely used approximate algorithms on account of its conceptual simplicity, computational speed and accuracy for  $z/\bar{m}_G$  ranging from 0 to 5 [5].

It is evident that in computations where moderate amounts of errors, which will be exhibited in three common aforementioned algorithms, are not allowed, the exact solution must be applied. Alternatively, in the case of perfect plasticity, for values of  $z$  below a certain limit, it is possible to reach high accuracy by



2. NAGHDI, P. M. and TRAPP, J. A. - 'Restrictions on Constitutive Equations of Finitely Deformed Elastic-Plastic Materials', Quart. J. Mech. Appl. Math., 1975, 28, 25.
3. SAVIĆ, Lj. - 'Some Geometrical Features of the Rate-Type Plasticity Theory for Structural Metals', Proceedings of the Second International Conference on Advances in Numerical Methods in Engineering, Theory and Application, NUMETA '87, Swansea, Martinus Nijhoff Publishers, Dordrecht, Boston, Lancaster, 1987, II, C14.
4. KRIEG, R. O. and KRIEG, D. B. - 'Accuracies of Numerical Solution Methods for the Elastic-Perfectly Plastic Model', J. Press. Vess. Techn. ASME, 1977, 99, 510.
5. SAVIĆ, Lj. - 'Static Analysis of Elastic-Plastic Behaviour of Metallic Structures', (in serbocroatian), PhD thesis, Civil Engineering Faculty, Belgrade (to be published).
6. MARCAL, P. V. - 'A Stiffness Method for Elastic-Plastic Problems', Int. J. Mech. Sci., 1965, 7, 229.
7. RICE, J. R. and TRACEY, D. M. - 'Computational Fracture Mechanics', Numerical and Computer Methods in Structural Mechanics, Ed. Fenves, S. J., Perrone, N., Robinson, A. R. and Schnobich, W. C., Academic Press, New York, 1973, p. 585.
8. WILKINS, M. L. - 'Calculations of Elastic-Plastic Flow', Methods of Computational Physics, Ed. Alder, B., Fernback, S. and Rotenberg, M., Vol. 3, Academic Press, New York, 1964.





## ANALYSIS OF THIN-WALLED BEAMS WITH DEFORMABLE CROSS SECTION

Rastislav Mandić

Faculty of Civil Engineering, University of Belgrade  
Yugoslavia

### SUMMARY

An analytical model for the analysis of thin-walled beams with deformable cross section is investigated. Starting from the rather general elastic solution a reinterpretation of Sedlacek's theory is presented. This theory has been implemented in the computer program capable of analysis of continuous box beams with or without side cantilevers under eccentric uniform and concentrated loading.

### 1. INTRODUCTION

The analysis of thin-walled beams attracted attention of many researches. An extensive list of references devoted to the above topic is given in [1]. Apart from the numerical (finite elements, finite strips) a special attention has been devoted to simplified models which are easy to apply in everyday engineering practice. In general, these models are expected to give correct insight into the global response of a thin-walled beam taking into account various aspects the structural behaviour (torsion, distortion, shear lag effect, etc.). Sedlacek's [2] theory falls into such category since by decoupling of different modes of actions a relatively simple analytical model can be obtained. The influence of various assumptions of Sedlacek's theory on the accuracy of the analysis is studied in [1] and [3].

In this article the above analytical simplified approach is presented but starting from the assumptions with generality beyond original Sedlacek's work. It is shown which additional assumptions have to be postulated in order to develop original Sedlacek's approach. Shear lag phenomenon is also introduced. At the final point results obtained by the computer program [7] based on the model with independent modes of action are compared with results obtained by some other methods of analysis.

### 2. FUNDAMENTALS OF THE THEORY

The basic assumptions of the theory are:

- a)  $\epsilon_s = 0$ . (in the middle surface of each individual plate)

b)  $\epsilon_n = \gamma_{sn} = \gamma_{zn} = 0$ . (Kirrchoff-Love's assumption used in the classical plate bending theory)

c) In the plane of the cross section cubic polynomials are used to describe the displacement in the direction  $n$  due to displacements and rotations of the nodal lines.

$$d) \gamma_{zs} = \gamma_{zs}^{SV} + \gamma_{zs}^W$$

$\gamma_{zs}^{SV}$  - primary, Saint-Venant shear deformation

$\gamma_{zs}^W$  - secondary, warping shear deformation

For comparison purposes it is worth noting that these assumptions yield the analytical approach which is closely related to the theory of folded plates with open cross section (Kollbrunner and Hajdin (Chapter V of reference [5])).

Using the above assumptions the components of displacement vector of an arbitrary point of the cross section are:

$$u = \sum_{i=1}^I V_i u_v^{(i)} + \sum_{k=1}^K \phi_k u_\phi^{(k)} + u_p \quad ( )' = \frac{\partial}{\partial z} ( ) \quad (2.1a)$$

$$v = \sum_{i=1}^I V_i (v^{(i)} - \dot{u}_v^{(i)} n) - \sum_{k=1}^K \phi_k \dot{u}_\phi^{(k)} n - \dot{u}_p n \quad ( )' = \frac{\partial}{\partial s} ( ) \quad (2.1b)$$

$$w = - \sum_{i=0}^I V_i' (\omega^{(i)} + u_v^{(i)} n) - \sum_{k=1}^K \phi_k' u_\phi^{(k)} n - u_p' n \quad (2.1c)$$

where generalised warping shape function  $\omega^{(i)}$  is:

$$\omega^{(i)} = \int_0^s (v^{(i)} - \tau^{(i)}) ds \quad i=1,2,\dots,I \quad \omega^{(0)} = 1.$$

In (2.1) generalised coordinates  $V_i(z)$  ( $i=1,2,\dots,I$ ) describe the displacement of the plane hinged mechanism consisting of axially stiff rods coinciding with the middle line of the cross section. It is assumed that  $V_1(z)$ ,  $V_2(z)$  and  $V_3(z)$  are two translational and one rotational rigid body movements respectively, while coordinates  $V_i(z)$   $i=4,5,\dots,I$  are associated with the distortion of the cross section. The function  $V_0(z)$  is related to the translation of the cross section in the longitudinal direction. The functions  $\phi_k(z)$  are rotations of the nodal lines

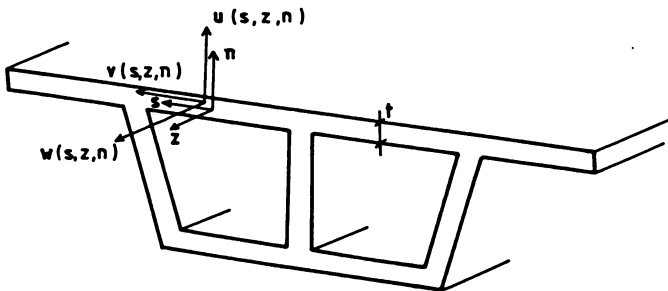


Fig. 1

while  $u_p(s,z)$  is displacement in direction  $n$  in the case of  $V_i = \phi_k = 0$ . The properties of the shape functions  $v^{(i)}(s)$ ,  $u_v^{(i)}(s)$  and  $u_\phi^{(k)}(s)$  follow from the basic assumptions.  $\tau^{(i)}$  is Saint Venant shear stress in the middle surface in the

case of  $GV_i = 1$ . On the wall between cells M and L  $\tau^{(i)}$  is given by:

$$\tau^{(i)} = \frac{q_M^{(i)} - q_L^{(i)}}{t} \quad i=3,4,\dots,I \quad (2.2)$$

In (2.2)  $q_M^{(i)}$  and  $q_L^{(i)}$  are Saint Venant shear flows in cells M and L respectively. They are calculated from the compatibility conditions:

$$\int_M \frac{\partial w}{\partial s} ds = 0 \quad M = 1, 2, \dots, M_{tot} \quad (2.3)$$

which can be transformed to a system of linear equations for torsional and each distortional degree of freedom. Note that integral in (2.3) is evaluated along the mid-line of each cell M of the cross section consisting of  $M_{tot}$  cells. For the open portions of the cross section  $\tau^{(i)} = 0$ , since there is no shear deformation in the middle surface. In this case kinematical relations (2.1) are the same as the relations (V.25) from reference [4].

The components of strain tensor are obtained by appropriate differentiation of the displacements:

$$\epsilon_z = \frac{\partial w}{\partial z} \quad \epsilon_s = \frac{\partial w}{\partial s} \quad \gamma_{zs} = \frac{\partial w}{\partial s} + \frac{\partial v}{\partial z} \quad (2.4)$$

Applying constitutive relations (Hook's law) following stress components can be expressed in terms of strains:

$$\sigma_z = E_1(\epsilon_z + \nu\epsilon_s) \quad \sigma_s = E_1(\epsilon_s + \nu\epsilon_z) \quad \tau_{zs}^{SV} = G\gamma_{zs} \quad (2.5)$$

$$E_1 = \frac{E}{1-\nu^2} \quad G = \frac{E}{2(1+\nu)}$$

It is worth noting that from (2.5) beside  $\sigma_z$  and Saint-Venant shear stress  $\tau_{zs}^{SV}$  only antisymmetrical component of  $\sigma_s$  (i.e. transverse bending moment  $m_s = \int \sigma_s n dn$ ) can be obtained. The rest components of the stress tensor can be found out from the equilibrium conditions in the similar manner as was presented in Chapter V of reference [5]. However in evaluating  $\tau_{zs}^W$  problem is statically indeterminate and shear deformation  $\gamma_{zs}^W$  must be additionally taken into account and the compatibility conditions (2.3) have to be solved again.

By virtue of the principle of virtual work the system of coupled differential equations, i.e. the governing equations of the problem, can be derived:

$$K_1 U^{IV} - K_2 U^{III} + K_3 U = \frac{1}{E_1} R \quad (2.6)$$

where  $U^T = \{v^T \phi^T\}$  is the displacement vector consisting of parameters  $v_s$  and nodal rotations  $\phi_k$  while  $R$  is load vector. Stiffness matrices  $K_1$ ,  $K_2$  and  $K_3$  depend on the geometry of the cross section and on the choice of parameters  $v_s$ . As was expected the equations (2.6) have the same form as governing equations for folded plates with open cross section (Eq.V86 from reference [5]). Because of that the above stiffness matrices can be obtained by adopting the corresponding matrices from [5] to the presence of Saint-Venant shear strain in the middle surface in the closed portions of the cross section.

In order to derive Sedlacek's model following additional assumptions have to be introduced:

- e) longitudinal normal stress  $\sigma_z$  is assumed to be constant throughout the wall thickness
- f) Torsional moment  $m_{zs} = \int \tau_{zs} n dn$  are assumed to be constant between nodal

lines:

$$m_{zs} = -\frac{Gt^3}{6} \left( \sum_{i=3}^I V_i' \dot{u}_v^{(i)} + \sum_{k=1}^K \phi_k' \dot{u}_\phi^{(k)} \right) - \frac{Gt^3}{6} u_p' \rho - \frac{Gt^3}{6} \sum_{i=3}^I V_i' \dot{u}_{v0}^{(i)} \quad (2.7)$$

where  $\dot{u}^{(i)}$  stands for the function which presents the rotation of the rods of the corresponding plane mechanism in case of  $V_i = 1$ .

g) Transverse bending moment  $m_s$  are assumed not to be affected by longitudinal curvature:

$$m_s = -\frac{E_1 t^3}{6} \left( \sum_{i=4}^I V_i u_v^{(i)} + \sum_{k=1}^K \phi_k u_\phi^{(k)} + u_p \right) - \underbrace{-\nu \frac{E_1 t^3}{12} \left( \sum_{i=1}^I V_i' u_v^{(i)} + \sum_{k=1}^K \phi_k' u_\phi^{(k)} + u_p' \right)}_{\text{neglected}} \quad (2.8)$$

Since the additional assumptions yield an algebraic relation between functions  $V_i$  and  $\phi_k$  the matrix equation (2.6) is transferred to the equations of terms of coordinates,  $V_i$  only:

$$E_1 A V^{IV} - G F V^{II} + E_1 E V = R_0 \quad (2.9)$$

In this case stiffness matrices can be recognised as axial, bending and warping stiffness (matrix  $A$ ), Saint-Venant shear stiffness (matrix  $F$ ) and transverse bending stiffness (matrix  $E$ ).

### 3. INTRODUCING SHEAR LAG

According to the presented theory longitudinal stress varies lineary between nodal points of the cross section. However, the behaviour of a real beam is somewhat different. Because of the shear strain  $\gamma_{zs}$  longitudinal stress is distributed non-

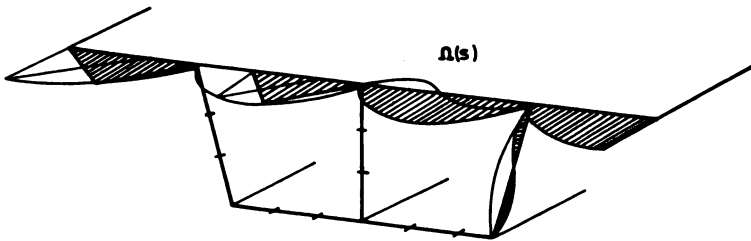


Fig. 2

uniformly throughout the width of each plate. In order to take this phenomenon, known as shear lag into account additional warping functions (Fig. 2) will be introduced. Instead of (2.1c) longitudinal displacement is now given by:

$$w = -\sum_{i=0}^I V_i' (\omega^{(i)} + u_v^{(i)} n) - \sum_{k=1}^K \phi_k' u_\phi^{(k)} n - u_p' n + \sum_{p=1}^P w_p \Omega^{(p)} \quad (3.1)$$

where:  $W_p(z)$  = warping functions

$\Omega^p(s)$  = linearly independent shape functions constant throughout the wall thickness

With displacement field established the procedure outlined in the previous section can be used in deriving strains, stresses and governing equation. Note that in this formulation shear strain which is calculated by virtue of (2.4) is not restricted to Saint-Venant shear strain. Because of that from the strain-stress relationships besides longitudinal normal stress, transverse bending stress and Saint-Venant shear stress, a part of warping shear stress can be obtained. However, in order to calculate total warping shear stress the procedure mentioned in previous section must be applied again.

The governing equation describing axial loading, bending, torsion, distortion and shear lag is in matrix form:

$$E_1 \begin{bmatrix} A & B \\ B^T & C \end{bmatrix} \begin{bmatrix} V \\ Z \end{bmatrix}^{IV} - G \begin{bmatrix} F & \phi \\ \phi & S \end{bmatrix} \begin{bmatrix} V \\ Z \end{bmatrix}^{II} + E_1 \begin{bmatrix} E & \phi \\ \phi & \phi \end{bmatrix} \begin{bmatrix} V \\ Z \end{bmatrix} = \begin{bmatrix} R_0 \\ R_s \end{bmatrix} \quad (3.2)$$

The equation (3.2) is derived introducing warping function  $Z_p$  instead of  $W_p$  so that  $W_p = -Z_p$ . The additional assumptions of Sedlacek's theory are also introduced, although the model described by the equation (2.6) can be modified by warping as well. In (3.2) matrices  $C$  and  $S$  are additional warping stiffness and warping shear stiffness respectively. The close examination of (3.2) shows that  $B$  presents coupling between primary and additional warping while shear coupling between Saint-Venant shear stress and additional warping shear stress does not exist at all.

It is important to notice that the idea with additional warping shape functions can be treated as a first step towards the approach in which longitudinal displacement field is expressed in terms of quite independent functions (Kollbrunner and Hajdin (Chapter VI of reference [5])). Further, if the same discrete points are used to describe warping and the motion in the plane of the cross section and if series are used to solve the governing equation, a similarity with finite strip method [6] can be recognised.

#### 4. SOLUTION OF THE DIFFERENTIAL EQUATION

For the solution of system (3.3) strategy suggested by Sedlacek [2] and Maisel [4] can be used to obtain a set of separate differential equation for each degree of freedom. The full orthogonalization is achieved performing appropriate transformation of generalised coordinates and neglecting the coupling effects which are of low structural significance. The influence of such an assumption on the accuracy in the analysis of single cell simple supported beams with or without side cantilevers under concentrated and uniform loading is studied in [3]. According to the results of this study in the case of concentrated loading the separate treatment of torsional and distortional effects is reasonable if the total value of  $\sigma_z$  due to bending, torsion and distortion is calculated. Transverse bending moments and stresses in girders subjected to uniform loading seem not to be sensitive to uncoupling torsional and distortional action.

Once the orthogonalization has been performed the following system of separate differential equations describe the behaviour of a thin walled beam:

$$E_1 a_{ii} V_i^{IV} - G f_{ii} V_i^{II} + E_1 e_{ii} V_i = R_i \quad i=1,2,\dots,I,I+1,\dots,I+P \quad (4.1)$$

where:

$$V_{I+P} = Z_p, \quad \omega^{(I+P)} = \Omega^{(P)} \dots \text{etc}$$

These equations are analogous to the equation of a straight prismatic beam on elastic foundation subjected to bending and axial loading. However the "elastic foundation" exists in distortional modes only, while for the bending even no "axial load" is present. Note that if antisymmetrical component of  $\tau_{zs}$  is neglected (i.e.  $m_{zs} = 0$ .) there is no "axial load" in substituting beam problem for the analysis of the distortional action in single cell girders. This yields to well known "Beam-on-Elastic-Foundation-Analogy" [11].

For the solution of each equation from system (4.1) ordinaty beam statics can be used. It is interest to say that the stresses and strains in thin-walled girder can be expressed in terms of deformations (and forces) of substituting beams. In case of  $p_z = 0$ . longitudinal normal membrane force  $n_z = \int \sigma_z dn$  and total warping shear force are:

$$n_z = \sum_{i=1}^{I+P} \frac{M_i \omega^{(i)}}{a_{ii}} t \quad n_{zs}^w = \sum_{i=1}^{I+P} \frac{Q_i S_i}{a_{ii}} \quad (4.2)$$

where  $M_i$  and  $Q_i$  are bending moments and shear forces in substituting beams while  $S_i$  are warping shear stress distribution functions:

$$S_i = \int_s \omega^{(i)} t ds - S_{i0} \quad i=1,2,\dots,I+P \quad (4.3)$$

which are obtained form the equilibrium conditions:

$$\dot{n}_{zs} + n'_z = 0 \quad (4.4)$$

The second term of (4.3) exists only in the closed portions of the cross section. On the wall between the adjacent cells M and L we have:  $S_{i0} = S_{i0}^M - S_{i0}^L$  where  $S_{i0}^M$  and  $S_{i0}^L$  are statically indeterminate warping shear flows (in case of  $GV_i^M = -1$ ). which are calculated using compatibility conditions as was already mentioned in the precious section. Note that in the case of shear lag modes shear stress is calculated by the above procedure and not out of strains.

Torsional moments  $m_{zs}$  (see Eq. 2.7) and Saint-Venant shear forces are proportional to the slopes of the substituting beams. For the latter we can write:

$$n_{zs}^{sv} = G t \sum_{i=3}^I V_i' \tau^{(i)} \quad (4.5)$$

In the case of loading acting along the nodal lines (i.e.  $u_D = 0$ . transverse bending moments are proportional to the deflections of substituting beams. It can be realised from equation (2.8) having in mind an algebraic relations between functions  $V_i$  and  $\phi_k$ .

A computer program for the analysis of continuous single cell beams with or without side cantilevers was developed [7] Rigid transverse diaphragms are supposed to be at supports only although with certain modifications girders with diaphragms with finite rigidity within each span could be considered as well. Torsional moments  $m_{zs}$  are neglected. At each mode of action the support moments are chosen to be redundants and they are computed restoring the continuity of displacements over the supports. However, for the analysis of torsional action a slight modified approach which allows for torsional warping shear deformation is used. The governing equation of the problem (Eq. III31 from Ref. [4]) is of the forth order again but the full beam analogy can not be established since warping is not more proportional to the first derivative of the angle of twist. The parametric study presented in [3] justifies this modification. In evaluating torsional warping shear stress equilibrium conditions (4.4) are used again. Three additional warping functions are introduced in order to describe shear lag in flanges due to symmetric loading component. For the shape functions second or forth order curves can be alternatively used.

## 5. NUMERICAL EXAMPLES

### EXAMPLE 1

Simply supported box beam (span 1524 mm) with side cantilevers subjected to concentrated loading is analysed. Rigid diaphragms which prevent torsion and distortion but show no resistance to warping are supposed to be at the supports only. Obtained values of longitudinal strain (solid line in Fig. 3) are compared experimental data from references [9] and [10]. For the warping fourth order curve is used.

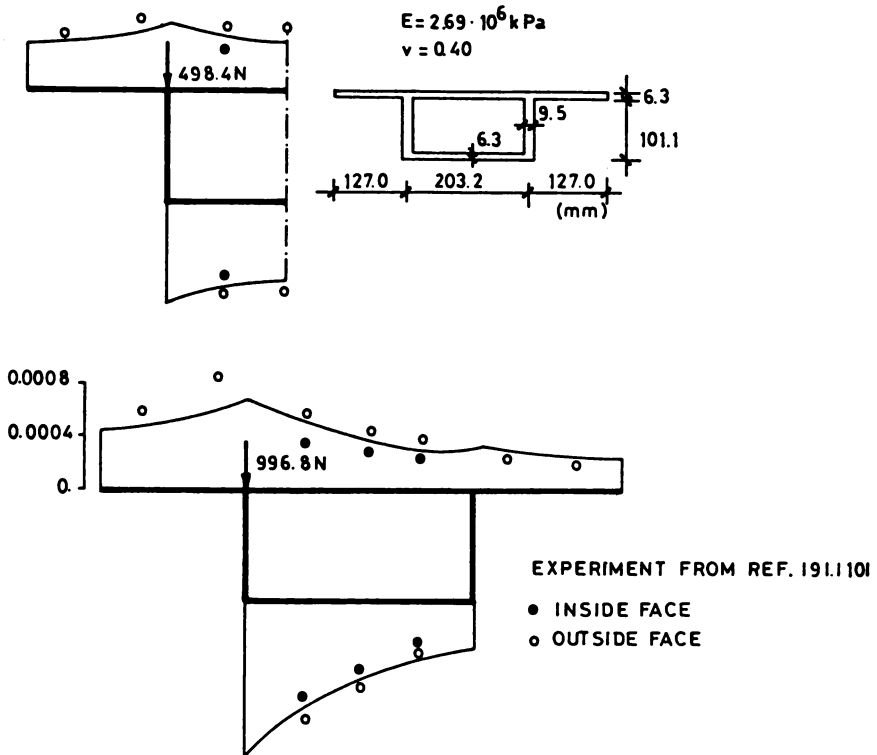


Fig. 3

### EXAMPLE 2

The effect of shear lag in simply supported box girders subjected to bending is analysed (Fig. 4). For the warping fourth order curve is used. The calculated values of effective breadth ratios are compared with those obtained by Moffatt and Dowling [8] by means of finite element method. In the case of concentrated loading greater differences are observed only in the girders with very short spans. For the uniform loading (these results are not presented here) there is almost no difference between analytically and numerically obtained values.



B/L	Z/L	$B_{EF}/B$		FEM
		FEM	ANALIT.	ANALIT.
0.10	0.25	1.00	1.0	1.00
	0.50	0.80	0.83	0.96
0.20	0.25	1.00	1.00	1.00
	0.50	0.67	0.71	0.94
0.40	0.25	0.98	0.95	1.03
	0.50	0.49	0.54	0.91
0.80	0.25	0.63	0.63	1.00
	0.50	0.30	0.36	0.83

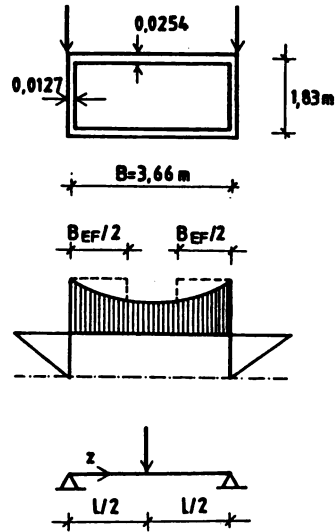


Fig. 4

#### REFERENCES

- [1] Maisel, B. I., "Analysis of concrete box beams using small computer capacity", Cement and Concrete Association, Development Report 5, 1982.
- [2] Sedlacek, G., "Systematische Darstellung des Biege und Verdrehvorganges für prismatische Stäbe mit dünnwandige Querschnitt unter Berücksichtigung der Profilverformung", Fortschritt-Berichte VDI-Zeitschrift, Reihe 4, Nr. 8, Sept. 1968.
- [3] Mandić, R., Hajdin, N. "A contribution to the analysis of box beams with deformable cross section", Proceedings of "International Conference on Steel Structures" (held in Budva Yugoslavia 1986), pp 431-440. See also: Journal of Constructional Steel Research, Vol. 9, No. 2, 1988.
- [4] Kollbrunner, C.F., Hajdin, N. "Dünnwandige Stäbe", Band 1, Springer-Verlag 1972.
- [5] Kollbrunner, C.F., Hajdin, N. "Dünnwandige Stäbe", Band 2, Springer-Verlag 1975.
- [6] Cheung, Y. K., "Finite strip method in structural analysis", Pergamon Press 1976.
- [7] Mandić, R. "Analysis of thin-walled beams with closed and deformable cross section" M.Sc. Thesis, Civil Engineering Faculty, University of Belgrade, 1985.
- [8] Moffatt, K. R., Dowling, P.J., "Shear lag in steel box girder bridges", The Structural Engineer, October 1975, No. 10, Vol. 53. pp. 439-448.
- [9] Sawko, F., Cope, R. J., "Analysis of spine beam bridges using finite elements", Civil Engineering and Public Works Review, Febr. 1970, pp 146-170.
- [10] Cope, R. J., "Discussion of "The Western Avenue Extension-The Design of Section Five"", The Structural Engineer, Vol. 49, No. 3, March 1971, pp. 157-160.
- [11] Wright, R. N., Abdel-Samad, S.R., Robinson, A. R. "BEF Analogy for the analysis of box girders", Proceeding of ASCE. Vol. 94, No. St.7, July 1968 pp. 1719-1743.

## ACADEMICIAN NIKOLA HAJDIN

### CURRICULUM VITAE

#### 1) BASIC INFORMATION

Nikola Hajdin was born on 4 April 1923 in Vrbovsko, Yugoslavia. He is of Serbian nationality.

He enrolled at the Civil Engineering Faculty in Belgrade in 1945, and graduated from its Structural Department in 1951.

The same year he was elected as a research assistant of the Civil Engineering Faculty in Belgrade, in Structural Mechanics. He took his Ph.D. degree at the Faculty of Engineering of Belgrade University in 1956.

In 1960 he was elected an assistant professor, in 1961 an associate professor and in 1966 a professor at the Civil Engineering Faculty in Belgrade.

In 1970 he was elected a corresponding member of the Serbian Academy of Sciences and Arts and in 1976 a full member.

In 1987 Nikola Hajdin was elected a member of the Slovenian Academy of Sciences and Arts.

#### 2) SCIENTIFIC ACTIVITIES

The scientific areas in which Hajdin has made a considerable contribution are:

- a) Numerical Methods in Structural Engineering
- b) Thin-Walled Structures
- c) Bridges.

Professor Hajdin has proposed and elaborated a method for the numerical analysis of boundary value problems in the Theory of Elasticity, which has proved to be suitable for one and two dimensional elastic systems. The method has been widely applied in various technical branches. This particular procedure has been exceptionally well applied in the analysis of large hydro-technical

structures such as arch dams.

Thin-Walled Members are another scientific field in which academician Hajdin has made an exceptional contribution. He was the first scientist to introduce this particular field into Yugoslav science and practice on a broad basis.

Papers by Prof. N. Hajdin in this field, mostly published abroad, are ranked among the most serious and essential works in this field.

He has spent several periods in Switzerland as guest of the Swiss Association for Steel Structures and taken part in research with Dr. C.F. Kollbrunner regarding the Theory of Thin-Walled Members.

### 3) LECTURING IN YUGOSLAVIA AND ABROAD

At the Civil Engineering Faculty in Belgrade, Prof. Hajdin has lectured in the following subjects: Strength of Materials, Structural Analysis, and Theory of Plates and Shells.

As a professor, Hajdin has held courses in special scientific fields for post-graduate students at the Civil Engineering and Natural Science and Mathematical Faculties (the Mechanics group) in Belgrade, the Civil Engineering and Mechanical Faculties in Skopje and Civil Engineering Faculties in Zagreb and Ljubljana.

As a visiting professor he delivered lectures on the subject of Thin-Walled Members at the Swiss Federal Institute of Technology (ETH) in Zurich, during the summer terms in 1970/71 and 1972/73.

In addition he has given lectures at scientific conferences in various countries, at universities, scientific and professional institutions, such as:

University College London (Great Britain),  
ETH - Lausanne (Switzerland),  
University of Prague, (Czechoslovakia),  
University of Bratislava, (Czechoslovakia),  
University of Stuttgart (Fed.Rep.Germay),  
University of Dresden (Ger.Dem.Republic),  
Chinese Academy of Sciences, Peking (China),  
Indian Institute of Structural Engineers, Calcutta,  
Bombay (India),  
Austrian Association of Engineers and Architects,  
Vienna (Austria),  
University of Baghdad, (Iraq),  
TH. Aachen (Fed.Rep.Germany),  
University of Hanover (Fed.Rep.Germany).

N. Hajdin has supervised a large number of theses for master's and doctor's degrees and has also been a member of various boards for the appraisal and defence of doctor's theses at almost all universities in Yugoslavia.

For the past five years he has been a coordinator for a complex scientific-research project: "Stability and Plasticity of Steel Structures and their Application in Design and Construction". This project has been developed by a large group of experts from the Serbian Academy of Sciences and Arts, the Civil Engineering Faculties in Belgrade and Niš, as well as the "GOŠA" Steel Structure Factory in Smederevska Palanka and "MIN" of Niš.

In the course of this project successful international cooperation has been developed with the Czechoslovakian Academy of Sciences, Imperial College London and University College Cardiff.

#### 4) CREATIVE ACTIVITIES IN CIVIL ENGINEERING DESIGN

Another field to which N. Hajdin has dedicated himself is that of civil-engineering design. Either as an author or as a consultant, Hajdin has taken part in many of the biggest Yugoslav Engineering achievements. A great deal of his work carries new design ideas and extends Yugoslav possibilities in this field.

Even as a young design engineer, he was given top awards in anonymous competitions for bridge designs over the Tisa river near Žablje and over the Sava near Orašje. Both bridges were later constructed on the basis of these designs.

During 1958 and 1959 he was employed as a design engineer and consultant with the Steel Construction Company, Zschokke, Switzerland.

For many years N. Hajdin has been a consultant in such companies as: "Energoprojekt" in Belgrade, "Energoinvest" in Sarajevo and "Metalna" in Maribor, participating in supervising works in various projects in the fields of hydro techniques and bridge construction.

In record of his rich professional activity, Hajdin's exceptionally successful participation in projects carried out by Yugoslav civil-engineering companies abroad should be stressed.

Two famous bridges of the structural type known as cable-stayed bridges comprise Prof. Hajdin's most important structural achievements.

#### 5) MEMBERSHIP AND DUTIES

N. Hajdin has carried out a number of duties at his own Faculty; inter alia he has held the positions of vice-dean, dean and president of the Faculty Council.

He has been very active in professional and scientific organizations. His numerous honorary offices have included:

President of the Union of Yugoslav Associations of Structural Engineers,

President of the Yugoslav Group of the International Association of Bridges and Structural Engineering and a Member of the Permanent Committee of this organization,

President of the Yugoslav Committee of the International Union for Theoretical and Applied Mechanics,

Member of the Urbanistic Council of Belgrade,

Member of the Scientific Committee of the Italian international magazine - "Construzioni Metaliche",

Member of several committees of the Serbian Academy of Sciences and Arts,

President of the Scientific Committee of the Institute of Technical Sciences (Serbian Academy Sciences and Arts),

Member of the Civil Engineering Committee of the Republican Community of Science of Serbia,

#### 6) PUBLIC RECOGNITIONS AND AWARDS

Prof. Hajdin has received the following awards:

October Award of Belgrade, 1959,

October Award of Novi Sad, 1979,

Order of Labour with Golden Wreath,

Order of National Merit with Golden Star,

The AVNOJ Award for Scientific Work, 1987 (the highest Yugoslav award in this field),

Plaque of the City of Belgrade on the 40th Anniversary of the city's liberation,

Honorary Member of the Yugoslav Association for Mechanics,

Honorary Member of the Union of Associations of Structural Engineers of Yugoslavia,

Honorary Member of the Union of Civil Engineers and Technicians of Yugoslavia,

and a number of recognitions, awards and plaques granted by industrial and other organization.

## LIST OF PAPERS AND BOOKS

BY NIKOLA HAJDIN

1. Torzija trouglaste cevi, (Torsion of triangular tube). Godišnjak Tehničkog fakulteta Univerziteta u Beogradu, 1949 (1946-1947), pp. 27-29.
2. Jedno tačnije rešenje poliedarske ljske, (A more rigorous solution of folded plate). Glas SAN, 1952, CCXX, Odeljenje tehničkih nauka, 3; pp. 101-112.
3. Contribution à la solution du problème plan. - Publications de l'Institut mathématique de l'Académie serbe des sciences, 1953., V; pp. 53-62, tab. 1.
4. Une méthode pour la solution numérique des problèmes de valeurs aux limites du type elliptique et son application à certains problèmes de la théorie de l'élasticité.- IX Congrès International de Mécanique appliquée. Actes, t. V., Bruxelles 1956; pp. 261-273.
5. Ein Verfahren zur numerischen Lösung der Randwertaufgaben von elliptischen Typus. - Publications de l'Institut mathématique de l'Académie serbe des sciences, 1956., IX; pp. 69-78.
6. Cilindrična ljska promenljive debljine, (Cylindrical Shell of Variable Thickness). - II Kongres gradjevinskih konstruktora Jugoslavije, 19-24 maja 1958., Opatija, Beograd, pp. 218-225.
7. A Contribution to the Analysis of Arch Dams with remarks concerning "Trial Load" method. - Paris, 1958; p. 21. - (Commission international des grands barrages. Bulletin 12).
8. Jedan postupak za numeričko rešavanje graničnih zadataka i njegova primena na neke probleme teorije elastičnosti, (A Method for Numerical Solution of Boundary Values Problems and its Applications to Certain Problems of the Theory of Elasticity (Doctor Thesis). - Zbornik Gradjevinskog fakulteta u Beogradu, 1958., 4; pp. 1-57.
9. Prilog statičkoj analizi lučnih brana sa osvrtom na "Trial Load" postupak, (A Contribution to the Statical Analysis of Arch Dams with the Coments Concerning "Trial Load" Method). - Saopštenje sa četvrtog savetovanja stručnjaka Jugoslavije o visokim branama. Skopje 14-16 juna 1957. Beograd, 1958.

10. Knickdiagramme für Stäbe mit sprungweise veränderlichen Trägheitsmoment, Eulerfälle I und II, (mit C.F.Kollbrunner und S.Milosavljević). Zürich, 1959; S. 45+ Diagr. 10. - (Mitteilungen über Forschung und Konstruktion in Stahlbau, 24).
11. An integral equations method for arch dam analysis. - Bulletin of the International Association for Shell Structures, 1960, 23; pp. 57-66.
12. Knickdiagramme für Stäbe mit sprungweise veränderlichen Trägheitsmoment, Eulerfälle III und IV, (Mit C.F.Kollbrunner und S.Milosavljević), Zürich, 1960; s. 36+ Diagr. 10. - (Mitteilungen über Forschung und Konstruktion in Stahlbau, 27).
13. Beitrag zur Berechnung von Stauwehrklappen, (mit C.F.Kollbrunner). Zürich, 1961; s. 52. - (Mitteilungen über Forschung und Konstruktion in Stahlbau, 28).
14. Jedno numeričko rešenje ravnog problema sa primenom na statičku analizu olakšanih brana, (A Numerical Solution of the Plane Stress Problem with Application to the Statical Analysis of Butress Dams (with D.Dimitrijević). Tehnika, 1963, XVIII, 6; pp. 1000-1004.
15. Die St.-Venantsche Torsion, (mit C.F.Kollbrunner), Zürich, 1963; S. 120.- (Mitteilungen der Technischen Kommission der Schweizer Stahlbau Vereinigung, 26).
16. An integral equations method for arch dam analysis. - International Symposium on the Theory of Arch Dams. Southampton, 1964; pp. 331-340.
17. Wölbkrafttorsion dünnwandiger Stäbe mit offenem Profil. Teil I, (mit C.F.Kollbrunner). Zürich, 1964; S. 121.- (Mitteilungen der Technischen Kommission der Schweizer Stahlbau Vereinigung, 29).
18. Štapovi sa tankim zidovima i otvorenim profilom. Autorizovana skripta. (Thin-Walled Members with Open Cross Section), (Text book). Beograd, 1965; /2/+128 str. - (Univerzitet u Beogradu, Gradjevinski fakultet).
19. Uvod u teoriju elastičnosti. Autorizovana skripta, (Introduction to the Theory of Elasticity . Text book). Pripremio za štampu D.Krajčinović. - Beograd, 1966; /6/+75 str. - (Univerzitet u Beogradu, Gradjevinski fakultet).
20. Wölbkrafttorsion dünnwandiger Stäbe mit offenem Profil. Teil II. (mit C.F.Kollbrunner). Zürich, 1965; S. 75+ T.23. (Mitteilungen der Technischen Kommission der Schweizer Stählbau Vereinigung,30)
21. Betrachtungen zur Theorie der dünnwandiger Stäbe und ihrer Anwendung im Bauwesen, (mit C.F.Kollbrunner). Schweizerische Bauzeitung, 1966, 84 Jg, Hft 41; s. 715-719.
22. Wölbkrafttorsion dünnwandiger Stäbe mit geschlossenem Profil. (mit C.F.Kollbrunner). Zürich, 1966; S. 175 + T.41. (Mitteilungen der Technischen Kommission der Schweizer Stahlbau Vereinigung,32).
23. Discussion. Section 1. - Arch Dams. A review of British Research and Development. Proceedings of the Symposium held at the Institution of Civil Engineers 20-21 March 1968. London, 1968; p.27.

24. Displacement Method in the Theory of Thin Walled Members, and a New Calculation Model for the Thin-Walled Bars with Deformable Contours, (with C.F.Kollbrunner). Publications of the International Association for Bridge and Structural Engineering. 1968, v. 28b; pp. 87-100.
25. Dünnwandige Stäbe mit in ihren Ebenen deformierbaren Querschnitten. Theorie der Faltwerke nach der Verschiebungsmethode, (mit C.F.Kollbrunner). Zürich, 1968; S. 98. Institut für bauwissenschaftliche Forschung, 1).
26. Beitrag zur Theorie der dünnwandiger Stäbe mit gekrümmter Achse, (mit C.F.Kollbrunner). Zürich, 1969; S. 56. (Institut für bauwissenschaftliche Forschung, 8).
27. Matrix Analysis of Thin-Walled Structures, (with C.F.Kollbrunner and D.Krajčinović). Zürich, 1969; p. 83. (Institut für bauwissenschaftliche Forschung, 10).
28. Numerički postupci i primena elektronskih računara u teoriji konstrukcija (Numerical Methods and Application of Computers in the Structural Mechanics). Savremene armirano-betonske konstrukcije. Beograd, 1969; str. 12-16. (Časopis "Izgradnja", specijalno izdanje).
29. Diferencijalne jednačine tankozidnog štapa sa kružnom osovinom (Differential Equations of the Thin-Walled Circular Bar). Zbornik radova posvećen preminulom akademiku Jakovu M. Hlitičijevu. Beograd, 1970; str. 401-415.
30. Der Einfluss des Kriechens und Schwindens des Betons in dünnwandigen Trägern mit gekrümmter Achse. L'influence du fluage et du retrait, l'effet des changements de température sur les constructions en béton. Symposium de l'Association internationale des ponts et charpentes. Madrid, 1970. Extrait du rapport final; p. 423-430.
31. Lučna brana Glažnja (sa D.Dimitrijevićem) (Arch Dam "Glaznja"). Saopštenja od VIII kongres na Juslovenskiot komitet za visoki brani. Ohrid 1970; Skopje, 1971; str. 21-33.
32. Prilog rešenju tankozidnog štapa u krivini sa deformabilnim poprečnim presekom (sa M.Stankovićem). (A Contribution to the Solution of a Curved Bar with Deformable Cross-Section). Zbornik radova X Jugoslovenskog kongresa za racionalnu i primenjenu mehaniku. Baško Polje 1970; str. 535-558.
33. Proračun linijskih sistema prema stadijumu granične ravnoteže. (Analysis of Linear Systems According to the Ultimate Limit State). Plastično ponašanje građevinskih konstrukcija. Materijali sa savetovanja, Beograd, 1971; str. 23-47.
34. Beitrag zur Lösung des durch die Querrahmen ausgesteiften dünnwandigen Stäbes. - Zbornik Posobenie tenkostenných otvorených a uzavretých jedno, alebo viacvážných prierezov, Symposium. Piešťany 20-22 IX 1972; p. 77-81.
35. Contribution to the numerical analysis of beams, grids and plates on elastic foundation, (with C.F.Kollbrunner and M.Sekulović). Zürich, 1972; p. 53. (Institut für bauwissenschaftliche Forschung, 23).



36. Dünnwandige Stäbe. Bd 1: Stäbe mit undeformierbaren Querschnitt-  
en, (mit C.F.Kollbrunner). Berlin, Springer-Verlag, 1972; S. XII  
+296.
37. Integral Equation Method for Solution of Boundary Value Problems  
of Structural Mechanics. Pt. I: Ordinary Differential Equations.  
Pt II: Elliptic Partial Differential Equations (with D.Krajčino-  
vić). International Journal for Numerical Methods in Engineering,  
1972., v.4, n.4, pp. 509-539.
38. Teorija tankozidnih štapova i njena primena u tehnici. (Theory  
of Thin-Walled Members and its Application in Engineering). -  
Spomenica u čast novoiyabranih članova Srpske akademije nauka i  
umetnosti. Beograd, 1972; str. 161-164. (Posebna izdanja SANU,  
CDLII, Spomenice, 55).
39. Uticaj ukrućenja na deformabilnost sandučastih nosača. (Influen-  
ce of Stiffeners on the Deformability of Box Girders). Savremena  
dostignuća u čeličnim konstrukcijama. Materijal sa savetovanja.  
Beograd, 1972; ref. III, str. 16.
40. Različite mogućnosti sprezanja betona i čelika u mostogradnji.  
(Different Possibility of Composite Action Between Steel and  
Concrete in Bridges). Spregnute konstrukcije. Beograd, 1973; str.  
30-37. Časopis "Izgradnja", posebno izdanje.
41. Folded Plates Stiffened by Diaphragms. International Association  
for Shell Structures, Symposium on Folded Plates and Spatial Pa-  
nel Structures. Udine, September 23-27, 1974. Preliminary Report,  
p. 8.
42. Granična nosivost tankozidnih preseka napregnutih na ograničenu  
torziju. (Ultimate State of Thin-Walled Cross-Section Loaded on  
Warping Torsion). XII jugoslovenski kongres racionalne i prime-  
njene mehanike. Sekcija C5. Ohrid, 1974; rf. 7, str. 10.
43. Izbočavanje vitkih vertikalnih limova (Buckling of Slender Webs).  
V kongres Jugoslovenskog društva građevinskih konstruktora.  
Budva, 30.9-5.10.1974; str. 203-216.
44. Približno rešenje vezanog bočnog izvijanja kontinualnog nosača  
deformabilnog I-preseka. (An Aproximate Solution of Lateral Buck-  
ling of a Continuous Girder with Deformable Contour). XII jugos-  
lovenski kongres racionalne i primenjene mehanike. Sekcija C3.  
Ohrid, 1974; ref. 6, str. 7.
45. Sopstvene vibracije grednih sistema sa kablovima (sa D.Dimitrije-  
vićem i Lj.Savićem), (Free Vibrations of Cable-Stayed Girders).  
V kongres Jugoslovenskog društva građevinskih konstruktora.  
Budva, 1974; str. 217-229.
46. Contribution to the analysis of diaphragms embedded into an elas-  
tic semi-infinite solid, (with C.F.Kollbrunner and M.Sekulović).  
Zürich, 1975; p. 78. Institut für bauwissenschaftliche Forschung,  
35).
47. Dünnwandige Stäbe. Bd 2: Stäbe mit deformierbaren Querschnitten.  
Nicht-elastisches Verhalten dünnwandiger Stäbe, (mit C.F.Kollb-  
runner). Berlin, 1975; S. XII+284. (Springer-Verlag).
48. Granična nosivost tankozidnih preseka napregnutih na ograničenu  
torziju. (Carrying Capacity of Thin-Walled Cross-Sections Loaded  
on Warping Torsion). Čelične konstrukcije, Beograd, 1975; str.  
37-40 (Časopis "Izgradnja", posebno izdanje).

49. Näherungslösung der gebendene Kippung des Durchlaufträgers mit I-Querschnitt, (mit C.F.Kollbrunner). Zürich, 1975; S. 23. (Institut für bauwissenschaftliche Forschung, 33).
50. Pregled radova iz mehanike čvrstog deformabilnog tela. (A Review of Papers on Mechanics of Solid Body). (sa N.Naerlović-Veljković) Tehnika, 1975., XXX 1; str. 12-16.
51. Proračun linijskih nosača prema stadijumu loma. (Design of Linear System on Ultimate Limit State). Čelične konstrukcije. Beograd, 1975; str. 3-12. (Časopis "Izgradnja", posebno izdanje).
52. Teorijske podloge za dimenzionisanje I-nosača sa tankim rebrom. (Theoretical Basis for Dimensioning of I-Girders with Slender Web). Čelične konstrukcije. Beograd, 1975; str. 168-192. (Časopis "Izgradnja", posebno izdanje).
53. Ispitivanje neelastičnog ponašanja i određivanje graničnog opterećenja uklještene konzole opterećene na savijanje sa torzijom, (sa B.Čorićem), (Investigation of Non-Elastic Behaviour and Ultimate Load Capacity of a Cantilever Beam Loaded on Bending and Torsion. Tehnika-Naše gradjevinarstvo, 1976., 12; str. 1-6.
54. Izbočavanje vitkih vertikalnih limova. (Buckling of the vertical Slender Webs). Glas SANU, 1976; CCXCV Odeljenje tehničkih nauka, 11, str. 61-74.
55. Undamped vibrations of elastic thin-walled beams of open deformable cross sections, (with C.F.Kollbrunner and S.Brčić). Zürich, 1976., p. 69. (Institut für bauwissenschaftliche Forschung, 38).
56. Vergleich zwischen den Paralleldrahtseilen und verschlossenen Seilen am Beispiel der Eisenbahnschrägseilbrücke über die Save in Belgrad. Dixième congrès de l'Association Internationale des ponts et charpentes. Tokyo, September 6-11, 1976. Extrait du rapport préliminaire. Zürich, p. 471-475.
57. Buckling of Plate Girders With Slender Webs. Bulletin de l'Académie serbe des Sciences et des Arts, 1977., LVII, Sciences techniques, 11; pp. 71-83.
58. Composite thin-walled member with closed cross section (with C.F. Kollbrunner and B.Stipanić). Zürich 1977; 1+66p. (Institut für bauwissenschaftliche Forschung, 39).
59. 20-20-2000 Zwanzig Jahre der Zusammenarbeit, (with C.F.Kollbrunner). Zürich, 1977; 40 S. (Institut für bauwissenschaftliche Forschung, 41).
60. Dinamička analiza mosta "23 oktobar" u Novom Sadu, (Dynamic Analysis of Bridge "23 oktobar" in Novi Sad (sa O. Djurić) . VI kongres Jugoslovenskog društva gradjevinskih konstruktera, Bled 26-29 IX 1978. Knj. Mostovi - M.Beograd, JDGK, 1978; str. 149-157. M14.
61. Eisenbahnschrägseilbrücke über die Save in Belgrad (mit Lj.Jevtović). Der Stahlbau, 1978., Jhrg. 47, Hft. 4; S. 97-106.
62. Elastic-Plastic Thin-Walled I-Section Beam Subjected to Bending and Warping Torsion, (with C.F.Kollbrunner and B.Čorić). Zürich, 1978; 40 p. (Institut für bauwissenschaftliche Forschung, 43).

63. Metod konačnih elemenata i njegova primena u mehanici čvrstog deformabilnog tela. (Finite Element Method and its Application in the Mechanics of Deformable Solid Body) (sa M.Sekulovićem). 14. Jugoslovenski kongres racionalne i primenjene mehanike, Portorož, 5-9 jun 1978. Knj. K., Beograd, JDM, 1978; str. 19-37.K3.
64. Most "23 oktobar" preko Dunava u Novom Sadu, (Bridge "23 oktobar" over River Danube in Novi Sad). VI kongres Jugoslovenskog društva gradjevinskih konstruktora, Bled 26-29 IX 1978. Knj. Mostovi - M.Beograd, JDGK, 1978; str. 133-148, M13.
65. Novi železnički most preko Save u Beogradu, (sa Lj.Jevtovićem, S.Cvetkovićem i V.Matićem), (New Railway Bridge over Sava River in Belgrade). VI kongres Jugoslovenskog društva gradjevinskih konstruktora, Bled 26-29 IX 1978. Knj. Mostovi - M.Beograd, JDGK 1978; str. 81-100, M9.
66. Proračun lokalnih naprezanja u konstrukciji mosta "23 oktobar" u Novom Sadu (sa M.Sekulovićem i G.Srećkovićem), (Calculation of Local Stresses in the Structure of the Bridge "23 Oktobar" in Novi Sad. VI kongres Jugoslovenskog društva gradjevinskih konstruktora, Bled 26-29 IX 1978. Knj. Mostovi - M.Beograd, JDGK, 1978; str. 159-167. M15.
67. Teorija konstrukcija II. Po predavanjima Nikole Hajdina, pripremili D.Dimitrijević i D.Krajčinović, (Structural Mechanics II). 3.izd. - Beograd, Gradjevinski fakultet, 1978. Deo I: Ploče, 101s.
68. Teorija konstrukcija i savremene gradjevinske konstrukcije, (Structural Mechanics and Contemporary Civil Engineering Structures). Spomenica posvećena novoizabranim članovima Odeljenja tehničkih nauka, Beograd, SANU, 1978; 41-47. (Spomenica, IV, Odeljenje tehničkih nauka, 1). (Pristupna beseda). Isto: - Tehnika - Naše gradjevinarstvo, 1979., XXXIII, 3; NG 1 (355) - NG 3 (357).
69. Elastic-plastic fixed ended Beam of I-section subjected to Bending and Warping Torsion, (with C.F.Kollbrunner and P.Obradović) Zürich, 1979; 40 p. (Institut für bauwissenschaftliche Forschung, 46).
70. Most "23 oktobar" preko Dunava u Novom Sadu, (Bridge "23 Oktobar" over river Danube in Novi Sad). Izgradnja, 1979.; XXXIII, 7; str. 9-18.
71. Proračun lokalnih naprezanja u konstrukciji mosta "23 oktobar" u Novom Sadu, (sa M.Sekulovićem), (Analysis of Local Stresses in the Structural System of the Bridge "23 Oktobar" in Novi Sad). Izgradnja 1979., XXXIII, 10; str. 1-4.
72. The Railway Cable-stayed Bridge over the River Sava in Belgrade, (with S.Cvetković and V.Matić). International Association for Bridge and Structural Engineering Periodica, 1979., 4: IABSE Structures C - 10/79. Constructions AIPC Bridges I; p. 30.
73. Teorija površinskih nosača (po predavanjima Nikole Hajdina, pripremio B.Kolundžija) (Plates and Shells). Beograd, Gradjevinski fakultet Univerziteta. Deo II: Ploče napregnute u svojoj ravni, 1979; 59 str. Deo 2: Ploče napregnute u svojoj ravni, 1980; 58str.
74. A Contribution on the Non-Linear Theory of Thin-Walled Member with open Cross Section - Bulletin de l'Académie serbe des Sciences et des Arts, 1980, LXXIII, Sciences techniques, 16; pp. 1-12.

75. Contribution to the Analysis of Cable-Stayed Bridges, (with C.F. Kollbrunner and B.Stipanić). Zürich, 1980; 45 p. (Institut für bauwissenschaftliche Forschung, 48).
76. Novija istraživanja stabilnosti limova i njihov uticaj na izmenu postojećih i budućih propisa, (Recent Investigations on Plate Stability and Their Influence on the Changes of Existing and Coming Standards). Simpozijum "O inovaciji jugoslovenskih propisa za betonske, metalne i spregnute konstrukcije" - Iskustva i nova saznanja, Trogir, 14-16. maja 1980. Beograd, JDGK, Institut za materijale i konstrukcije Gradjevinskog fakulteta Univerziteta, 1980; str. 267-285, MK-4.
77. Prilog nelinearnoj teoriji tankozidnog štapa otvorenog poprečnog preseka, (A Contribution to the Non-Linear Theory of the Bar with Open Cross-Section). Glas SANU, 1980; CCCXXI, Odeljenje tehničkih nauka, 16; str. 17-28.
78. Application of Parallel Wire Cables in Cable-Stayed Bridges for Higways and Railways. - 42nd Indian Roads Congress, Amritsar, December 1981; pp. 1-19.
79. Miodrag Milosavljević (23. april 1905 - 16. septembar 1980.). Godišnjak SANU, 1981, LXXXVII za 1980; str. 465-466. (Nekrolog).
80. Novi Železnički most preko Save u Beogradu (sa Lj.Jevtovićem i S.Cvetkovićem), (New Railway Bridge over Sava River in Belgrade). Izgradnja, 1981., XXXV, 11; str. 63-76.
81. Udeo mehanike u projektovanju gradjevinskih konstrukcija sa posebnim osvrtom na mostove, (Role of Mechanics in Structural Design with the Emphasis on Bridges). 15. jugoslovenski kongres teorijske i primenjene mehanike. Kupari, 1-5 juna 1981. (Beograd), Savez društva za mehaniku Jugoslavije, (1981.); str. 51-65. K-2.
82. Construction of the Cable-Stayed Bridge "Sloboda" (bridge of freedom) over River Danube in Novi Sad, Yugoslavia (with S.Dinić and H.R.Müller). The Ninth International Congress of the FIP, Stockholm June 6-10.1982. Stockholm, FIP, 1982; pp. 1-16.
83. The Non-Linear Theory of Thin-Walled Member With Open Cross Section. - Teorijska i primenjena mehanika, 1982, 8; pp. 29-39. Isto: - Festschrift Prof. Dr Bruno Thürlimann zum 60. Geburtstag. Zürich, "Schweizer Ingenieur und Architekt", 1983; S. 317-326.
84. Primer proračuna sadejstva objekta i tla (sa D.Šumarcem), (An Example of Interaction Between Structure and Soil). Seminar o "Metodi konačnih elemenata", Beograd 1982. Beograd, Jugoslovenski gradjevinski centar, 1982; str. 339-346.
85. Contribution to the Analysis of Cable-Stayed Bridges (with C.F. Kollbrunner and B.Stipanić). Bridge Engineering Japan (in Japanese) , 1983., vol 19, n.6,7; pp. 16-23, 20-28.
86. Izgradnja mosta Slobode preko Dunava u Novom Sadu, (Construction of the Bridge "Sloboda" ("23 Oktobar") over river Danube in Novi Sad). Naše gradjevinarstvo, 1983, XXXVII 8; str. 1051-1058.
87. Prilog rešenju granične nosivosti proizvoljnog nedeformabilnog poprečnog preseka tankozidnog nosača (sa M.Stankovićem i D.Veličkovićem), (A Contribution to the Carrying Capacity of an Arbitrary Undeformable Cross Section of the Thin-Walled Bar). Zbornik radova Gradjevinskog fakulteta u Nišu, 1983, 4; str. 77-86.

88. Prilog rešenju tankozidnog štapa sa zakrivljenom osom u ravni, proizvoljnog nedeformabilnog poprečnog preseka u elastičnoj oblasti (sa M.Stankovićem i D.Veličkovićem), (A Contribution to the Solution of the Thin-Walled Curved Bar, with the Arbitrary Undeformable Cross-Section in the Elastic Range). Zbornik radova Gradjevinskog fakulteta u Nišu, 1983., 4; str. 67-75.
89. Primena prednapregnutih visokovrednih anker-zavrtnjeva na mostu Slobode preko Dunava u Novom Sadu (sa Lj.Vlajićem), (Application of High Strength Prestressed Anchor-Bolts in the Construction of the Bridge "Sloboda" ("23 Oktobar") over Danube River in Novi Sad). VII kongres Saveza društava gradjevinskih konstruktora Jugoslavije, Cavtat 25-28 aprila 1983. Knj. Mostovi, M. Beograd, SDGKJ, 1983; str. 81-90. M-7.
90. Probno opterećenje glavne čelične konstrukcije mosta Sloboda preko Dunava u Novom Sadu (sa Lj.Vlajićem), (Test Loading of the Main Structural System of the Bridge "Sloboda" over Danube River in Novi Sad). VII kongres Saveza društava gradjevinskih konstruktora Jugoslavije, Cavtat 25-28. april 1983. Knj. Mostovi, M. Beograd, SDGKJ, 1983; str. 59-80. M-6.
91. Proračun mostova sa kosim kablovima po teoriji drugog reda (sa G.Srećkovićem, B.Stipanićem i M.Momčilovićem), (Analysis of Cable-Stayed Bridges Using the Second Order Theory). VII kongres Saveza društava gradjevinskih konstruktora Jugoslavije, Cavtat 25-28. april 1983. Knj. Mostovi, M. Beograd, SDGKJ, 1983; str. 91-99.M-8.
92. Računska analiza lokalnih koncentracija napona u pilonu mosta Slobode preko Dunava u Novom Sadu (sa B.Stipanićem, G.Srećkovićem i B.Pujevićem), (Numerical Analysis of Local Stress Concentrations in the Pylon of the Bridge "Sloboda" over River Danube in Novi Sad). VII kongres Saveza društava gradjevinskih konstruktora Jugoslavije, Cavtat 25-28. april 1983. Knj. Mostovi, M. Beograd, SDGKJ, 1983; str. 101-108. M-9.
93. Strassenrücke "Sloboda" über die Donau in Novi Sad. - Der Stahlbau, 1983., Jhrg. 52, Heft. 4; S. 97-103.
94. Bočno izvijanje čeličnog i nosača deformabilnog poprečnog preseka (sa B.Čorićem), (Lateral Buckling of a Girder with Deformable Cross-Section). Zbornik radova Matematičkog instituta, n.s., 1984, 4(12); str. 75-80.
95. Dejstvo vetra na rashladne kule oblika rotacionog hiperboloida (sa M.Sekulovićem, B.Kolundžijom i Š.Dunicom), (Influence of Wind on the Colling Tower in the form of Hyperboloid of Revolution). 16. jugoslovenski kongres "Teorijske i primenjene mehanike", C, Bečići, 28. maj - 1. juni 1984., Beograd, JDM, 1984; str. 329-338. C7-13.
96. Sekundarni uticaji usled savijanja u kosim kablovima sa paralelnim žicama (sa B.Stipanićem), (Bending Stresses in the Stay Cables with Parallel Wires). 16. jugoslovenski kongres "Teorijske i primenjene mehanike", C: Mehanika čvrstog deformabilnog tela, Bečići, 28.maj-1.juni 1984. Beograd, JDM, 1984; str. 177-184. C1-24.
97. Teorija površinskih nosača. Deo 1 i 2,3 (Theory of Plates and Shells). Beograd, Gradjevinski fakultet Univerziteta, Naučna knjiga, 1984. Deo 1 i 2: Ploče napregnute na savijanje, ploče napregnute u svojoj ravni; 101 str. (Deo 3: Ljuske);105 str.

98. Kongres međunarodnog udruženja za mostove i visokogradnju (IABSE održan u Vancouveru septembra 1984.godine, (12th Congress of Int. Association for bridge and Structural Engineering (IABSE), Vancouver, Sept., 1984.)). Simpozijum Saveza društava građevinskih konstruktora Jugoslavije. Knj. GR-K: Generalni referati i konferencije, Dubrovnik 23-26. april 1985. Beograd, SDGKJ, 1985; str. 165-172. K-7. (Kratak prikaz).
99. Granično stanje deformacije iskustva sa Al-Khulafa Street Development Project-a (sa V.Perićem i Lj.Vlajićem), (Ultimate Limit State of Deformation; Experiences from Al-Khulafa Street Development Project). Simpozijum Saveza društava građevinskih konstruktora Jugoslavije. Knj. IV: Jugoslovensko građevinsko konstruktorstvo u inostranstvu, Dubrovnik, 23-26. april 1985. Beograd, SDGKJ, 1985; str. 92-100. IN-11.
100. Einige Beispiele der Kombination von Stahl und Beton im Brückenbau.- Schweizer Ingenieur und Architekt. Pierre Dubas zum 60. Geburtstag, 1985, Jhrg. 103, Hft. 3; S. 37-39.  
Und : - Festschrift Pierre Dubas zum 60. Geburtstag. Zürich, Schweizer Ingenieur und Architekt, 1985; S. 29-31.
101. Interakcija između tla i panelne zgrade fundirane na lošem tlu, (sa B.Kolundžijom, Š.Dunicom, N.Grubićem i B.Škorom), (Interaction Between the Panel Building and the Subsoil with Low Carrying Capacity). - Simpozijum Saveza društava građevinskih konstruktora Jugoslavije. Knj. IN: Jugoslovensko građevinsko konstruktorstvo u inostranstvu. Dubrovnik, 23-26. april 1985. Beograd, SDGKJ, 1985; str. 85-91. IN-10.
102. Neki problemi projektovanja i izvođenja građevinskih konstrukcija u inostranstvu, (Some Problems of Design and Construction of Civil Engineering Structures in Foreign Countries). Simpozijum Saveza društava građevinsko konstruktorstvo u inostranstvu. Dubrovnik 23-26. april 1985. Beograd, SDGKJ, 1985; str. 1-20. IN-1.  
Isto; (See also): - Izgradnja, 1985, XXXIX, 5; str. 5-14.
103. Elasto-Plastic Behaviour of Thin Walled I-Section Members Subjected to Bending and Warping Torsion. - Steel Structures. Recent Research Advances and Their Applications to Design. (Conference Budva 1986). Ed. by M.N.Pavlović. London and New York, Elsevier Applied Science Publishers, 1986; pp. 193-218.
104. A Contribution to the Analysis of Box Beams With Deformable Cross Section, (with R.Mandić). - Proceedings of the International Conference held at Budva, Yugoslavia, 28th September - 1st October, 1986. Steel Structures. Recent Research Advances and Their Applications to Design. Pt. II. Ed. by N.Hajdin, M.Sekulović. Belgrade, Civil Engineering Faculty, 1986; pp. 431-440.  
See also: Journal of Constructional Steel Research, London, 1988. Vol. 9, No. 2, Elsevier Applied Science.
105. Granična nosivost tankozidnog nosača proizvoljnog zatvorenog profila sa deformabilnom konturom (sa M.Stankovićem i D.Veličkom), (Ultimate Limit State of Thin-Walled Girder with Closed Deformable Contour). 17. jugoslovenski kongres teorijske i primjenjene mehanike. Zadar, 1986., Beograd, JDM, 1986; str. 105-110.

106. Neki aspekti proračuna platformi za porinuće brodova (sa Dj.Vuk-sanovićem i R.Mandićem), (Some Aspects of the Stress and Strain Analysis of the Platforms for Launching Ships). I kongres Društva građevinskih konstruktora Srbije, Vrnjačka Banja 30. i 31. oktobar 1986. Beograd, DGKS, 1986; str. 199-204. R-5.
107. Proračun tankozidnih nosača zatvorenog deformabilnog poprečnog preseka sa zanemarenjem sekundarne smičuće deformacije (sa R. Mandićem), (Analysis of the Thin-Walled Girder with Deformable Cross-Section Neglecting the Secondary Shear Strain). 17. jugoslovenski kongres teorijske i primenjene mehanike. Zadar, 1986. Beograd, JDM, 1986; str. 87-92. C1-15.
108. Naučni i stručni aspekti međunarodne konferencije "Čelične konstrukcije", (Scientific Aspects of International Conference "Steel Structures"). Izgradnja, 1987., XLI, 2; str. 5-9.
109. Some Yugoslav Experiences in Design and Construction of Long-Span Bridges, (with S.Cvetković). Steel Structures. Advances, Design and Construction. Ed. by R.Narayanan (Proceedings of the International Conference on Steel and Aluminium Structures, Cardiff, UK, 8-10 July 1987.). London and New York, Elsevier Applied Science, 1987; pp. 44-53.
110. Vladimir Bogunović (1912-1986). Godišnjak SANU, 1987., XCIII za 1986; str. 509-510. (Nekrolog), (Necrology).
111. Box Girders. - ECCS/BCSA International Symposium on Steel Bridges. London, Shameleon Press Limited Conference Proceedings, 1988., pp. 12/1-12/12.

## SOME OF THE MORE IMPORTANT STRUCTURES DESIGNED BY NIKOLA HAJDIN

N. Hajdin was involved as designer, consultant and expert in the construction of many different structures built in Yugoslavia and abroad.

The following are some of the more important:

1. Cable-stayed railway bridge over the Sava river in Belgrade, with Lj. Jevtović.

A double track bridge, length 556 m, max. span 254 m. The first long-span bridge in this system for rail traffic alone. Completed in 1979. See Eng. News Record, July 1976, p. 17 and Ref.: 57, 60, 61, 65, 75, 78, 80, 109.

2. Cable-stayed road bridge over the Danube river in Novi Sad. Max. span. 351 m. One of the biggest spans in the world for a cable-stayed bridge with cables in a single vertical plane. Completed in 1981. Ref.: 60, 64, 70, 75, 78, 82, 85, 86, 89, 90, 92, 93, 96, 109.

3. Composite continuous bridge over the Sava river in Orašje (Yug.). Central span 134 m; side spans 85,4 m. One of the largest spans for a continuous composite structure. Completed in 1968. First use of concrete slab for the upper and lower flanges in the zone of intermediate supports. Ref.: 40, 100.

4. Composite continuous bridge over the Špilje hydro-electric power station reservoir (Yug.), with G. Nenadić. Length 300 m, max. span 85 m. First use of precast concrete slab elements in Yugoslavia for a composite prestressed bridge. Ref.: 40, 100. Completed in 1965.

5. Two prestressed composite railway bridges in Ljubljana. Length 30 m. Frame system with the prestressed concrete slab in the lower zone. Ref.: 40, 60. Completed in 1964.

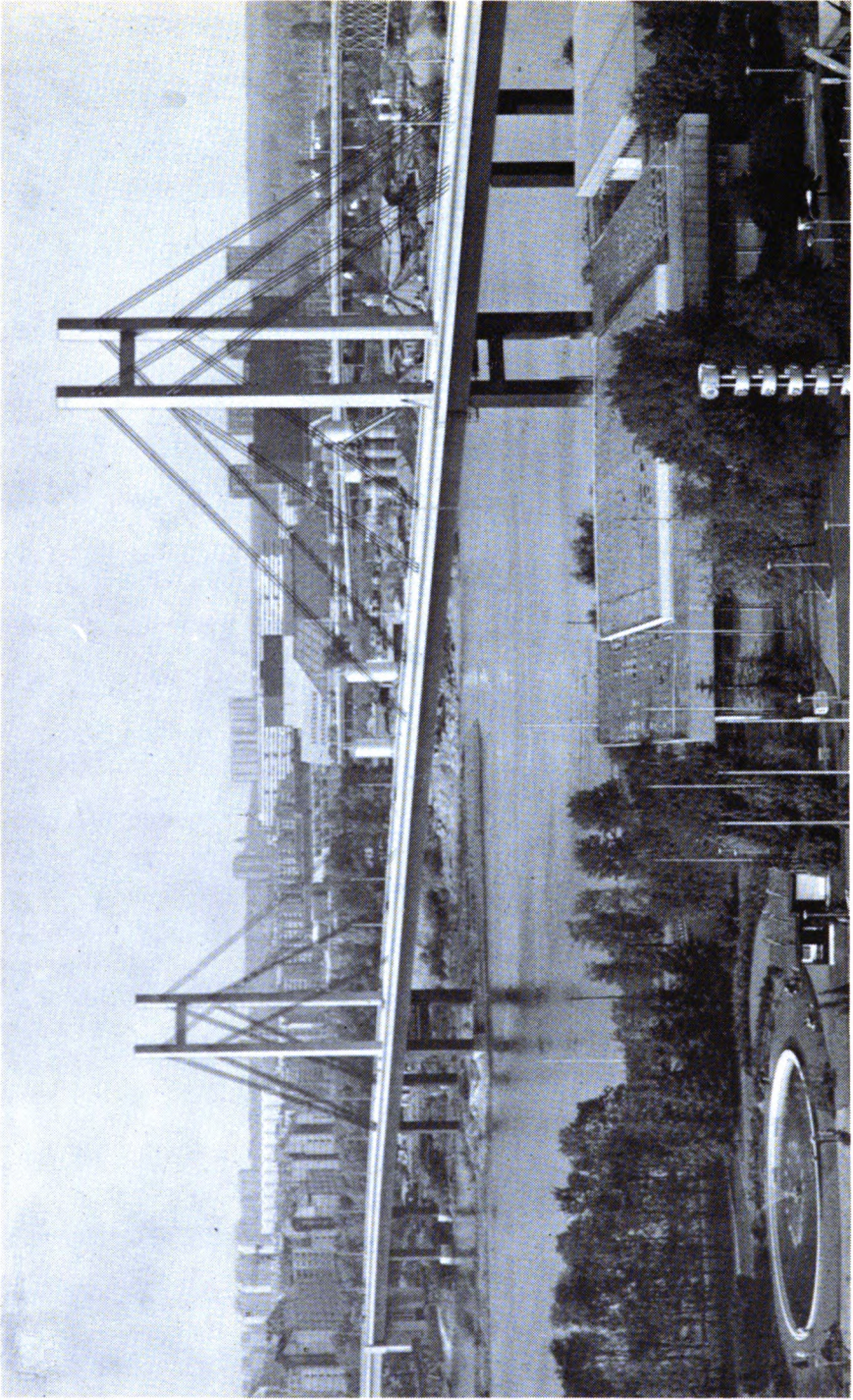
6. Composite prestressed continuous bridge over the Lim river at Rožaj (Yug.), with G. Nenadić. Max span 80 m. Completed in 1965.

7. Glažnja arch dam (Yug.), with D. Dimitrijević and D. Krajčinović. Height 85 m. One of the largest arch dams in Yugoslavia. Completed in 1970.



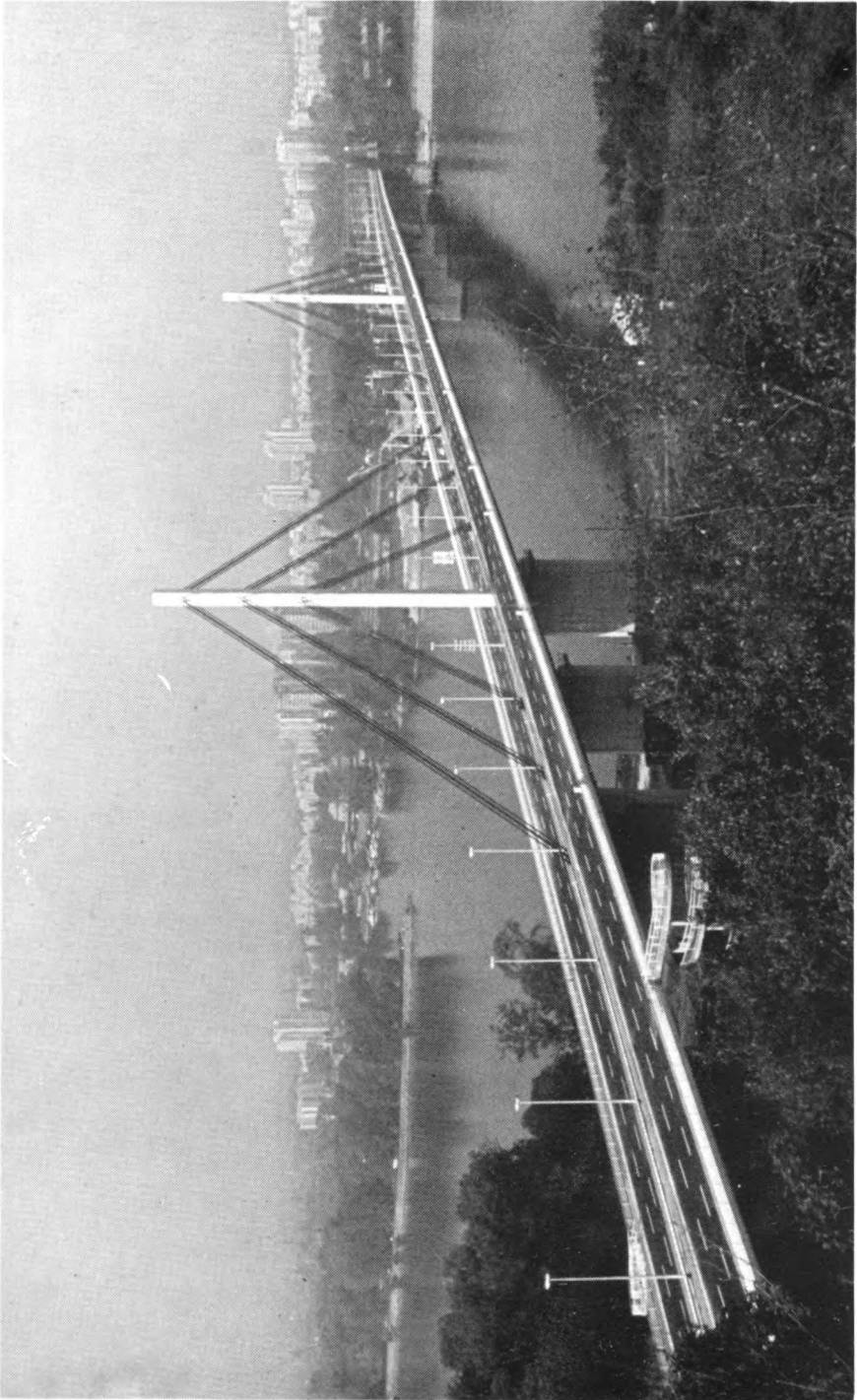
8. Cylindrical continuous shells as a roof system, for the Superphosphat factory in Prahovo (Yug.). Length 30 m. Completed in 1960.

9. Preliminary design for the steel railway bridge over the Tisa river near Titel (Yug.), with M. Djurić, Ž. Hiba and M. Hiba. Awarded in anonymous competition in 1956.



**THE RAILWAY BRIDGE OVER THE SAVA RIVER IN BELGRADE**





THE ROAD BRIDGE OVER THE DANUBE RIVER IN NOVI SAD







U.C. BERKELEY LIBRARIES



C029277315



**U.C. BERKELEY  
ENGINEERING LIBRARY**





